# Two-State Systems with Non-Markovian Thermal and Squeezed Quantum Noise Inputs

A thesis submitted to the University of Waikato

for the degree of

Doctor of Philosophy in Physics

by

**Andrew Scott Parkins**

November 1990

# Abstract

The effect of quantum noise on the two-state system is studied in the context of (i) coherent quantum tunnelling in a double-well system subject to low temperature quantum noise, and (ii) the two-level atom subject to finite bandwidth squeezed noise. Our approach to these problems is based on the adjoint equation, which describes the evolution of a quantum stochastic density operator. This equation is amenable to solution by ordinary stochastic methods, of which numerical simulation plays the most significant role in our calculations.

The dissipative double-well system is relevant to the search for macroscopic quantum coherence in superconducting quantum interference devices, and previous work, starting from a two-state model and using path integral methods, has established the so-called "noninteracting-blip approximation" as a central result. The adjoint equation, applied to this problem in the weak coupling limit, is shown to closely reproduce this result. The noninteracting-blip approximation entails a Markovian-type assumption about the noise, and, by means of stochastic simulation, we are able to check, and confirm, the validity of this assumption, even for the case of a zero-temperature bath.

Squeezed light, which has reduced quantum fluctuations in one quadrature phase, has been produced experimentally, and possible applications are under active consideration. Analyses of the effect of squeezed light on fundamental radiative processes in simple atoms have revealed interesting possibilities, most notably line-narrowing in the fluorescence spectrum. The original analyses in this field of research have been based on the assumption of broad bandwidth squeezing, and we review the primary results found in this limit. Also in this limit, we study in more detail the phenomenon of squeezed-light-induced photon echoes.

For broad bandwidth squeezing, line-narrowing in resonance fluorescence is restricted to the central fluorescence peak, while the Rabi sidebands exhibit broadening. We examine strongly driven resonance fluorescence for the case in which squeezing is confined to relatively small regions of frequency space about individual fluorescence peaks. It is shown that the noisy component associated with the unsqueezed quadrature phase can be effectively decoupled from the atomic dynamics, which allows narrowing to occur in all three peaks of the spectrum.

Finally, we address the practical problem of producing an effective coupling between an atom and a realistic three-dimensional squeezed field of modest angular spread. We show that this can be achieved, in principle, inside a microscopic plane mirror cavity, provided the injected squeezed field is suitably mode-matched to the cavity.

# Acknowledgements

My deepest thanks go to Prof. Crispin Gardiner, whose knowledge and understanding of physics have been, and will continue to be, a valuable influence on my career in the field of quantum optics. I thank him for supporting me in a trip to the Rochester Conference on Quantum Optics in 1989, and also for his considerable help with the technical side of producing this thesis; that is, with MacTeX, MacPlPlot, Illustrator, ....

I have also benefited immensely from discussions with Barry Sanders, Margaret Reid, and Moira and Alistair Steyn-Ross, to all of whom I express my thanks.

Thanks also to all of the physics graduates for their companionship and help over the past few years. This has been a much-valued part of my experience at the University of Waikato.

I thank the New Zealand University Grants Committee for its support through a Postgraduate Scholarship and a Shirtcliffe Fellowship.

Finally, I thank my parents, once again, for their unerring support throughout my time at university.

# Contents

# 1. Introduction

The rich variety of phenomena exhibited by the dissipative two-state system, and, more especially, its direct relevance to many practical situations, have ensured that this system occupies an important place in theoretical physics. From the point of view of quantum optics, the two-level model of an atom provides a fundamental tool for the examination of optical systems and has been quite central to the development of this field. Correspondingly, it has served as a testbed for the methods of quantum noise theory which have been developed in connection with quantum optics. This particular aspect is very pertinent to the present study, which, although concentrating on the dynamics of the two-level system, serves to highlight a particular approach to quantum noise based on the so-called *adjoint equation*. The adjoint equation is derived from the more familiar quantum Langevin equation, and its value arises from the fact that it can be treated as an ordinary (classical) linear stochastic differential equation. This, of course, opens the door to solution via the well-established methods of classical stochastic theory, including numerical simulation. More significantly (certainly from the point of view of this thesis), the adjoint equation requires no assumptions to be made about the correlation properties of the noise. Thus, it offers a clear opportunity for the treatment of non-Markovian dynamics, which is central to much of this thesis.

Appropriately, we begin, in Chapter 2, with a review of the adjoint equation formulation. This formulation is due to Gardiner and co-workers (Gardiner, Parkins, and Collett, 1987, Gardiner, 1988), and encompasses a unified treatment of inputs and outputs in damped quantum systems and operator quantum Langevin equations. As a first demonstration of the significance of the adjoint equation, and to make a connection with more familiar results, we apply the cumulant expansion method of van Kampen (1974, 1981) for linear stochastic differential equations to derive the quantum master equation.

Our first application of the adjoint equation approach is to the treatment of coherent quantum tunnelling in a double-well system. This particular problem has been

popularised in connection with the search for macroscopic quantum coherence in superconducting quantum interference devices (SQUID's), in which suitable double-well potentials are realisable. For sufficiently low temperatures, only the lowest doublet of states is appreciably populated, and a two-state model follows quite naturally. However, the rising spectrum of thermal quantum noise ensures that, even with this truncated system, an exact solution is not possible. Previous work has focussed primarily on path integral analyses (Leggett *et al*, 1987), which have yielded, as a central result, the "noninteracting-blip approximation." This approximation is based on the assumption that memory effects resulting from the system-bath coupling can be neglected. A stochastic interpretation of this approximation is therefore one of Markovian dynamics, which motivates our interest in this problem, since, in fact, low temperature thermal quantum noise exhibits a very long correlation time.

Restricting our considerations to the limit in which the system is weakly coupled to the environment, the adjoint equation approach leads to a relatively simple set of stochastic differential equations, which can be dealt with in a number of ways. By approximate analytical means, it is possible to obtain a result that is in close agreement with the noninteracting-blip approximation. More notably, however, we are able to numerically simulate the equations of motion, thereby avoiding the need for analytical approximations to the behaviour of thermal quantum noise. This allows us to check our earlier results, and, in fact, we find good agreement, which lends support to the analytical methods, whilst also demonstrating a very new approach to this particular problem.

The remaining chapters of this thesis deal with the two-level system in the context of atomic spectroscopy, and, in particular, with the effects one finds when *squeezed light* is incident upon the system. Squeezed light has reduced quantum fluctuations in one quadrature phase, and can be produced in certain nonlinear optical processes, such as four-wave mixing and parametric amplification. The successful generation of squeezed light in the laboratory has encouraged theoreticians to look for possible applications, and in the field of atomic spectroscopy this has lead to the discovery of some very interesting phenomena.

In a study of spontaneous emission in a squeezed vacuum, Gardiner (1986) found that the radiative processes of a two-level atom can be fundamentally altered, leading to spectral line-narrowing in the fluorescence spectrum. Analyses of resonance fluorescence

in a squeezed vacuum soon followed (Carmichael, Lane, and Walls, 1987a,b), and the field of (theoretical) squeezed light spectroscopy has continued to expand since then. However, the great majority of the work done in this field has been based on two very idealistic conditions; namely, that (i) the bandwidth of squeezed light is very broad, and (ii) the atom couples exclusively to squeezed modes of the radiation field.

The assumption of broad bandwidth squeezing means that, to the atom, the squeezed vacuum appears as quantum white noise, and hence the interaction can be described in terms of a Markov process. The cumulant expansion method alluded to earlier in connection with the adjoint equation is precisely suited to this regime, and is used in Chapter 4 to derive the (now standard) squeezed white noise master equation. The overall purpose of Chapter 4 is then to review some of the major results obtained in the white noise limit as a precursor to the work of Chapter 5 with finite bandwidth squeezing. We include a more detailed study of a particular phenomenon derived from the field of photon echo spectroscopy. Pulses of squeezed light are shown to induce photon echoes in inhomogeneously-broadened two-level media, offering a novel application of squeezed light that stands somewhat apart from the work on (steady-state) fluorescence spectra.

Work involving finite bandwidth squeezed light has been carried out in the past, but the main aim of this work has been to identify the detrimental effects such squeezing has on earlier predictions regarding spontaneous emission and atomic absorption spectra (Parkins and Gardiner, 1988, Ritsch and Zoller, 1988a,b). In Chapter 5, we examine the process of resonance fluorescence in a squeezed vacuum for the case in which the squeezing exhibits a spectral structure on the scale of the Rabi frequency. In contrast to the previous studies of finite bandwidth squeezing, we uncover some interesting dynamical effects which open the door to a new range of squeezing phenomena in the fluorescence spectrum. We concentrate on strongly driven resonance fluorescence and on the situation in which squeezing is confined to relatively small regions of frequency space about individual fluorescence peaks. Under these circumstances, we show that it is possible for the narrow bandwidth component of one quadrature phase noise operator to be decoupled from the atomic dynamics. Through an appropriate choice of driving field phase, this quadrature can be made to correspond to the unsqueezed or noisy quadrature of the input field. As a result, we find that it is possible for all three peaks in the fluorescence spectrum to exhibit narrowing. This represents a clear departure from previous white noise squeez-

ing analyses, which only predicted narrowing of the central fluorescence peak. Again, the adjoint equation forms the basis for our study, and we concentrate on the technique of stochastic simulation as a means of solution.

Finally, in Chapter 6, we address the second condition raised above concerning the coupling of the atom to only squeezed modes of the field. This is certainly the most serious problem facing experimentalists, and the purpose of Chapter 6 is to propose a possible experimental configuration based on the *microscopic Fabry-Pérot cavity*. Such cavities, in which plane mirrors are separated by a distance of the order of the emission wavelength, have been constructed (De Martini *et al*, 1986, 1987), and provide an environment in which field modes can be selectively coupled to atoms within the cavity. Using this configuration, we show that it is possible to manufacture an effective squeezed-field-atom coupling with an input squeezed field of modest angular dimensions, provided the input field is suitably mode-matched to the cavity.

Most of the original work in this thesis has been published in a series of papers, which, together with the appropriate chapters, are listed as follows:

**Chapter 3**

Parkins, A.S., and C.W. Gardiner, 1989, *Effect of dissipation on macroscopic quantum coherence in a double-well system*, in *Coherence and Quantum Optics VI*, edited by L. Mandel and E. Wolf (Plenum, New York).

Parkins, A.S., C.W. Gardiner, and M.L. Steyn-Ross, 1990, *The effect of dissipation on coherent quantum tunnelling in a double-well system: two-level model using an adjoint equation approach*, submitted to Z. Phys. B - Condensed Matter.

**Chapter 4**

Parkins, A.S., and C.W. Gardiner, 1989, *Photon echoes with coherent and squeezed pulses*, Phys. Rev. A **40**, 2534.

**Chapter 5**

Parkins, A.S., 1990, *Rabi sideband narrowing via strongly driven resonance fluorescence in a narrow-bandwidth squeezed vacuum*, Phys. Rev. A **42**, 4352.

Parkins, A.S., 1990, *Resonance fluorescence of a two-level atom in a two-mode squeezed vacuum*, to appear in Phys. Rev. A.

**Chapter 6**

Parkins, A.S., and C.W. Gardiner, 1989, *Inhibition of atomic phase decays by squeezed light in a microscopic Fabry-Pérot cavity*, Phys. Rev. A **40**, 3796, and erratum (to be published).

# 2. Quantum Langevin Equations

The body of formal theory upon which this thesis is based ties together in a coherent form several important concepts from the field of theoretical quantum optics. Specifically, it presents a unified approach to the formulation of (i) inputs and outputs in dissipative quantum systems, (ii) operator quantum Langevin equations, and (iii) the quantum master equation. The particular version that we shall present has been elucidated in detail a number of times (Collett, 1983, Gardiner, Parkins, and Collett, 1987, Gardiner, 1988), and represents a progression from the earlier input-output formalism of Gardiner and Collett (1985), which provided the first authoritative treatment of inputs and outputs and their interrelations with the familiar equations of quantum optics.

We begin by reviewing the input-output formalism for a system interacting with a one-dimensional electromagnetic field. This is presented in a form that is valid at all frequencies, and does not rely on either the rotating-wave approximation or any white noise assumptions. The primary result of this formulation takes the form of a simple boundary condition relating input and output fields to each other via the internal dynamics of the system.

To describe the time development of system operators, we derive a general quantum Langevin equation in the standard fashion. However, the input-output formalism now allows an explicit identification of the Langevin noise term with the input field, and thus the quantum Langevin equation provides the final link-up between input, output, and system fields.

From the quantum Langevin equation, we derive the *adjoint equation*, which describes the evolution of a quantum stochastic density operator, and is formulated in such a way that we are able to define a commuting noise operator. This means that the adjoint equation can be written in the form of a linear stochastic differential equation, amenable to solution using any of the methods of classical stochastic theory. One such method is the cumulant expansion technique of van Kampen (1974, 1981), which, for a white noise input, provides a direct and straightforward route to the familiar master equation of quantum

optics.

However, the adjoint equation itself makes no particular assumptions about the noise, and thus provides a starting point for the alternative analyses that are necessary when the dynamics are non-Markovian. Analyses of this sort, based largely on stochastic simulation, form the basis for much of this thesis.

## 2.1 The Model

The starting point for all of our calculations is the model of a system, characterised by the set of operators $\mathbf{Z}$, interacting with a bath of harmonic oscillators. The bath operators are denoted by $p(\omega)$ and $q(\omega)$, and the interaction is described by the linear coupling of a particular system operator $X$ to the bath degrees of freedom. The Hamiltonian for the interacting system and bath is

$$H = H_{sys}(\mathbf{Z}) + \frac{1}{2}\int_0^\infty d\omega \left\{[p(\omega) - \kappa(\omega)X]^2 + \omega^2 q(\omega)^2\right\}, \qquad (2.1.1)$$

where $\kappa(\omega)$ is a smooth function of $\omega$. A field interpretation can be formulated by introducing the Fourier transform variables

$$A(x,t) = \sqrt{\frac{2}{\pi c}}\int_0^\infty d\omega\, q(\omega,t)\cos(\omega x/c), \qquad (2.1.2)$$

$$\tilde{\kappa}(x) = \sqrt{\frac{2}{\pi c}}\int_0^\infty d\omega\kappa(\omega)\cos(\omega x/c), \qquad (2.1.3)$$

using which a Lagrangian can be derived in the form

$$\begin{aligned} L =& L_{sys}(\mathbf{Z}) + \frac{1}{2}\int_0^\infty dx\, \left\{\dot{A}(x,t)^2 - c^2[\partial_x A(x,t)]^2\right\} \\ &+ X\int_0^\infty dx\, \tilde{\kappa}(x)\dot{A}(x,t). \end{aligned} \qquad (2.1.4)$$

This Lagrangian describes the interaction of a system with a one-sided one-dimensional electromagnetic field. The range of the interaction is determined by the function $\tilde{\kappa}(x)$, which, in general, is assumed to be sharply peaked about $x = 0$, corresponding to a localised system and interaction. In atomic physics, this corresponds, of course, to the electric dipole approximation.

## 2.2 Input and Output Fields

### 2.2.1 Solutions for the field

The Heisenberg equations of motion for the bath operators $p(\omega)$ and $q(\omega)$ are

$$\dot{q}(\omega) = p(\omega,t) - \kappa(\omega)X, \tag{2.2.1}$$

$$\dot{p}(\omega) = -\omega^2 q(\omega,t). \tag{2.2.2}$$

The solutions to (2.2.1,2), expressed in terms of the annihilation operator

$$a(\omega,t) = \frac{\omega q(\omega,t) + ip(\omega,t)}{\sqrt{2\hbar\omega}}, \tag{2.2.3}$$

exists in two distinct forms, depending on whether we choose to solve the equations in terms of the initial conditions at time $t_0 < t$,

$$a(\omega,t) = e^{-i\omega(t-t_0)}a(\omega,t_0) - \kappa(\omega)\sqrt{\frac{\omega}{2\hbar}}\int_{t_0}^{t} dt'\, e^{-i\omega(t-t')}X(t'), \tag{2.2.4}$$

or in terms of the final conditions at time $t_1 > t$,

$$a(\omega,t) = e^{-i\omega(t-t_1)}a(\omega,t_1) + \kappa(\omega)\sqrt{\frac{\omega}{2\hbar}}\int_{t}^{t_1} dt'\, e^{-i\omega(t-t')}X(t'). \tag{2.2.5}$$

To this end, we define *in* and *out* fields as

$$A_{in}(t) = \frac{1}{2}\int_0^\infty d\omega\sqrt{\frac{\hbar}{\pi\omega c}}\left\{a(\omega,t_0)e^{-i\omega(t-t_0)} + a^\dagger(\omega,t_0)e^{i\omega(t-t_0)}\right\}, \tag{2.2.6}$$

and

$$A_{out}(t) = \frac{1}{2}\int_0^\infty d\omega\sqrt{\frac{\hbar}{\pi\omega c}}\left\{a(\omega,t_1)e^{-i\omega(t-t_1)} + a^\dagger(\omega,t_1)e^{i\omega(t-t_1)}\right\}, \tag{2.2.7}$$

which we note differ only in their dependence on, respectively, the initial time $t_0$ and the final time $t_1$.

Solving for $q(\omega,t)$ and hence for $A(x,t)$, one obtains after some manipulation

$$\begin{aligned} A(x,t) =& A_{in}(t + x/c) + A_{in}(t - x/c) \\ &- \frac{1}{2}\int_{x/c-(t-t_0)}^{x/c+(t-t_0)} d\tau\, \tilde{\kappa}(c\tau)X(t - |\tau - x/c|) \end{aligned} \tag{2.2.8}$$

$$\begin{aligned} =& A_{out}(t - x/c) + A_{out}(t + x/c) \\ &+ \frac{1}{2}\int_{x/c+(t-t_1)}^{x/c-(t-t_1)} d\tau\, \tilde{\kappa}(c\tau)X(t + |\tau - x/c|). \end{aligned} \tag{2.2.9}$$

Considerable simplification of these results is possible if we take note of the following points. Although these solutions are valid for arbitrary $\tilde{\kappa}(x)$, in practice $\tilde{\kappa}(x)$ will be nonzero only in some small finite range about $x = 0$. If we take $x$ to be outside this range, then, in the integrals above, $\tau$ will always be less than $x/c$ for nonzero $\tilde{\kappa}(c\tau)$, and we can replace $|\tau - x/c|$ with $(x/c - \tau)$. Further, if $t_0$ is taken to be in the remote past, and $t_1$ in the remote future, then the integral limits can be set equal to $\pm\infty$. With these approximations, the expressions on the right hand sides of (2.2.8,9) can be written as the sum of a function of $t - x/c$ and a function of $t + x/c$. We can equate functions of $t + x/c$ in (2.2.8) with those in (2.2.9) (and similarly for functions of $t - x/c$) to obtain

$$A_{in}(t + x/c) = A_{out}(t + x/c) + \frac{1}{2}\int_{-\infty}^{\infty} d\tau\, \tilde{\kappa}(c\tau) X(t + x/c - \tau), \qquad (2.2.10)$$

which, for any $x$ outside the range of $\tilde{\kappa}(x)$, can be generalised to

$$A_{out}(t) = A_{in}(t) - \frac{1}{2}\int_{-\infty}^{\infty} d\tau\, \tilde{\kappa}(c\tau) X(t - \tau). \qquad (2.2.11)$$

Returning to (2.2.8), and using the result (2.2.11), it is then possible to derive the additional result

$$A(t, x) = A_{in}(t + x/c) + A_{out}(t - x/c), \qquad (2.2.12)$$

for which there exists a very straightforward interpretation. Away from the region of interaction the total field is given by the sum of an outgoing *out* field and an incoming *in* field, which are related by (2.2.11). The *out* field consists of a *reflection* of the *in* field, plus a *radiated* field, which is determined by the behaviour of the system operator $X$.

### 2.2.2 System-field commutation relations

The system and bath represent different degrees of freedom, and hence the equal-times commutators of system operators with bath operators must be zero. That is, for an arbitrary system operator $Y(t)$, we have

$$[Y(t), q(\omega, t)] = [Y(t), p(\omega, t)] = 0. \qquad (2.2.13)$$

Hence, using the result (2.2.4) for $a(\omega, t)$, we can derive

$$[a(\omega, t_0), Y(t)] = \kappa(\omega)\sqrt{\frac{\omega}{2\hbar}}\int_{t_0}^{t} dt'\, e^{i\omega(t'-t_0)}[X(t'), Y(t)], \qquad (2.2.14)$$

which, in combination with the definition (2.2.6) of $A_{in}(t)$, leads to the commutation relation

$$[A_{in}(t'),Y(t)] = \frac{1}{2}\int_{t'-t}^{\infty} d\tau\, \tilde{\kappa}(c\tau)[X(t'-\tau),Y(t)]. \qquad (2.2.15)$$

Commutation relations involving $A_{out}(t)$ and $A(t)$ are derived in a similar fashion.

## 2.3 Quantum Langevin Equations

The Heisenberg equation of motion for an arbitrary system operator $Y(t)$ has the form

$$\dot{Y} = \frac{i}{\hbar}[H_{sys},Y] + \frac{i}{2\hbar}\int_0^{\infty} d\omega\ \left[(p(\omega,t)-\kappa(\omega)X)^2\ ,Y\right] \qquad (2.3.1)$$

$$= \frac{i}{\hbar}[H_{sys},Y] + \frac{i}{2\hbar}\int_0^{\infty} d\omega\ [p(\omega,t)-\kappa(\omega)X,[p(\omega,t)-\kappa(\omega)X,Y]\ ]_+\ , \qquad (2.3.2)$$

which, using (2.2.1) and the identity $[p(\omega,t),Y(t)] = 0$, can be simplified to

$$\dot{Y} = \frac{i}{\hbar}[H_{sys},Y] - \frac{i}{2\hbar}\int_0^{\infty} d\omega\ \kappa(\omega)\ [\dot{q}(\omega,t),[X,Y]]_+\ . \qquad (2.3.3)$$

In the previous section, we solved formally for the field operators in terms of initial conditions at time $t_0$ in the remote past. Using these solutions, we substitute for $\dot{q}(\omega,t)$ in (2.3.3) to obtain the quantum Langevin equation

$$\dot{Y} = \frac{i}{\hbar}[H_{sys},Y] + \frac{i}{2\hbar}[\ \Gamma(t)-\xi(t),[X,Y]\ ]_+\ , \qquad (2.3.4)$$

where

$$\Gamma(t) = \frac{1}{4c}\int_{-\infty}^{\infty}\int_{-\infty}^{\infty} dx dy\ \tilde{\kappa}(x)\tilde{\kappa}(y)\dot{X}(t-|x-y|/c), \qquad (2.3.5)$$

and

$$\xi(t) = \int_0^{\infty} dx\ \tilde{\kappa}(x)\left\{\dot{A}_{in}(t-x/c)+\dot{A}_{in}(t+x/c)\right\} \qquad (2.3.6)$$

$$= i\int_0^{\infty} d\omega\kappa(\omega)\sqrt{\frac{\hbar\omega}{2}}\left\{-a(\omega,t_0)e^{-i\omega(t-t_0)}+a^{\dagger}(\omega,t_0)e^{i\omega(t-t_0)}\right\} \qquad (2.3.7)$$

The term proportional to $\dot{X}$ represents radiation damping, which may or may not be Markovian in nature, depending on the choice of $\tilde{\kappa}(x)$. In what may be called the *first*

*Markov approximation*, one chooses $\tilde{\kappa}(x) \propto \delta(x)$ (i.e. $\kappa(\omega)$ constant), in which case the equation of motion simply becomes a first-order differential equation, with the time development of any system operator determined only by system operators in the present. However, this does not by itself lead to Markovian dynamics, since this also depends on the "noise" term $\xi(t)$. The term $\xi(t)$ depends on the initial quantum state of the bath through the operators $a(\omega, t_0)$ and $a^\dagger(\omega, t_0)$, and is quite arbitrary. In practice, $\xi(t)$ will be stochastic in nature and may exhibit a finite correlation time, so that computation of averages will require treatment of non-Markovian noise.

## 2.4 The Adjoint Equation

The quantum Langevin equation (2.3.4) is a nonlinear operator equation, which makes it difficult to deal with directly. However, an alternative approach that is far more amenable to calculation has been developed by Gardiner *et al* (Gardiner, Parkins, and Collett, 1987, Gardiner, 1988, Parkins and Gardiner, 1988) that has, as its central result, the *adjoint equation*. This equation describes the evolution of a quantum stochastic density operator, $\mu(t)$, that is a functional of the impressed quantum noise $\xi(t)$. A detailed derivation and discussions of this equation have been given in the aforementioned references.

Briefly, it is assumed that initially the system and bath are independent, so that the density operator factorises in the Heisenberg picture. We suppose that $\{e_i\}$ is a complete set of Schrödinger picture operators, such that any system operator can be expressed as a linear combination of them. We assume further that they are orthogonal with respect to the trace:

$$Tr_{sys}\{e_i^\dagger e_j\} = \delta_{ij}. \tag{2.4.1}$$

It follows that any Schrödinger picture system operator $Y$ can be written as

$$Y = \sum_i Tr_{sys}\{Y e_i^\dagger\} e_i \ , \tag{2.4.2}$$

and the corresponding Heisenberg picture operator as

$$Y(t) = \sum_i Tr_{sys}\{Y e_i^\dagger\} e_i(t) \ , \tag{2.4.3}$$

which follows from the fact that the evolution is unitary, and hence all algebraic relations are preserved. We construct the operator $\mu(t)$ as

$$\mu(t) = \sum_i Tr_{sys}\{e_i(t)\rho_{sys}\}e_i^\dagger, \tag{2.4.4}$$

from which it is clear that

$$Tr_{sys}\{e_i\mu(t)\} = Tr_{sys}\{e_i(t)\rho_{sys}\}, \tag{2.4.5}$$

and, therefore, that

$$Tr_{sys}\{Y(t)\rho_{sys}\} = Tr_{sys}\{Y\mu(t)\}. \tag{2.4.6}$$

To evaluate $\dot{\mu}(t)$, one must evaluate $Tr_{sys}\{\dot{e}_i(t)\rho_{sys}\}$, and this is done by Parkins and Gardiner (1988), notably, however, only in the first Markov approximation, when all of the system operators appearing in the quantum Langevin equation are evaluated at time $t$.

If the function $\tilde{\kappa}(x)$ remains general, the equation for $\dot{\mu}(t)$ cannot be derived exactly (in a simple closed form) from the quantum Langevin equation, owing to the operator function $\Gamma(t)$, which contains a term of the form $\dot{X}(t-\tau)$, and which therefore cannot be expressed directly in terms of system operators at time $t$. However, if we invoke the approximation that the noise is weak, and that $H_{sys}$ is almost time independent, then we can write

$$X(t-\tau) \simeq \exp\left(\frac{-iH_{sys}\tau}{\hbar}\right) X(t) \exp\left(\frac{iH_{sys}\tau}{\hbar}\right), \tag{2.4.7}$$

after which it is possible to derive the equation of motion for $\mu(t)$ in the form

$$\dot{\mu}(t) = -\frac{i}{\hbar}[H_{sys}, \mu(t)] + \frac{i}{2\hbar}[\,[\Gamma - \xi(t), \mu(t)]_+, X\,], \tag{2.4.8}$$

where now $\Gamma$ is expressed entirely in terms of Schrödinger operators as

$$\Gamma = \frac{1}{4c}\int_{-\infty}^{\infty}\int_{-\infty}^{\infty} dxdy\ \tilde{\kappa}(x)\tilde{\kappa}(y)\dot{X}(-|x-y|/c). \tag{2.4.9}$$

The equation of motion (2.4.8) is called the *adjoint equation.* The quantity $\mu(t)$ is related to the more familiar Schrödinger picture system density matrix, $\rho_{sys}(t)$, through

$$\rho_{sys}(t) = Tr_B\{\mu(t)\rho_B\} \equiv \langle\mu(t)\rangle. \tag{2.4.10}$$

Thus, we have in (2.4.8) an equation of motion for a density matrix $\mu(t)$ that is a functional of the impressed quantum noise as represented by the operator input $\xi(t)$.

We reiterate that, in the first Markov approximation, the adjoint equation (2.4.8) is completely equivalent to the quantum Langevin equation. Without this approximation, this is not the case, but the adjoint equation will still be valid in weak noise situations, such as one finds in quantum optical systems.

**A commuting form of quantum noise**

The operator nature of $\xi(t)$ can be almost completely eliminated from the adjoint equation with the introduction of an operator $\beta(t)$ defined by

$$\beta(t)\mu(t) \equiv \frac{1}{2}[\xi(t), \mu(t)]_+. \tag{2.4.11}$$

Noting that the commutator $[\xi(t), \xi(t')]$ is a complex number, it follows that

$$[\beta(t), \beta(t')]\mu = \frac{1}{4}[\,[\xi(t), \xi(t')], \mu\,] = 0, \tag{2.4.12}$$

and, hence, that

$$\beta(t)\beta(t') = \beta(t')\beta(t), \tag{2.4.13}$$

for all $t, t'$. Hence, $\beta(t)$ can be treated as a $c$-number random function, and the adjoint equation can be written in the form of a linear stochastic differential equation

$$\dot{\mu}(t) = [A_0 + \beta(t)A_1]\mu(t), \tag{2.4.14}$$

where $A_0$ and $A_1$ are linear operators in the system space and are defined by

$$A_0\mu(t) = -\frac{i}{\hbar}[H_{sys}, \mu(t)] + \frac{i}{2\hbar}[\,[\Gamma, \mu(t)]_+, X\,], \tag{2.4.15}$$

$$A_1\mu(t) = \frac{i}{\hbar}[\,X, \mu(t)\,]. \tag{2.4.16}$$

Clearly, then, (2.4.14) may be treated as a classical stochastic differential equation, and, hence, solutions may be attempted with the well-studied methods of classical stochastic theory at our disposal. One such method is the cumulant expansion technique of van Kampen (1974, 1981), which we shall use in Section 2.5 to derive the familiar master equation. Eigenfunction methods (Ritsch and Zoller, 1988a,b), and stochastic simulation (Parkins and Gardiner, 1988) have also been used in connection with the adjoint equation to investigate effects associated with finite bandwidth squeezed noise. This particular example is also notable for the use of complex noise sources to model the negative correlations that

characterise squeezing. This necessitates a doubling of the dimensionality of the problem, following the approach introduced with the generalised P-representations of Drummond and Gardiner (1980) for the description of nonclassical states of light.

## 2.5 The Master Equation

In practice, we want to evaluate the properties of a system via the averages of system variables. These averages are obtained from the density matrix $\mu(t)$ through the relationship

$$\begin{aligned}\langle Y(t)\rangle &= Tr_{sys}\{Tr_B\{Y(t)\rho_{sys}\otimes\rho_B\}\} = Tr_B\{Tr_{sys}\{Y\mu(t)\}\rho_B\} \\ &= Tr_{sys}\{YTr_B\{\mu(t)\rho_B\}\}.\end{aligned} \tag{2.5.1}$$

It follows that we must determine the average of $\mu(t)$ over the noise $\beta(t)$. The form (2.4.14) of the adjoint equation leads us quite naturally to the cumulant expansion technique of van Kampen (1974, 1981). This method yields an equation of motion for $\rho(t) \equiv \langle\mu(t)\rangle$ in the form of a perturbation expansion in a smallness parameter. The equation, to second order in this parameter, is

$$\begin{aligned}\dot{\rho}(t) =& A_0\rho(t) \\ &+ \int_0^\infty d\tau\,\langle\beta(t)A_1\exp(A_0\tau)\beta(t-\tau)A_1\exp(-A_0\tau)\rangle\,\rho(t).\end{aligned} \tag{2.5.2}$$

The actual smallness parameter is $(\|A_1\|\,\|\beta\|\,\tau_c)$, where $\|A_1\|$ is a measure of the magnitude of the operator $A_1$, $\|\beta\|$ is the root mean square amplitude of $\beta(t)$, and $\tau_c$ is the correlation time of $\beta(t)$. Clearly, this method is suited to the treatment of near-white noise sources that exhibit very short correlation times.

To evaluate the integral in (2.5.2), we note firstly that $A_0$ and $A_1$ involve only operators in the system space, and hence $\beta(t)$ is statistically independent of, and commutes with, these operators. Secondly, we make the approximation

$$\exp(A_0\tau)X\exp(-A_0\tau) \simeq X(-\tau) \simeq \exp(-iH_{sys}\tau/\hbar)X\exp(iH_{sys}\tau/\hbar), \tag{2.5.3}$$

which amounts to the assumption of weak system-bath coupling. However, it may also be the case that $\exp(A_0\tau)$ does not vary significantly over the correlation time of $\beta(t)$.

To convert the equation to the form found most often in quantum optics, we define eigenstates of the system Hamiltonian $H_{sys}$ by

$$H_{sys}|i\rangle = \hbar\omega_i|i\rangle, \tag{2.5.4}$$

(where $\omega_i > \omega_j$ if $i > j$) and expand $X$ in eigenoperators of the system Hamiltonian as

$$X = \sum_{m<n}(q_{mn}A_{mn} + q_{nm}A_{nm}), \tag{2.5.5}$$

where

$$A_{mn} = |m\rangle\langle n| \tag{2.5.6}$$

corresponds in the summation (2.5.5) to a lowering operator. With these definitions, it follows that

$$[H_{sys}, A_{mn}] = \hbar\omega_{mn}A_{mn}, \tag{2.5.7}$$

where $\omega_{mn} = \omega_m - \omega_n$. Hence, we can write

$$X(t) = \sum_{m<n}(q_{mn}A_{mn}e^{i\omega_{mn}t} + q_{nm}A_{nm}e^{i\omega_{nm}t}), \tag{2.5.8}$$

and working out (2.5.2) in detail yields the master equation

$$\begin{aligned}
\dot{\rho}(t) = &-\frac{i}{\hbar}[H_{sys}, \rho(t)] \\
&- \sum_{m<n}\sum_{k<l}\frac{\pi\omega_{mn}}{4\hbar}\kappa(\omega_{mn})^2[\,[q_{mn}A_{mn} - q_{nm}A_{nm}, \rho(t)]_+, q_{kl}A_{kl} + q_{lk}A_{lk}\,] \\
&+ \sum_{m<n}\sum_{k<l}\frac{i\omega_{mn}}{4\hbar}P\int_{-\infty}^{\infty}d\omega\frac{\kappa(\omega)^2}{\omega_{mn}-\omega} \\
&\qquad\times[\,[q_{mn}A_{mn} + q_{nm}A_{nm}, \rho(t)]_+, q_{kl}A_{kl} + q_{lk}A_{lk}\,] \\
&+ \frac{1}{2\hbar^2}\sum_{m<n}\sum_{k<l}F(\omega_{mn}, t)[\,[q_{mn}A_{mn}, \rho(t)], q_{kl}A_{kl} + q_{lk}A_{lk}\,] \\
&+ \frac{1}{2\hbar^2}\sum_{m<n}\sum_{k<l}F(\omega_{nm}, t)[\,[q_{nm}A_{nm}, \rho(t)], q_{kl}A_{kl} + q_{lk}A_{lk}\,],
\end{aligned} \tag{2.5.9}$$

with

$$F(\omega_{mn}, t) = 2\int_0^{\infty}d\tau\, e^{-i\omega_{mn}\tau}\langle\beta(t)\beta(t-\tau)\rangle. \tag{2.5.10}$$

In practice, the form (2.5.9) can be simplified considerably by invoking the rotating-wave approximation, and by neglecting the principal value integrals (frequency shift terms).

# 3. Coherent Quantum Tunnelling in a Double Well System

Coherent quantum tunnelling in a double-well system is sensitively dependent on dissipation that results from the coupling of the tunnelling coordinate to the environment. A considerable amount of research has been dedicated to this problem, motivated by its relevance to the possible observation of macroscopic quantum coherence in, for instance, the SQUID (superconducting quantum interference device), where the motion of the trapped magnetic flux may be governed by a symmetric double-well potential (of a microscopic order of magnitude). Hence, it is possible, in principle, for the flux to exhibit coherent oscillations between two metastable states. In practice, dissipation due to the system-environment coupling plays a vital role in the dynamics, leading to a loss of coherence which may ultimately preclude any observation of coherent oscillations. Consequently, many efforts have been made to identify the most favourable regions of parameter-space (see in particular Leggett *et al*, 1987, and Weiss *et al*, 1987a, and references therein).

The case of most interest is one in which quantum tunnelling through the potential barrier yields two closely-spaced low-lying states that are together well separated in energy from the higher states. Hence, the standard approach in previous treatments has been to truncate the system to just these two levels, and to model the dissipative interaction of the system with its environment by a linear coupling to a thermal bath of harmonic oscillators. Even with this reduced model, an exact solution is not possible, and various approximate treatments have been proposed in the literature, based largely on path integral formulations and instanton techniques. A central result amongst all of these analyses is the much celebrated "noninteracting-blip approximation" (first introduced by Chakravarty and Leggett, 1984), which can be obtained from a long and detailed analysis of path integrals, the end result being a single integro-differential equation for the variable of interest.

Interestingly, however, the same result has been derived using a Heisenberg equation approach together with a standard second-order Born approximation (Aslangul *et al*, 1985,1986, Dekker, 1987). This basically amounts to a master equation approach, which,

as we know, relies in general on the characteristic correlation time of the reservoir being very small. However, for sufficiently low temperatures, thermal quantum noise exhibits a very long correlation time, thereby bringing into question master equation methods.

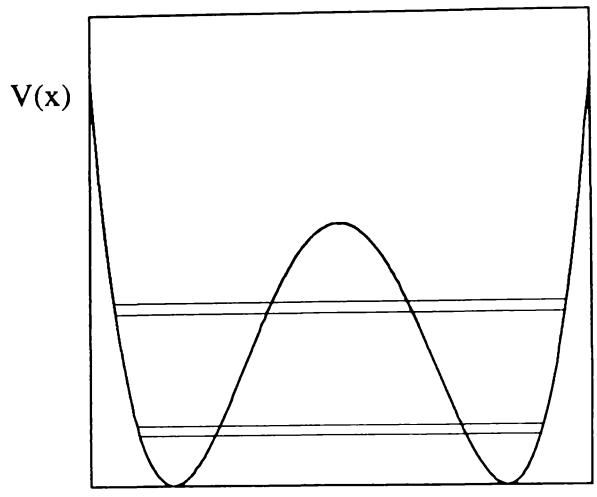


**Fig.3.1** Double-well potential with energy levels

Our interest in this problem arises from the inherently non-Markovian behaviour of thermal quantum noise, and, more particularly, from the opportunity offered by the adjoint equation for an investigation of just this sort of non-white noise system. We will consider a number of possible methods of solution using the adjoint equation, including stochastic simulation. Naturally, the rising spectrum exhibited by thermal quantum noise presents a significant practical problem, and, in practice, we must introduce a cutoff. Even with this cutoff, the treatment of noise at very high frequencies can be very difficult. However, with the recognition that the frequencies of interest (i.e. around the tunnelling frequency) are relatively small compared to much of the bath, we can divide the noise into high and low frequency parts, and perform a stochastic average over the high frequency portion of the bath using the cumulant expansion technique outlined in the previous chapter. The low frequency portion is then dealt with numerically.

## 3.1 The Double-Well System

### 3.1.1 The coupling operator $X$

We consider a double-well system in which quantum tunnelling through the potential barrier lifts the degeneracy of the groundstate to yield a doublet of states, as depicted in Fig.3.1. This doublet is assumed to be well separated in energy from the remaining higher states, so that for sufficiently low temperatures, the population of all but these two lowest-energy states is negligible. A reduction of the problem to that of a simple two-state system should then be a reliable approximation.

For the moment, however, the formulation of Chapter 2 allows us to retain complete generality, and eigenstates of the double-well system Hamiltonian are defined as before by

$$H_{sys}|i\rangle = \hbar\omega_i|i\rangle, \tag{3.1.1}$$

as is the coupling operator $X$, which we write once again as

$$X = \sum_{m<n}(q_{mn}A_{mn} + q_{nm}A_{nm}), \tag{3.1.2}$$

where

$$A_{mn} = |m\rangle\langle n|, \tag{3.1.3}$$

and

$$q_{mn} = \langle m|X|n\rangle = \int dx\ \psi_m^*(x)x\psi_n(x), \tag{3.1.4}$$

with $\psi_n(x)$ the wavefunctions of the undamped system. Hence, detailed information on the nature and shape of the potential is contained in the parameters $q_{mn}$. It is also reflected to some extent by the transition frequencies. In particular, for the system we have in mind, the potential is assumed to be such that $\omega_{21} \ll \omega_{32}$ ($\omega_{nm} = \omega_n - \omega_m$); that is, the ground-state splitting is much less than the energy gap to the next highest level.

Finally, we note that if our results are to be considered in the context of macroscopic quantum coherence, then $\pm|q_{21}|$ (which give the positions of the minima of the potential) would have to be of such a magnitude as to allow a description in terms of macroscopically-distinguishable states.

### 3.1.2 High and low frequency behaviour

The double-well system that we have in mind possesses two distinct frequency scales; (i) the tunnelling frequency between the two lowest levels, $\omega_{21}$, and (ii) the much larger frequency of the transitions connecting these levels to higher energy states (e.g. $\omega_{32}$). It is appropriate, therefore, in dealing with the bath to which the system is coupled, to consider separately the contributions from the high-frequency and low-frequency oscillators. For this purpose, we write the noise $\beta(t)$ as a sum of two (independent) noises $\beta_{hf}(t)$ and $\beta_{lf}(t)$, which correspond respectively to the high and low frequency portion of the bath. That is, we write

$$\beta(t) \equiv \beta_{hf}(t) + \beta_{lf}(t), \tag{3.1.5}$$

where

$$\langle \beta_{hf}(t)\beta_{hf}(t')\rangle = \frac{\hbar}{2}\int_0^\infty d\omega \kappa_{hf}(\omega)^2 \omega \coth\left(\frac{\hbar\omega}{2kT}\right)\cos[\omega(t-t')], \tag{3.1.6}$$

and

$$\langle \beta_{lf}(t)\beta_{lf}(t')\rangle = \frac{\hbar}{2}\int_0^\infty d\omega \kappa_{lf}(\omega)^2 \omega \coth\left(\frac{\hbar\omega}{2kT}\right)\cos[\omega(t-t')]. \tag{3.1.7}$$

The coupling functions $\kappa_{hf}(\omega)$ and $\kappa_{lf}(\omega)$ shall remain general at this stage, but we note that the following properties will hold,

$$\kappa_{hf}(\omega)^2 \simeq 0 \quad \text{for} \quad \omega \ll \omega_c, \tag{3.1.8}$$

$$\kappa_{lf}(\omega)^2 \simeq 0 \quad \text{for} \quad \omega \gg \omega_c, \tag{3.1.9}$$

where $\omega_c$ is a frequency that characterises the division between the high and low frequency portions of the bath, and is such that $\omega_{21} \ll \omega_c \ll \omega_{32}$.

### 3.1.3 Average over high frequency noise

The dynamics of the two lowest states will be of the most interest to us, and these dynamics will be influenced most strongly by the "low" frequency noise $\beta_{lf}(t)$. While the high frequency bath oscillators play no part in the dynamics of these levels, they are expected to provide a renormalisation of the tunnelling frequency.

Returning to the adjoint equation, our approach to the high frequency portion of the bath is to perform a stochastic average over the noise $\beta_{hf}(t)$ using the cumulant expansion

technique described in the previous chapter. This technique is particularly suitable for this purpose because this portion of the bath exhibits a very short correlation time. The expansion gives an equation of motion in the form

$$\begin{aligned}\dot{\mu}_{hf}(t) &= [A_0 + \beta_{lf}(t)A_1]\mu_{hf}(t) \\ &\quad + \int_0^\infty d\tau \langle \beta_{hf}(t)A_1 \exp(A_0\tau)\beta_{hf}(t-\tau)A_1 \exp(-A_0\tau)\rangle\, \mu_{hf}(t),\end{aligned} \tag{3.1.10}$$

where the subscript $hf$ denotes that we have taken the average over the high-frequency portion of the bath. As in Section 2.5, we make the approximation

$$\exp(A_0\tau)X\exp(-A_0\tau) \simeq X(-\tau) = \exp(-iH_{sys}\tau/\hbar)X\exp(iH_{sys}\tau/\hbar), \tag{3.1.11}$$

and, writing

$$X(t) = \sum_{m<n}(q_{mn}A_{mn}e^{i\omega_{mn}t} + q_{nm}A_{nm}e^{i\omega_{nm}t}), \tag{3.1.12}$$

we can evaluate the coefficients in (3.1.10) to obtain

$$\begin{aligned}\dot{\mu}_{hf}(t) &= -\frac{i}{\hbar}[H_{sys}, \mu_{hf}(t)] \\ &\quad - \frac{i}{\hbar}\beta_{lf}(t)\sum_{m<n}[\mu_{hf}(t), q_{mn}A_{mn} + q_{nm}A_{nm}] \\ &\quad - \sum_{m<n}\sum_{k<l}\frac{\pi\omega_{mn}}{4\hbar}\kappa(\omega_{mn})^2[\,[q_{mn}A_{mn} - q_{nm}A_{nm}, \mu_{hf}(t)]_+, q_{kl}A_{kl} + q_{lk}A_{lk}\,] \\ &\quad + \sum_{m<n}\sum_{k<l}\frac{i\omega_{mn}}{4\hbar}P\int_{-\infty}^{\infty}d\omega\frac{\kappa(\omega)^2}{\omega_{mn}-\omega} \\ &\qquad \times [\,[q_{mn}A_{mn} + q_{nm}A_{nm}, \mu_{hf}(t)]_+, q_{kl}A_{kl} + q_{lk}A_{lk}\,] \\ &\quad + \frac{1}{2\hbar^2}\sum_{m<n}\sum_{k<l}F(\omega_{mn})[\,[q_{mn}A_{mn}, \mu_{hf}(t)], q_{kl}A_{kl} + q_{lk}A_{lk}\,] \\ &\quad + \frac{1}{2\hbar^2}\sum_{m<n}\sum_{k<l}F(\omega_{nm})[\,[q_{nm}A_{nm}, \mu_{hf}(t)], q_{kl}A_{kl} + q_{lk}A_{lk}\,],\end{aligned} \tag{3.1.13}$$

with

$$\begin{aligned}F(\omega_{mn}) &= 2\int_0^\infty d\tau\, e^{-i\omega_{mn}\tau}\langle\beta_{hf}(t)\beta_{hf}(t-\tau)\rangle \\ &= \frac{\pi\hbar}{2}\kappa_{hf}(\omega_{mn})^2\omega_{mn}\coth\left(\frac{\hbar\omega_{mn}}{2kT}\right) \\ &\quad + \frac{i\hbar}{2}P\int_0^\infty d\omega\,\kappa_{hf}(\omega)^2\omega\coth\left(\frac{\hbar\omega}{2kT}\right)\left(\frac{1}{\omega-\omega_{mn}} - \frac{1}{\omega+\omega_{mn}}\right).\end{aligned} \tag{3.1.14}$$

Noting that $\kappa_{hf}(\omega_{21})^2 \simeq 0$, this equation is seen to possess the standard master equation terms for the higher states of the system, together with frequency renormalisation terms

(corresponding to the Lamb shift terms of quantum optics). These renormalisation terms must be taken into account when we concentrate on the two lowest states.

It is a relatively straightforward matter to compute, from (3.1.13), the equation of motion for an arbitrary matrix element of $\mu_{hf}(t)$. This has the form

$$\begin{aligned}\langle a|\dot{\mu}_{hf}|b\rangle = &-i\omega_{ab}\langle a|\mu_{hf}|b\rangle - \frac{i}{\hbar}\beta_{lf}(t)\sum_n \left(q_{nb}\langle a|\mu_{hf}|n\rangle - q_{an}\langle n|\mu_{hf}|b\rangle\right)\\ &+\sum_{n,k} q_{an}q_{kb}\langle n|\mu_{hf}|k\rangle(-\gamma_{an}-i\Delta_{an})\\ &+\sum_{n,k} q_{kn}q_{ak}\langle n|\mu_{hf}|b\rangle(\gamma_{kn}+i\Delta_{kn})\\ &+\sum_{n,k} q_{nk}q_{kb}\langle a|\mu_{hf}|n\rangle(\gamma_{kn}-i\Delta_{kn})\\ &+\sum_{n,k} q_{nb}q_{ak}\langle k|\mu_{hf}|n\rangle(-\gamma_{bn}+i\Delta_{bn}),\end{aligned} \tag{3.1.15}$$

where

$$\gamma_{kn} = \frac{\pi}{4\hbar}\omega_{kn}\left\{\kappa(\omega_{kn})^2 - \kappa_{hf}(\omega_{kn})^2\coth\left(\frac{\hbar\omega_{kn}}{2kT}\right)\right\}, \tag{3.1.16}$$

and

$$\begin{aligned}\Delta_{kn} = &\frac{1}{4\hbar}P\int_0^\infty d\omega\,\omega_{kn}\kappa(\omega)^2\left(\frac{1}{\omega-\omega_{kn}}-\frac{1}{\omega+\omega_{kn}}\right)\\ &-\frac{1}{4\hbar}P\int_0^\infty d\omega\,\omega\kappa_{hf}(\omega)^2\coth\left(\frac{\hbar\omega}{2kT}\right)\left(\frac{1}{\omega-\omega_{kn}}-\frac{1}{\omega+\omega_{kn}}\right).\end{aligned} \tag{3.1.17}$$

### 3.1.4 Specification of cutoff functions

Before proceeding further, we should specify the functions $\kappa(\omega)^2$, $\kappa_{lf}(\omega)^2$, and $\kappa_{hf}(\omega)^2$ that appear above. We will assume smooth cutoff behaviour of the form

$$\kappa(\omega)^2 = \kappa^2\exp(-|\omega|/\omega_b), \tag{3.1.18}$$

$$\kappa_{lf}(\omega)^2 = \kappa^2\exp(-|\omega|/\omega_c), \tag{3.1.19}$$

$$\kappa_{hf}(\omega)^2 = \kappa^2\left[\exp(-|\omega|/\omega_b) - \exp(-|\omega|/\omega_c)\right], \tag{3.1.20}$$

with $\omega_b \gg \omega_c$. The frequency $\omega_c$ is a parameter characterising the division between the high and low frequency portions of the bath. The exponential is a commonly-chosen form of cutoff function. We note, however, that our final results should, in principle, be largely

independent of $\omega_c$, and of the form of cutoff behaviour. While $\omega_c$ is an artificial frequency, chosen for our convenience, the upper cutoff frequency $\omega_b$ reflects the finite size of the system, and gives a measure of the highest frequency response of the bath. Hence, $\omega_b$ represents a real frequency, characteristic of the particular system we are considering.

By assumption, we have $\hbar\omega_c \gg 2kT$, and hence the hyperbolic cotangent that multiplies $\kappa_{hf}(\omega)^2$ in (3.1.16) and (3.1.17) can be set equal to one without significant error. With this simplification, and using (3.1.18-20), the quantities $\gamma_{kn}$ and $\Delta_{kn}$ take the form

$$\begin{aligned}\gamma_{kn} &= \frac{\pi}{4\hbar}\left[\omega_{kn}\kappa(\omega_{kn})^2 - |\omega_{kn}|\kappa_{hf}(\omega_{kn})^2\right] \\ &= \frac{\pi\kappa^2}{4\hbar}\left\{\omega_{kn}\exp(-|\omega_{kn}|/\omega_b) - |\omega_{kn}|\left[\exp(-|\omega_{kn}|/\omega_b) - \exp(-|\omega_{kn}|/\omega_c)\right]\right\},\end{aligned} \tag{3.1.21}$$

and

$$\begin{aligned}\Delta_{kn} = &\frac{\kappa^2}{2\hbar}\omega_{kn}\exp(\omega_{kn}/\omega_b)\,\mathrm{Ei}(-\omega_{kn}/\omega_b) \\ &- \frac{\kappa^2}{4\hbar}\omega_{kn}\left[\exp(-\omega_{kn}/\omega_c)\,\mathrm{Ei}(\omega_{kn}/\omega_c) + \exp(\omega_{kn}/\omega_c)\,\mathrm{Ei}(-\omega_{kn}/\omega_c)\right],\end{aligned} \tag{3.1.22}$$

where

$$\mathrm{Ei}(x) = C + \ln(|x|) + \sum_{k=1}^{\infty}\frac{x^k}{k.k!} \tag{3.1.23}$$

is the exponential integral function, with $C = 0.577\ldots$ (Gradshteyn and Ryzhik, 1965).

### 3.1.5 Truncation to a two-level problem

At sufficiently low temperatures, it is a justifiable approximation to assume that only the two lowest energy levels are occupied. The only matrix elements that should differ significantly from zero are then $\langle i|\mu_{hf}|j\rangle$ with $i,j = 1,2$. The equations of motion for these elements are, from (3.1.15),

$$\begin{aligned}\langle 2|\dot{\mu}_{hf}|1\rangle &= \langle 1|\dot{\mu}_{hf}|2\rangle^* \\ &= -i\omega_{21}\langle 2|\mu_{hf}|1\rangle - \frac{i}{\hbar}q_{21}\beta_{lf}(t)\left(\langle 2|\mu_{hf}|2\rangle - \langle 1|\mu_{hf}|1\rangle\right) \\ &\quad - q_{21}^2\left[(\gamma_{12}+\gamma_{21}) + i(\Delta_{21}-\Delta_{12})\right]\langle 1|\mu_{hf}|2\rangle \\ &\quad + \sum_k\left[|q_{k2}|^2(\gamma_{k2}+i\Delta_{k2}) + |q_{k1}|^2(\gamma_{k1}-i\Delta_{k1})\right]\langle 2|\mu_{hf}|1\rangle, \qquad (3.1.24) \\ \langle 1|\dot{\mu}_{hf}|1\rangle &= -\frac{i}{\hbar}\beta_{lf}(t)\left(q_{21}\langle 1|\mu_{hf}|2\rangle - q_{12}\langle 2|\mu_{hf}|1\rangle\right)\end{aligned}$$

$$- 2|q_{21}|^2\gamma_{12}\langle 2|\mu_{hf}|2\rangle + 2\sum_k |q_{k1}|^2\gamma_{k1}\langle 1|\mu_{hf}|1\rangle, \qquad (3.1.25)$$

$$\langle 2|\dot{\mu}_{hf}|2\rangle = -\frac{i}{\hbar}\beta_{lf}(t)\left(q_{12}\langle 2|\mu_{hf}|1\rangle - q_{21}\langle 1|\mu_{hf}|2\rangle\right)$$
$$- 2|q_{21}|^2\gamma_{21}\langle 1|\mu_{hf}|1\rangle + 2\sum_k |q_{k2}|^2\gamma_{k2}\langle 2|\mu_{hf}|2\rangle. \qquad (3.1.26)$$

In deriving these equations, we have set equal to zero any summations involving products of the form $q_{2k}q_{k1}$, since $\psi_1(x)$ and $\psi_2(x)$ have opposite parity, and, hence, one of $q_{2k}$ or $q_{k1}$ is necessarily zero.

Further simplification is possible by noting that $\gamma_{k1}, \gamma_{k2} \simeq 0$ for $k \geq 3$ (which follows from the assumption that $\omega_{32} \gg \omega_c$). In addition, we assume that the dominant frequency shift terms occurring in (3.1.24) are those involving only $k = 1, 2$, and hence we neglect the remaining terms. We shall return to this point later when comparing our results with other work. We note, however, that while this truncation does simplify the equations that follow, it is not, in principle, essential.

Using the fact that $\omega_{21} \ll \omega_c$, we can write

$$\gamma_{21} = -\gamma_{12} \simeq \frac{\pi}{4\hbar}\kappa^2\omega_{21}, \qquad (3.1.27)$$

and

$$\Delta_{21} \simeq \frac{\kappa^2}{2\hbar}\omega_{21}\ln\left(\frac{\omega_c}{\omega_b}\right) = -\Delta_{12}. \qquad (3.1.28)$$

Finally, we introduce the familiar notation for a two-level system, defining

$$\begin{aligned} S_x &= \langle 2|\mu_{hf}|1\rangle + \langle 1|\mu_{hf}|2\rangle, \\ S_y &= i(\langle 2|\mu_{hf}|1\rangle - \langle 1|\mu_{hf}|2\rangle), \\ S_z &= \langle 2|\mu_{hf}|2\rangle - \langle 1|\mu_{hf}|1\rangle, \end{aligned} \qquad (3.1.29)$$

and setting

$$\langle 1|\mu_{hf}|1\rangle + \langle 2|\mu_{hf}|2\rangle = 1. \qquad (3.1.30)$$

Incorporating a factor of $(2q_{21}/\hbar)$ into the definition of $\beta_{lf}(t)$, the equations of motion for the variables $S_x$, $S_y$, and $S_z$ are (taking $q_{21} = q_{12}$),

$$\begin{aligned} \dot{S}_x &= -\Delta_y S_y, \\ \dot{S}_y &= \Delta_x S_x + \beta_{lf}(t) S_z, \\ \dot{S}_z &= -\pi\alpha\omega_{21} - \beta_{lf}(t) S_y, \end{aligned} \qquad (3.1.31)$$

where

$$\Delta_y = \omega_{21}\,,$$
$$\Delta_x = \omega_{21}[\,1 - 2\alpha \ln(\omega_b/\omega_c)\,]\,, \tag{3.1.32}$$

and we have introduced the basic coupling parameter $\alpha$, defined by

$$\alpha = \frac{\kappa^2 q_{21}^2}{\hbar}. \tag{3.1.33}$$

The correlation function of the noise $\beta_{lf}(t)$ can be evaluated explicitly as

$$\begin{aligned}
&\langle \beta_{lf}(t)\,\beta_{lf}(0)\rangle \\
&\quad = 2\alpha \int_0^\infty d\omega\; \omega \exp(-\omega/\omega_c)\, \coth\left(\frac{\hbar\omega}{2kT}\right) \cos(\omega t) \\
&\quad = 2\alpha \left\{ \frac{\omega_c^2(1-\omega_c^2 t^2)}{(1+\omega_c^2 t^2)^2} + \frac{1}{t^2} - \left(\frac{\pi kT}{\hbar}\right)^2 \mathrm{cosech}^2\left(\frac{\pi kTt}{\hbar}\right) \right\}.
\end{aligned} \tag{3.1.34}$$

This correlation function exhibits a long-time tail, which, for finite temperatures, takes the form

$$\langle \beta_{lf}(t)\,\beta_{lf}(0)\rangle \simeq -2\alpha \left(\frac{2\pi kT}{\hbar}\right)^2 \exp\left(-\frac{2\pi kTt}{\hbar}\right) \quad \text{as} \quad t \to \infty. \tag{3.1.35}$$

It follows that the noise exhibits a characteristic thermal correlation time $\hbar/2\pi kT$, which, in principle, becomes infinite as $T \to 0$. In fact, the zero temperature limit of the correlation function, for long times, is no longer exponential, but inverse quadratic,

$$\langle \beta_{lf}(t)\,\beta_{lf}(0)\rangle \to -\frac{2\alpha}{t^2} \quad \text{as} \quad t \to \infty. \tag{3.1.36}$$

### 3.1.6 Higher order terms in the cumulant expansion

In fact, Eqs.(3.1.31) are not quite in their final form. As we show in Appendix A, higher order terms in the cumulant expansion lead to a correction of the inhomogeneous term in the equation for $\dot{S}_z$; in particular, we make the replacement

$$\begin{aligned}
-\pi\alpha\omega_{21} \;&\to\; -\pi\alpha\omega_{21} \\
&\quad \times \left\{ 1 - \frac{q_{21}^2}{\hbar} P \int_0^\infty d\omega \kappa_{hf}(\omega)^2 \omega \left[ \frac{1}{(\omega-\omega_{21})^2} + \frac{1}{(\omega+\omega_{21})^2} \right] \right\} \\
&= -\pi\alpha\omega_{21} \left[ 1 - \frac{2\kappa^2 q_{21}^2}{\hbar} \ln(\omega_b/\omega_c) \right] \\
&\equiv -\pi\alpha\Delta_z.
\end{aligned} \tag{3.1.37}$$

The inclusion of this correction is consistent with the order of the frequency correction terms already appearing in (3.1.31). We have left the working to an appendix so as to not unnecessarily complicate the equations leading up to (3.1.31).

## 3.2 Methods of Solution

### 3.2.1 Lowest order perturbation theory

It is worthwhile to examine the results one obtains by using the cumulant expansion method to average over the *entire* bath, that is, over $\beta(t)$, rather than merely $\beta_{hf}(t)$. To first order in the expansion parameter, one finds

$$\begin{aligned}
\langle \dot{S}_x \rangle &= -\omega_{21} \langle S_y \rangle, \\
\langle \dot{S}_y \rangle &= (\omega_{21} + \delta) \langle S_x \rangle - \alpha\pi\omega_{21} \coth\left(\frac{\hbar\omega_{21}}{2kT}\right) \langle S_y \rangle, \\
\langle \dot{S}_z \rangle &= -\alpha\pi\omega_{21} - \alpha\pi\omega_{21} \coth\left(\frac{\hbar\omega_{21}}{2kT}\right) \langle S_z \rangle,
\end{aligned} \tag{3.2.1}$$

where

$$\delta = -\alpha P \int_0^\infty d\omega\, \omega \exp(-\omega/\omega_b) \coth\left(\frac{\hbar\omega}{2kT}\right) \left(\frac{1}{\omega - \omega_{21}} - \frac{1}{\omega + \omega_{21}}\right) \tag{3.2.2}$$

This is the standard lowest-order perturbation theory result. Since the expansion parameter is proportional to the correlation time of the noise and this becomes, in principle, infinite at zero temperature, we expect (3.2.1) to be an adequate description only for extremely weak coupling, especially at low temperatures. The limitations of this approach will be demonstrated in Section 3.2.3.

It is possible, of course, to follow the working of Appendix A and extend the expansion to higher orders in the expansion parameter. However, for non-zero temperatures in particular, the additional terms quickly become intractable and it is very difficult to obtain analytic results. In the previous section, in which the average was only being taken over the high frequency component of the noise, $\beta_{hf}(t)$, most of these additional terms could be ignored as they only described corrections to (damping) terms that had already been neglected because $\kappa_{hf}(\omega_{21})^2 \simeq 0$. In addition, temperature was not a significant

factor as $\hbar\omega_b \gg kT$. This demonstrates in part the advantage in dividing the bath into high and low frequency components.

### 3.2.2 Decorrelation approximation

The quantity of most interest is, of course, $\langle S_x(t)\rangle$, where now $\langle\ \rangle$ denotes the average over $\beta_{lf}(t)$. In the undamped limit, $\langle S_x(t)\rangle$ displays coherent oscillations between $-1$ and $+1$, that is, between the left and right wells. By solving firstly for $S_y(t)$ and $S_z(t)$, and substituting the result for $S_y(t)$ into the equation of motion for $S_x(t)$, we can reduce our analysis to a single stochastic integro-differential equation of the form

$$\begin{aligned}\dot{S}_x(t) = &-\Delta_y\int_0^t dt'\left\{\Delta_x\cos[\int_{t'}^t ds\beta_{lf}(s)]S_x(t') - \alpha\pi\Delta_z\sin[\int_{t'}^t ds\beta_{lf}(s)]\right\}\\ &-\Delta_y\left\{\cos[\int_0^t ds\beta_{lf}(s)]S_y(0) + \sin[\int_0^t ds\beta_{lf}(s)]S_z(0)\right\}.\end{aligned} \tag{3.2.3}$$

On averaging this equation over the noise $\beta_{lf}(t)$, and noting that $\beta_{lf}(t)$ is a Gaussian random variable, and hence that

$$\langle\sin[\int_{t'}^t ds\beta_{lf}(s)]\rangle = 0, \tag{3.2.4}$$

we derive

$$\begin{aligned}\langle\dot{S}_x(t)\rangle = &-\Delta_x\Delta_y\int_0^t dt'\langle\cos[\int_{t'}^t ds\beta_{lf}(s)]S_x(t')\rangle\\ &-\Delta_y\left\{\langle\cos[\int_0^t ds\beta_{lf}(s)]S_y(0)\rangle + \langle\sin[\int_0^t ds\beta_{lf}(s)]S_z(0)\rangle\right\}.\end{aligned} \tag{3.2.5}$$

This equation is not straightforward to solve, particularly as $\beta_{lf}(s)$ is not a white noise. This precludes a strictly legitimate decorrelation of the products appearing in (3.2.5).

If, however, we do make such a decorrelation, we are able to make a connection with previous results, in particular, with the so-called "noninteracting-blip" approximation (Leggett *et al*, 1987). Making a decorrelation approximation, and setting $\langle S_y(0)\rangle = \langle S_z(0)\rangle = 0$, we find

$$\begin{aligned}\langle\dot{S}_x(t)\rangle &= -\Delta_x\Delta_y\int_0^t dt'\langle\cos[\int_{t'}^t ds\beta_{lf}(s)]\rangle\langle S_x(t')\rangle\\ &= -\Delta_x\Delta_y\int_0^t dt'\ \exp\left[-\frac{1}{2}\int_{t'}^t\int_{t'}^t dsds'\langle\beta_{lf}(s)\beta_{lf}(s')\rangle\right]\ \langle S_x(t')\rangle,\end{aligned} \tag{3.2.6}$$

which, using the explicit form for $\langle \beta_{lf}(s)\beta_{lf}(s')\rangle$, becomes

$$\langle \dot{S}_x(t)\rangle = -\Delta_x\Delta_y \int_0^t dt' \times \exp\left[-2\alpha \int_0^\infty d\omega\, e^{-\omega/\omega_c} \coth\left(\frac{\hbar\omega}{2kT}\right) \frac{1-\cos[\omega(t-t')]}{\omega}\right] \langle S_x(t')\rangle . \tag{3.2.7}$$

The region of most interest for the observation of (macroscopic) quantum coherence is that of weak damping or weak coupling to the environment, which corresponds to $\alpha$ being very small (i.e. $\alpha \ll 1$). For small $\alpha$, we can write

$$\begin{aligned}\Delta_x\Delta_y &\simeq \omega_{21}^2 \exp\left[-\alpha \ln\left(\frac{\omega_b^2}{\omega_c^2}\right)\right] \\ &= \omega_{21}^2 \left(\frac{\omega_c}{\omega_b}\right)^{2\alpha}\end{aligned} \tag{3.2.8}$$

The equation (3.2.7) can be solved formally by Laplace transform. Taking $\langle S_x(0)\rangle = 1$, the Laplace transform solution can be written

$$\langle S_x(\lambda)\rangle = \frac{1}{\lambda + f(\lambda)}\,, \tag{3.2.9}$$

where $f(\lambda)$ is the Laplace transform of

$$f(t) \simeq \omega_{21}^2 \left(\frac{\omega_c}{\omega_b}\right)^{2\alpha} \exp\left[-2\alpha \int_0^\infty d\omega\, e^{-\omega/\omega_c} \coth\left(\frac{\hbar\omega}{2kT}\right) \frac{1-\cos(\omega t)}{\omega}\right]. \tag{3.2.10}$$

**Comparison with the noninteracting-blip approximation**

The noninteracting-blip approximation relies on essentially the same decorrelation assumption made above; that is, memory effects generated by the system-environment interaction can be regarded as negligible. The approximation yields a result (Leggett *et al*, 1987) (for ohmic dissipation, as we are considering) of the form (3.2.9), with

$$\begin{aligned}f(t) =& \Delta^2 \cos\left[2\alpha \int_0^\infty d\omega\, e^{-\omega/\omega_c} \frac{\sin(\omega t)}{\omega}\right] \\ &\times \exp\left[-2\alpha \int_0^\infty d\omega\, e^{-\omega/\omega_c} \coth\left(\frac{\hbar\omega}{2kT}\right) \frac{1-\cos(\omega t)}{\omega}\right].\end{aligned} \tag{3.2.11}$$

The argument of the cosine factor varies between 0 and $\alpha\pi$ at $t = 0$ and $t = \infty$ respectively. Hence, for $\alpha \ll 1$ (to which we restrict our approach), this factor is essentially constant and equal to one. Leggett *et al* (1987) do not give an explicit expression for the renormalized frequency $\Delta$, but refer to the work of Dorsey *et al* (1986), who perform the

reduction of a double-well system to an equivalent two-state system using instanton techniques. To leading order in $\alpha \rightarrow 0$, they obtain, for a quartic double-well potential (in the WKB limit), the expression

$$\Delta = \left(\frac{\omega_c}{\omega_b}\right)^{\alpha} e^{-0.24\alpha}\omega_{21}. \qquad (3.2.12)$$

Hence, for small $\alpha$, there is close agreement between the expressions (3.2.10) and (3.2.11). The exponential factor that appears in (3.2.12) is related to the detailed shape of the quartic potential considered by Dorsey *et al* (1986), but, in general, this factor is close to unity (Weiss *et al*, 1987b, have considered potential wells with quadratic forms, and reach the same conclusion for small $\alpha$). This is evidently related to the assumption that we have made in neglecting the frequency shift terms in (3.1.24-26) involving $\Delta_{k1}$ and $\Delta_{k2}$ with $k \geq 3$.

The integral appearing in (3.2.10) can be evaluated explicitly, and $f(t)$ rewritten as

$$f(t) = \omega_{21}^2 \left(\frac{\omega_c}{\omega_b}\right)^{2\alpha} \exp\left\{-\alpha \ln\left[1+\omega_c^2 t^2\right] - 2\alpha \ln\left[\frac{\hbar}{\pi kTt}\sinh\left(\frac{\pi kTt}{\hbar}\right)\right]\right\} \qquad (3.2.13)$$

We are interested in the dynamics of the system for times $t \gg \omega_c^{-1}$. We note that for such times, $f(t)$ is indeed independent of the arbitrary cutoff frequency $\omega_c$, as required.

We shall not consider for now the precise form of the solutions for $\langle S_x(t)\rangle$ obtained using the decorrelation approximation; such solutions have been discussed in depth by (for example) Leggett *et al* (1986). Briefly, for small $\alpha$, and temperatures less than $\sim \hbar\,\Delta_r/k\pi\alpha$, damped oscillations of frequency

$$\Delta_r \simeq \omega_{21}\left(\frac{\omega_{21}}{\omega_b}\right)^{\alpha/(1-\alpha)} \qquad (3.2.14)$$

are predicted.

Finally, we note the work of Aslangul *et al* (1985, 1986), and Dekker (1987), who have derived the noninteracting-blip results from a two-state Hamiltonian using a Heisenberg equation approach, and applying a standard second-order Born approximation. Our approach is therefore related to theirs, but, of course, we begin from a more general Hamiltonian and incorporate a treatment of the reduction to an effective two-level system. Our formulation also produces, as its basic result, a system of (classical) stochastic differential

equations describing the dynamics of the two lowest states. Hence, instead of employing the decorrelation approximation, we may also consider direct stochastic simulation as a means of obtaining a solution.

### 3.2.3 Solution through stochastic simulation

Our previous experience with stochastic simulation of the adjoint equation has involved noise sources exhibiting simple exponential correlation functions (Parkins and Gardiner, 1988). We are faced here by a far more complicated correlation function, given by

$$\langle \beta_{lf}(t)\beta_{lf}(0)\rangle = 2\alpha\left\{\frac{\omega_c^2(1-\omega_c^2t^2)}{(1+\omega_c^2t^2)^2}+\frac{1}{t^2}-\left(\frac{\pi kT}{\hbar}\right)^2 \mathrm{cosech}^2\left(\frac{\pi kTt}{\hbar}\right)\right\}. \quad (3.2.15)$$

Fortunately, however, we are able to formulate a means of producing a sequence of random numbers with the appropriate correlation properties by using Fourier transforms. In particular, we write

$$\beta_{lf}(t) = \int_{-\infty}^{\infty} d\omega\; g(\omega)\sqrt{S(\omega)}e^{i\omega t}, \quad (3.2.16)$$

where

$$S(\omega) = \alpha\omega\exp(-|\omega|/\omega_c)\coth\left(\frac{\hbar\omega}{2kT}\right), \quad (3.2.17)$$

and $g(\omega)$ is a random function, with the properties

$$\langle g(\omega)\rangle = 0 \quad , \quad \langle g(\omega)g(\omega')\rangle = \delta(\omega-\omega'). \quad (3.2.18)$$

The form (3.2.16) can be discretised, with $g(\omega)$ becoming a sequence of Gaussian random numbers $\{g_i\}$ with zero mean and unit variance ($\langle g_i g_j\rangle = \delta_{ij}$). The resulting discrete summation is then computed using a Fast Fourier Transform routine, yielding a sequence of random numbers $\{\beta_{lf}^n\}$ that may be used in simulations of the equations (3.1.31). More precise details are given in Appendix B.

Simulation of the equations (3.1.31) is carried out using a fully-implicit numerical integration scheme. We follow the approach of Smith and Gardiner (1989), and McNeil and Craig (1990), approximating equations (3.1.31) with the discrete form

$$\Delta\mathbf{S}^n = \mathbf{S}^{n+1} - \mathbf{S}^n \quad (3.2.19)$$

$$= \mathbf{A}(\mathbf{S}^{n+\theta_1})\Delta t + \mathbf{B}(\mathbf{S}^{n+\theta_2})\beta_{lf}^n\Delta t\,, \quad (3.2.20)$$

where

$$\mathbf{S} = \begin{pmatrix} S_x \\ S_y \\ S_z \end{pmatrix} \quad , \quad \mathbf{A}(\mathbf{S}) = \begin{pmatrix} -\Delta_y S_y \\ \Delta_x S_x \\ -\alpha\pi\Delta_z \end{pmatrix} \quad , \quad \mathbf{B}(\mathbf{S}) = \begin{pmatrix} 0 \\ S_z \\ -S_y \end{pmatrix} , \qquad (3.2.21)$$

$\Delta t$ is the timestep, and

$$\mathbf{A}(\mathbf{S}^{n+\theta_1}) = \mathbf{A}(\mathbf{S}^n) + \underline{J}_A^n \theta_1 \Delta \mathbf{S}^n \quad , \quad [\underline{J}_A^n]_{ij} = \left[\frac{\partial A_i}{\partial S_j}\right]_{\mathbf{S}=\mathbf{S}^n} , \qquad (3.2.22)$$

$$\mathbf{B}(\mathbf{S}^{n+\theta_2}) = \mathbf{B}(\mathbf{S}^n) + \underline{J}_B^n \theta_2 \Delta \mathbf{S}^n \quad , \quad [\underline{J}_B^n]_{ij} = \left[\frac{\partial B_i}{\partial S_j}\right]_{\mathbf{S}=\mathbf{S}^n} ; \qquad (3.2.23)$$

that is, we linearise about the point $\mathbf{S}^n$. It is straightforward to show that

$$\underline{J}_A^n = \begin{bmatrix} 0 & -\Delta_y & 0 \\ \Delta_x & 0 & 0 \\ 0 & 0 & 0 \end{bmatrix} \quad , \quad \underline{J}_B^n = \begin{bmatrix} 0 & 0 & 0 \\ 0 & 0 & 1 \\ 0 & -1 & 0 \end{bmatrix} \qquad (3.2.24)$$

Substitution of (3.2.22,3) into (3.2.20) leads to the integration scheme

$$\Delta \mathbf{S}^n = [\, 1 - \theta_1 \underline{J}_A^n \Delta t - \theta_2 \underline{J}_B^n \beta_{lf}^n \Delta t]^{-1} \, [\mathbf{A}(\mathbf{S}^n)\Delta t + \mathbf{B}(\mathbf{S}^n)\beta_{lf}^n \Delta t] \, . \qquad (3.2.25)$$

The choice $\theta_{1,2} = 0$ corresponds to the Euler method of integration, but we find this method to be highly unstable for our particular problem. This is related to the fact that the only explicit damping term occurs in the equation for $\dot{S}_z$, and this term is also very small. Hence, we adopt the time-centered choice $\theta_{1,2} = 1/2$, which exhibits much better properties of stability.

**Numerical results**

Our numerical results should in large part be independent of the artificial cutoff frequency $\omega_c$, subject to the constraint $\omega_{21} \ll \omega_c \ll \omega_b$. In Fig.3.2 we demonstrate that this is the case by comparing results as $\omega_c$ is changed by an order of magnitude. This corresponds to a change in the variance of the noise $\langle \beta_{lf}^2 \rangle$ by a factor of 100, which, as shown in Fig.3.2(a,b), substantially increases the noise in a typical trajectory. However, this difference is largely removed once the average is taken over a sufficient number of trajectories, although we do find a small shift in the period exhibited by $\langle S_x(t) \rangle$. This shift is still smaller as $\alpha$ is decreased. The integration timestep used in both cases was $\Delta t = 0.0005$ (units of $\omega_{21}^{-1}$). For $\omega_c/\omega_{21} = 50$ (with corresponding period $2\pi/\omega_c = 0.13\omega_{21}^{-1}$), this is certainly small enough, and indeed a much coarser timestep ($\Delta t = 0.005$) gives virtually identical results. For $\omega_c/\omega_{21} = 500$, a much smaller timestep was not practical for the parameters

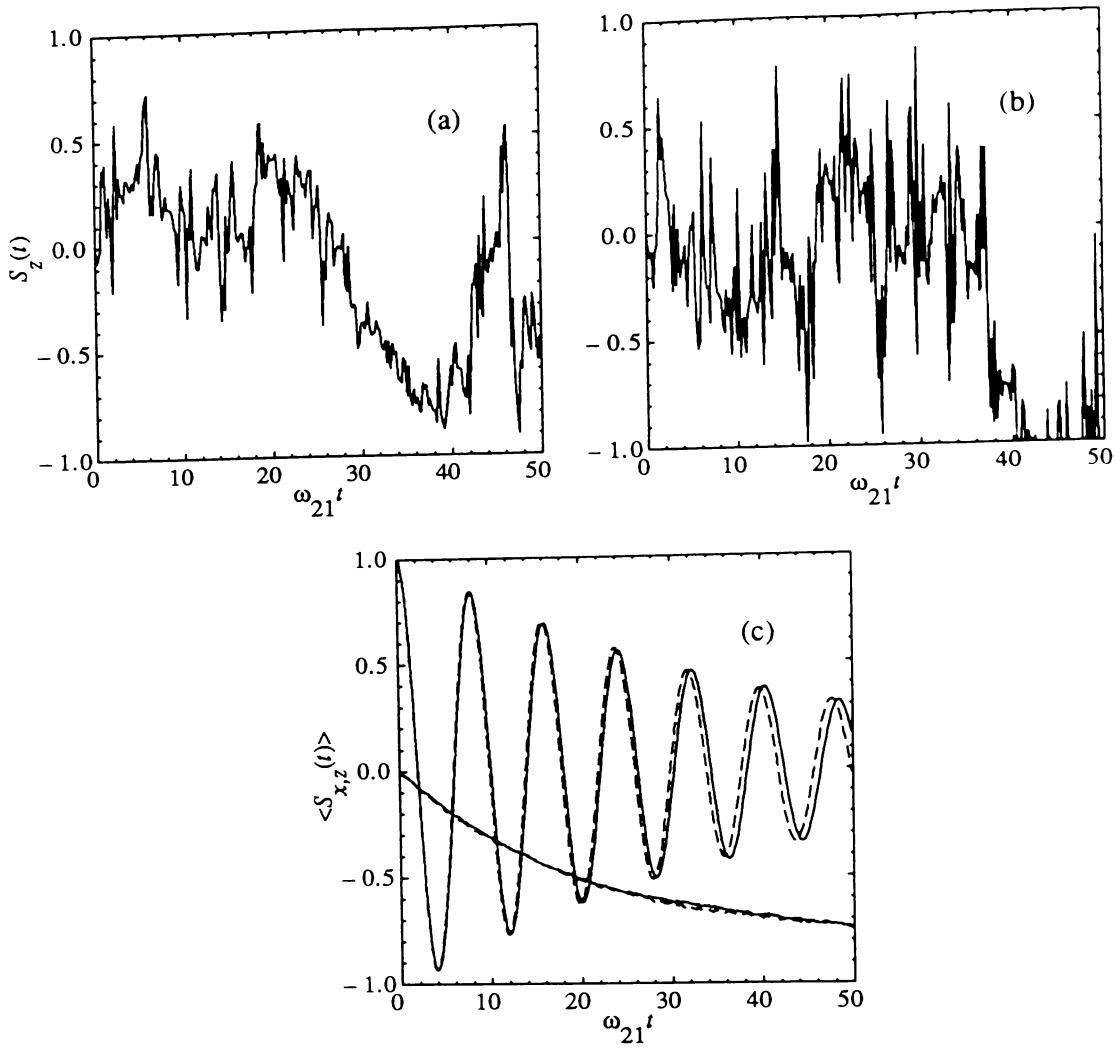


**Fig.3.2** Effect of varying the cutoff frequency $\omega_c$, $\alpha = 0.02$, $T = 0$, $\omega_b = 10^5\omega_{21}$, (a) single trajectory, $S_z(t)$, $\omega_c/\omega_{21} = 50$, (b) single trajectory, $S_z(t)$, $\omega_c/\omega_{21} = 500$, (c) average of 8000 trajectories, $\langle S_{x,z}(t) \rangle$, $\omega_c/\omega_{21} = 50$ (solid line), and $\omega_c/\omega_{21} = 500$ (dashed line).

considered, but $\Delta t = 0.0005$ is still sufficiently small that the simulation procedure should work well. However, because of the large difference in the bandwidths of the noise being simulated, we cannot fully discount the possibility of some of the (small) discrepancy being due to the numerical procedure.

In the remaining calculations we use $\Delta t = 0.0005$, $\omega_c/\omega_{21} = 200$, and $\omega_b/\omega_{21} = 10^5$, and we compute averages from 8000 trajectories.

Our choice of $\omega_b/\omega_{21}$ is somewhat arbitrary, although, in the context of macroscopic quantum coherence in a SQUID, in which one might expect a frequency $\omega_{21} \simeq 10^6 - 10^7 s^{-1}$, the value $\omega_b \simeq 10^{11} - 10^{12} s^{-1}$ corresponds to a wavelength in the millimetre range. In principle, it is quite possible to omit the high frequency averaging

procedure of Section 3, and to simulate $\beta(t)$ rather than simply $\beta_{lf}(t)$, in which case the argument above concerning $\omega_c$ becomes redundant. However, there are practical limitations associated with the Fourier transform method for producing the noise when $\omega_b/\omega_{21}$ is so large, and hence the cumulant expansion average is not only a very nice way of dealing with the high frequency bath oscillators, but it is also quite essential from the point of view of simulation. Of course, for much smaller values of $\omega_b/\omega_{21}$, simulation of $\beta(t)$ becomes a viable option.

In Fig.3.3, we display the results obtained with $\alpha = 0.02$, for varying temperatures of the bath. As the temperature is increased, the oscillations are gradually destroyed, ultimately giving way to purely incoherent relaxation at a temperature given approximately by $\hbar\Delta_r/k\pi\alpha$. Again, in the context of coherent tunnelling in a SQUID, one might envisage a coherent oscillation frequency $\Delta_r \simeq 10^6 - 10^7 s^{-1}$, in which case a quantitative estimate of the crossover temperature (for $\alpha = 0.02$) is $\sim 1\text{mK}$.

Also in Fig.3.3, we compare the simulation results with the results obtained from the decorrelation approximation; that is, from the equations

$$\begin{aligned}
\langle \dot{S}_x(t) \rangle &= -\int_0^t dt'\ f(t-t') \langle S_x(t') \rangle, \\
\langle \dot{S}_y(t) \rangle &= \Delta_x - \int_0^t dt'\ \{\Delta_x\Delta_y + \langle \beta_{lf}(t)\beta_{lf}(t') \rangle\} \langle S_y(t') \rangle, \\
\langle \dot{S}_z(t) \rangle &= -\alpha\pi\Delta_z - \int_0^t dt'\ \cos\left[\sqrt{\Delta_x\Delta_y}(t-t')\right]\ \langle \beta_{lf}(t)\beta_{lf}(t') \rangle\ \langle S_z(t') \rangle,
\end{aligned} \tag{3.2.26}$$

with $f(t)$ given by

$$f(t) = \Delta_x\Delta_y \exp\left\{-\alpha \ln\left[1+\omega_c^2 t^2\right] - 2\alpha \ln\left[\frac{\hbar}{\pi kTt}\sinh\left(\frac{\pi kTt}{\hbar}\right)\right]\right\}, \tag{3.2.27}$$

and with $\Delta_x = \Delta_z = \omega_{21}[1 - 2\alpha\ln(\omega_b/\omega_c)]$ and $\Delta_y = \omega_{21}$. The initial conditions have been chosen as $\langle S_x(0) \rangle = 1$, $\langle S_y(0) \rangle = \langle S_z(0) \rangle = 0$. We solve (3.2.26,27) numerically, using Euler's method and the trapezium rule.

The agreement between the two approaches is generally very good. At the lower temperatures, where the thermal correlation time is very long (e.g. in principle infinite at $T = 0$), there is a slight discrepancy, mainly at long times. As the temperature is increased, however, a comparison of the thermal correlation time with the approximate decay time of the oscillations reveals that we are essentially in a white-noise (Markovian) regime. Hence, we expect the decorrelation approximation to be a very good approximation, and this is indeed what we find, as demonstrated, in particular, by Fig.3.3(c,d).

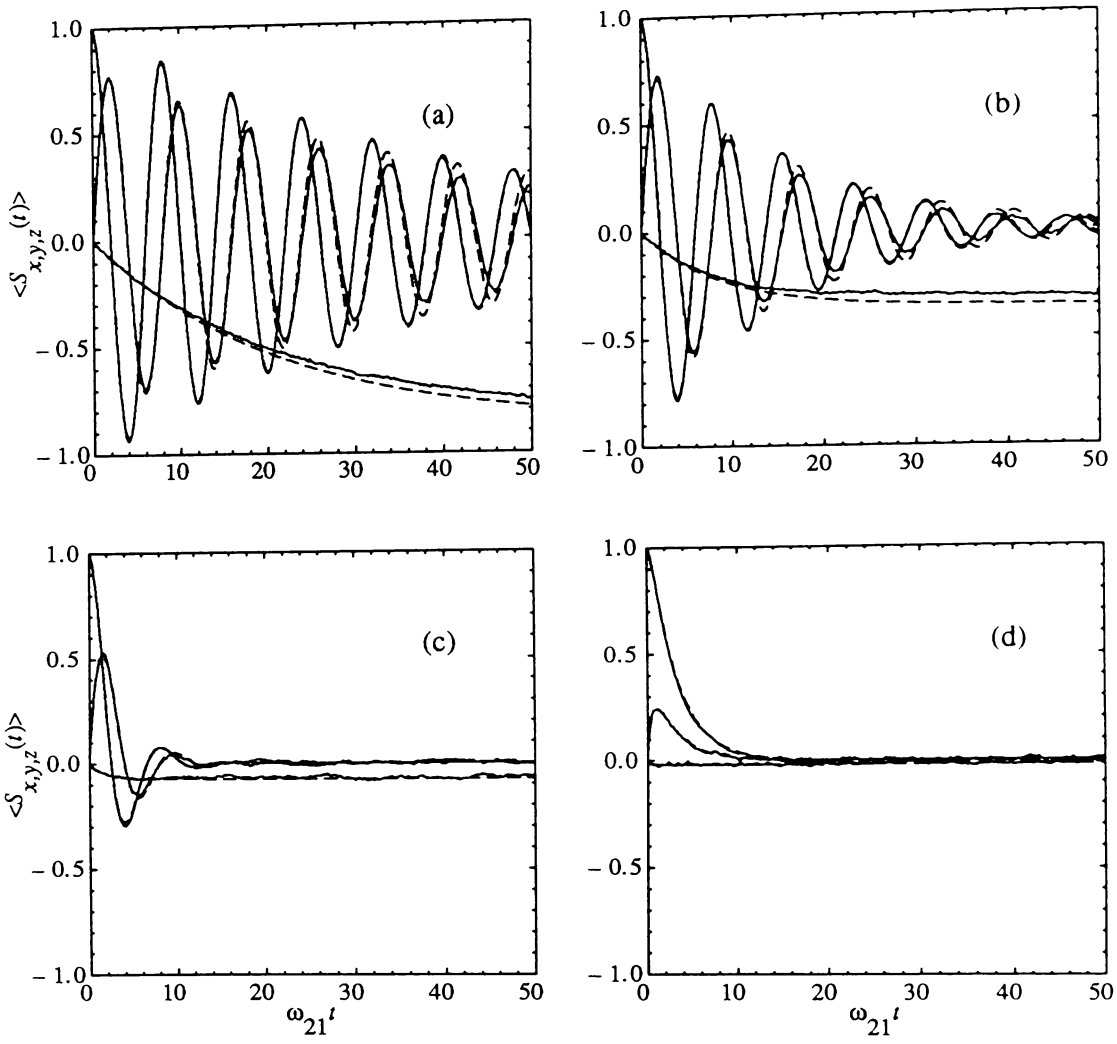


**Fig.3.3** Averages of 8000 trajectories $\langle S_{x,y,z}(t) \rangle$, for $\alpha = 0.02$, $\omega_b = 10^5 \omega_{21}$, (a) $\hbar\omega_{21}/kT = \infty$, (b) $\hbar\omega_{21}/kT = 1$, (c) $\hbar\omega_{21}/kT = 0.2$, (d) $\hbar\omega_{21}/kT = 0.05$, computed from simulation (solid lines) and from the decorrelation approximation (dashed lines).

In contrast, a comparison of simulation results with the lowest order perturbation theory of Section 3.2.1, for $\alpha = 0.02$ and $T = 0$, does not yield good agreement, as shown in Fig.3.4(a). The perturbation theory evidently does not suit this regime of parameter space, and we have to reduce $\alpha$ in order to obtain better agreement. Alternatively, one can increase the temperature, and hence reduce the effective correlation time of the noise (and hence the size of the cumulant expansion parameter). This also leads to improved agreement, as shown in Fig.3.4(b).

**Effect of bias**

Finally, we consider briefly the influence of bias, that is, an applied field giving rise to an *asymmetric* double well potential. In our formulation, this corresponds simply to allowing

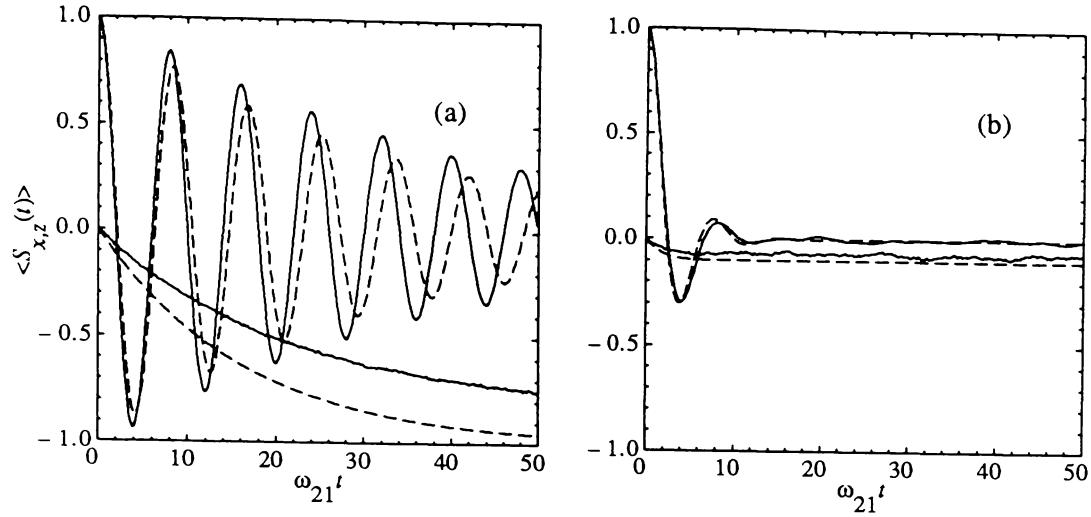


**Fig.3.4** Comparison of simulation (solid lines) with lowest order perturbation theory, Eqs.(3.2.1) (dashed lines), for $\alpha = 0.02$, $\omega_b = 10^5 \omega_{21}$, (a) $\hbar\omega_{21}/kT = \infty$, (b) $\hbar\omega_{21}/kT = 0.2$.

the noise $\beta_{lf}(t)$ a nonzero coherent amplitude. We accommodate this by defining

$$\beta'_{lf}(t) = \beta_{lf}(t) - \epsilon\,, \tag{3.2.28}$$

where $\epsilon = \langle \beta_{lf}(t) \rangle$, and making the appropriate substitution in (3.1.31). The equations we then simulate are

$$\begin{aligned} \dot{S}_x &= -\Delta_y S_y, \\ \dot{S}_y &= \Delta_x S_x + \epsilon S_z + \beta'_{lf}(t) S_z, \\ \dot{S}_z &= -\alpha\pi\Delta_z - \epsilon S_y - \beta'_{lf}(t) S_y. \end{aligned} \tag{3.2.29}$$

In Fig.3.5 we display simulation results for $\alpha = 0.01$, with bias $\epsilon = 0.25\omega_{21}$, and for two different temperatures. The results for zero bias are given for comparison. With non-zero bias, oscillations appear in $\langle S_z(t) \rangle$, and $\langle S_x(t) \rangle$ approaches a non-zero steady state value. With an increase in temperature however, the effect of the bias is less significant, as thermal noise starts to dominate, and $\langle S_x(t) \rangle$ again approaches zero in the long time limit.

We note that in the presence of a non-zero bias, the decorrelation approximation (and the noninteracting-blip approximation) predicts localisation of the quantum "particle" ($\langle S_x(\infty) \rangle = \pm 1$) at zero temperature. For weak damping ($\alpha \ll 1$) and small bias (relative to the tunnel splitting), this is not the correct behaviour (Leggett *et al*,1987, Weiss *et al*,

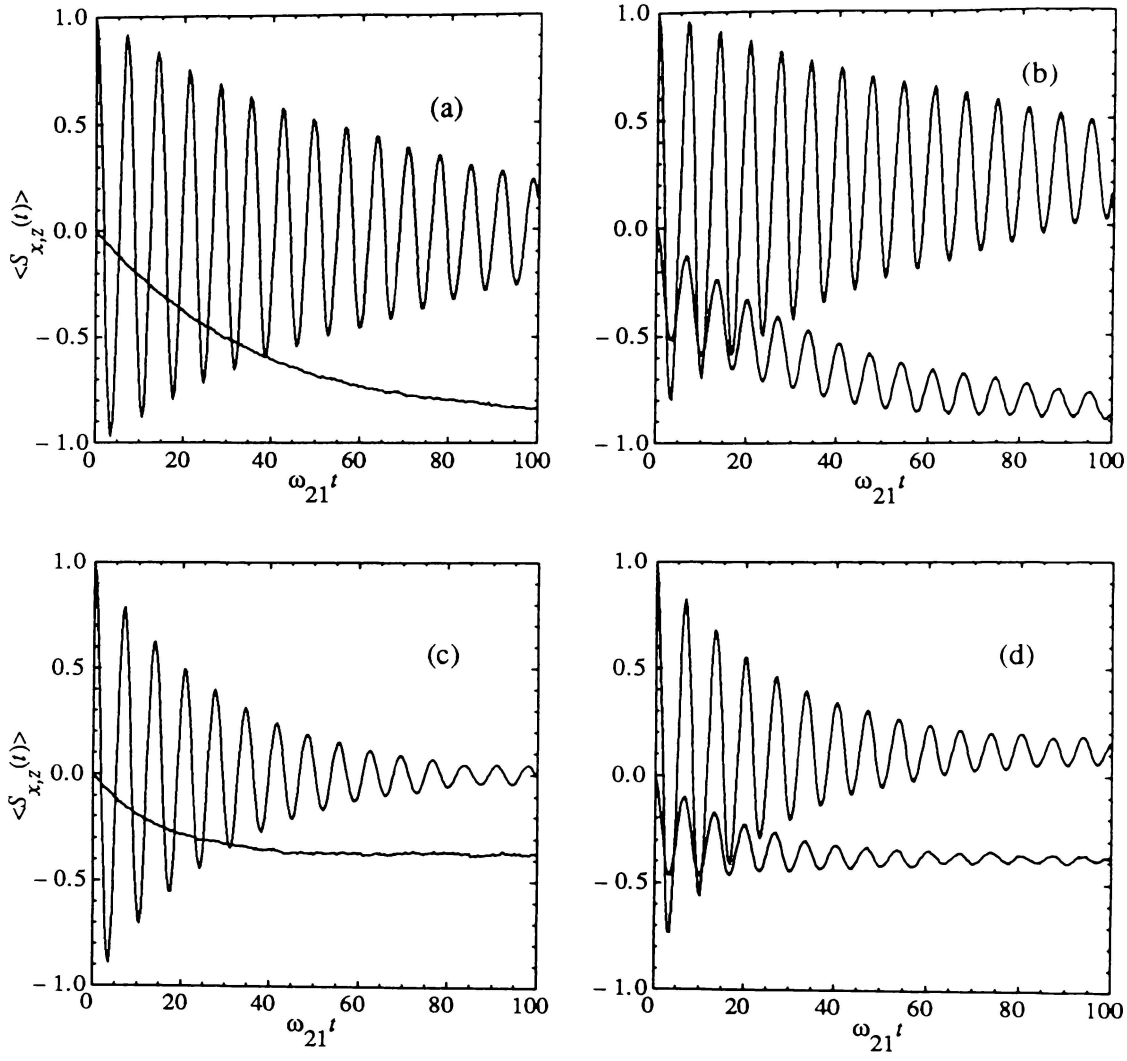


**Fig.3.5** Averages of 8000 trajectories $\langle S_{x,z}(t) \rangle$, $\alpha = 0.01$, $\omega_b = 10^5$, for $\hbar\omega_{21}/kT = \infty$ with (a) $\epsilon = 0$, (b) $\epsilon = 0.25\omega_{21}$, and for $\hbar\omega_{21}/kT = 1$ with (c) $\epsilon = 0$, (d) $\epsilon = 0.25\omega_{21}$.

1987a), but modifications to the theory can be made (Weiss *et al*, 1987a) which lead to

$$\langle S_x(\infty) \rangle_{T=0} = \frac{\epsilon}{(\Delta_r^2 + \epsilon^2)^{1/2}}. \qquad (3.2.30)$$

This formula gives good agreement with the simulation result displayed in Fig.3.5(b).

# 4. Two-Level Atoms in Broad Bandwidth Squeezed Light

The successful generation of squeezed light in the laboratory has opened the door to a variety of possible applications. In the field of atomic spectroscopy, it was recognised by Gardiner (1986) that the phase-sensitive field correlations that characterise a squeezed field can significantly alter the dynamics of an atomic dipole. The decay of one atomic polarisation quadrature can, in principle, be inhibited, leading to subnatural spectral linewidths. With the addition of a coherent driving field, the familiar Mollow triplet is found to exhibit a striking dependence on the relative phases of the squeezed vacuum field and the coherent field (Carmichael, Lane, and Walls, 1987a,b). In particular, the central peak of the triplet can possess either a subnatural or supernatural linewidth depending on the relative phases.

Following on from these investigations, a variety of other problems in atomic spectroscopy have been reexamined with squeezed light incorporated into the formulation. Atomic absorption spectra (Ritsch and Zoller, 1987, 1988a,b, An *et al*, 1988), energy level shifts (Milburn, 1986), and the laser (Marte and Walls, 1988, Marte *et al*, 1988a,b) are but a few examples. The majority of these studies, including the original works of Gardiner and Carmichael *et al*, have assumed broad bandwidth squeezing, thus allowing a formulation in terms of squeezed white noise (Gardiner and Collett, 1985). The advantage of this formulation is that it enables the use of standard master equation methods to solve for the system dynamics.

Since much of this thesis deals with squeezed light spectroscopy, it is necessary that we background the original results in this field, and review the techniques and approximations with which they were derived, so that later work can be clearly contrasted with the original findings. This is the primary objective of this chapter, but, in addition, we shall describe in some detail one recent application of squeezing (Parkins and Gardiner, 1989a) that arises in the study of photon echoes, and which thus expands the field of squeezed light atomic spectroscopy to include transient optical phenomena.

## 4.1 Squeezed Light: Degenerate Parametric Amplification

The degenerate parametric amplifier is the prototype for all squeezing devices and has, to date, yielded the largest amount of experimentally-observed squeezing (Wu *et al*, 1986, 1987). Theoretical analyses of this device are numerous, so a detailed exposition of its properties is not necessary. However, in view of its fundamental importance to our particular study, a brief description seems appropriate.

The systematic Hamiltonian for the process of degenerate parametric amplification, with a classical pump, can be written as

$$H_{sys} = \hbar\omega_0 a^\dagger a + \frac{1}{2} i\hbar \left[\epsilon_c e^{-i\omega_p t}(a^\dagger)^2 - \epsilon_c^* e^{i\omega_p t} a^2\right], \qquad (4.1.1)$$

where $a$ is the annihilation operator for the cavity mode of frequency $\omega_0$, $\omega_p$ is the frequency of the pump beam, and $\epsilon_c$ is the pump driving strength. It is assumed that the cavity and pump are tuned so that $\omega_p = 2\omega_0$. Downconversion from frequency $2\omega_0$ to frequency $\omega_0$ occurs through the action of a nonlinear optical medium placed inside the cavity. The cavity itself is treated as a one-sided cavity; that is, it possesses one near-perfect mirror and one output mirror of finite transmissivity (at the frequency $\omega_0$). This configuration yields the optimum amount of squeezing in the output field (i.e. in the field emerging from the cavity), the properties of which have been computed by Collett and Gardiner (1984) using an input-output formulation (see also Collett *et al*, 1987). The correlation functions of the output field quadrature phase operators $E_1(t)$ and $E_2(t)$ (suitably defined with respect to the phase of the driving field) take the form

$$\langle E_1(t)E_1(t')\rangle = -\frac{|\epsilon_c|\gamma_c}{\frac{1}{2}\gamma_c + |\epsilon_c|} e^{-(\frac{1}{2}\gamma_c + |\epsilon_c|)|t-t'|} + \delta(t-t'), \qquad (4.1.2)$$

$$\langle E_2(t)E_2(t')\rangle = \frac{|\epsilon_c|\gamma_c}{\frac{1}{2}\gamma_c - |\epsilon_c|} e^{-(\frac{1}{2}\gamma_c - |\epsilon_c|)|t-t'|} + \delta(t-t'), \qquad (4.1.3)$$

where $\gamma_c$ is the loss rate through the output mirror. The exponential terms in the expressions give the effect of squeezing, while the $\delta$-correlated terms represent vacuum fluctuations. Strong squeezing occurs in one quadrature, over a finite bandwidth, as we approach threshold, i.e. as $|\epsilon_c| \to \frac{1}{2}\gamma_c$. Fluctuations in the unsqueezed quadrature naturally become very large in the same limit. It is worthwhile noting that the form of these correlation functions has been confirmed in the experiments of Wu *et al* (1986, 1987).

Two distinct timescales characterise the correlation functions, corresponding to the two decay rates $(\frac{1}{2}\gamma_c + \epsilon_c)$ and $(\frac{1}{2}\gamma_c - \epsilon_c)$. In the case that both of these decay rates are very large (and hence the bandwidth of squeezing is very large), the exponentials may be approximated by $\delta$-functions to yield the squeezed white noise limit

$$\begin{aligned}\langle E_1(t)E_1(t')\rangle &= \left[-\frac{2|\epsilon_c|\gamma_c}{(\frac{1}{2}\gamma_c + |\epsilon_c|)^2} + 1\right]\delta(t-t') \\ &\equiv (2N - 2M + 1)\delta(t-t'), \qquad (4.1.4)\\ \langle E_2(t)E_2(t')\rangle &= \left[\frac{2|\epsilon_c|\gamma_c}{(\frac{1}{2}\gamma_c - |\epsilon_c|)^2} + 1\right]\delta(t-t') \\ &\equiv (2N + 2M + 1)\delta(t-t'), \qquad (4.1.5)\end{aligned}$$

where we have introduced the "standard" squeezing parameters $N$ and $M$ defined by

$$N = \frac{1}{2}|\epsilon_c|\gamma_c\left[\frac{1}{(\frac{1}{2}\gamma_c - |\epsilon_c|)^2} - \frac{1}{(\frac{1}{2}\gamma_c + |\epsilon_c|)^2}\right], \qquad (4.1.6)$$

$$M = \frac{1}{2}|\epsilon_c|\gamma_c\left[\frac{1}{(\frac{1}{2}\gamma_c - |\epsilon_c|)^2} + \frac{1}{(\frac{1}{2}\gamma_c + |\epsilon_c|)^2}\right]. \qquad (4.1.7)$$

With these definitions, $N$ and $M$ satisfy

$$M^2 = N(N+1), \qquad (4.1.8)$$

corresponding to a minimum uncertainty state, or ideal squeezing. Once again, the experiments of Wu *et al* support such a description of squeezing produced in degenerate parametric amplification below threshold.

## 4.2 Master Equation for a Two-Level Atom in a Squeezed Vacuum

Although obviously an idealisation, the two-level model of an atom is fundamental to the field of quantum optics, and provides the logical starting point for the study of the interaction of squeezed light with atomic systems. If the bandwidth of squeezing is sufficiently broad compared to the linewidth of the atomic transition, then the squeezed vacuum can be expected to appear as squeezed white noise to the atom, and the atom-field interaction should be adequately described by a suitable master equation. The adjoint equation approach of Chapters 2 and 3 provides a route to such a master equation once the system and

input have been suitably prescribed. This particular approach has been described in detail by Gardiner *et al* (1987).

### 4.2.1 Derivation of the master equation

The two-level atomic system can be described by the familiar spin operators $S^{\pm}$ and $S_z$, such that

$$H_{sys} = \frac{1}{2}\hbar\omega_a S_z, \tag{4.2.1}$$

and

$$X = \sqrt{\frac{\hbar}{\omega_a}}(S^+ + S^-), \tag{4.2.2}$$

where $\omega_a$ is the atomic transition frequency. The initial quantum state of the bath is, of course, taken to be squeezed, which we qualify by choosing the input correlation functions as

$$\langle a^\dagger(\omega,t_0)a(\omega',t_0)\rangle = N\,\delta(\omega-\omega'), \tag{4.2.3}$$

$$\langle a(\omega,t_0)a(\omega',t_0)\rangle = M\,\delta(2\omega_0-\omega-\omega'), \tag{4.2.4}$$

with $N$ and $M$ as defined in (4.1.6,7). Following the notation of the earlier chapters, we find the function $F(\omega_a,t)$ to be

$$\begin{aligned} F(\omega_a,t) &= 2\int_0^\infty d\tau\, e^{-i\omega_a\tau}\langle\beta(t)\beta(t-\tau)\rangle \\ &= \pi\hbar\omega_a\kappa(\omega_a)^2\left(N+\frac{1}{2}\right) \\ &\quad - i\hbar P\int_0^\infty d\omega\,\omega\kappa(\omega)^2\left(N+\frac{1}{2}\right)\left(\frac{1}{\omega_a-\omega}+\frac{1}{\omega_a+\omega}\right) \\ &\quad - \pi\hbar\sqrt{(2\omega_0-\omega_a)\omega_a}\,\kappa(\omega_a)\kappa(2\omega_0-\omega_a)Me^{-i2\omega_0 t} \\ &\quad - i\hbar P\int_0^{2\omega_0} d\omega\,\sqrt{(2\omega_0-\omega)\omega}\,\kappa(\omega)\kappa(2\omega_0-\omega) \\ &\quad\times\left[\frac{Me^{-i2\omega_0 t}}{2\omega_0-\omega-\omega_a}-\frac{M^*e^{i2\omega_0 t}}{2\omega_0-\omega+\omega_a}\right]. \end{aligned} \tag{4.2.5}$$

The principal value integrals represent frequency shifts, which have been discussed in detail elsewhere (Milburn, 1986, Ford and O'Connell, 1987), and which we shall assume to be negligible. Furthermore, we assume that the coupling function $\kappa(\omega)$ is independent of frequency over the bandwidth of interest, and can be set equal to its value at $\omega = \omega_a$.

In the rotating-wave approximation (assuming that $\omega_0 \simeq \omega_a$), the master equation then follows in the form

$$\begin{aligned}\dot{\rho} = & -i\frac{1}{2}\omega_a[S_z, \rho] \\ & + \frac{\gamma_a}{2}(N+1)(2S^-\rho S^+ - S^+S^-\rho - \rho S^+S^-) \\ & + \frac{\gamma_a}{2}N(2S^+\rho S^- - S^-S^+\rho - \rho S^-S^+) \\ & - \gamma_a M e^{-i2\omega_0 t}S^+\rho S^+ - \gamma_a M^* e^{i2\omega_0 t}S^-\rho S^-,\end{aligned} \tag{4.2.6}$$

where we have defined $\gamma_a = \pi\kappa(\omega_a)^2$ to be the natural atomic linewidth.

A major assumption implicit in the above master equation is that the atom interacts only with squeezed modes of the radiation field. This is perhaps the most significant practical problem facing experimentalists, but we shall not delve into this aspect at this stage - this is the purpose of Chapter 6. However, it should be noted that the majority of investigations undertaken so far have been based upon this assumption.

### 4.2.2 Reflections of the input squeezed field

Once the master equation has been formulated, it is a straightforward matter to compute one-time and two-time averages of the atomic variables, and to therefore describe the behaviour of the atom. However, a further consideration in the computation of output spectra from systems that are subjected to squeezed light is the effect of reflections of the input squeezed light. One must allow not only for the nonzero power spectrum of the squeezed vacuum, but also for correlations (or interferences) that are established between the reflected squeezed light and the light radiated from the atom. These correlations can substantially affect the total fluorescence spectrum.

Once again, this aspect of squeezed light spectroscopy has been dealt with in detail by Gardiner *et al* (1987). The input-output formulation specifies that the output electric field, $E_{out}(t) = -\dot{A}_{out}(t)$, is related to the input and atomic fields via the simple relationship

$$E_{out}(t) = E_{in}(t) + \sqrt{\gamma_a}\,\dot{X}(t) \tag{4.2.7}$$

(for simplicity we have set $2c \rightarrow 1$ in the definitions of Chapter 2, with $\kappa(x) = \sqrt{\gamma_a}\delta(x)$). Using the commutation relations derived in Section 2.2.2, the correlation function for the

output field can be expressed in the form

$$\langle E_{out}(t)\,E_{out}(t')\rangle = \langle E_{in}(t)\,E_{in}(t')\rangle + \frac{\gamma_a}{2}\langle[\dot{X}(t),\dot{X}(t')]_+\rangle + \frac{1}{2}\sqrt{\gamma_a}\left\{\langle[\dot{X}(t),E_{in}(t')]_+\rangle + \langle[\dot{X}(t'),E_{in}(t)]_+\rangle\right\}. \quad (4.2.8)$$

The last two correlation functions can be computed using the general formula (for an arbitrary system operator $Y(t)$)

$$\langle[Y(t),E_{in}(t')]_+\rangle = \frac{i}{\hbar}\sqrt{\gamma_a}\int_{-\infty}^{t} ds\,\langle[E_{in}(t'),E_{in}(s)]_+\rangle\,\langle[X(s),Y(t)]\rangle, \quad (4.2.9)$$

which Gardiner *et al* (1987) have shown to be valid to the same order as that to which the master equation is valid.

The added complication of reflections could, in principle, be avoided with the introduction of a small "window" of unsqueezed vacuum modes through which to observe the fluorescence (small because our formulation assumes that the atom sees only squeezed vacuum modes), and, indeed, this has been the configuration most commonly assumed in the variety of applications considered since Gardiner's original work on spontaneous emission. In practice, this may well be a reasonable assumption, since experiments with squeezed light are likely to employ cavity configurations, in which the squeezed light is incident on the atom through the cavity modes. The reflections could then be avoided by simply observing the fluorescent light out the side of the cavity (provided the cavity is not a microcavity, as we shall consider in Chapter 6, in which case the light must be observed through the cavity modes).

### 4.2.3 Spontaneous emission and the inhibition of atomic phase decays

The master equation (4.2.6) describes spontaneous emission of a two-level atom in a squeezed vacuum, given that the atom interacts only with squeezed modes. Under conditions of resonance ($\omega_0 = \omega_a$), and making a choice of phase such that $M$ is real, we derive equations of motion for the averaged atomic variables. Defining atomic polarisation quadratures $S_x$ and $S_y$ by

$$S^{\pm} = \frac{1}{2}(S_x \pm iS_y), \quad (4.2.10)$$

and working in a frame rotating at frequency $\omega_0$, these equations can be written in the

form

$$\begin{aligned}
\langle \dot{S}_x \rangle &= -\gamma_a \left( N + M + \frac{1}{2} \right) \langle S_x \rangle \equiv -\gamma_x \langle S_x \rangle, \\
\langle \dot{S}_y \rangle &= -\gamma_a \left( N - M + \frac{1}{2} \right) \langle S_y \rangle \equiv -\gamma_y \langle S_y \rangle, \\
\langle \dot{S}_z \rangle &= -\gamma_a - \gamma_a (2N + 1) \langle S_z \rangle \equiv -\gamma_a - \gamma_z \langle S_z \rangle,
\end{aligned} \tag{4.2.11}$$

from which it is clear that the two polarisation quadratures are damped at different rates, given by $\gamma_x$ and $\gamma_y$. These rates are proportional, respectively, to the variances of the maximally unsqueezed and maximally squeezed quadrature phases of the incoming squeezed vacuum field. Hence, while the quadrature $\langle S_x \rangle$ decays rapidly to its steady state value of zero, the decay of the $\langle S_y \rangle$ quadrature is inhibited. In fact, the decay rate $\gamma_y$ can, in principle, approach zero, as evidenced by the large squeezing limit

$$N - M + \frac{1}{2} \rightarrow \frac{1}{8N} \quad \text{as} \quad N \rightarrow \infty. \tag{4.2.12}$$

In other terms, one says that the projection of the original orientation of the Bloch vector (with components $\langle S_x \rangle$, $\langle S_y \rangle$, and $\langle S_z \rangle$) on the direction of the low-noise quadrature phase is preserved, while the remaining components decay rapidly to their stationary values.

Of course, one must keep in mind that the limit $N \rightarrow \infty$ corresponds to the approach to threshold in the parametric amplifier providing the squeezed light. In this limit, the time constant $(\frac{1}{2}\gamma_c - |\epsilon_c|)^{-1}$, which characterises the unsqueezed quadrature phase, approaches infinity, thereby invalidating the squeezed white noise formulation. It is possible to estimate more precisely the range of validity of the white noise theory, and, as one might expect, it is found (Gardiner *et al*, 1987) that the approximation requires that the largest correlation time of the squeezed field, $(\frac{1}{2}\gamma_c - |\epsilon_c|)^{-1}$, be much smaller than the smallest characteristic time constant of the atom, $\gamma_x^{-1}$.

Parkins and Gardiner (1988), using simulation methods based on the adjoint equation, and Ritsch and Zoller (1988a,b), using eigenfunction methods based on the same equation, have gone beyond the white noise limit to examine the effect of finite bandwidth squeezing on the inhibition of atomic phase decays. They have found that the basic effects predicted by the white noise theory still exist (although reduced in magnitude) for bandwidths of squeezing only a few times greater than the atomic linewidth. As $(\frac{1}{2}\gamma_c - \epsilon_c)$ is reduced further, however, inhibition of the decay ultimately ceases to occur, and, hence, for a given value of $\gamma_c$, there is a limit to the reduction in the decay rate of a particular polarisation quadrature.

With the above limitations understood, we now return to the squeezed white noise formulation of spontaneous emission to consider the observable consequences of the inhibited phase decay. In particular, we consider the spectrum of fluorescent light. The stationary correlation functions of the atom can be computed with the aid of the quantum regression theorem, after which the correlation function of the total output field incorporating reflections can be found using (4.2.8,9). The fluorescence spectrum is given by the Fourier transform of the correlation function $\langle E_{out}^{(-)}(t)\, E_{out}^{(+)}(t')\rangle$, which is found to be

$$\langle E_{out}^{(-)}(t)\, E_{out}^{(+)}(t')\rangle = \hbar\,\omega_0\, e^{i\omega_0(t-t')} \times \left\{ N\delta(t-t') + \frac{\gamma_a}{2}\frac{M}{2N+1}\left[e^{-\gamma_y|t-t'|} - e^{-\gamma_x|t-t'|}\right]\right\}. \qquad (4.2.13)$$

The spectrum thus consists of a flat background arising from the squeezed vacuum field, plus two Lorentzians centered at the transition frequency. One of these is a negative peak of width $\gamma_x$, and consequently will be very broad, whereas the other is a positive peak of width $\gamma_y$, possessing a subnatural linewidth. The extent of the narrowing of this linewidth is, of course, directly proportional to the degree of squeezing in the input light, and thus provides a direct measurement of squeezing.

### 4.2.4 Resonance fluorescence

Resonance fluorescence from a two-level atom is a classic problem in quantum optics, and has been well studied theoretically (Mollow, 1969, Carmichael and Walls, 1976, Cresser *et al*, 1982) and experimentally (for references see Cresser *et al*, 1982). For strong driving fields, the spectrum of fluorescent light exhibits three peaks, which are often referred to as the Mollow triplet. A study of the effect of squeezed light on resonance fluorescence represents a natural progression from the work on spontaneous emission, and such a study was first carried out in detail by Carmichael *et al* (1987a,b).

Using our formulation, a coherent driving field is accommodated by giving the input field a nonzero mean value, i.e. $\langle E_{in}(t)\rangle \neq 0$. The master equation that results can be written

$$\dot{\rho} = -i\frac{1}{2}\Omega_0\left[e^{-i\omega_0 t + i\phi_0}S^{+} + e^{i\omega_0 t - i\phi_0}S^{-}, \rho\right] + (\dot{\rho})_{spon}, \qquad (4.2.14)$$

where $(\dot{\rho})_{spon}$ is given by (4.2.6), and $\Omega_0$ (proportional to $\sqrt{\gamma_a}\ |\langle E_{in}\rangle|$) and $\phi_0$ are the Rabi frequency and phase respectively of the coherent driving field. The frequency of the

coherent field is assumed to be resonant with the central squeezing frequency. From an experimental point of view this is a natural assumption, since one would envisage using a single laser to provide the pump for both the parametric amplifier (after frequency doubling, as is actually done in the experiments of Wu *et al*, 1987) and for the atoms. In this way, one also has control of the relative phase between the coherent and squeezed fields, which, as we shall see, plays a vital role in the atomic dynamics.

From (4.2.14), we derive the Bloch equations for the atom. For simplicity, we ignore detuning between the atomic and driving field frequencies. In a frame rotating at frequency $\omega_0$, and choosing polarisation quadratures that are in-phase and out-of-phase with the coherent field,

$$\begin{aligned} \langle S_x \rangle &= \langle S^+ \rangle e^{-i\omega_0 t + i\phi_0} + \langle S^- \rangle e^{i\omega_0 t - i\phi_0}, \\ \langle S_y \rangle &= -i \left( \langle S^+ \rangle e^{-i\omega_0 t + i\phi_0} - \langle S^- \rangle e^{i\omega_0 t - i\phi_0} \right), \end{aligned} \tag{4.2.15}$$

we find

$$\begin{aligned} \langle \dot{S}_x \rangle &= -\gamma_a \left[ N + M\cos(2\phi_0) + \frac{1}{2} \right] \langle S_x \rangle - \gamma_a M \sin(2\phi_0) \langle S_y \rangle, \\ \langle \dot{S}_y \rangle &= -\gamma_a \left[ N - M\cos(2\phi_0) + \frac{1}{2} \right] \langle S_y \rangle - \gamma_a M \sin(2\phi_0) \langle S_x \rangle - \Omega_0 \langle S_z \rangle, \\ \langle \dot{S}_z \rangle &= -\gamma_a - \gamma_a (2N+1) \langle S_z \rangle + \Omega_0 \langle S_y \rangle, \end{aligned} \tag{4.2.16}$$

where, again, we have adopted a choice of phase for the squeezed vacuum such that $M$ is real and positive. This does not lead to a loss of generality, as the dynamics are sensitive only to the relative phase between the coherent field and the squeezed field, which can obviously be varied through $\phi_0$.

This dependence of the dynamics on phase represents a striking departure from traditional studies of resonance fluorescence, and leads, of course, to some interesting new phenomena. These phenomena are described in detail by Carmichael *et al* (1987a,b). Perhaps the most significant of these, and certainly the one in which we shall be most interested, is the phase dependence exhibited by the fluorescence spectrum under strong driving field conditions (such that Rabi splitting occurs). Two notable limiting cases arise for the choices of phase $\phi_0 = 0$ and $\phi_0 = \pi/2$, for which the equations (4.2.16) take the

form

$$\begin{aligned}
\langle \dot{S}_x \rangle &= -\gamma_a \left( N \pm M + \frac{1}{2} \right) \langle S_x \rangle \equiv -\gamma_x \langle S_x \rangle , \\
\langle \dot{S}_y \rangle &= -\gamma_a \left( N \mp M + \frac{1}{2} \right) \langle S_y \rangle - \Omega_0 \langle S_z \rangle \equiv -\gamma_y \langle S_y \rangle - \Omega_0 \langle S_z \rangle , \\
\langle \dot{S}_z \rangle &= -\gamma_a - \gamma_a (2N + 1) \langle S_z \rangle + \Omega_0 \langle S_y \rangle \equiv -\gamma_a - \gamma_z \langle S_z \rangle + \Omega_0 \langle S_y \rangle .
\end{aligned} \tag{4.2.17}$$

The fluorescence spectrum that one then computes, after use of the quantum regression theorem to determine atomic correlation functions (for simplicity, we omit reflections, although these have been dealt with in the context of resonance fluorescence in a squeezed vacuum by Lane, 1988), exhibits three peaks at the frequencies $\omega = \omega_0$ and $\omega = \omega_0 \pm \Omega_0$, with linewidths determined by the decay rates $\gamma_x$, $\gamma_y$, and $\gamma_z$. In particular, the halfwidth of the central peak is given by $\gamma_x$, while that of the two Rabi sidebands is given by the averaged value $(\gamma_y + \gamma_z)/2$. If we again consider the large squeezing limit, $N \gg 1$, we find, for $\phi_0 = 0$,

$$\gamma_x \simeq 2N\gamma_a \quad , \quad \frac{1}{2}(\gamma_y + \gamma_z) \simeq N\gamma_a \ , \tag{4.2.18}$$

while for $\phi_0 = \pi/2$,

$$\gamma_x \simeq \frac{\gamma_a}{8N} \quad , \quad \frac{1}{2}(\gamma_y + \gamma_z) \simeq 2N\gamma_a \ . \tag{4.2.19}$$

Hence, the Mollow triplet is now sensitively dependent on the phase of the coherent field, with the width of the central peak varying between subnatural and supernatural values. Noticeably, however, the sidebands only exhibit broadening compared to their normal (unsqueezed) vacuum profile. To illustrate these features, we plot the fluorescence spectrum in Fig.4.1, for the two limiting choices of phase.

We conclude this section on resonance fluorescence by re-emphasising that the results presented thus far have been derived in the squeezed white noise limit. In fact, the conditions for the validity of the white noise theory are more stringent for strongly driven resonance fluorescence than for spontaneous emission, since the squeezed noise must appear $\delta$-correlated even on the timescale of the Rabi oscillations. In frequency space, this corresponds to a squeezing bandwidth that is much broader than the Rabi splitting appearing in the fluorescence triplet.

In the case of simple spontaneous emission, it is apparent that a relaxation of the broad bandwidth squeezing assumption only leads to a degradation of the squeezing effects. However, it is not so clear as to what occurs as this condition is relaxed when dealing

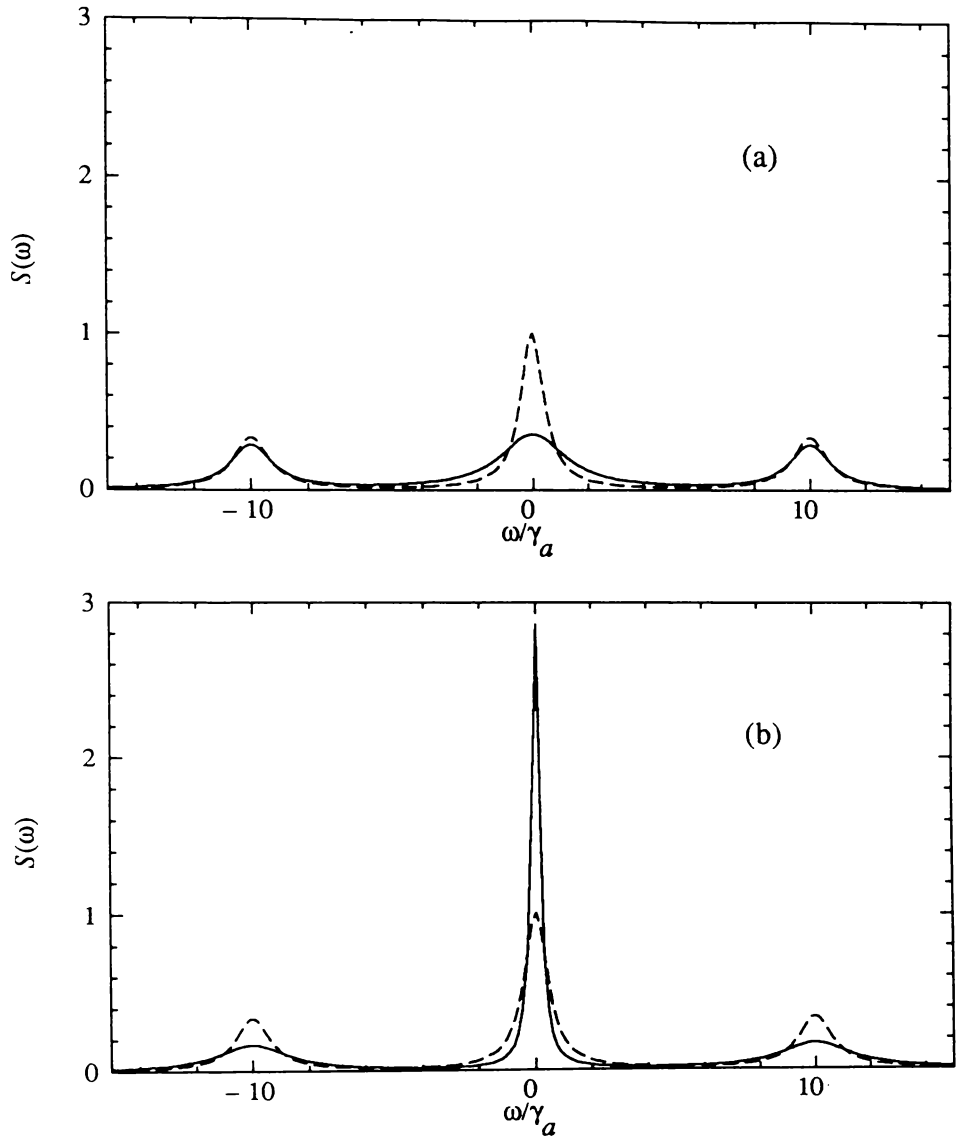


**Fig.4.1** Incoherent fluorescence spectrum for $N = 0.3$, with (a) $\phi_0 = 0$, and (b) $\phi_0 = \pi/2$. The dashed curve is the ordinary fluorescence spectrum ($N = 0$).

with resonance fluorescence, and, in particular, when the Rabi splitting starts to exceed the bandwidth of squeezing. This is the subject of the next chapter.

## 4.3 Photon Echoes with Coherent and Squeezed Pulses of Light

The application of coherent optical pulses to samples of atoms and molecules can lead to a variety of interesting coherent transient phenomena. These phenomena make possible a close examination of the various relaxation processes at work within a sample. The photon echo is an example of such a phenomenon that also has a relatively long history in the field of quantum optics (Allen and Eberly, 1975). In the simplest case, a photon echo is produced by a sequence of two coherent pulses incident upon a system of inhomogeneously-broadened atoms. The first pulse serves to induce in the sample a macroscopic polarisation. Inhomogeneous broadening then causes dephasing of the individual dipole moments throughout the sample in a process that manifests itself as a rapid dissipation of the macroscopic dipole moment. Hence, the collection of atoms as a whole may cease radiating in only a fraction of the natural lifetime of the atomic transition involved.

If a second coherent pulse (of suitable intensity) is applied at a time $\tau$ after the first pulse, the dephasing process may, however, be reversed. The system then rephases at the same rate at which it dephased, resulting in a momentary reformation of the macroscopic dipole moment, at a time $2\tau$ after the first excitation pulse. The pulse of light that is subsequently emitted is known as a photon echo.

Of course, throughout the sequence of events described above, each individual dipole moment is incoherently damped by spontaneous emission at the rate $\gamma_a/2$. By varying the pulse delay time, it is therefore possible to change the amplitude of the echo, and so in fact obtain a measure of $\gamma_a$. This application of the photon echo phenomenon leads us to examine theoretically the effects one might expect when squeezed light, in the form of (long) pulses, is added to such an experiment.

As we have seen, squeezed light incident upon a two-level atom gives rise to two different transverse relaxation times that are inversely proportional to the variances of the two quadrature phases of the incident field. In a strongly squeezed field the variance in one quadrature phase approaches zero. The corresponding atomic relaxation time may, therefore, become extremely long.

In this section, we shall show how the difference in transverse decay rates produced in this way, during exposure to a pulse of squeezed light, can in principle lead to a

new form of photon echo which does not rely on a second coherent pulse to initiate the rephasing process. We shall also examine how conventional two-coherent-pulse echoes are modified with the addition of a squeezed pulse. Before commencing our analysis, however, it is worthwhile clarifying our use of the term squeezed "pulse". Although pulses of squeezed light have been produced experimentally (Slusher *et al*, 1987), the duration of these pulses is probably too short for the application that we have in mind, and, hence, our pulses correspond more realistically to a continuous wave source of squeezed light that is switched on and off suddenly.

### 4.3.1 Bloch equations with detuning

The system we shall consider is a spatially-degenerate two-level system, in which cooperative effects are neglected, as is common in analyses of photon echoes. A typical sequence of events that we might wish to examine is depicted in Fig.4.2.

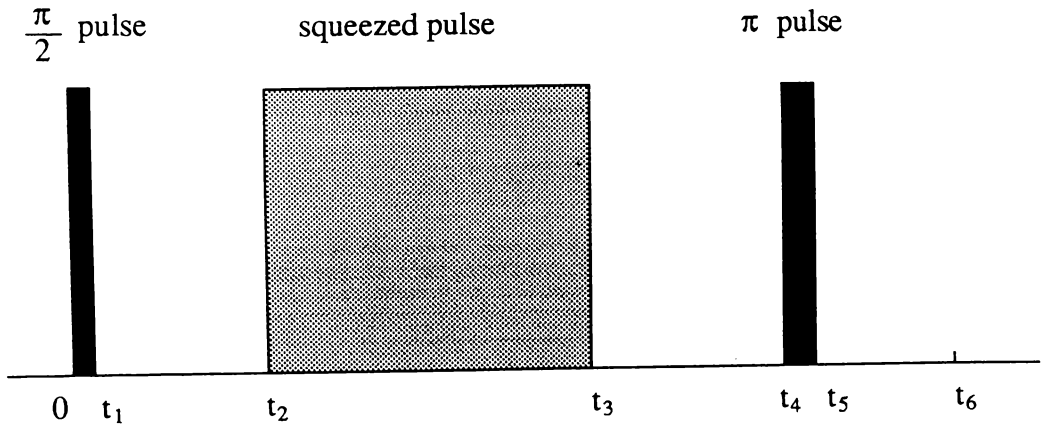


**Fig.4.2** Typical sequence of events in time (not to scale).

Our description of the system is, as usual, made through the Bloch equations. We shall assume that the coherent pulses are of sufficiently short duration for damping to be neglected during the time that they act on the system. The equations for the intervals $0 \rightarrow t_1$ and $t_4 \rightarrow t_5$ are thus

$$\begin{aligned} \langle \dot{S}_x \rangle &= -\Delta_a \langle S_y \rangle, \\ \langle \dot{S}_y \rangle &= \Delta_a \langle S_x \rangle - \Omega_0 \langle S_z \rangle, \\ \langle \dot{S}_z \rangle &= \Omega_0 \langle S_y \rangle, \end{aligned} \tag{4.3.1}$$

where $\Delta_a = \omega_a - \omega_0$ is the detuning. As with previous analyses of two-pulse photon echoes, we shall assume that the first and second coherent pulses are, respectively, '$\pi/2$' and '$\pi$' pulses; that is $(\Omega_0 t_1) = \pi/2$, and $[\Omega_0 (t_5 - t_4)] = \pi$.

For the periods between and after the coherent pulses, the Bloch equations can be written in the general form

$$\begin{aligned} \langle \dot{S}_x \rangle &= -\gamma_x \langle S_x \rangle - \Delta_a \langle S_y \rangle, \\ \langle \dot{S}_y \rangle &= -\gamma_y \langle S_y \rangle + \Delta_a \langle S_x \rangle, \\ \langle \dot{S}_z \rangle &= -\gamma_z \langle S_z \rangle - \gamma_a, \end{aligned} \tag{4.3.2}$$

where, for the intervals $t_1 \rightarrow t_2$ and $t_3 \rightarrow t_4$,

$$\gamma_x = \gamma_y = \frac{\gamma_a}{2} \quad , \quad \gamma_z = \gamma_a \ , \tag{4.3.3}$$

while, for the interval $t_2 \rightarrow t_3$, during which the system is exposed to an ideal broad bandwidth squeezed light source,

$$\gamma_x = \gamma_a \left( N + M + \frac{1}{2} \right) \quad , \quad \gamma_y = \gamma_a \left( N - M + \frac{1}{2} \right) \quad , \quad \gamma_z = \gamma_a (2N + 1), \tag{4.3.4}$$

where $M = [N(N+1)]^{1/2}$. We note finally that all other possible sources of decay (such as collision-induced decay) have been neglected in the above.

### 4.3.2 Solutions

The equations can be solved sequentially to give the components of the Bloch vector at any time $t$. The polarisation $P(t)$ induced in the sample is obtained by summing the contributions from individual dipole moments, weighted by some appropriate detuning distribution. In a continuum limit, we define

$$P(t) = \frac{\mathcal{N} d_a}{2\delta\sqrt{\pi}} \int_{-\infty}^{+\infty} d\Delta_a \, [\langle S_x(t, \Delta_a) \rangle + i \langle S_y(t, \Delta_a) \rangle] e^{i\omega_0 t} \exp(-\Delta_a^2 / \delta^2) \ + \ c.c., \tag{4.3.5}$$

where $d_a$ is the transition dipole moment, and $\mathcal{N}$ is the atomic density. The particular weight function used is a Gaussian of 'width' $\delta$, which simply corresponds to a Doppler-broadened medium. We do not exclude the possibility, however, of a distribution of detunings due to some other effect. For instance, photon echo experiments were first carried out using ruby, in which inhomogeneous crystal strains give rise to such a distribution.

We note further that $\langle S_x(t,\Delta_a)\rangle$ is an odd function of $\Delta_a$, while $\langle S_y(t,\Delta_a)\rangle$ is an even function, and hence

$$P(t) \propto \int_0^\infty d\Delta_a \, \langle S_y(t,\Delta_a)\rangle \exp(-\Delta_a^2/\delta^2) \equiv y(t). \qquad (4.3.6)$$

Solution of the Bloch equations in the presence of squeezing yields eigenvalues of the form

$$\lambda_{1,2} = -\gamma_a \left[ N + \frac{1}{2} \mp \sqrt{M^2 - (\Delta_a/\gamma_a)^2} \right]. \qquad (4.3.7)$$

From these it is apparent that squeezing offers the possibility of both inhibiting the phase decay and preventing the precession of the Bloch vector about the z-axis. With $N$ large and for $t_{32}$ ($t_{ij} = t_i - t_j$) sufficiently long, those atoms with detunings of the order of, or greater than $\gamma_a M$ will experience rapid damping of their $\langle S_y\rangle$ components. Only those atoms with sufficiently small detunings will maintain a significant $\langle S_y\rangle$ component. The $\langle S_x\rangle$ components of all atoms will decay quickly to zero.

**(a) $\frac{\pi}{2}$ pulse / squeezed pulse**

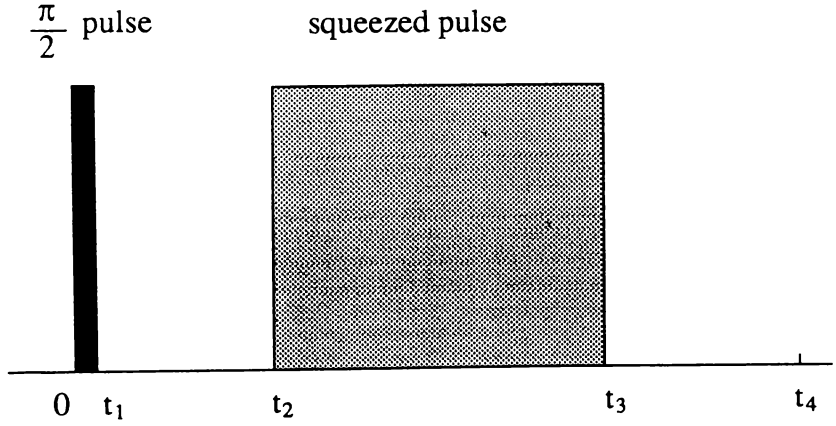


**Fig.4.3** Sequence of events for part (a).

The first situation that we shall examine is depicted in Fig.4.3, and corresponds to a single $\pi/2$ coherent pulse, followed after a time $t_{21}$ by a much longer squeezed pulse. We find that even in this case, without any subsequent $\pi$ coherent pulse, an echo may be produced. The approximate position of this echo can be found by considering those atoms with detunings that satisfy $\Delta_a \ll \Omega_0, 2\gamma_a M$, in which case one derives

$$\begin{aligned} \langle S_y(t_4)\rangle \simeq -\frac{1}{2} \{ &\cos[\Delta_a(t_{43} - t_{21})] + \cos[\Delta_a(t_{43} + t_{21})]\} \\ &\times \exp[-\frac{\gamma_a}{2}(t_{43} + t_{21}) - \gamma_y t_{32}]. \end{aligned} \qquad (4.3.8)$$

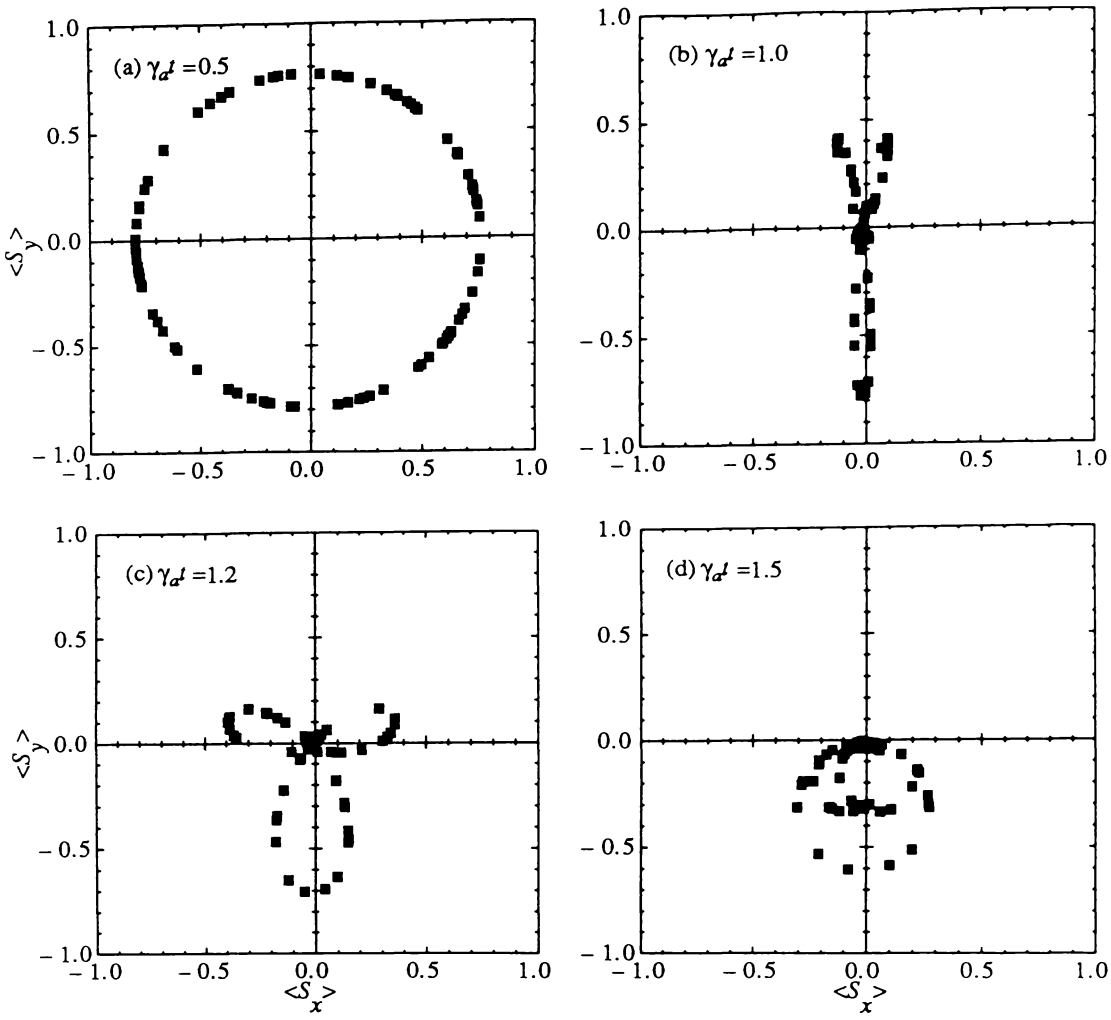


**Fig.4.4** Time development of the $\langle S_x \rangle$ and $\langle S_y \rangle$ components corresponding to 100 (Gaussian) random detunings, for a single $\pi/2$ coherent pulse, followed after a time $\gamma_a t_{21} = 0.5$ by a squeezed pulse of duration $\gamma_a t_{32} = 0.5$, with $N = 10$ (98% squeezing). The time shown is taken from the conclusion of the $\pi/2$ pulse.

Hence, evaluation of $P(t)$ will yield a peak at $t_{43} \simeq t_{21}$, that is, an echo can be expected at a time $t_{43}$ after the squeezed pulse approximately equal to the time $t_{21}$ between the coherent and squeezed pulses.

The mechanism for producing such an echo is quite different from that of a normal echo, and is illustrated in the sequence of diagrams shown in Fig.4.4. These diagrams show the time development of the $\langle S_x \rangle$ and $\langle S_y \rangle$ components corresponding to 100 random detunings $\Delta_a$ chosen from a Gaussian distribution with standard deviation $10\,\gamma_a$. The first $\pi/2$ pulse serves to prepare the atoms in a state with $\langle S_y \rangle \simeq -1$. The vectors are then allowed to precess freely for the interval $\gamma_a t_{21} = 0.5$, during which time the individual vectors dephase, distributing themselves equally about the origin, as in Fig.4.4(a). The

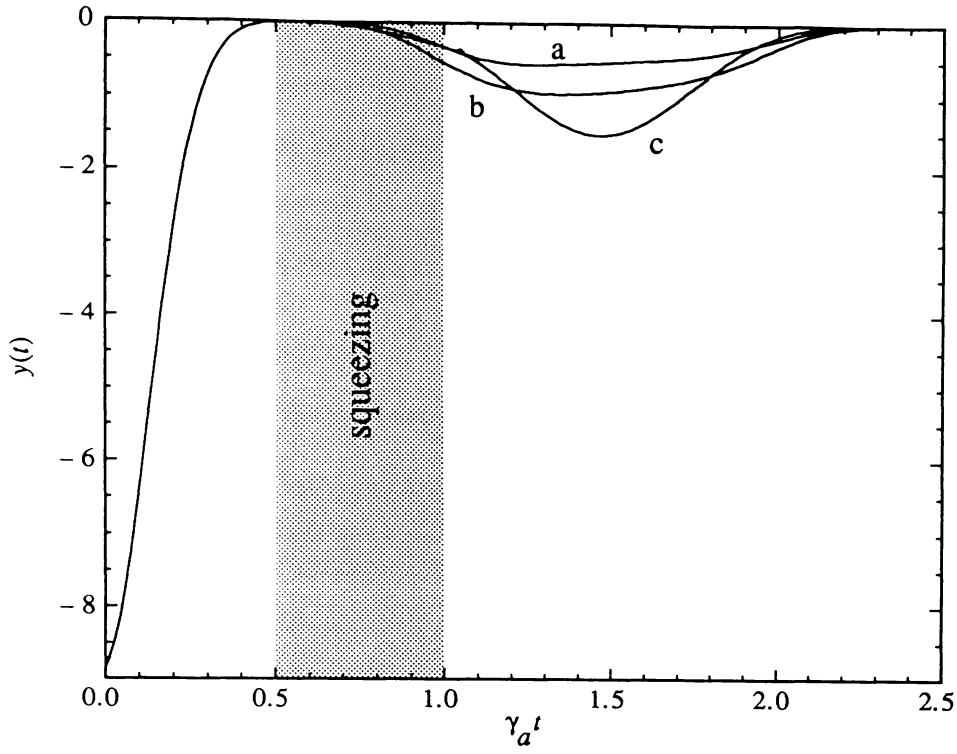


**Fig.4.5** $y(t)$ vs. $\gamma_a t$ for $\chi/\gamma_a = 200, \delta/\gamma_a = 10$, with (a) $N = 0.5$ (73% squeezing), (b) $N = 2$ (90%), (c) $N = 10$ (98%). Time is measured from the conclusion of the $\pi/2$ pulse.

application of squeezing (N=10) rapidly aligns the vectors along the line $\langle S_x \rangle = 0$ , with vectors corresponding to larger detunings quickly attenuated to zero (Fig.4.4(b)). Once the squeezing is removed after a time $\gamma_a t_{32} = 0.5$, a separation of vectors with different rates of precession is revealed (Fig.4.4(c)), and a partial realignment occurs, roughly at the time predicted by the approximate analysis above (Fig.4.4(d)).

The addition of squeezing complicates the exact solution for $\langle S_y(t) \rangle$, and the integration over detunings to evaluate $y(t)$ is best carried out numerically. In Fig.4.5 we plot $y(t)$ for the pulse sequence used in Fig.4.4, but with varying amounts of squeezing. We note that the effects we are describing will work best when the squeezing is able to inhibit the decay and precession of a large proportion of the inhomogeneously-broadened sample. An increase in $\delta/\gamma_a$ could in theory be counteracted with an increase in the squeezing parameter $N$.

The change in amplitude, width, and position of the echo with varying $N$ indicates the possible use of this technique in measuring the squeezing in the incident field. Alternatively, one might vary the time $t_{32}$ during which squeezing is present to obtain a

measure of $\gamma_y$ (and hence $N$).

**(b) $\frac{\pi}{2}$ pulse / squeezed pulse / $\pi$ pulse**

In the case that a second coherent pulse is added to the above analysis, as depicted in Fig.4.2 (which corresponds most directly to the usual photon echo experiments), we find that a sequence of echoes may be generated, depending on pulse delays. Again, one may show with an approximate analysis (for $\Delta_a \ll \gamma_a M$)

$$\langle S_y(t_6)\rangle \simeq \frac{1}{2}\{\cos[\Delta_a(t_{65} - t_{43} + t_{21})] + \cos[\Delta_a(t_{65} - t_{43} - t_{21})]\} \times \exp\left[-\frac{\gamma_a}{2}(t_{65} + t_{43} + t_{21}) - \gamma_y t_{32}\right]. \quad (4.3.9)$$

If $t_{43} > t_{21}$, an echo may occur before the $\pi$ pulse, which is then followed by two further echoes at times $t_{65} \simeq t_{43} - t_{21}$ and $t_{65} \simeq t_{43} + t_{21}$. A conventional echo generated by the two coherent pulses alone would occur at $t_{65} \simeq t_{21} + t_{32} + t_{43}$. Hence, compared to the normal echo, the echoes produced with this sequence of pulses arrive earlier, as shown in Fig.4.6.

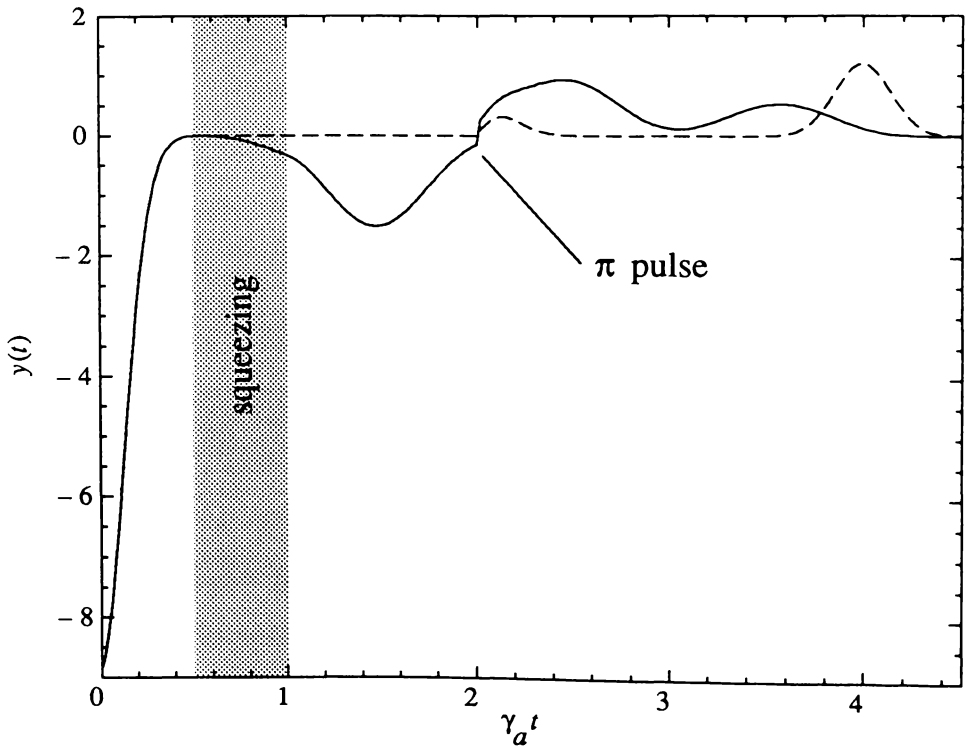


**Fig.4.6** $y(t)$ vs. $\gamma_a t$ for the sequence of pulses depicted in Fig.4.2, with $N = 0$ (dashed curve) and $N = 10$ (98% squeezing) (solid curve). Here $\chi/\gamma_a = 200$ and $\delta/\gamma_a = 10$.

A variety of possible combinations of pulses exist. For example, one can consider

placing the squeezed pulse after the $\pi$ pulse, in which case

$$\langle S_y(t_6)\rangle \simeq \frac{1}{2}\{\cos[\Delta_a(t_{65}+t_{43}-t_{21})]+\cos[\Delta(t_{65}-t_{43}+t_{21})]\} \times \exp\left[-\frac{\gamma_a}{2}(t_{65}+t_{43}+t_{21})-\gamma_y t_{54}\right], \quad (4.3.10)$$

where now $t_{21}$ is the time between coherent pulses, $t_{43}$ is the time between the $\pi$ pulse and squeezed pulse, and $t_{65}$ is the time after the squeezed pulse. If $t_{43} < t_{21}$ then a single "delayed" echo may be produced at time $t_{65} \simeq t_{21} - t_{43}$, while if $t_{43} > t_{21}$ a "delayed" echo may be generated in addition to the conventional echo.

**(c) $\frac{\pi}{2}$ pulse / squeezed pulse / squeezed pulse**

Similar sequences of echoes may be produced if we replace the $\pi$ pulse with a second squeezed pulse, as depicted in Fig.4.7. For instance, if the separation between the $\pi/2$ pulse and first squeezed pulse is $t_{21}$, and the separation between squeezed pulses is $t_{43}$, with $t_{43} > t_{21}$, then three echoes may be produced, the first between the squeezed pulses, and the other two at times $\sim (t_{43}-t_{21})$ and $\sim (t_{43}+t_{21})$ after the second squeezed pulse. Such a case is illustrated in Fig.4.8.

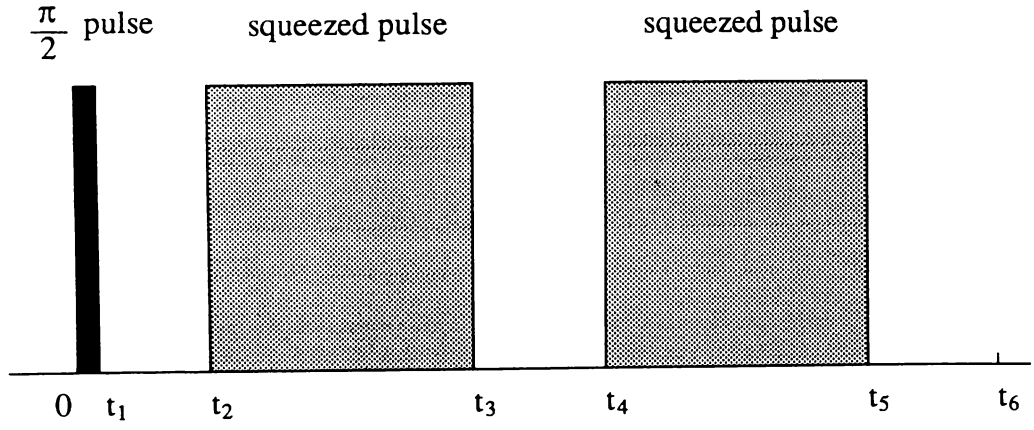


**Fig.4.7** Sequence of events for part (c).

**(d) A few experimental considerations**

The echoes produced with squeezing present are generally smaller and much broader than normal echoes, but they should still be detectable with current technology. We have concentrated here mainly on the occurrence and position of echoes, but further information is clearly to be found in the actual shapes of the echoes. For maximum effect one would prefer only a small amount of inhomogeneous broadening, which suggests (in the case of gases) velocity compression (cooling) techniques. If the squeezing is to be incident over

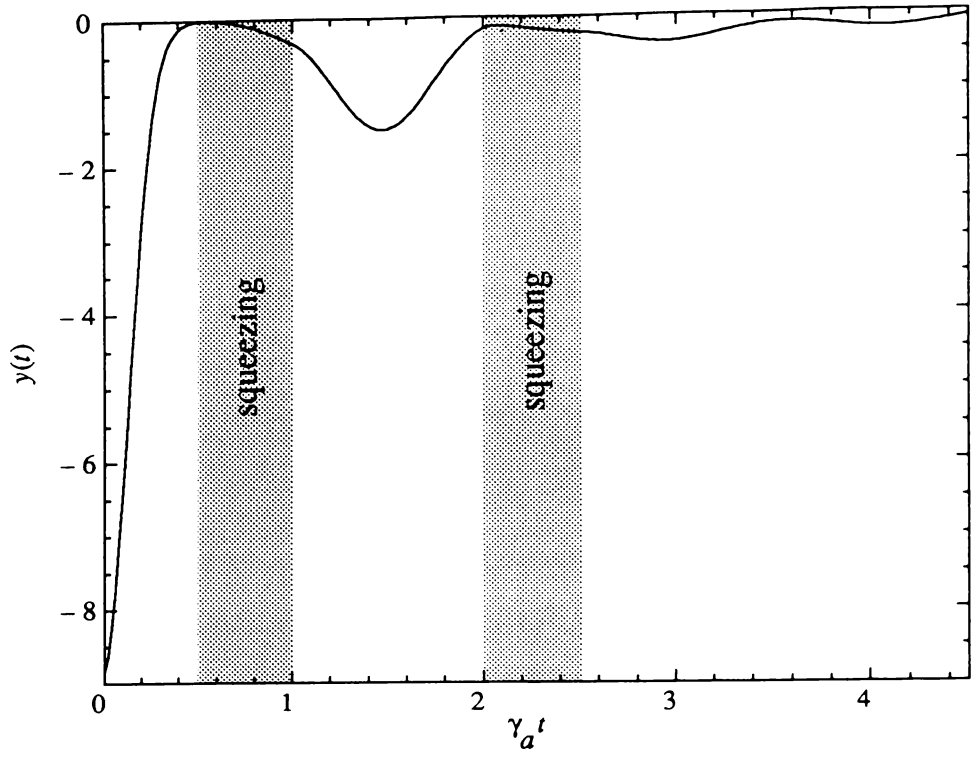


**Fig.4.8** $y(t)$ vs. $\gamma_a t$ for the sequence of pulses depicted in Fig.4.7, with $N = 10$ (98% squeezing), $\chi/\gamma_a = 200$, and $\delta/\gamma_a = 10$.

some large solid angle a significant problem arises in that the Doppler shift will differ for squeezed modes incident from different directions. This can nullify the effect of squeezing (Ritsch, 1989). Such a problem could be avoidable using the microcavity method we shall discuss later. However, it might be advantageous to consider a crystal or dye in which the distribution of detunings is not governed by the Doppler effect.

# 5. Two-Level Atoms in Narrow Bandwidth Squeezed Light

As we have already seen, the introduction of squeezed light to a number of classic problems in atomic spectroscopy has led to predictions of novel and interesting phenomena. The most dramatic of these has been the prediction of line-narrowing in the fluorescence spectrum of a two-level atom. The squeezed white noise formulation, from which these predictions have been made, is, of course, an idealisation. Indeed, present squeezed light sources, most notably the degenerate parametric amplifier (Wu *et al*, 1986, 1987), exhibit bandwidths only of the order of typical atomic linewidths. The effect of finite bandwidth squeezing on spontaneous emission and atomic absorption spectra has been analysed in detail (Parkins and Gardiner, 1988, Ritsch and Zoller, 1988a,b), with the overall conclusion that line-narrowing effects are degraded, and eventually cease to occur, as the squeezing bandwidth is reduced.

The spectrum of resonance fluorescence under finite bandwidth conditions has not, however, been investigated in such detail. While one might expect a similar degradation of line-narrowing effects to occur, it is also possible that the presence of a reservoir spectral structure on the scale of the Rabi frequency may allow for some interesting dynamical effects to come into play. An investigation of the possibilities offered by a finite bandwidth squeezed vacuum is the purpose of this chapter.

The particular scenarios that we have in mind are depicted in Fig.5.1, where we superimpose the squeezed vacuum power spectrum on the spectrum of resonance fluorescence emitted by the atom. The first scenario represents a situation in which the bandwidth of squeezing, though possibly broad compared to the natural atomic linewidth, falls well within the Rabi splitting of the Mollow triplet. In the second scenario, the squeezed vacuum is assumed to exhibit *two* spectral peaks, that we shall take to be centered on the two sidebands of the fluorescence triplet. This kind of squeezing is what one expects from (frequency) *nondegenerate* parametric amplification, and we shall refer to it as *two-mode* squeezing, in the sense that two cavity modes are excited in the parametric amplification

process. Correspondly, we shall refer to the squeezing in the first scenario as *single-mode* squeezing.

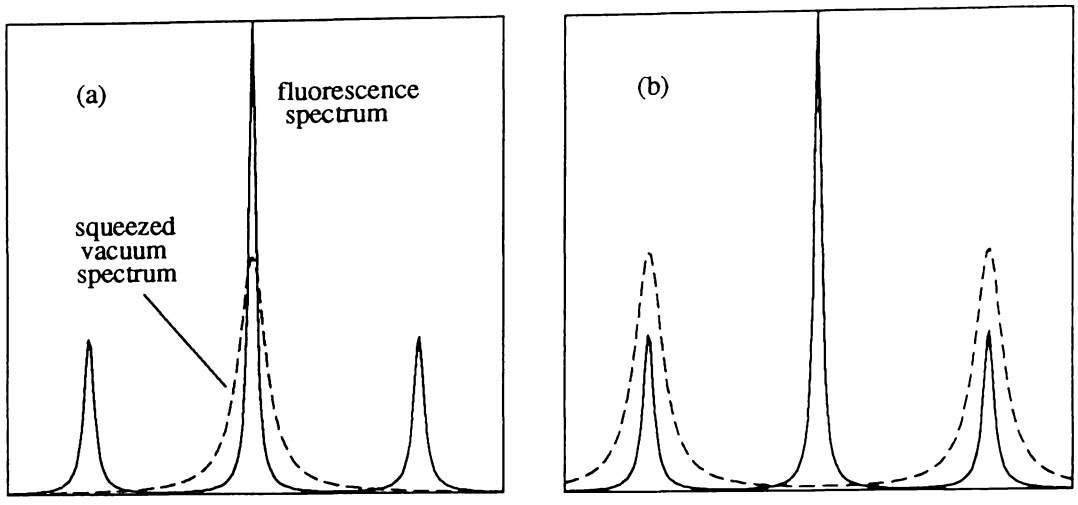


**Fig.5.1** (a) Single-mode and (b) two-mode squeezing scenarios.

These investigations can be related to recent work on dynamical modifications of spontaneous emission via strongly-driven resonance fluorescence in a cavity (Lewenstein *et al*, 1987, Lewenstein and Mossberg, 1988). In this case, the cavity spectral density facilitates a vacuum reservoir with finite bandwidth noise properties. In the final section of this chapter, we modify the work of Lewenstein *et al* to incorporate squeezing. This yields a model that closely parallels that of the earlier section, whilst also offering a possible experimental configuration.

## 5.1 Equations of Motion

The approach we shall adopt in treating this problem was first described in detail in a study by Parkins and Gardiner (1988) of the effect of finite bandwidth squeezing on the inhibition of atomic phase decays in spontaneous emission. The only added complication in the present study is the presence of a coherent driving field.

The dynamics of our two-level atom are completely described through the equations of motion for the atomic "spin" operators $S^+$, $S^-$, $S_z$. The quantum Langevin equa-

tions for the operators $S^+$ and $S_z$ can be written in the form

$$\dot{S}^+ = i\omega_a S^+ - i\Omega_0 \cos(\omega_0 t - \phi_0) S_z - \frac{i}{2}\sqrt{\frac{\gamma_a}{\hbar\omega_a}}\,[E_{in}(t), S_z]_+, \qquad (5.1.1)$$

$$\dot{S}_z = -\gamma_a - 2i\Omega_0 \cos(\omega_0 t - \phi_0)(S^+ - S^-) - i\sqrt{\frac{\gamma_a}{\hbar\omega_a}}\,[E_{in}(t), S^+ - S^-]_+ , \qquad (5.1.2)$$

where $\omega_a$ is the atomic transition frequency, $\gamma_a$ is the natural linewidth of the transition, and $\Omega_0$ and $\phi_0$ are the Rabi frequency and phase respectively of the coherent driving field. The incoming electric field operator $E_{in}(t)$ (representing the incoherent portion of the field) is evaluated at the position of the atom, and we shall express it in terms of quadrature phase operators as

$$E_{in}(t) = \sqrt{\hbar\omega_0}\,[E_1(t)\cos(\omega_0 t) + E_2(t)\sin(\omega_0 t)]\,, \qquad (5.1.3)$$

where $\omega_0$ is the frequency of the coherent driving field.

We move to a frame rotating at frequency $\omega_0$, and define polarisation quadratures that are in-phase and out-of-phase with the coherent driving field,

$$S_x = S^+ e^{-i\omega_0 t + i\phi_0} + S^- e^{i\omega_0 t - i\phi_0}, \qquad (5.1.4)$$

$$S_y = -i\left(S^+ e^{-i\omega_0 t + i\phi_0} - S^- e^{i\omega_0 t - i\phi_0}\right). \qquad (5.1.5)$$

With rapidly rotating terms removed (rotating wave approximation), the equations of motion become

$$\dot{S}_x = -\Delta_a S_y + \frac{1}{2}\sqrt{\gamma_a}\,[E_1(t)\sin(\phi_0) - E_2(t)\cos(\phi_0), S_z]_+, \qquad (5.1.6)$$

$$\dot{S}_y = \Delta_a S_x - \Omega_0 S_z - \frac{1}{2}\sqrt{\gamma_a}\,[E_1(t)\cos(\phi_0) + E_2(t)\sin(\phi_0), S_z]_+, \qquad (5.1.7)$$

$$\dot{S}_z = -\gamma_a + \Omega_0 S_y + \frac{1}{2}\sqrt{\gamma_a}\,[E_1(t)\cos(\phi_0) + E_2(t)\sin(\phi_0), S_y]_+ - \frac{1}{2}\sqrt{\gamma_a}\,[E_1(t)\sin(\phi_0) - E_2(t)\cos(\phi_0), S_x]_+, \qquad (5.1.8)$$

where $\Delta_a = \omega_a - \omega_0$. The adjoint equation, as described in Chapter 2, provides an equivalent description of the dynamics in terms of the density operator $\mu(t)$, which in this particular case is a $2 \times 2$ matrix functional of the incoming electric field operator $E_{in}(t)$. Defining

$$\bar{S}_i(t) \equiv Tr_{sys}\{S_i \mu(t)\} \qquad (5.1.9)$$

as the *atomic* average of the spin operators, the equations of motion for the matrix elements of $\mu(t)$ can be derived in the form

$$\begin{aligned}
\dot{\bar{S}}_x &= -\Delta_a \bar{S}_y - \beta_X(t)\bar{S}_z, \\
\dot{\bar{S}}_y &= \Delta_a \bar{S}_x - \Omega_0 \bar{S}_z - \beta_Y(t)\bar{S}_z, \\
\dot{\bar{S}}_z &= -\gamma_a + \Omega_0 \bar{S}_y + \beta_X(t)\bar{S}_x + \beta_Y(t)\bar{S}_y,
\end{aligned} \tag{5.1.10}$$

where $\beta_X(t)$ and $\beta_Y(t)$ are defined by

$$\begin{aligned}
\beta_X(t)\rho &= \frac{1}{2}\sqrt{\gamma_a}\{-\sin(\phi_0)[E_1(t),\rho]_+ + \cos(\phi_0)[E_2(t),\rho]_+\} \\
&\equiv \{-\sin(\phi_0)\beta_1(t) + \cos(\phi_0)\beta_2(t)\}\rho, \qquad (5.1.11) \\
\beta_Y(t)\rho &= \frac{1}{2}\sqrt{\gamma_a}\{\cos(\phi_0)[E_1(t),\rho]_+ + \sin(\phi_0)[E_2(t),\rho]_+\} \\
&\equiv \{\cos(\phi_0)\beta_1(t) + \sin(\phi_0)\beta_2(t)\}\rho. \qquad (5.1.12)
\end{aligned}$$

Having introduced these definitions, we now have a commuting form of quantum noise, that is, the operators $\beta_X(t)$ and $\beta_Y(t)$ satisfy

$$[\beta_X(t),\beta_X(t')] = [\beta_Y(t),\beta_Y(t')] = [\beta_X(t),\beta_Y(t')] = 0, \tag{5.1.13}$$

for all $t, t'$. This means, of course, that the equations can be treated as classical $c$-number equations, amenable to solution by ordinary stochastic methods. Hence, we need only specify the statistics of $\beta_X(t)$ and $\beta_Y(t)$, as determined by the initial quantum state of the incoming electric field.

## 5.2 Resonance Fluorescence in a Single-Mode Squeezed Vacuum

### 5.2.1 Single-mode squeezing statistics

The degenerate parametric amplifier, as described in Section 4.1, will once again serve as our source of squeezed light, only now the exponential character of the correlation functions (which is approximated by $\delta$-functions in the white noise limit) is central to our problem and must be retained. With the assumption that the amplifier is operating below threshold in a single-ended cavity (around the frequency $\omega_0$), the correlation functions of

the output light are

$$\langle \beta_1(t)\beta_1(t')\rangle = \gamma_a \langle E_1(t)E_1(t')\rangle$$
$$= \gamma_a \left\{ -\frac{\epsilon_c \gamma_c}{\frac{1}{2}\gamma_c + \epsilon_c} e^{-(\frac{1}{2}\gamma_c + \epsilon_c)|t-t'|} + \delta(t-t') \right\}, \qquad (5.2.1)$$
$$\langle \beta_2(t)\beta_2(t')\rangle = \gamma_a \langle E_2(t)E_2(t')\rangle$$
$$= \gamma_a \left\{ \frac{\epsilon_c \gamma_c}{\frac{1}{2}\gamma_c - \epsilon_c} e^{-(\frac{1}{2}\gamma_c - \epsilon_c)|t-t'|} + \delta(t-t') \right\}, \qquad (5.2.2)$$
$$\langle \beta_1(t)\beta_2(t')\rangle = 0, \qquad (5.2.3)$$

where again $\gamma_c$ is the cavity damping, and $\epsilon_c$ is the (real) amplifier driving strength ($\epsilon_c > 0$). Once again, we have made a particular choice of phase for the squeezed vacuum, which, as explained previously, does not cause any loss of generality.

With these definitions, and introducing the familiar $N$ and $M$ notation as defined in (4.1.6,7), the correlation properties of $\beta_X(t)$ and $\beta_Y(t)$ take the form

$$\langle \beta_X(t)\beta_X(t')\rangle = \gamma_a \sin^2(\phi_0)(N-M)\left(\frac{1}{2}\gamma_c + \epsilon_c\right) e^{-(\frac{1}{2}\gamma_c + \epsilon_c)|t-t'|}$$
$$+ \gamma_a \cos^2(\phi_0)(N+M)\left(\frac{1}{2}\gamma_c - \epsilon_c\right) e^{-(\frac{1}{2}\gamma_c - \epsilon_c)|t-t'|}$$
$$+ \gamma_a \delta(t-t'), \qquad (5.2.4)$$
$$\langle \beta_Y(t)\beta_Y(t')\rangle = \gamma_a \cos^2(\phi_0)(N-M)\left(\frac{1}{2}\gamma_c + \epsilon_c\right) e^{-(\frac{1}{2}\gamma_c + \epsilon_c)|t-t'|}$$
$$+ \gamma_a \sin^2(\phi_0)(N+M)\left(\frac{1}{2}\gamma_c - \epsilon_c\right) e^{-(\frac{1}{2}\gamma_c - \epsilon_c)|t-t'|}$$
$$+ \gamma_a \delta(t-t'), \qquad (5.2.5)$$
$$\langle \beta_X(t)\beta_Y(t')\rangle = -\frac{\gamma_a}{2}\sin(2\phi_0)(N-M)\left(\frac{1}{2}\gamma_c + \epsilon_c\right) e^{-(\frac{1}{2}\gamma_c + \epsilon_c)|t-t'|}$$
$$+ \frac{\gamma_a}{2}\sin(2\phi_0)(N+M)\left(\frac{1}{2}\gamma_c - \epsilon_c\right) e^{-(\frac{1}{2}\gamma_c - \epsilon_c)|t-t'|}. \qquad (5.2.6)$$

### 5.2.2 Qualitative analysis of the equations

Before commencing our analysis of the equations of motion, we find it convenient to average firstly over the white noise portions of $\beta_X(t)$ and $\beta_Y(t)$. We do this by writing $\beta_X(t)$ as a sum of independent coloured and white noise sources

$$\beta_X(t) = \beta_X^c(t) + \beta_X^w(t), \qquad (5.2.7)$$

with

$$\langle \beta_X^w(t)\beta_X^w(t')\rangle = \gamma_a \delta(t-t'), \tag{5.2.8}$$

$$\langle \beta_X^c(t)\beta_X^c(t')\rangle = \gamma_a \sin^2(\phi_0)(N-M)\left(\frac{1}{2}\gamma_c + \epsilon_c\right) e^{-(\frac{1}{2}\gamma_c+\epsilon_c)|t-t'|} + \gamma_a \cos^2(\phi_0)(N+M)\left(\frac{1}{2}\gamma_c - \epsilon_c\right) e^{-(\frac{1}{2}\gamma_c-\epsilon_c)|t-t'|}, \tag{5.2.9}$$

and similarly for $\beta_Y(t)$. The equations (5.1.10) are in the form of Stratonovich stochastic differential equations. For the purpose of averaging over the white noises $\beta_X^w(t)$ and $\beta_Y^w(t)$, we convert to the Ito form of the stochastic equations (Gardiner, 1983) with respect to the white noises. Averaging is then straightforward and results in the equations

$$\begin{aligned}
\dot{\bar{S}}_x &= -\frac{\gamma_a}{2}\bar{S}_x - \Delta_a \bar{S}_y - \beta_X^c(t)\bar{S}_z, \\
\dot{\bar{S}}_y &= -\frac{\gamma_a}{2}\bar{S}_y + \Delta_a \bar{S}_x - \Omega_0 \bar{S}_z - \beta_Y^c(t)\bar{S}_z, \\
\dot{\bar{S}}_z &= -\gamma_a - \gamma_a \bar{S}_z + \Omega_0 \bar{S}_y + \beta_X^c(t)\bar{S}_x + \beta_Y^c(t)\bar{S}_y,
\end{aligned} \tag{5.2.10}$$

where the bar is now understood to incorporate the white noise average. It remains therefore to perform the average over $\beta_X^c(t)$ and $\beta_Y^c(t)$ to obtain $\langle S_i(t)\rangle$, where $\langle\ \rangle$ denotes the total average.

Considerable insight into the nature of our problem can be gained from a simple qualitative inspection of the equations above. In the lowest order (neglecting noise terms), and for zero detuning, $\langle S_x(t)\rangle$ displays a simple exponential decay, while $\langle S_y(t)\rangle$ and $\langle S_z(t)\rangle$ undergo Rabi oscillations at frequency $\Omega_0$ and also decay exponentially. The contribution to the time development of $\langle S_x(t)\rangle$ from the additional noise terms is proportional to the time average of $\beta_X^c(t)\bar{S}_z(t)$. Since $\bar{S}_z(t)$ undergoes Rabi oscillations, it follows that this contribution will be significant only if $\beta_X^c(t)$ contains Fourier components at the frequencies $\pm\Omega_0$. Clearly, if $\beta_X^c(t)$ is a narrow bandwidth noise source, with significant spectral components only at frequencies much smaller than $\Omega_0$, then this term will play little part in the time evolution of $\langle S_x(t)\rangle$. A similar argument can be applied to $\langle S_y(t)\rangle$ and $\langle S_z(t)\rangle$. The time development of both $\langle S_y(t)\rangle$ and $\langle S_z(t)\rangle$ will be sensitive to the spectral components of $\beta_Y^c(t)$ around zero frequency, while in the equation of motion for $\bar{S}_z(t)$, the term $\beta_X^c(t)\bar{S}_x(t)$ will be significant only if, once again, $\beta_X^c(t)$ has non-negligible frequency components at $\pm\Omega_0$. Hence, $\langle S_y(t)\rangle$ and $\langle S_z(t)\rangle$ will be sensitive to spectral components of the noise sources at both zero frequency and at the frequencies $\pm\Omega_0$.

The above argument raises the interesting possibility of effectively decoupling the noise source $\beta_X^c(t)$ from the dynamics of the atom. This possibility takes on special significance in the case of a squeezed vacuum input when, through an appropriate choice of phase $\phi_0$, the unsqueezed (noisy) quadrature can be made to correspond to $\beta_X^c(t)$. We shall now investigate this possibility, firstly by using an approximate analytical method, and then by direct numerical simulation of the equations (5.2.10).

### 5.2.3 Solution by decorrelation approximation

The basic features of our scheme can be illustrated using a decorrelation approximation approach, whereby, for example, averages of the form $\langle \beta_X^c(t)\beta_X^c(t')S_x(t')\rangle$ are replaced by $\langle \beta_X^c(t)\beta_X^c(t')\rangle\langle S_x(t')\rangle$. We solve for two of the system variables and substitute the results into the equation of motion for the third variable, after which averaging is performed in the decorrelation approximation. Two distinct limiting cases characterise our problem, corresponding to the choices of phase $\phi_0 = 0$ and $\phi_0 = \pi/2$. For simplicity, we shall consider only these two cases, and therefore we have

$$\langle \beta_X^c(t)\beta_X^c(t')\rangle = \gamma_a(N \pm M)b_\pm e^{-b_\pm|t-t'|}, \tag{5.2.11}$$

$$\langle \beta_Y^c(t)\beta_Y^c(t')\rangle = \gamma_a(N \mp M)b_\mp e^{-b_\mp|t-t'|}, \tag{5.2.12}$$

$$\langle \beta_X^c(t)\beta_Y^c(t')\rangle = 0, \tag{5.2.13}$$

where $b_+ = \frac{1}{2}\gamma_c - \epsilon_c$ and $b_- = \frac{1}{2}\gamma_c + \epsilon_c$. With the further assumption of a strong driving field ($\Omega_0 \gg \gamma_a/4$), we find, after some work,

$$\begin{aligned}
\langle \dot{S}_x(t)\rangle = &-\frac{\gamma_a}{2}\langle S_x(t)\rangle \\
&+ \gamma_a(N \pm M)b_\pm \int_0^t dt' \exp\left[-(\frac{3\gamma_a}{4} + b_\pm)(t-t')\right] \\
&\quad \times \frac{\gamma_a}{4\Omega_0}\sin[\Omega_0(t-t')]\langle S_x(t')\rangle \\
&- \gamma_a(N \pm M)b_\pm \int_0^t dt' \exp\left[-(\frac{3\gamma_a}{4} + b_\pm)(t-t')\right] \\
&\quad \times \cos[\Omega_0(t-t')]\langle S_x(t')\rangle,
\end{aligned} \tag{5.2.14}$$

$$\begin{aligned}
\langle \dot{S}_y(t)\rangle = &-\frac{\gamma_a}{2}\langle S_y(t)\rangle - \Omega_0\langle S_z(t)\rangle \\
&+ \gamma_a(N \mp M)b_\mp \int_0^t dt' \exp\left[-(\frac{3\gamma_a}{4} + b_\mp)(t-t')\right] \\
&\quad \times \frac{\gamma_a}{4\Omega_0}\sin[\Omega_0(t-t')]\langle S_y(t')\rangle
\end{aligned}$$

$$
\begin{aligned}
&- \gamma_a(N \mp M) b_{\mp} \int_0^t dt' \ \exp\left[-(\frac{3\gamma_a}{4} + b_{\mp})(t-t')\right] \\
&\qquad \times \cos[\Omega_0(t-t')]\langle S_y(t')\rangle \\
&+ \gamma_a(N \mp M) b_{\mp} \int_0^t dt' \ \exp\left[-(\frac{3\gamma_a}{4} + b_{\mp})(t-t')\right] \\
&\qquad \times \sin[\Omega_0(t-t')]\langle S_z(t')\rangle, \qquad (5.2.15)
\end{aligned}
$$

$$
\begin{aligned}
\langle \dot{S}_z(t)\rangle = &- \gamma_a - \gamma_a\langle S_z(t)\rangle + \Omega_0\langle S_y(t)\rangle \\
&- \gamma_a(N \pm M) b_{\pm} \int_0^t dt' \ \exp\left[-(\frac{\gamma_a}{2} + b_{\pm})(t-t')\right] \langle S_z(t')\rangle \\
&- \gamma_a(N \mp M) b_{\mp} \int_0^t dt' \ \exp\left[-(\frac{3\gamma_a}{4} + b_{\mp})(t-t')\right] \\
&\qquad \times \frac{\gamma_a}{4\Omega_0} \sin[\Omega_0(t-t')]\langle S_z(t')\rangle \\
&- \gamma_a(N \mp M) b_{\mp} \int_0^t dt' \ \exp\left[-(\frac{3\gamma_a}{4} + b_{\mp})(t-t')\right] \\
&\qquad \times \cos[\Omega_0(t-t')]\langle S_z(t')\rangle \\
&- \gamma_a(N \mp M) b_{\mp} \int_0^t dt' \ \exp\left[-(\frac{3\gamma_a}{4} + b_{\mp})(t-t')\right] \\
&\qquad \times \sin[\Omega_0(t-t')]\langle S_y(t')\rangle. \qquad (5.2.16)
\end{aligned}
$$

In the white noise limit, one has $b_{\pm} \gg \Omega_0$, and to a good approximation $\langle S_i(t')\rangle$ can be replaced in the integrals by $\langle S_i(t)\rangle$. However, we are interested in the opposite limit, $\Omega_0 \gg b_{\pm}$. Provided $b_+$ and $b_-$ are larger than the decay rates of the various spin components, then the appropriate substitutions in this limit are

$$
\begin{aligned}
&\langle S_x(t')\rangle \simeq \langle S_x(t)\rangle, \\
&\langle S_y(t')\rangle \simeq \cos[\Omega_0(t-t')]\langle S_y(t)\rangle + \sin[\Omega_0(t-t')]\langle S_z(t)\rangle, \qquad (5.2.17) \\
&\langle S_z(t')\rangle \simeq \cos[\Omega_0(t-t')]\langle S_z(t)\rangle - \sin[\Omega_0(t-t')]\langle S_y(t)\rangle.
\end{aligned}
$$

The integrals that remain can then be evaluated. The time dependent terms that result from the integrals are assumed to give only small transient effects, and so we neglect them. Hence, we derive the modified Bloch equations

$$
\begin{aligned}
&\langle \dot{S}_x\rangle \simeq -\gamma_x\langle S_x\rangle, \\
&\langle \dot{S}_y\rangle \simeq -\gamma_y\langle S_y\rangle - \Omega_z\langle S_z\rangle, \qquad (5.2.18) \\
&\langle \dot{S}_z\rangle \simeq -\gamma_a - \gamma_z\langle S_z\rangle + \Omega_y\langle S_y\rangle,
\end{aligned}
$$

where

$$\gamma_x = \frac{\gamma_a}{2}\left\{1 + 2(N \pm M)\frac{b_\pm(b_\pm + \gamma_a/2)}{(b_\pm + 3\gamma_a/4)^2 + \Omega_0^2}\right\}, \tag{5.2.19}$$

$$\gamma_y = \frac{\gamma_a}{2}\left\{1 + 2(N \mp M)\frac{b_\mp}{b_\mp + 3\gamma_a/4} - (N \mp M)\frac{\gamma_a b_\mp/2}{(b_\mp + 3\gamma_a/4)^2 + 4\Omega_0^2}\right\}, \tag{5.2.20}$$

$$\gamma_z = \gamma_a\left\{1 + (N \mp M)\frac{b_\mp}{b_\mp + 3\gamma_a/4} + (N \mp M)\frac{b_\mp\gamma_a/4}{(b_\mp + 3\gamma_a/4)^2 + 4\Omega_0^2} + (N \pm M)\frac{b_\pm(b_\pm + \gamma_a/2)}{(b_\pm + \gamma_a/2)^2 + \Omega_0^2}\right\}, \tag{5.2.21}$$

and

$$\Omega_z = \Omega_0\left\{1 - (N \mp M)\frac{\gamma_a^2}{8\Omega_0^2}\frac{b_\mp}{b_\mp + 3\gamma_a/4} + (N \mp M)\frac{\gamma_a^2}{8\Omega_0^2}\frac{b_\mp(b_\mp + 3\gamma_a/4)}{(b_\mp + 3\gamma_a/4)^2 + 4\Omega_0^2}\right\}, \tag{5.2.22}$$

$$\Omega_y = \Omega_0\left\{1 + (N \mp M)\frac{\gamma_a^2}{8\Omega_0^2}\frac{b_\mp}{b_\mp + 3\gamma_a/4} - (N \mp M)\frac{\gamma_a^2}{8\Omega_0^2}\frac{b_\mp(b_\mp + 3\gamma_a/4)}{(b_\mp + 3\gamma_a/4)^2 + 4\Omega_0^2} + (N \pm M)\frac{\gamma_a b_\pm}{(b_\pm + \gamma_a/2)^2 + \Omega_0^2}\right\}. \tag{5.2.23}$$

In view of the limit we are considering ($\Omega_0 \gg b_\pm$), many of the terms appearing in (5.2.19-23) are negligible. Removing these terms, we arrive finally at the results

$$\gamma_x \simeq \frac{\gamma_a}{2}, \tag{5.2.24}$$

$$\gamma_y \simeq \frac{\gamma_a}{2}\left\{1 + 2(N \mp M)\frac{b_\mp}{b_\mp + 3\gamma_a/4}\right\}, \tag{5.2.25}$$

$$\gamma_z \simeq \gamma_a\left\{1 + (N \mp M)\frac{b_\mp}{b_\mp + 3\gamma_a/4}\right\}, \tag{5.2.26}$$

and

$$\Omega_z \simeq \Omega_y \simeq \Omega_0. \tag{5.2.27}$$

These permit the following observations:

(i) The component $\langle S_x(t)\rangle$ is damped at its normal vacuum rate independent of the choice of phase. This is to be expected, as the spectral distribution of the noises $\beta_X^c(t)$ and $\beta_Y^c(t)$ does not extend to the frequencies $\pm\Omega_0$. In the fluorescence spectrum, we can therefore expect the central peak of the Mollow triplet to remain essentially unchanged.

(ii) The components $\langle S_y(t)\rangle$ and $\langle S_z(t)\rangle$ are damped at the rate

$$\frac{1}{2}(\gamma_y + \gamma_z) = \frac{3\gamma_a}{4} + \gamma_a(N \mp M)\frac{b_\mp}{b_\mp + 3\gamma_a/4}, \tag{5.2.28}$$

which, if we consider the optimum case, $b_\mp \gg \gamma_a$, can be further simplified to

$$\frac{1}{2}(\gamma_y + \gamma_z) \simeq \gamma_a\left(\frac{3}{4} + N \mp M\right). \tag{5.2.29}$$

For large squeezing ($N \gg 1$), we have

$$\begin{aligned} N - M &\simeq -\frac{1}{2} + \frac{1}{8N}, \\ N + M &\simeq 2N + \frac{1}{2}, \end{aligned} \tag{5.2.30}$$

and hence the two choices of phase lead to widely different behaviour. For the case $\phi_0 = 0$,

$$\frac{1}{2}(\gamma_y + \gamma_z) \simeq \gamma_a\left(\frac{1}{4} + \frac{1}{8N}\right), \tag{5.2.31}$$

and the decay of $\langle S_y(t)\rangle$ and $\langle S_z(t)\rangle$ is found to be *inhibited* from its normal vacuum rate by an amount which could approach 66%. It follows that the Rabi sidebands should be *narrowed* compared to their natural width. For the case $\phi_0 = \pi/2$,

$$\frac{1}{2}(\gamma_y + \gamma_z) \simeq 2N\gamma_a, \tag{5.2.32}$$

and the decay rate is greatly enhanced, leading to a broadening of the Rabi peaks.

(iii) These results are in marked contrast to those found in the white noise limit of Chapter 4, where $b_\pm \gg \Omega_0$. Repeating these results, one finds, for $\phi_0 = 0$ (and for $N \gg 1$),

$$\begin{aligned} \gamma_x &= \gamma_a\left(N + M + \frac{1}{2}\right) \simeq 2N\gamma_a, \\ \frac{1}{2}(\gamma_y + \gamma_z) &= \gamma_a\left(\frac{3}{2}N - \frac{1}{2}M + \frac{3}{4}\right) \simeq N\gamma_a, \end{aligned} \tag{5.2.33}$$

while for $\phi_0 = \pi/2$,

$$\begin{aligned} \gamma_x &= \gamma_a\left(N - M + \frac{1}{2}\right) \simeq \frac{\gamma_a}{8N}, \\ \frac{1}{2}(\gamma_y + \gamma_z) &= \gamma_a\left(\frac{3}{2}N + \frac{1}{2}M + \frac{3}{4}\right) \simeq 2N\gamma_a. \end{aligned} \tag{5.2.34}$$

Hence, for strong squeezing, the central peak can be narrowed with an appropriate choice of phase ($\phi_0 = \pi/2$), but the sidebands can only be broadened relative to their natural width.

### 5.2.4 Solution by stochastic simulation

As we have seen already, the technique of stochastic simulation is a viable option in obtaining solutions to the equations of motion. We shall now adopt this technique once more to provide confirmation of the approximate analytical results found in the previous section.

The equations (5.2.10) are simulated using the fully-implicit numerical integration scheme (McNeil and Craig, 1990, Smith and Gardiner, 1989) that we first introduced in Chapter 3. For the present problem, this scheme takes the form

$$\begin{aligned}\Delta \mathbf{S}^n &= \mathbf{S}^{n+1} - \mathbf{S}^n \\ &= \mathbf{A}(\mathbf{S}^{n+\theta_1})\Delta t + \mathbf{B}(\mathbf{S}^{n+\theta_2})\beta_X^{c,n}\Delta t + \mathbf{C}(\mathbf{S}^{n+\theta_2})\beta_Y^{c,n}\Delta t\,, \end{aligned} \tag{5.2.35}$$

where

$$\mathbf{S} = \begin{pmatrix} \bar{S}_x \\ \bar{S}_y \\ \bar{S}_z \end{pmatrix}, \tag{5.2.36}$$

$$\mathbf{A}(\mathbf{S}) = \begin{pmatrix} -\frac{\gamma_a}{2}\bar{S}_x - \Delta_a \bar{S}_y \\ -\frac{\gamma_a}{2}\bar{S}_y + \Delta_a \bar{S}_x - \Omega_0 \bar{S}_z \\ -\gamma_a - \gamma_a \bar{S}_z + \Omega_0 \bar{S}_y \end{pmatrix}, \tag{5.2.37}$$

$$\mathbf{B}(\mathbf{S}) = \begin{pmatrix} -\bar{S}_z \\ 0 \\ \bar{S}_x \end{pmatrix}, \tag{5.2.38}$$

$$\mathbf{C}(\mathbf{S}) = \begin{pmatrix} 0 \\ -\bar{S}_z \\ \bar{S}_y \end{pmatrix}, \tag{5.2.39}$$

$\Delta t$ is the timestep, $\theta_1, \theta_2 \in [0, 1]$, and

$$\mathbf{A}(\mathbf{S}^{n+\theta_1}) = \mathbf{A}(\mathbf{S}^n) + \underline{J}_A^n \theta_1 \Delta \mathbf{S}^n \quad , \quad [\underline{J}_A^n]_{ij} = \left[\frac{\partial A_i}{\partial S_j}\right]_{\mathbf{S}=\mathbf{S}^n}, \tag{5.2.40}$$

$$\mathbf{B}(\mathbf{S}^{n+\theta_2}) = \mathbf{B}(\mathbf{S}^n) + \underline{J}_B^n \theta_2 \Delta \mathbf{S}^n \quad , \quad [\underline{J}_B^n]_{ij} = \left[\frac{\partial B_i}{\partial S_j}\right]_{\mathbf{S}=\mathbf{S}^n}, \tag{5.2.41}$$

$$\mathbf{C}(\mathbf{S}^{n+\theta_2}) = \mathbf{C}(\mathbf{S}^n) + \underline{J}_C^n \theta_2 \Delta \mathbf{S}^n \quad , \quad [\underline{J}_C^n]_{ij} = \left[\frac{\partial C_i}{\partial S_j}\right]_{\mathbf{S}=\mathbf{S}^n}. \tag{5.2.42}$$

It is straightforward to show that

$$\underline{J}_A^n = \begin{bmatrix} -\gamma_a/2 & -\Delta_a & 0 \\ \Delta_a & -\gamma_a/2 & -\Omega_0 \\ 0 & \Omega_0 & -\gamma_a \end{bmatrix}, \tag{5.2.43}$$

$$\underline{J}_B^n = \begin{bmatrix} 0 & 0 & -1 \\ 0 & 0 & 0 \\ 1 & 0 & 0 \end{bmatrix}, \tag{5.2.44}$$

$$\underline{J}_C^n = \begin{bmatrix} 0 & 0 & 0 \\ 0 & 0 & -1 \\ 0 & 1 & 0 \end{bmatrix}. \tag{5.2.45}$$

Substitution of (5.2.40-42) into (5.2.35) leads to the integration scheme

$$\Delta \mathbf{S}^n = [1 - \theta_1 \underline{J}_A^n \Delta t - \theta_2 \underline{J}_B^n \beta_X^{c,n} \Delta t - \theta_2 \underline{J}_C^n \beta_Y^{c,n} \Delta t]^{-1} \times [\mathbf{A}(\mathbf{S}^n)\Delta t + \mathbf{B}(\mathbf{S}^n)\beta_X^{c,n}\Delta t + \mathbf{C}(\mathbf{S}^n)\beta_Y^{c,n}\Delta t]. \quad (5.2.46)$$

The Euler method of integration, corresponding to the choice $\theta_1 = \theta_2 = 0$, suffers stability problems when large Rabi frequencies are involved, and hence our simulations have been carried out with $\theta_{1,2} = 1/2$. This fully implicit method has very good stability properties, which have already been demonstrated in Chapter 3.

Noise sources with the correct statistics are constructed using summations of suitably weighted Gaussian-distributed random numbers. The exact details of this procedure are given in Appendix C. The negative correlations which characterise squeezing require that these sources be complex. This enables $\bar{S}_x(t)$, $\bar{S}_y(t)$, and $\bar{S}_z(t)$ to develop imaginary parts, but in practice these average to zero after a sufficient number of trials, provided that the integration routine is stable.

**(a) Results for $\langle S_z(t) \rangle$**

The averages $\langle S_i(t) \rangle$ $(i = x, y, z)$ have typically been computed from 5000 trajectories. Our first aim is to confirm the basic predictions of the decorrelation approximation, and so, for Fig.5.2, we have chosen parameters to roughly suit the assumptions made in obtaining the approximate analytical results (i.e. $\Omega_0 \gg b_+, b_- \gg \gamma_{x,y,z}$). The decay of $\langle S_z(t) \rangle$ is clearly inhibited or enhanced, depending on the choice of phase. An exponential fit to the curves yields decay rates of $0.32\gamma_a$ and $4.9\gamma_a$ for $\phi_0 = 0$ and $\phi_0 = \pi/2$ respectively. These can be compared with the approximate theoretical result (5.2.28), which predicts decay rates

$$\frac{3\gamma_a}{4} + \gamma_a(N \mp M)\frac{b_\mp}{b_\mp + 3\gamma_a/4} = 0.35\gamma_a \ , \ 3.8\gamma_a. \quad (5.2.47)$$

The disagreement between the decay rates for $\phi_0 = \pi/2$ is not surprising, as the bandwidth of noise in the unsqueezed quadrature, $b_+ = 2.5\gamma_a$, is actually smaller than the decay rate of the $\langle S_y \rangle$ and $\langle S_z \rangle$ components, which clearly limits the accuracy of the decorrelation method.

In Fig.5.3, we examine the case in which the bandwidth of squeezed light is only marginally greater than $\gamma_a$. In particular, we now consider the choice $\Omega_0 = 20\gamma_a$, with $\gamma_c = 3\gamma_a$, and $\epsilon_c = 0.75\gamma_a$ ($b_+ = 0.75\gamma_a$, $b_- = 2.25\gamma_a$). Approximate exponential fits to

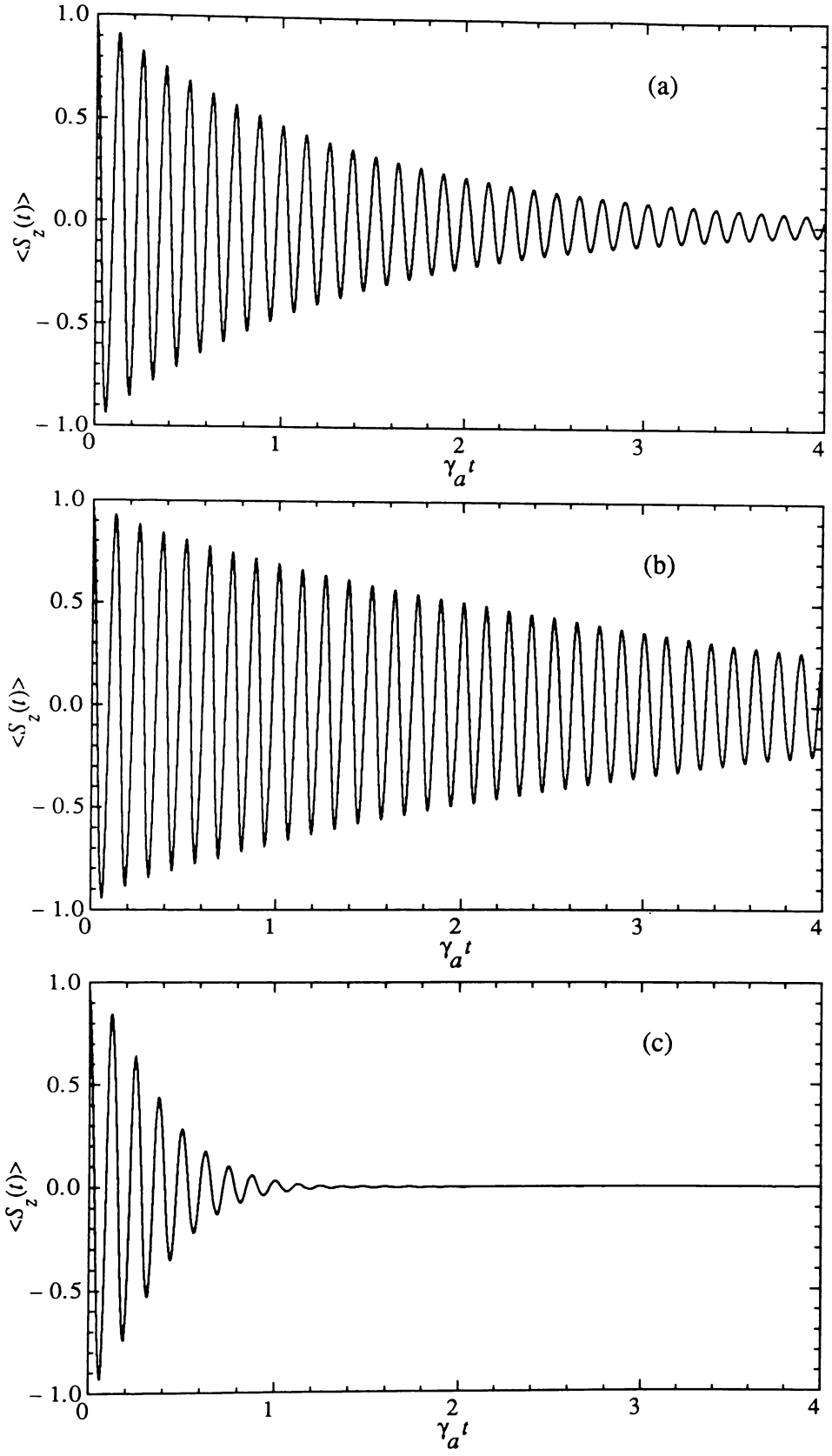


**Fig.5.2** Population inversion $\langle S_z(t) \rangle$ computed by simulation for $\Omega_0 = 50\gamma_a$, $\gamma_c = 10\gamma_a$, with (a) $\epsilon_c = 0$ (no squeezing), (b) $\epsilon_c = 2.5\gamma_a$ (89% squeezing), $\phi_0 = 0$, (c) $\epsilon_c = 2.5\gamma_a$, $\phi_0 = \pi/2$. The squeezing bandwidths in the two quadratures are $b_+ = 2.5\gamma_a$ and $b_- = 7.5\gamma_a$.

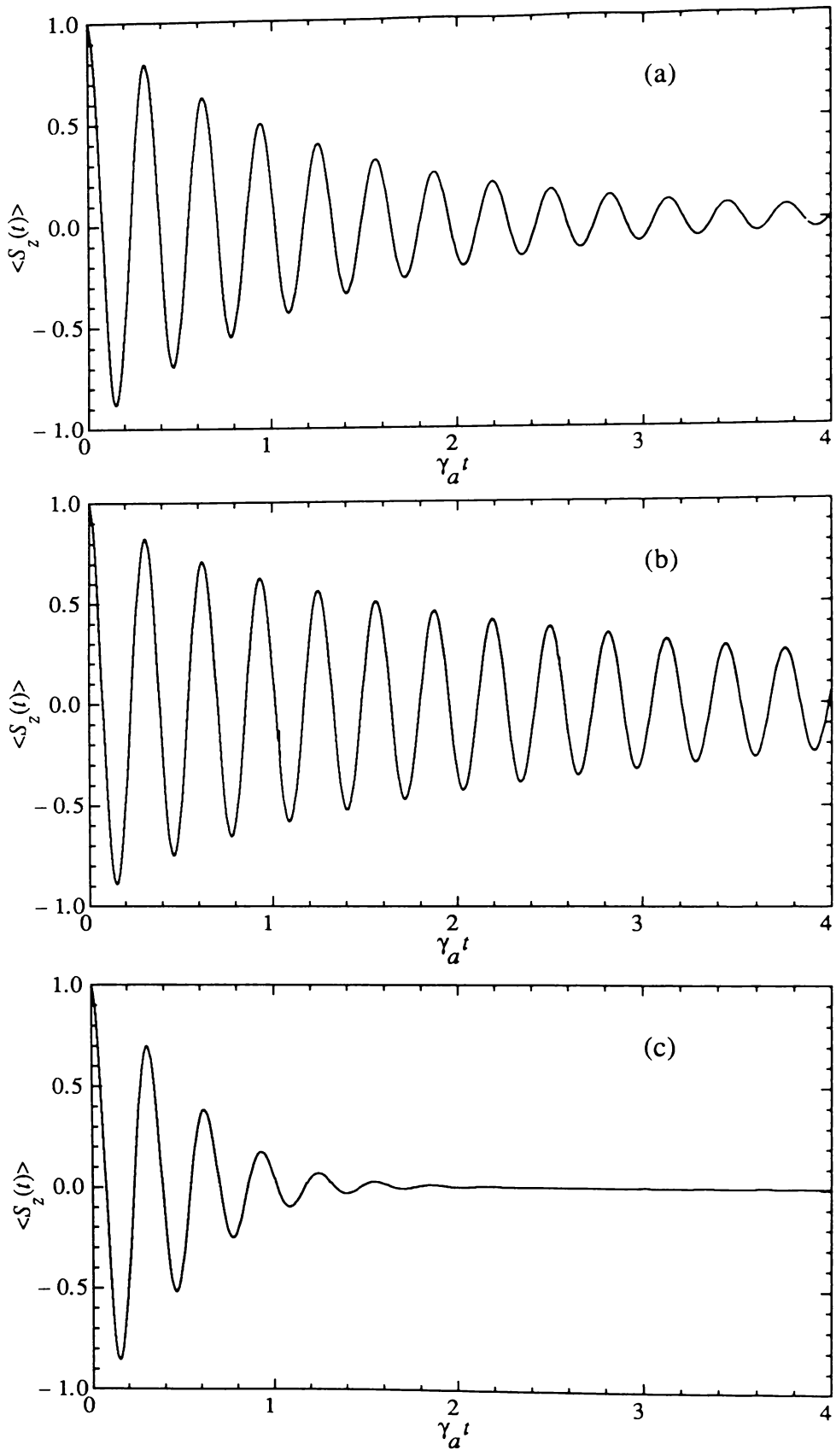


**Fig.5.3** Population inversion $\langle S_z(t) \rangle$ computed by simulation for $\Omega_0 = 20\gamma_a$, $\gamma_c = 3\gamma_a$, with (a) $\epsilon_c = 0$ (no squeezing), (b) $\epsilon_c = 0.75\gamma_a$ (89% squeezing), $\phi_0 = 0$, (c) $\epsilon_c = 0.75\gamma_a$, $\phi_0 = \pi/2$. The squeezing bandwidths in the two quadratures are $b_+ = 0.75\gamma_a$ and $b_- = 2.25\gamma_a$.

the simulation results now yield inhibited and enhanced decay rates of $0.32\gamma_a$ and $3.2\gamma_a$ respectively (the expression (5.2.47) agrees only poorly with these results, as one would expect), so strong inhibition and enhancement persists for parameters that are far from ideal from the point of view of the decorrelation method. However, we note that as we increase the parametric driving strength $\epsilon_c$ further, an optimum value is reached, $\epsilon_c \approx 1$ (at which inhibition is maximised), after which the degree of inhibition is reduced.

**(b) Correlation functions and spectra**

The computation of correlation functions and spectra is somewhat more difficult than the evaluation of the simple spin averages. The non-Markov nature of the processes being studied means that the familiar quantum regression theorem cannot be applied. However, methods have been developed for the simulation of the correlation functions (Parkins and Gardiner, 1988), based on the adjoint equation, from which spectra can be computed using a fast Fourier transform routine. In particular, if the solutions of the equations of motion (5.2.10) are written in the form

$$\bar{S}_i(t) = \sum_j f_{ij}(t,t')\bar{S}_j(t') + g_i(t,t'), \tag{5.2.48}$$

then the stationary correlation functions are given by

$$\begin{aligned}\langle S_i(t)S_k(t')\rangle = {} & \langle f_{ik}(t,t')\rangle + \langle g_i(t,t')g_k^{st}(t')\rangle \\ & + i\sum_{l,m}\epsilon_{lkm}\langle f_{il}(t,t')g_m^{st}(t')\rangle,\end{aligned} \tag{5.2.49}$$

where $g_i(t,t') \rightarrow g_i^{st}(t)$ as $t \rightarrow \infty$.

To evaluate (5.2.49) by stochastic simulation, we first allow the equations to evolve to a stationary state, thereby obtaining $g_i^{st}(t')$. A new trajectory is then initiated, with four different sets of initial conditions, so that we may identify $f_{ij}(t,t')$ and $g_i(t,t')$. The procedure is then repeated, and after approximately 10000 trials, the average is taken. We remove the coherent contribution to the correlation functions, and sample to a time at which the correlation functions are small (so as to avoid aliasing in the fast Fourier transform).

We shall concentrate for the moment on the fluorescence spectrum without reflections included, which is computed by fast Fourier transforming the correlation function $\langle S^+(t)S^-(0)\rangle$. In our first series of graphs, in Figs.5.4-6, we return to the squeezing parameters of Fig.5.2, and consider the variation in the fluorescence spectrum with changing

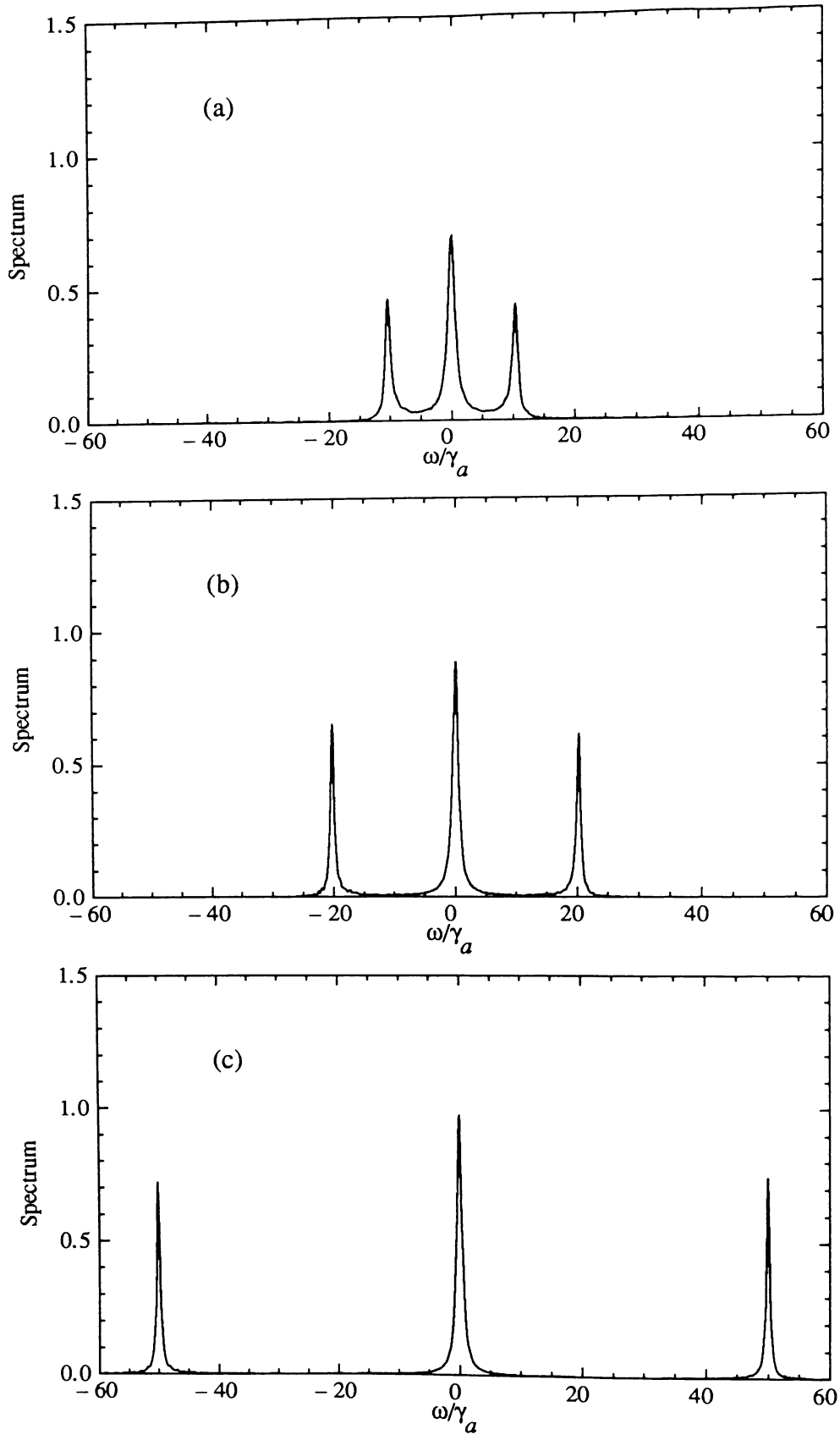


**Fig.5.4** Incoherent fluorescence spectrum, omitting reflections, computed by simulation for $\gamma_c = 10\gamma_a$, $\epsilon_c = 2.5\gamma_a$, $\phi_0 = 0$, with (a) $\Omega_0 = 10\gamma_a$, (b) $\Omega_0 = 20\gamma_a$, (c) $\Omega_0 = 50\gamma_a$.

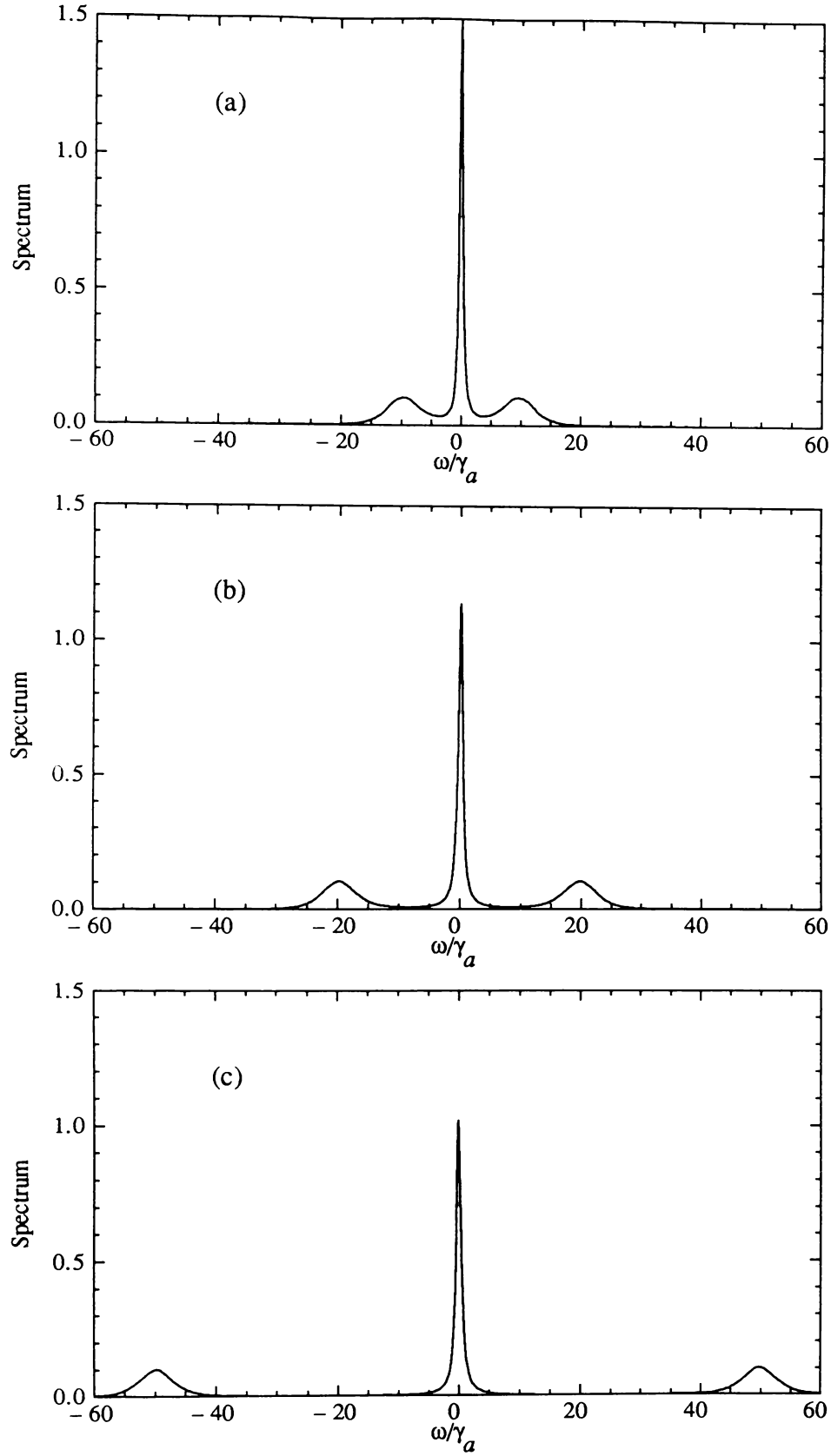


**Fig.5.5** Incoherent fluorescence spectrum, omitting reflections, computed by simulation for $\gamma_c = 10\gamma_a$, $\epsilon_c = 2.5\gamma_a$, $\phi_0 = \pi/2$, with (a) $\Omega_0 = 10\gamma_a$, (b) $\Omega_0 = 20\gamma_a$, (c) $\Omega_0 = 50\gamma_a$.

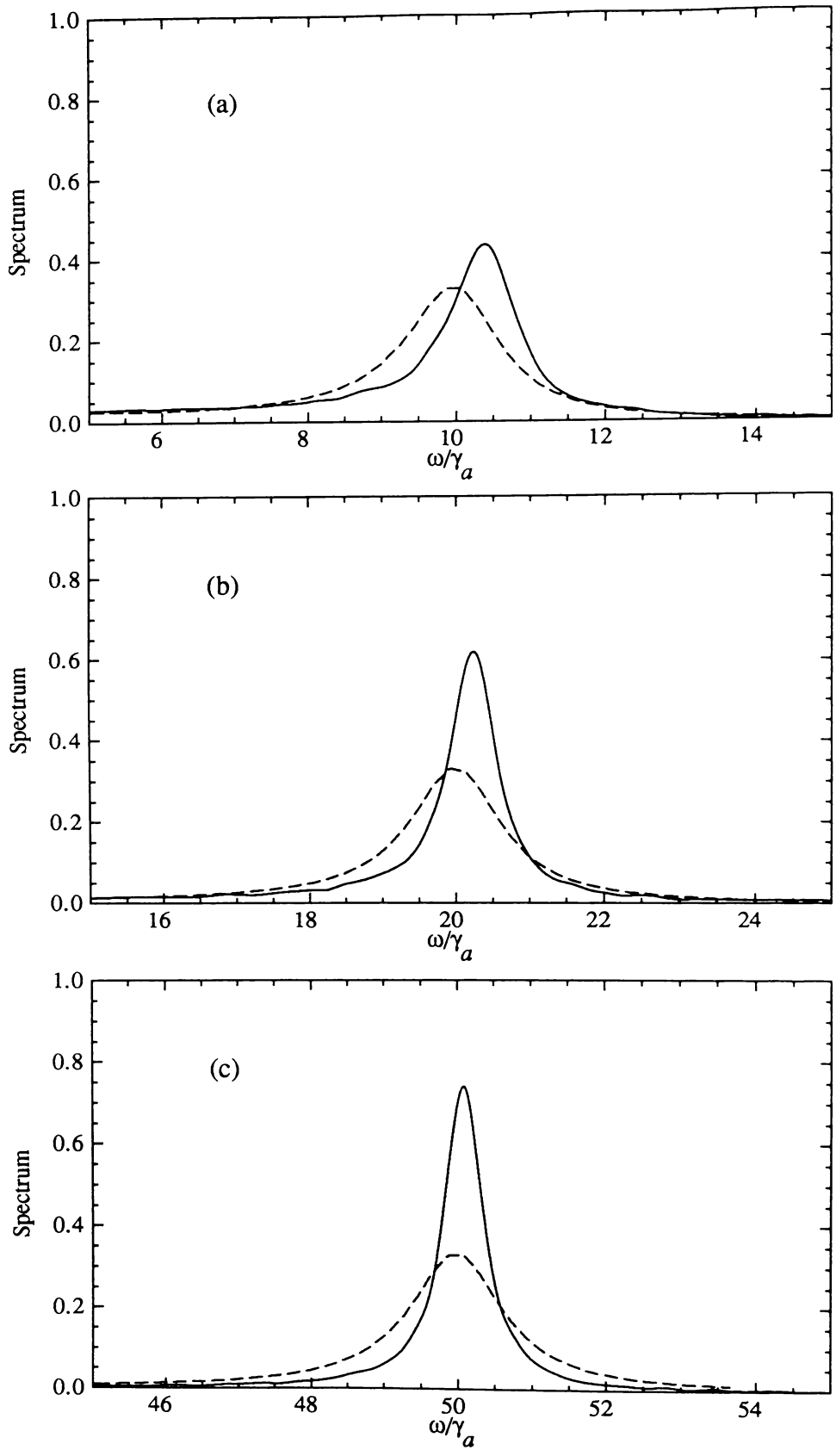


**Fig.5.6** Rabi sidebands of Fig.5.4 compared with normal vacuum results (dashed lines).

Rabi frequency $\Omega_0$. For $\Omega_0 = 50\gamma_a$ (Figs.5.4-6(c)) and $\Omega_0 = 20\gamma_a$ (Figs.5.4-6(b)), the Rabi sideband narrowing and broadening that we have described in previous sections is the dominant feature, with the central peak essentially unchanged from its normal vacuum form. However, for $\Omega_0 = 10\gamma_a$ (Figs.5.4-6(a)), we start to see features that characterise the white noise results, since now the bandwidth of squeezed light is comparable to the Rabi splitting. The Rabi sidebands are, for the choice of phase $\phi_0 = 0$, no longer significantly narrowed compared to their natural width, and the width of the central peak is now strongly phase dependent, alternating between supernatural and subnatural values for $\phi_0 = 0$ and $\phi_0 = \pi/2$ respectively.

In Fig.5.6, where we concentrate on the Rabi peaks of Fig.5.4, comparing them in each case with the normal (unsqueezed) vacuum result, we also note a slight shift in the position of the sidebands with the addition of squeezing. This shift decreases with increasing Rabi frequency, as one would expect from the form of $\Omega_y$ and $\Omega_z$ given in (5.2.22,23). The width of the peak for $\Omega_0 = 50\gamma_a$ agrees well with the decay rate computed earlier from the behaviour of $\langle S_z(t) \rangle$.

Finally, in Fig.5.7, we plot the spectra obtained with the squeezing parameters of Fig.5.3 for two values of the Rabi frequency, $\Omega_0 = 10\gamma_a$ and $\Omega_0 = 20\gamma_a$. Again, the sideband narrowing is enhanced as $\Omega_0$ is increased, and, in spite of the fact that the squeezing bandwidth is not optimum, significant effects are still clearly visible.

**(c) Reflections**

Using the simulation approach, it is not difficult to incorporate reflections of the input squeezed vacuum in the output. The formula relating the output field to input and atomic fields has the specific form

$$E_{out}(t) = E_{in}(t) - i\sqrt{\gamma_a \hbar \omega_a}\left[S^-(t) - S^+(t)\right], \qquad (5.2.50)$$

with which we can develop expressions for the correlation functions of the total output field. These expressions can then be computed numerically from the simulations in a straightforward manner. The fluorescence spectrum including reflections is given by the Fourier transform of the correlation function $\langle E_{out}^{(-)}(t) E_{out}^{(+)}(0) \rangle$.

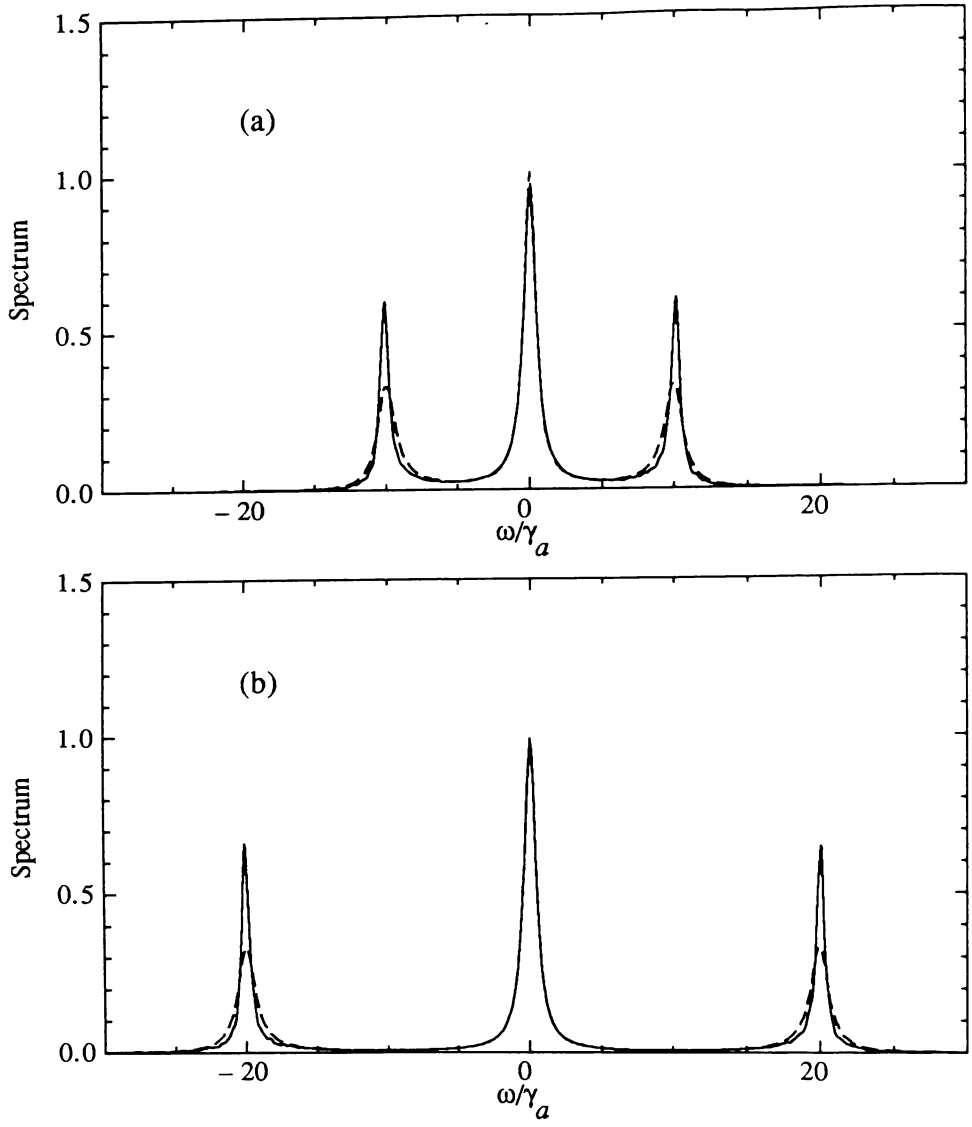


**Fig.5.7** Incoherent fluorescence spectrum, omitting reflections, computed by simulation for $\gamma_c = 3\gamma_a$, $\epsilon_c = 0.75\gamma_a$, $\phi_0 = 0$, with (a) $\Omega_0 = 10\gamma_a$, (b) $\Omega_0 = 20\gamma_a$, compared with normal vacuum results (dashed lines).

We have investigated (by simulation) the effect of reflections on the total fluorescence spectrum, and we find that, in our domain of interest ($\Omega_0 \gg b_\pm$), the Rabi peaks are unaffected, while the central peak is dominated by the squeezed vacuum spectrum (i.e. by a Lorentzian of width $b_+$). Hence, the significant features of our work, Rabi sideband narrowing and broadening, can still be seen in the fluorescence spectrum when reflections of the input are included. This is demonstrated in Fig.5.8.

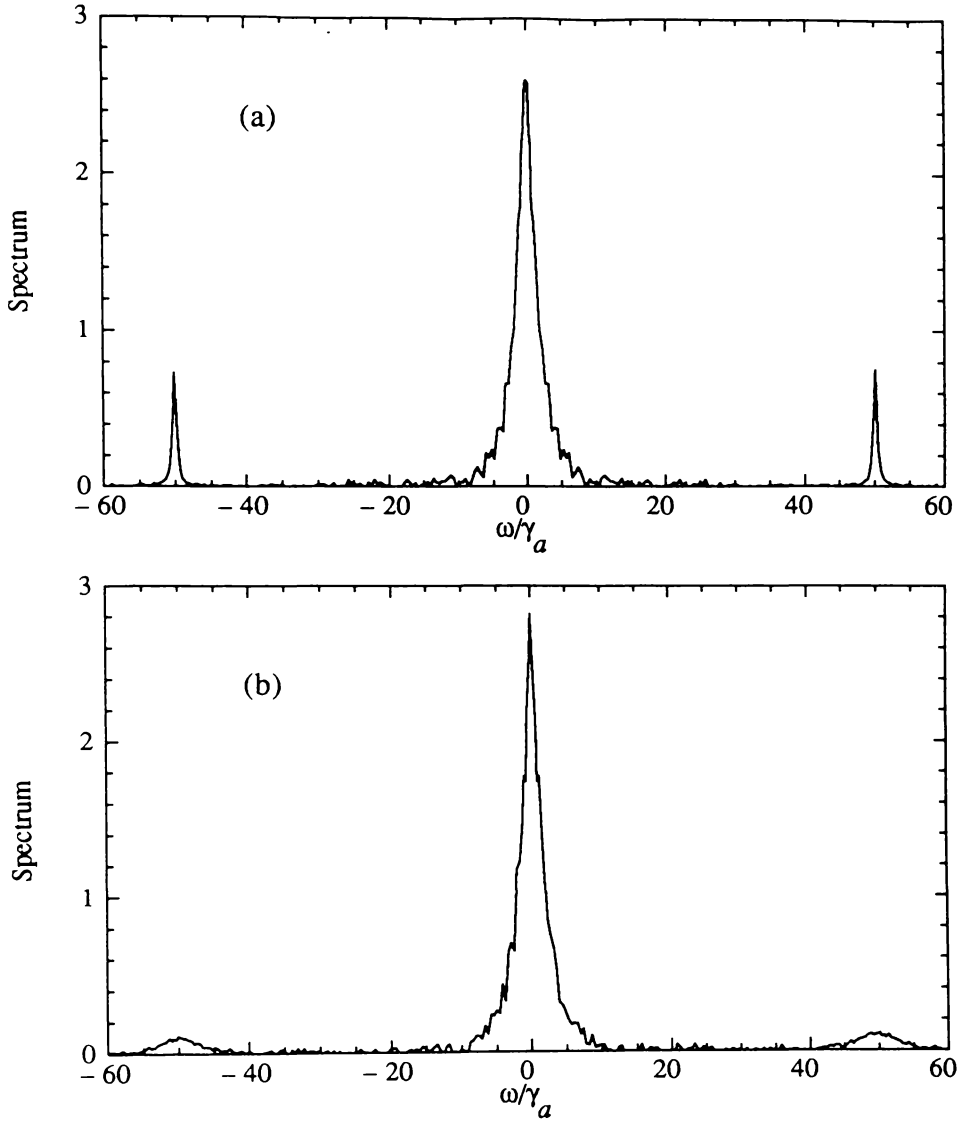


**Fig.5.8** Incoherent fluorescence spectrum, including reflections, computed by simulation for $\gamma_c = 10\gamma_a$, $\epsilon_c = 2.5\gamma_a$, $\Omega_0 = 50\gamma_a$, with (a) $\phi_0 = 0$ and (b) $\phi_0 = \pi/2$.

## 5.3 Resonance Fluorescence in a Two-Mode Squeezed Vacuum

The second scenario that we wish to pursue makes use of a two-mode squeezed vacuum exhibiting two (well-separated) spectral peaks centered on the frequencies $\omega_0 \pm \Omega_0$. Once again, it should be possible to decouple the narrow bandwidth component of one quadrature from the dynamics. It must be emphasised that this form of squeezed vacuum input is not merely a construction of convenience, since squeezing spectra with this double-peaked form are found in the output of a number of practical squeezing devices. The particular source we shall employ in this work is the nondegenerate parametric oscillator operating below threshold, but similar spectra are also found, for example, in optical bistability (Raizen *et al*, 1987, Orozco *et al*, 1987).

### 5.3.1 Two-mode squeezing statistics

Our source of squeezed light is now taken to be a nondegenerate parametric amplifier operating (below threshold) in a single-ended cavity. In this configuration, a pump beam at frequency $2\omega_0$ is coupled, via a nonlinear medium, to two cavity modes at frequencies $\omega_0 \pm \delta_c = \omega_\pm$. The two modes excited in this way (known as the signal and idler modes) may become highly correlated, leading to squeezed frequency components in two (separated) spectral peaks, centered respectively at the mode frequencies $\omega_+$ and $\omega_-$.

The correlation functions for the output mode operators of the non-degenerate parametric oscillator operating below threshold (with a classical pump) have been given by Collett *et al* (1987) (see also Reid and Drummond, 1990). We consider, of course, the case in which the signal and idler components are combined in a single beam. With a particular choice of phase that makes the parametric driving rate $\epsilon_c$ real ($\theta = 0$ in Eqs.(A18-19) of Collett *et al*), the correlation functions of $\beta_1(t)$ and $\beta_2(t)$ can be derived in the form (in a frame rotating at frequency $\omega_0$)

$$\langle \beta_1(t)\beta_1(t')\rangle = \gamma_a \left\{ -\frac{\epsilon_c\gamma_c}{\frac{1}{2}\gamma_c + \frac{1}{2}\epsilon_c} e^{-\frac{1}{2}(\gamma_c+\epsilon_c)|t-t'|} \cos[\delta_c(t-t')] + \delta(t-t') \right\}, \quad (5.3.1)$$

$$\langle \beta_2(t)\beta_2(t')\rangle = \gamma_a \left\{ \frac{\epsilon_c\gamma_c}{\frac{1}{2}\gamma_c - \frac{1}{2}\epsilon_c} e^{-\frac{1}{2}(\gamma_c-\epsilon_c)|t-t'|} \cos[\delta_c(t-t')] + \delta(t-t') \right\}, \quad (5.3.2)$$

$$\langle \beta_1(t)\beta_2(t')\rangle = 0\,, \tag{5.3.3}$$

where the cavity mode decay rate, $\gamma_c/2$, is assumed to be the same for both modes, and the results are derived with the assumption that $\omega_+ - \omega_- = 2\delta_c \gg \gamma_c$. We have removed a factor of one half from $\epsilon_c$ as defined by Collett *et al* (1987), so that perfect squeezing is approached in the limit $\epsilon_c \to \gamma_c$.

From the definitions (5.3.1-3), it follows that $\beta_1(t)$ exhibits reduced fluctuations in two spectral peaks centered at frequencies $\pm\delta_c$, with linewidth $\frac{1}{2}(\gamma_c + \epsilon_c)$, while $\beta_2(t)$ exhibits enhanced fluctuations in two spectral peaks of linewidth $\frac{1}{2}(\gamma_c - \epsilon_c)$.

### 5.3.2 Qualitative analysis of the equations

As before, we first perform an average over the white noise portions of $\beta_1(t)$ and $\beta_2(t)$ to obtain equations of motion in the form

$$\begin{aligned}
\dot{\bar{S}}_x &= -\frac{\gamma_a}{2}\bar{S}_x - \Delta_a\bar{S}_y - \beta_X^c(t)\bar{S}_z,\\
\dot{\bar{S}}_y &= -\frac{\gamma_a}{2}\bar{S}_y + \Delta_a\bar{S}_x - \Omega_0\bar{S}_z - \beta_Y^c(t)\bar{S}_z,\\
\dot{\bar{S}}_z &= -\gamma_a - \gamma_a\bar{S}_z + \Omega_0\bar{S}_y + \beta_X^c(t)\bar{S}_x + \beta_Y^c(t)\bar{S}_y,
\end{aligned} \tag{5.3.4}$$

where now

$$\langle \beta_1^c(t)\beta_1^c(t')\rangle = -\gamma_a \frac{\epsilon_c\gamma_c}{\frac{1}{2}\gamma_c + \frac{1}{2}\epsilon_c} e^{-\frac{1}{2}(\gamma_c+\epsilon_c)|t-t'|}\cos[\delta_c(t-t')], \tag{5.3.5}$$

$$\langle \beta_2^c(t)\beta_2^c(t')\rangle = \gamma_a \frac{\epsilon_c\gamma_c}{\frac{1}{2}\gamma_c - \frac{1}{2}\epsilon_c} e^{-\frac{1}{2}(\gamma_c-\epsilon_c)|t-t'|}\cos[\delta_c(t-t')]. \tag{5.3.6}$$

The small noise analysis of the Bloch equations presented in Section 5.2.2 revealed that the decay rates of the Bloch vector components are sensitive to the spectral components of $\beta_X^c(t)$ at the frequencies $\omega_0 \pm \Omega_0$, and to the spectral components of $\beta_Y^c(t)$ at the frequency $\omega_0$. In the case of single-mode narrow bandwidth squeezing centered at frequency $\omega_0$, this leads to a dynamical decoupling of $\beta_X^c(t)$ from the atomic dynamics.

With two-mode squeezing of the sort specified by (5.3.5,6), $\beta_X^c(t)$ and $\beta_Y^c(t)$ possess significant spectral components in two well-separated peaks that are centered on the frequencies $\omega_0 \pm \delta_c$. Hence, for two-mode squeezing, we now predict that $\beta_Y^c(t)$ will be decoupled from the dynamics, and that $\beta_X^c(t)$ will be the dominant noise term, provided, of course, that the atom is suitably "tuned" to the two-mode squeezed vacuum, such that $\delta_c \simeq \Omega_0$.

### 5.3.3 Decorrelation approximation

The same decorrelation approach developed in Section 5.2.3 provides a route to relatively simple analytical results for the case of two-mode squeezing. Again, we focus on the two limiting cases that characterise our problem, corresponding to the choices of phase $\phi_0 = 0$ and $\phi_0 = \pi/2$. We write

$$\langle \beta_X^c(t)\beta_X^c(t')\rangle = 2\gamma_a(N \pm M)b_\pm e^{-b_\pm|t-t'|}\cos[\delta_c(t-t')], \tag{5.3.7}$$

$$\langle \beta_Y^c(t)\beta_Y^c(t')\rangle = 2\gamma_a(N \mp M)b_\mp e^{-b_\mp|t-t'|}\cos[\delta_c(t-t')], \tag{5.3.8}$$

$$\langle \beta_X^c(t)\beta_Y^c(t')\rangle = 0, \tag{5.3.9}$$

where $b_+ = \frac{1}{2}(\gamma_c - \epsilon_c)$ and $b_- = \frac{1}{2}(\gamma_c + \epsilon_c)$, and the squeezing parameters $N$ and $M$ are now defined by

$$N = \epsilon_c\gamma_c\left[\frac{1}{(\gamma_c-\epsilon_c)^2} - \frac{1}{(\gamma_c+\epsilon_c)^2}\right], \tag{5.3.10}$$

$$M = \epsilon_c\gamma_c\left[\frac{1}{(\gamma_c-\epsilon_c)^2} + \frac{1}{(\gamma_c+\epsilon_c)^2}\right]. \tag{5.3.11}$$

We assume a strong driving field ($\Omega_0 \gg \gamma_a$), and set $\Delta_a = 0$. We find, after some work,

$$\begin{aligned}\langle \dot{S}_x(t)\rangle = &-\frac{\gamma_a}{2}\langle S_x(t)\rangle \\ &+\frac{\gamma_a^2}{2\Omega_0}(N \pm M)b_\pm\int_0^t dt'\,\exp\left[-(\frac{3\gamma_a}{4}+b_\pm)(t-t')\right] \\ &\quad\times\sin[\Omega_0(t-t')]\cos[\delta_c(t-t')]\langle S_x(t')\rangle \\ &-2\gamma_a(N \pm M)b_\pm\int_0^t dt'\,\exp\left[-(\frac{3\gamma_a}{4}+b_\pm)(t-t')\right] \\ &\quad\times\cos[\Omega_0(t-t')]\cos[\delta_c(t-t')]\langle S_x(t')\rangle,\end{aligned} \tag{5.3.12}$$

$$\begin{aligned}\langle \dot{S}_y(t)\rangle = &-\frac{\gamma_a}{2}\langle S_y(t)\rangle - \Omega_0\langle S_z(t)\rangle \\ &+\frac{\gamma_a^2}{2\Omega_0}(N \mp M)b_\mp\int_0^t dt'\,\exp\left[-(\frac{3\gamma_a}{4}+b_\mp)(t-t')\right] \\ &\quad\times\sin[\Omega_0(t-t')]\cos[\delta_c(t-t')]\langle S_y(t')\rangle \\ &-2\gamma_a(N \mp M)b_\mp\int_0^t dt'\,\exp\left[-(\frac{3\gamma_a}{4}+b_\mp)(t-t')\right] \\ &\quad\times\cos[\Omega_0(t-t')]\cos[\delta_c(t-t')]\langle S_y(t')\rangle \\ &+2\gamma_a(N \mp M)b_\mp\int_0^t dt'\,\exp\left[-(\frac{3\gamma_a}{4}+b_\mp)(t-t')\right] \\ &\quad\times\sin[\Omega_0(t-t')]\cos[\delta_c(t-t')]\langle S_z(t')\rangle,\end{aligned} \tag{5.3.13}$$

$$
\begin{aligned}
\langle \dot{S}_z(t)\rangle = &-\gamma_a - \gamma_a\langle S_z(t)\rangle + \Omega_0\langle S_y(t)\rangle \\
&- 2\gamma_a(N \pm M)b_\pm \int_0^t dt' \exp\left[-(\frac{\gamma_a}{2} + b_\pm)(t-t')\right] \\
&\quad \times \cos[\delta_c(t-t')]\langle S_z(t')\rangle \\
&- \frac{\gamma_a^2}{2\Omega_0}(N \mp M)b_\mp \int_0^t dt' \exp\left[-(\frac{3\gamma_a}{4} + b_\mp)(t-t')\right] \\
&\quad \times \sin[\Omega_0(t-t')]\cos[\delta_c(t-t')]\langle S_z(t')\rangle \\
&- 2\gamma_a(N \mp M)b_\mp \int_0^t dt' \exp\left[-(\frac{3\gamma_a}{4} + b_\mp)(t-t')\right] \\
&\quad \times \cos[\Omega_0(t-t')]\cos[\delta_c(t-t')]\langle S_z(t')\rangle \\
&- 2\gamma_a(N \mp M)b_\mp \int_0^t dt' \exp\left[-(\frac{3\gamma_a}{4} + b_\mp)(t-t')\right] \\
&\quad \times \sin[\Omega_0(t-t')]\cos[\delta_c(t-t')]\langle S_y(t')\rangle .
\end{aligned}
\tag{5.3.14}
$$

As mentioned earlier, we expect the most interesting results when $\delta_c$ and $\Omega_0$ are comparable, so for simplicity we choose $\delta_c = \Omega_0$. We know further that $\delta_c \gg b_\pm$. If $b_+$ and $b_-$ are much larger than the decay rates of the various spin components, then to a good approximation we can use (5.2.17) inside the integrals, relating $\langle S_{x,y,z}(t')\rangle$ to $\langle S_{x,y,z}(t)\rangle$ via the zeroth order (undamped) solutions. The assumption of large $b_\pm$ does, of course, restrict the maximum amount of squeezing one should consider for a particular value of $\gamma_c$, since $b_+ \to 0$ in the large squeezing limit.

With the substitutions given in (5.2.17), we have simply to evaluate some straightforward integrals as before. This produces time-dependent terms, but, once again, with the assumptions made above these are expected to give only small transient effects and so we neglect them. The modified Bloch equations that result are of the same form obtained in the single-mode squeezing analysis,

$$
\begin{aligned}
\langle \dot{S}_x\rangle &\simeq -\gamma_x\langle S_x\rangle, \\
\langle \dot{S}_y\rangle &\simeq -\gamma_y\langle S_y\rangle - \Omega_z\langle S_z\rangle, \\
\langle \dot{S}_z\rangle &\simeq -\gamma_a - \gamma_z\langle S_z\rangle + \Omega_y\langle S_y\rangle,
\end{aligned}
\tag{5.3.15}
$$

but with different coefficients, given by

$$
\gamma_x = \frac{\gamma_a}{2}\left\{1 + 2(N \pm M)b_\pm\left[\frac{1}{b_\pm + 3\gamma_a/4} + \frac{b_\pm + \gamma_a/4}{(b_\pm + 3\gamma_a/4)^2 + 4\Omega_0^2}\right]\right\}, \tag{5.3.16}
$$

$$
\begin{aligned}
\gamma_y = &\frac{\gamma_a}{2}\{1 + 2(N \mp M)b_\mp \\
&\times \left[\frac{b_\mp + 11\gamma_a/8}{(b_\mp + 3\gamma_a/4)^2 + \Omega_0^2} - \frac{3\gamma_a/8}{(b_\mp + 3\gamma_a/4)^2 + 9\Omega_0^2}\right]\},
\end{aligned}
\tag{5.3.17}
$$

$$
\gamma_z = \gamma_a\left\{1 + (N \pm M)\frac{b_\pm}{b_\pm + \gamma_a/2} + (N \pm M)\frac{b_\pm(b_\pm + \gamma_a/2)}{(b_\pm + \gamma_a/2)^2 + 4\Omega_0^2}\right.
$$

$$+ 2(N \mp M)\frac{b_\mp(b_\mp + 3\gamma_a/4)}{(b_\mp + 3\gamma_a/4)^2 + \Omega_0^2} \tag{5.3.18}$$
$$+\frac{1}{8}(N \mp M)\left[\frac{\gamma_a b_\mp}{(b_\mp + 3\gamma_a/4)^2 + \Omega_0^2} + \frac{3\gamma_a b_\mp}{(b_\mp + 3\gamma_a/4)^2 + 9\Omega_0^2}\right]\Bigg\},$$

and

$$\Omega_z = \Omega_0\left\{1 - \frac{\gamma_a^2}{8\Omega_0^2}(N \mp M)b_\mp \times\left[\frac{b_\mp + 3\gamma_a/4}{(b_\mp + 3\gamma_a/4)^2 + \Omega_0^2} - \frac{b_\mp + 3\gamma_a/4}{(b_\mp + 3\gamma_a/4)^2 + 9\Omega_0^2}\right]\right\}, \tag{5.3.19}$$

$$\Omega_y = \Omega_0\left\{1 + \frac{\gamma_a^2}{8\Omega_0^2}(N \mp M)b_\mp \times\left[\frac{b_\mp + 3\gamma_a/4}{(b_\mp + 3\gamma_a/4)^2 + \Omega_0^2} - \frac{b_\mp + 3\gamma_a/4}{(b_\mp + 3\gamma_a/4)^2 + 9\Omega_0^2}\right] + 2\gamma_a(N \pm M)\frac{b_\pm}{(b_\pm + \gamma_a/2)^2 + 4\Omega_0^2}\right\}. \tag{5.3.20}$$

The limit we are considering ($\Omega_0 \gg b_\pm, \gamma_x, \gamma_y, \gamma_z$) again allows for considerable simplification of the above expressions. Retaining only the leading order terms, and assuming that $b_\pm \gg \gamma_a$, we find

$$\gamma_x \simeq \frac{\gamma_a}{2}\left[1 + 2(N \pm M)\frac{b_\pm}{b_\pm + 3\gamma_a/4}\right] \simeq \frac{\gamma_a}{2}[1 + 2(N \pm M)], \tag{5.3.21}$$

$$\gamma_y \simeq \frac{\gamma_a}{2}, \tag{5.3.22}$$

$$\gamma_z \simeq \gamma_a\left[1 + (N \pm M)\frac{b_\pm}{b_\pm + \gamma_a/2}\right] \simeq \gamma_a[1 + (N \pm M)], \tag{5.3.23}$$

and

$$\Omega_z \simeq \Omega_y \simeq \Omega_0. \tag{5.3.24}$$

For large squeezing ($N \gg 1$), we have, of course,

$$N - M \simeq -\frac{1}{2} + \frac{1}{8N}, \qquad N + M \simeq 2N + \frac{1}{2}, \tag{5.3.25}$$

and hence, as we alter the phase $\phi_0$, *both* of the decay rates $\gamma_x$ and $\gamma_z$ may be enlarged or reduced compared to their normal vacuum values. In particular (for $N \gg 1$):

(i) The component $\langle S_x(t)\rangle$ decays at an enhanced rate $\gamma_x \approx 2N\gamma_a$ for $\phi_0 = 0$, and at an inhibited rate $\gamma_x \approx \gamma_a/8N$ for $\phi_0 = \pi/2$. The decay rate $\gamma_x$ gives the width of the central peak observed in the resonance fluorescence spectrum (Mollow triplet), and

hence we predict a phase-sensitive central peak width, varying between supernatural and subnatural values. The maximum reduction in width may in principle approach 100%.
(ii) The components $\langle S_y(t)\rangle$ and $\langle S_z(t)\rangle$ decay at the enhanced rate

$$\frac{1}{2}(\gamma_y + \gamma_z) \simeq \gamma_a N, \tag{5.3.26}$$

for $\phi_0 = 0$, and at the inhibited rate

$$\frac{1}{2}(\gamma_y + \gamma_z) \simeq \frac{3\gamma_a}{4}\left(\frac{2}{3} + \frac{1}{12N}\right), \tag{5.3.27}$$

for $\phi_0 = \pi/2$. Hence, the width of the Rabi sidebands should exhibit a phase sensitivity similar to that shown by the central peak, but with a smaller degree of broadening and narrowing.

For the choice of phase $\phi_0 = 0$, the results for $\gamma_x$ and $\frac{1}{2}(\gamma_y + \gamma_z)$ are identical to those found in the single-mode white noise limit of Section 4.2.4. However, for $\phi_0 = \pi/2$ an important difference is apparent. The two-mode squeezed vacuum result predicts a value for $\frac{1}{2}(\gamma_y + \gamma_z)$ that is much less than its single-mode white noise counterpart, and which may in fact be less than its normal vacuum value. Hence, it is possible for all three peaks in the fluorescence triplet to exhibit subnatural linewidths for a particular choice of phase. In the white noise analysis of Section 4.2.4, line narrowing is seen only in the central fluorescence peak, while in the narrow bandwidth scenario of Section 5.2, significant line narrowing occurs only in the Rabi sidebands.

Hence, the two-mode squeezing scheme offers still further possibilities in the field of squeezed light spectroscopy. The difference that it exhibits in comparison to the white noise theory can be explained qualitatively as follows. In the single-mode broad bandwidth squeezing analysis, the atom "sees" enhanced vacuum fluctuations at frequency $\omega_0$ due to the noisy quadrature. In the two-mode formulation, in which the spectral peaks of the squeezed vacuum are well separated at the frequencies $\omega_0 \pm \delta_c$, the atom "sees" only ordinary vacuum fluctuations at frequency $\omega_0$. This means that broadening need not occur in the fluorescence spectrum, and that all three lines in the fluorescence triplet may exhibit some degree of narrowing.

### 5.3.4 Solution by stochastic simulation

For a more accurate description of the dynamics than that given above, we have at our disposal, once again, the technique of stochastic simulation. With some minor modifications to the noise terms, the simulation scheme of Section 5.2.4 is readily adapted to the treatment of two-mode squeezing. Following the single-mode analysis, we begin with the simple spin averages.

**(a) Results for the spin averages**

Our first set of results are obtained for parameters that should roughly satisfy the conditions of the decorrelation approximation ($\Omega_0 \gg b_\pm \gg \gamma_a$). In Fig.5.9, the squeezing parameters correspond to a 64% reduction in noise (below the vacuum level) at the frequencies $\pm\delta_c$. This reduction in fluctuations extends over a bandwidth $2b_- = 12.5\gamma_a$.

As predicted by the decorrelation approximation, $\langle S_x(t)\rangle$ and $\langle S_z(t)\rangle$ exhibit enhanced decay rates for $\phi_0 = 0$, and reduced decay rates for $\phi_0 = \pi/2$. The simultaneous inhibition of the decay of $\langle S_x(t)\rangle$ and $\langle S_z(t)\rangle$ is perhaps the most significant feature of the two-mode squeezed vacuum scheme. This feature is more dramatically demonstrated in Fig.5.10, where the maximum squeezing has been increased to 89%.

It is interesting to compare decay rates obtained from the simulations and from the decorrelation approximation. An exponential fit to the curves of Fig.5.9(b,c) yields decay rates $\gamma_x \simeq 1.4\gamma_a$, $(\gamma_y + \gamma_z)/2 \simeq 1.2\gamma_a$ for $\phi_0 = 0$, and $\gamma_x \simeq 0.20\gamma_a$, $(\gamma_y + \gamma_z)/2 \simeq 0.60\gamma_a$ for $\phi_0 = \pi/2$. In comparison, the results (5.3.21-23) give

$$\gamma_x \simeq \frac{\gamma_a}{2}\left\{1 + 2(N \pm M)\frac{b_\pm}{b_\pm + 3\gamma_a/4}\right\} = 1.2\gamma_a\ ,\ 0.21\gamma_a\ , \qquad (5.3.28)$$

and

$$\frac{1}{2}(\gamma_y + \gamma_z) \simeq \frac{\gamma_a}{2}\left\{\frac{3}{2} + (N \pm M)\frac{b_\pm}{b_\pm + \gamma_a/2}\right\} = 1.1\gamma_a\ ,\ 0.60\gamma_a\ , \qquad (5.3.29)$$

for $\phi_0 = 0$ and $\phi_0 = \pi/2$ respectively. This level of agreement does not persist as the bandwidths $b_\pm$ are reduced, once again highlighting the limitations of the decorrelation approximation. However, the basic predictions of decorrelation approximation results are confirmed.

**(b) Correlation functions and spectra**

To begin, we compute the fluorescence spectrum for the parameters used in Fig.5.9. The results are displayed in Fig.5.11, and they confirm earlier predictions regarding narrowing

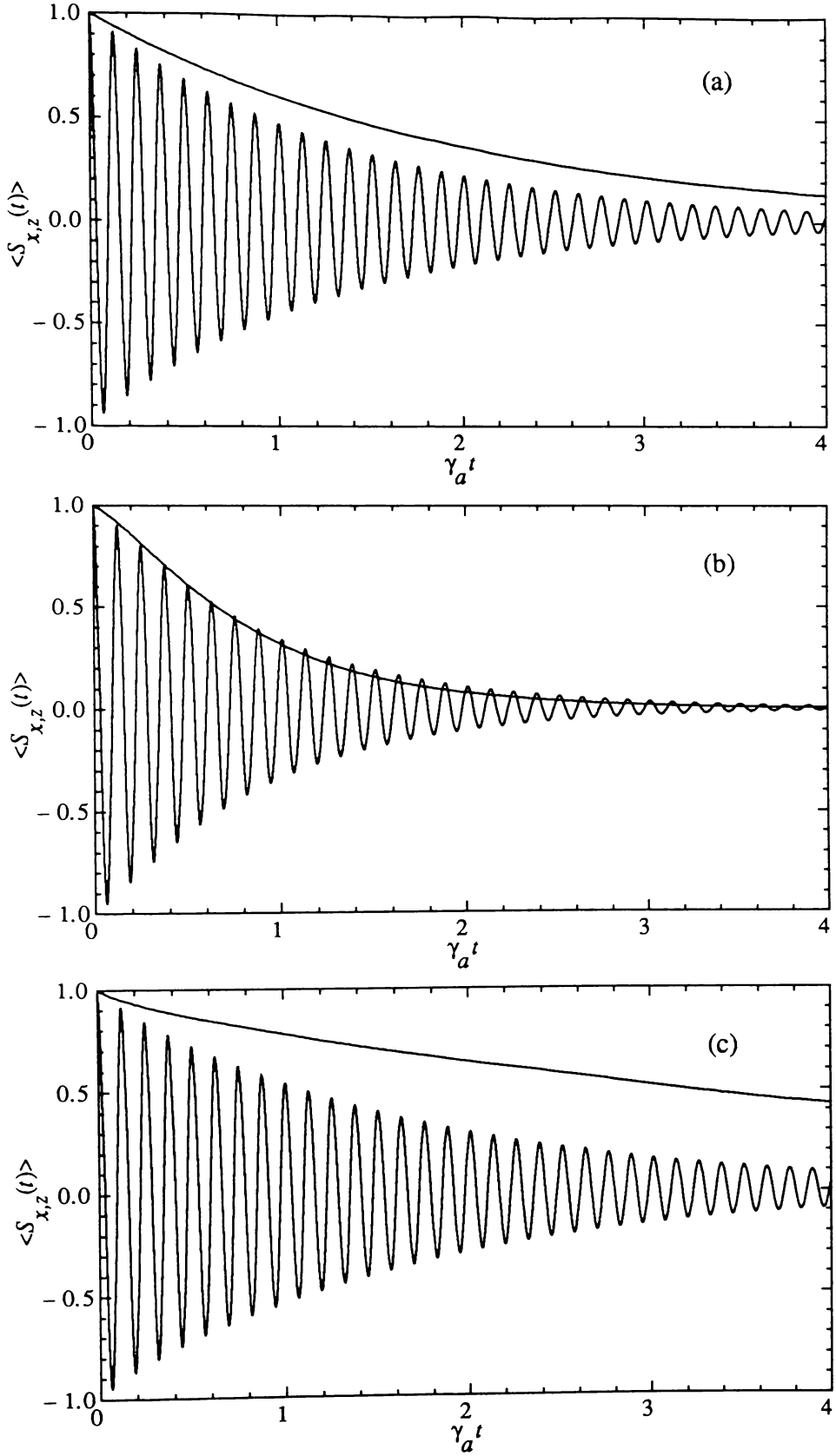


**Fig.5.9** Spin averages $\langle S_x(t) \rangle$ and $\langle S_z(t) \rangle$ (oscillating) computed by simulation (5000 trials) for $\Omega_0 = 50\gamma_a$, $\Delta_a = 0$, $\delta_c = 50\gamma_a$, $\gamma_c = 10\gamma_a$, with (a) $\epsilon_c = 0$ (no squeezing), (b) $\epsilon_c = 2.5\gamma_a$ (64% maximum squeezing), $\phi_0 = 0$, (c) $\epsilon_c = 2.5\gamma_a$, $\phi_0 = \pi/2$.

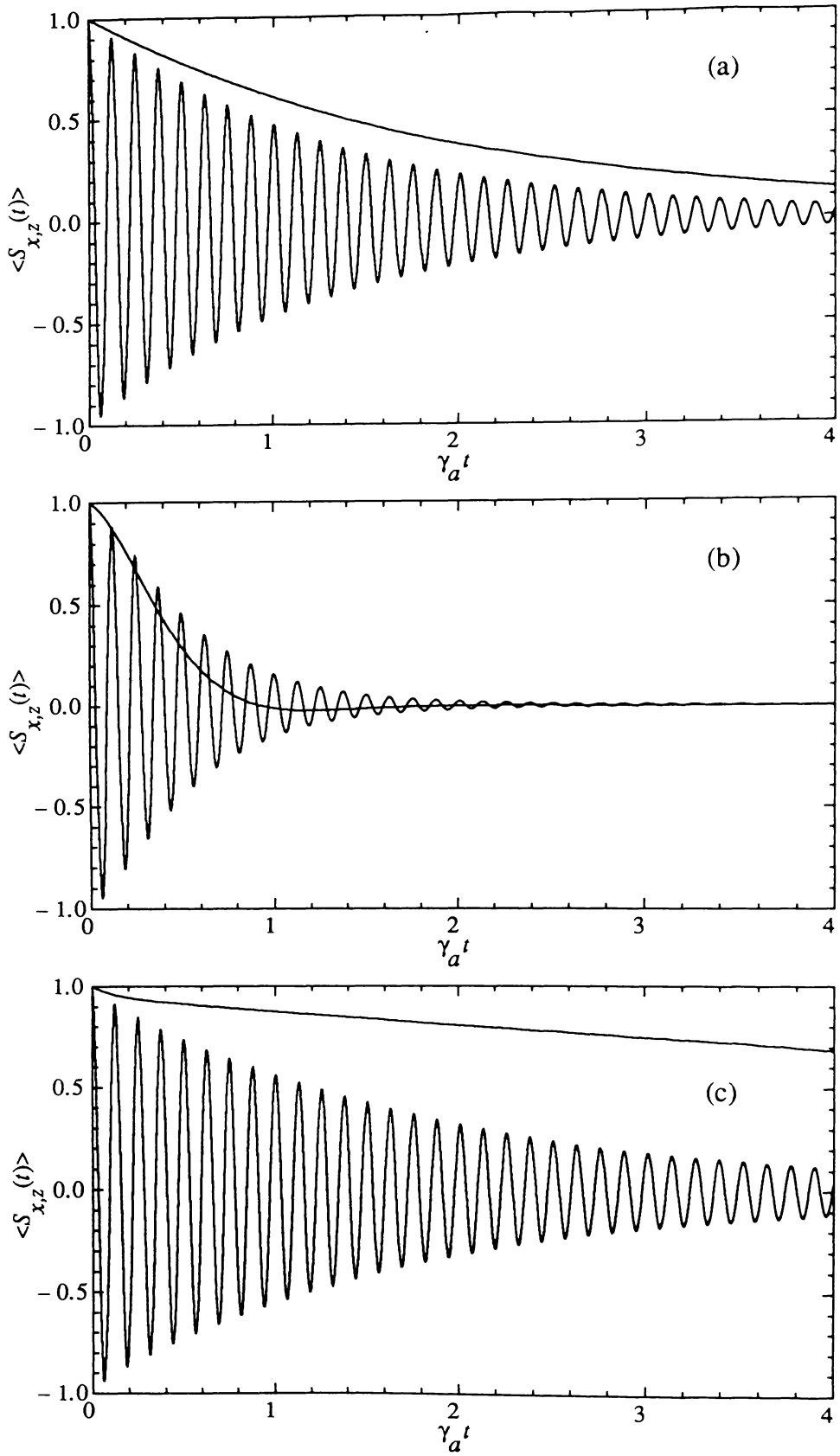


**Fig.5.10** Spin averages $\langle S_x(t) \rangle$ and $\langle S_z(t) \rangle$ (oscillating) computed by simulation (5000 trials) for $\Omega_0 = 50\gamma_a$, $\Delta_a = 0$, $\delta_c = 50\gamma_a$, $\gamma_c = 10\gamma_a$, with (a) $\epsilon_c = 0$ (no squeezing), (b) $\epsilon_c = 5.0\gamma_a$ (89% maximum squeezing), $\phi_0 = 0$, (c) $\epsilon_c = 5.0\gamma_a$, $\phi_0 = \pi/2$.

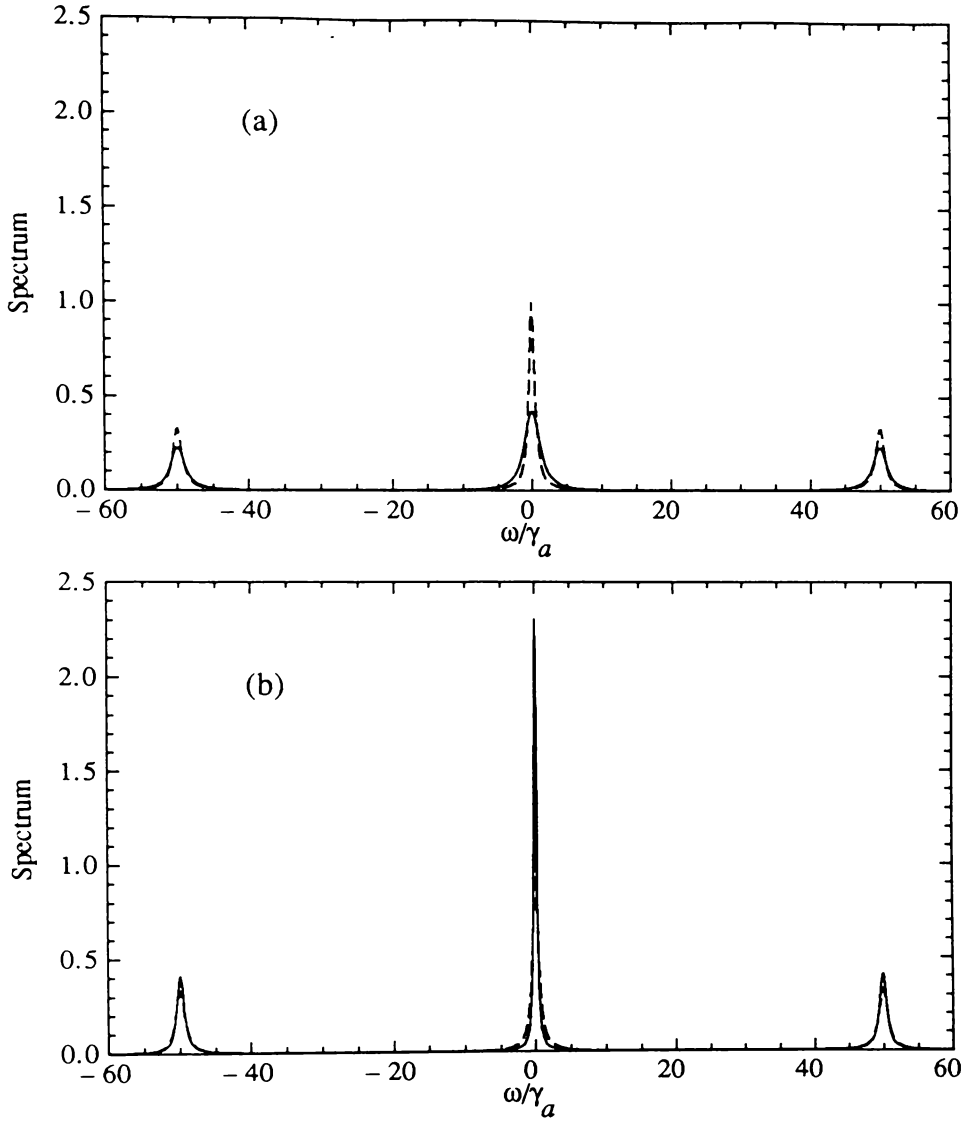


**Fig.5.11** Incoherent fluorescence spectrum, omitting reflections, computed by simulation (20000 trials) for the parameters of Fig.5.9 with (a) $\phi_0 = 0$, (b) $\phi_0 = \pi/2$. The dashed curve in each figure is the ordinary vacuum spectrum.

and broadening of the spectral peaks. For $\phi_0 = 0$, all three peaks are broadened, while for $\phi_0 = \pi/2$, all three peaks exhibit some degree of narrowing compared to their ordinary vacuum profiles. Although the extent of narrowing in the sidebands is modest (remember we are considering an input with only 64% maximum squeezing), it is important to note the contrast with the single-mode white noise squeezing model, which, for the same amount of squeezing yields sidebands with significantly broadened linewidths. With increased levels of squeezing, more substantial narrowing of the sidebands occurs in the two-mode model, and the contrast is even more pronounced. We note that the linewidths observed in the fluorescence spectra of Fig.5.11 are in good agreement with the decay rates exhibited

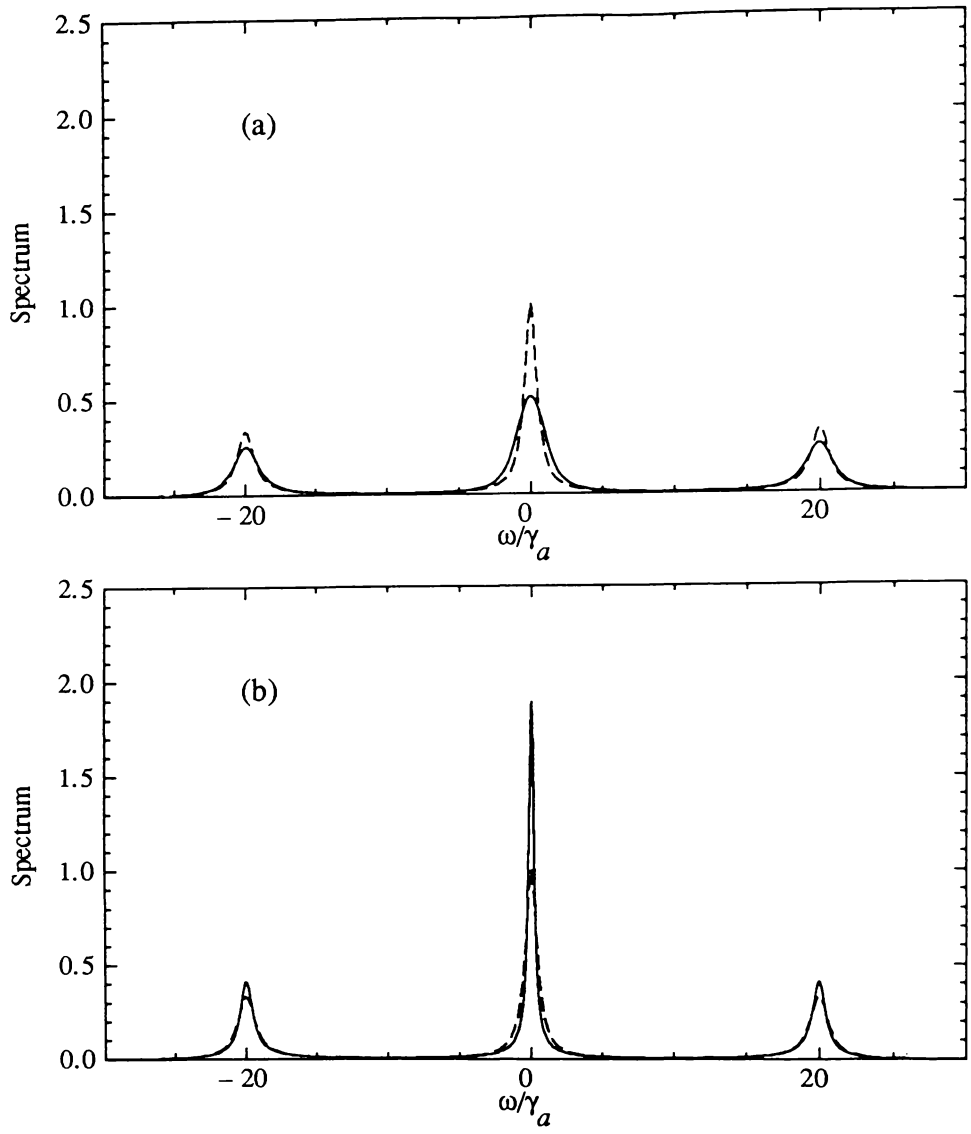


**Fig.5.12** Incoherent fluorescence spectrum, omitting reflections, computed by simulation (8000 trials) for $\Omega_0 = 20\gamma_a$, $\Delta_a = 0$, $\delta_c = 20\gamma_a$, $\gamma_c = 2\gamma_a$, $\epsilon_c = 0.6\gamma_a$ (71% maximum squeezing), with (a) $\phi_0 = 0$, (b) $\phi_0 = \pi/2$. The dashed curve in each figure is the ordinary vacuum spectrum.

by the simple spin averages in Fig.5.9.

As in the single-mode squeezing analysis, it is a worthwhile exercise to gauge the extent to which the effects of narrowing and broadening in the fluorescence spectrum persist for values of the parameters that do not strictly satisfy the conditions upon which earlier predictions were made. This may well be a problem facing any realistic experiment. We consider the case in which the squeezed vacuum bandwidth is only of the order of the atomic linewidth (i.e. $b_\pm \sim \gamma_a$), and, in addition, we reduce the Rabi frequency to the value $\Omega_0 = 20\gamma_a$. The fluorescence spectra are shown in Fig.5.12. As one might

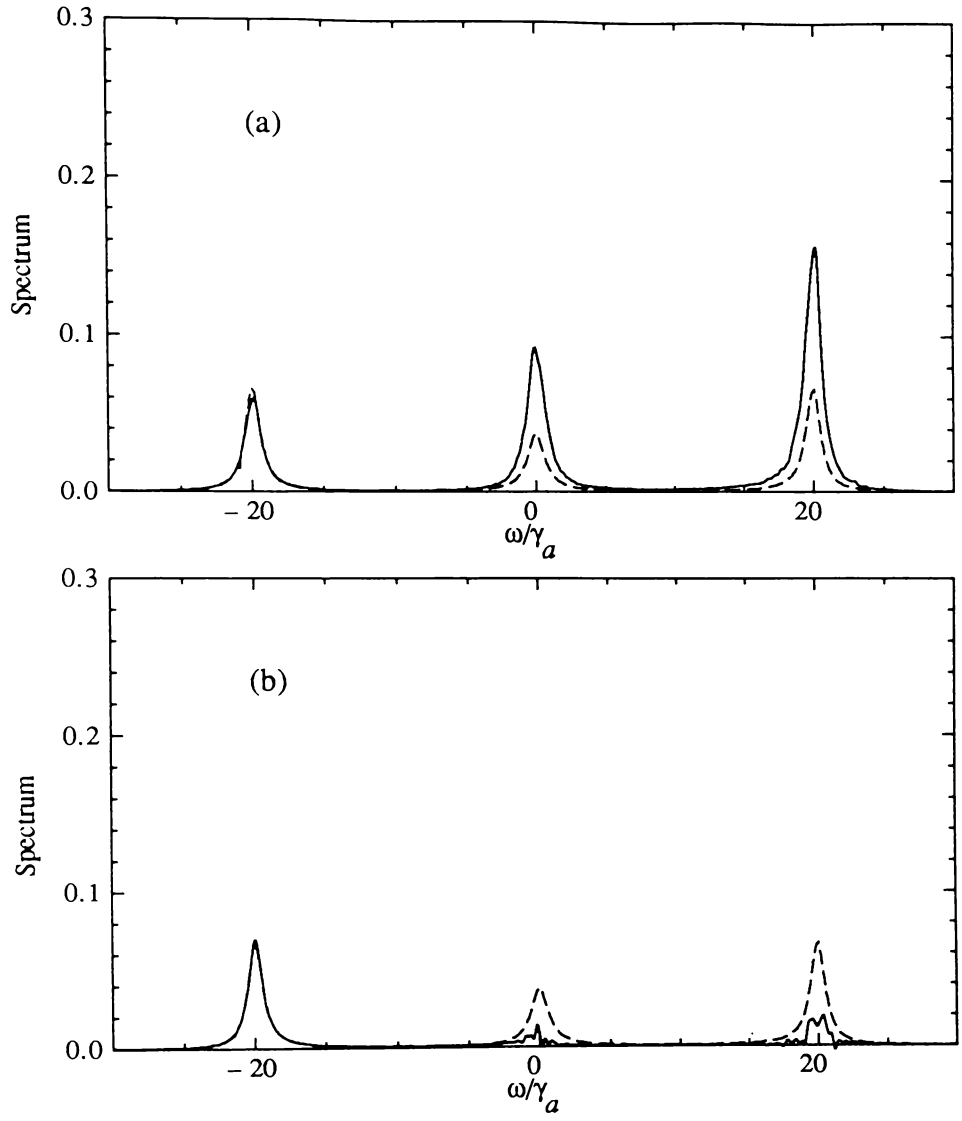


**Fig.5.13** Incoherent fluorescence spectrum, omitting reflections, computed by simulation (20000 trials) for $\Omega_0 = 14.14\gamma_a$, $\Delta_a = 14.14\gamma_a$, $\delta_c = 20\gamma_a$, $\gamma_c = 2\gamma_a$, $\epsilon_c = 0.173\gamma_a$ (29% maximum squeezing), with (a) $\phi_0 = 0$, (b) $\phi_0 = \pi/2$. The dashed curve in each figure is the ordinary vacuum spectrum.

expect, the extent of line narrowing and broadening is somewhat reduced compared to the results obtained under more ideal conditions, as in Fig.5.11. However, the effects are still plainly visible, which enables us to conclude that the basic predictions of Section 5.3.3 are reasonably robust in the face of non-ideal inputs.

The inclusion of a nonzero laser-atom detuning ($\Delta_a \neq 0$) substantially complicates any analytical computation. However, nonzero detuning presents no substantial additional difficulties from the point of view of simulation. In view of the unusual spectrum of noise experienced by the atom, we might expect some interesting phenomena, especially when

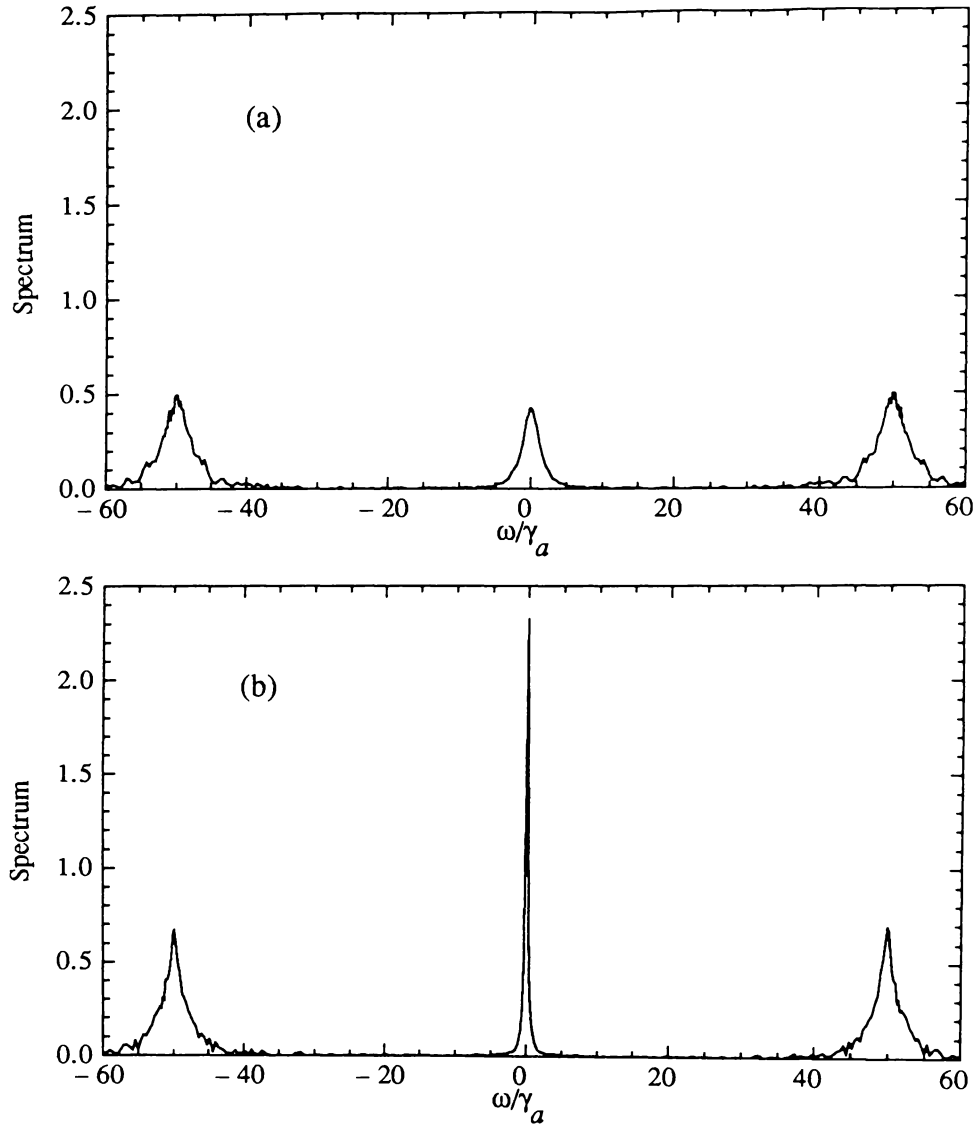


**Fig.5.14** Incoherent fluorescence spectrum, including reflections, computed by simulation (20000 trials) for the parameters of Fig.5.11 with (a) $\phi_0 = 0$, (b) $\phi_0 = \pi/2$.

$\Omega_0^2 + \Delta_a^2 = \delta_c^2$. This is indeed the case, as we demonstrate in Fig.5.13. It is clear that the response of the zero-frequency and oscillating components of the Bloch vector to the squeezed noise allows for a significant modification of the ordinary fluorescence spectrum. The asymmetry in the spectrum, and the enhancement or suppression of peaks (to an extent that is dependent also on the phase $\phi_0$), is quite dramatic and suggests alternative signatures one might look for in detecting squeezed light. Indeed, it is interesting to note the relatively small amount of squeezing required to produce significant effects. Similar phenomena have been seen in analyses of the interaction of (single-mode) broad bandwidth squeezed light with two-level atoms (Courty and Reynaud, 1989, Kennedy and Walls, 1990) and have been described in terms of dressed state population trapping

(Courty and Reynaud, 1989). We shall return to this feature in the next section.

**(c) Reflections**

With the inclusion of reflections in the output field, the squeezed vacuum power spectrum contributes peaks at the frequencies $\omega_0 \pm \delta_c$. In general, these peaks dominate the much smaller Rabi sidebands that appear at the same frequencies ($\Omega_0 = \delta_c$, $\Delta_a = 0$). However, the central atomic fluorescence peak, which is well separated from the sidebands, is essentially unaffected by the inclusion of reflections, so the most significant line narrowing and broadening is still clearly visible in the spectrum. To highlight these points, we display, in Fig.5.14, the fluorescence spectrum with reflections of the squeezed input included. The spectra obtained with reflections included are inherently more noisy than the simple atomic fluorescence spectra. This can, of course, be alleviated by averaging over a greater number of trials.

## 5.4 Resonance Fluorescence with Detuning: A General Approach

In the previous section, we touched briefly upon the additional possibilities that arise in the fluorescence spectrum when a nonzero laser-atom detuning is included. Courty and Reynaud (1989) have highlighted some of these possibilities in a study of strongly-driven resonance fluorescence in a broad bandwidth squeezed vacuum. They showed that a suitable choice of detuning can lead to the disappearance of inelastic peaks in the fluorescence triplet, and, moreover, that this effect does not require a large amount of squeezing.

The result presented in Fig.5.13 clearly exhibits some of these same features, and thus we are prompted to attempt an approximate analytical solution that will reveal more clearly the available possibilities. In doing so, we will develop an approach that can be adapted, under suitable conditions, to any of the three kinds of squeezing so far considered in this thesis (single-mode broad and narrow bandwidth, and two-mode), and which thus allows us to assess their respective merits, as regards the effects of nonzero detuning.

### 5.4.1 General equations of motion

The stochastic equations of motion, after averaging over the ordinary vacuum noise, can be written in the general form

$$\dot{\mathbf{S}} = (\underline{D} + \underline{A})\mathbf{S} + \mathbf{G} + \beta_X^c(t)\underline{X}\,\mathbf{S} + \beta_Y^c(t)\underline{Y}\,\mathbf{S}\ , \tag{5.4.1}$$

where

$$\mathbf{S} = \begin{pmatrix} \bar{S}_x \\ \bar{S}_y \\ \bar{S}_z \end{pmatrix} \quad , \quad \mathbf{G} = \begin{pmatrix} 0 \\ 0 \\ -\gamma_a \end{pmatrix} , \tag{5.4.2}$$

$$\underline{D} = \begin{bmatrix} -\gamma_a/2 & 0 & 0 \\ 0 & -\gamma_a/2 & 0 \\ 0 & 0 & -\gamma_a \end{bmatrix} \quad , \quad \underline{A} = \begin{bmatrix} 0 & -\Delta_a & 0 \\ \Delta_a & 0 & -\Omega_0 \\ 0 & \Omega_0 & 0 \end{bmatrix} , \tag{5.4.3}$$

and

$$\underline{X} = \begin{bmatrix} 0 & 0 & -1 \\ 0 & 0 & 0 \\ 1 & 0 & 0 \end{bmatrix} \quad , \quad \underline{Y} = \begin{bmatrix} 0 & 0 & 0 \\ 0 & 0 & -1 \\ 0 & 1 & 0 \end{bmatrix} \tag{5.4.4}$$

The noise terms, $\beta_X^c(t)$ and $\beta_Y^c(t)$, which represent the squeezing, can be written in terms of the independent noise sources $\beta_1^c(t)$ and $\beta_2^c(t)$ as

$$\beta_X^c(t) = -\sin(\phi_0)\beta_1^c(t) + \cos(\phi_0)\beta_2^c(t), \tag{5.4.5}$$

$$\beta_Y^c(t) = \cos(\phi_0)\beta_1^c(t) + \sin(\phi_0)\beta_2^c(t), \tag{5.4.6}$$

where $\phi_0$ is the phase of the coherent driving field. The statistics of these noises depend, of course, on the particular type of squeezing being considered.

We are interested in the situation in which the generalised Rabi frequency, $\Omega = \sqrt{\Omega_0^2 + \Delta_a^2}$, is large, in which case the solutions to (5.4.1) are rapidly oscillating functions of time, and the three peaks of the fluorescence triplet are well-separated. We can remove this rapid time dependence from the equations of motion by transforming to a frame defined by

$$\mathbf{S}(t) = e^{\underline{A}t}\,\mathbf{S}'(t), \tag{5.4.7}$$

where the exponential $e^{\underline{A}t}$ is given by (Allen and Eberly, 1975)

$$e^{\underline{A}t} = \begin{bmatrix} \frac{\Omega_0^2}{\Omega^2} + \frac{\Delta_a^2}{\Omega^2}\cos(\Omega t) & -\frac{\Delta_a}{\Omega}\sin(\Omega t) & \frac{\Delta_a}{\Omega}\sin(\Omega t) \\ \frac{\Delta_a}{\Omega}\sin(\Omega t) & \cos(\Omega t) & -\frac{\Omega_0}{\Omega}\sin(\Omega t) \\ \frac{\Delta_a}{\Omega}\sin(\Omega t) & \frac{\Omega_0}{\Omega}\sin(\Omega t) & \frac{\Delta_a^2}{\Omega^2} + \frac{\Omega_0^2}{\Omega^2}\cos(\Omega t) \end{bmatrix} \tag{5.4.8}$$

The equation of motion for $\mathbf{S}'$ takes the form

$$\begin{aligned} \dot{\mathbf{S}}' = &\left(e^{-\underline{A}t}\,\underline{D}\,e^{\underline{A}t}\right)\mathbf{S}' + e^{-\underline{A}t}\,\mathbf{G} \\ &+ \left(e^{-\underline{A}t}\,\underline{X}\,e^{\underline{A}t}\right)\beta_X^c(t)\mathbf{S}' + \left(e^{-\underline{A}t}\,\underline{Y}\,e^{\underline{A}t}\right)\beta_Y^c(t)\mathbf{S}'. \end{aligned} \tag{5.4.9}$$

The components of $\mathbf{S}'$ are considered to be slowly varying, which allows us to invoke the secular approximation in the deterministic part of this equation; that is, we drop any rapidly-rotating terms from the first two terms in (5.4.9), but we leave the stochastic terms for the moment, as we have not yet specified the type of squeezing. The equations of motion for the components of $\mathbf{S}'$ are thus

$$\begin{aligned} \dot{\bar{S}}_x{}' = &-\frac{\gamma_a}{2}\left[1 + \frac{3}{2}\left(\frac{\Delta_a\Omega_0}{\Omega^2}\right)^2\right]\bar{S}_x{}' + \frac{\gamma_a}{2}\frac{\Delta_a\Omega_0}{\Omega^2}\left(\frac{\Omega_0^2 - 2\Delta_a^2}{2\Omega^2}\right)\bar{S}_z{}' \\ &+ \beta_X^c(t)\left\{-\frac{\Omega_0}{\Omega}\sin(\Omega t)\bar{S}_y{}' - \cos(\Omega t)\bar{S}_z{}'\right\} \\ &+ \beta_Y^c(t)\left\{-\frac{\Delta_a\Omega_0}{\Omega^2}[1 - \cos(\Omega t)]\bar{S}_y{}' - \frac{\Delta_a}{\Omega}\sin(\Omega t)\bar{S}_z{}'\right\} \\ &- \gamma_a\frac{\Delta_a\Omega_0}{\Omega^2}, \end{aligned} \tag{5.4.10}$$

$$\begin{aligned} \dot{\bar{S}}_y{}' = &-\frac{\gamma_a}{2}\left(1 + \frac{\Omega_0^2}{2\Omega^2}\right)\bar{S}_y{}' \\ &+ \beta_X^c(t)\left\{\frac{\Omega_0}{\Omega}\sin(\Omega t)\bar{S}_x{}' + \frac{\Delta_a}{\Omega}\sin(\Omega t)\bar{S}_z{}'\right\} \\ &+ \beta_Y^c(t)\left\{\frac{\Delta_a\Omega_0}{\Omega^2}[1 - \cos(\Omega t)]\bar{S}_x{}' - \left[\frac{\Omega_0^2}{\Omega^2} + \frac{\Delta_a^2}{\Omega^2}\cos(\Omega t)\right]\bar{S}_z{}'\right\}, \end{aligned} \tag{5.4.11}$$

$$\dot{\bar{S}}_z{}' = -\gamma_a\left(\frac{\frac{3}{4}\Omega_0^4 + \Delta_a{}^2\Omega_0^2 + \Delta_a^4}{\Omega^4}\right)\bar{S}_z{}' + \frac{\gamma_a}{2}\frac{\Delta_a\Omega_0}{\Omega^2}\left(\frac{\Omega_0^2 - 2\Delta_a{}^2}{2\Omega^2}\right)\bar{S}_x{}'$$
$$+ \beta_X^c(t)\left\{\cos(\Omega t)\bar{S}_x{}' - \frac{\Delta_a}{\Omega}\sin(\Omega t)\bar{S}_y{}'\right\}$$
$$+ \beta_Y^c(t)\left\{\frac{\Delta_a}{\Omega}\sin(\Omega t)\bar{S}_x{}' + \left[\frac{\Omega_0^2}{\Omega^2} + \frac{\Delta_a^2}{\Omega^2}\cos(\Omega t)\right]\bar{S}_y{}'\right\} \qquad (5.4.12)$$
$$- \gamma_a\frac{\Delta_a^2}{\Omega^2}.$$

### 5.4.2 Stochastic secular approximation

The noise sources $\beta_X^c(t)$ and $\beta_Y^c(t)$ appearing in (5.4.10-12) are multiplied either by a rapidly oscillating cosine or sine function, or by a constant. Since the components of $\mathbf{S}'$ are slowly varying functions of time, it follows that the contributions of the stochastic terms to the time development of $\mathbf{S}'$ will be significant only if these terms exhibit Fourier components about zero frequency. This same argument was, of course, used in Sections 5.2.2 and 5.3.2 to qualitatively predict the effects of finite bandwidth squeezing. We now wish to use this approach more explicitly, simply dropping those terms that are not "resonant" with the time behaviour exhibited by $\mathbf{S}'$. The remaining stochastic terms are then treated as white noise terms, after which averaging may be carried out in a standard fashion.

(a) Single-mode broad bandwidth squeezing

In this case, none of the stochastic terms can be neglected, as $\beta_X^c(t)$ and $\beta_Y^c(t)$ are in fact white noises, with significant spectral components over the whole of frequency space. Averaging must therefore be carried out with the equations as they appear in (5.4.10-12), and with

$$\langle\beta_1^c(t)\beta_1^c(t')\rangle = 2\gamma_a(N - M)\delta(t - t'), \qquad (5.4.13)$$

$$\langle\beta_2^c(t)\beta_2^c(t')\rangle = 2\gamma_a(N + M)\delta(t - t'). \qquad (5.4.14)$$

This process is straightforward, but somewhat tedious.

(b) Single-mode narrow bandwidth squeezing

The noise terms for this case satisfy

$$\langle\beta_1^c(t)\beta_1^c(t')\rangle = \gamma_a(N - M)b_- e^{-b_-|t-t'|}, \qquad (5.4.15)$$

$$\langle\beta_2^c(t)\beta_2^c(t')\rangle = \gamma_a(N + M)b_+ e^{-b_+|t-t'|}, \qquad (5.4.16)$$

with $b_\pm \ll \Omega$. Hence, many of the stochastic terms appearing in (5.4.10-12) can be dropped, and we are left with the equations

$$\dot{\bar{S}}_x' \simeq -\frac{\gamma_a}{2}\left[1+\frac{3}{2}\left(\frac{\Delta_a\Omega_0}{\Omega^2}\right)^2\right]\bar{S}_x' + \frac{\gamma_a}{2}\frac{\Delta_a\Omega_0}{\Omega^2}\left(\frac{\Omega_0^2-2\Delta_a^2}{2\Omega^2}\right)\bar{S}_z' - \frac{\Delta_a\Omega_0}{\Omega^2}\left[\beta_1^c(t)\cos(\phi_0)+\beta_2^c(t)\sin(\phi_0)\right]\bar{S}_y' - \gamma_a\frac{\Delta_a\Omega_0}{\Omega^2}, \tag{5.4.17}$$

$$\dot{\bar{S}}_y' \simeq -\frac{\gamma_a}{2}\left(1+\frac{\Omega_0^2}{2\Omega^2}\right)\bar{S}_y' + \frac{\Omega_0}{\Omega}\left[\beta_1^c(t)\cos(\phi_0)+\beta_2^c(t)\sin(\phi_0)\right]\left(\frac{\Delta_a}{\Omega}\bar{S}_x' - \frac{\Omega_0}{\Omega}\bar{S}_z'\right), \tag{5.4.18}$$

$$\dot{\bar{S}}_z' \simeq -\gamma_a\left(\frac{\frac{3}{4}\Omega_0^4+\Delta_a^2\Omega_0^2+\Delta_a^4}{\Omega^4}\right)\bar{S}_z' + \frac{\gamma_a}{2}\frac{\Delta_a\Omega_0}{\Omega^2}\left(\frac{\Omega_0^2-2\Delta_a^2}{2\Omega^2}\right)\bar{S}_x' + \frac{\Omega_0^2}{\Omega^2}\left[\beta_1^c(t)\cos(\phi_0)+\beta_2^c(t)\sin(\phi_0)\right]\bar{S}_y' - \gamma_a\frac{\Delta_a^2}{\Omega^2}. \tag{5.4.19}$$

If we now assume that $b_+$ and $b_-$ are much greater than the decay rates of the spin components, then, in (5.4.17-19), we can approximate $\beta_{1,2}^c(t)$ with white noises, setting

$$b_\pm e^{-\overset{b}{\beta_\pm}|t-t'|} \rightarrow 2\delta(t-t'), \tag{5.4.20}$$

and carrying out the average as before.

(c) Two-mode narrow bandwidth squeezing

This is more complicated than the other cases, as $\beta_1^c(t)$ and $\beta_2^c(t)$ satisfy

$$\langle\beta_1^c(t)\beta_1^c(t')\rangle = 2\gamma_a(N-M)b_-e^{-b_-|t-t'|}\cos[\delta_c(t-t')], \tag{5.4.21}$$

$$\langle\beta_2^c(t)\beta_2^c(t')\rangle = 2\gamma_a(N+M)b_+e^{-b_+|t-t'|}\cos[\delta_c(t-t')], \tag{5.4.22}$$

and, hence, we must write $\beta_1^c(t)$ and $\beta_2^c(t)$ in terms of four independent noise sources as

$$\beta_1^c(t) = \beta_{1a}^c(t)\cos(\delta_c t) + \beta_{1b}^c(t)\sin(\delta_c t), \tag{5.4.23}$$

$$\beta_2^c(t) = \beta_{2a}^c(t)\cos(\delta_c t) + \beta_{2b}^c(t)\sin(\delta_c t), \tag{5.4.24}$$

with the statistics of $\beta_{1a,b}^c(t)$ and $\beta_{2a,b}^c(t)$ following from (5.4.21,22). As in Section 5.3, we expect the most significant effects to occur when $\delta_c$ is "tuned" to the sidebands of the

fluorescence triplet, so we choose $\delta_c = \Omega$. In the equations (5.4.10-12), we then retain only those stochastic terms involving the factors $\cos(\delta_c t)\cos(\Omega t)$ and $\sin(\delta_c t)\sin(\Omega t)$, and we replace these factors by $1/2$. The equations that result are somewhat more complicated than (5.4.17-19), but, again, we treat $\beta^c_{1a,b}(t)$ and $\beta^c_{2a,b}(t)$ as white noises, and perform the average accordingly.

### 5.4.3 Solutions for the spin averages

The solutions for the spin averages, after transforming back to the original frame, are identical in form for the three cases, differing only in the eigenvalues $\lambda_{1,2}$. The solutions are

$$\begin{aligned}\langle S_x(t)\rangle = &\left[\frac{\Omega_0^2}{\Omega^2}e^{\lambda_2 t} + \frac{\Delta_a^2}{\Omega^2}e^{\lambda_1 t}\cos(\Omega t)\right]\langle S_x(0)\rangle - \frac{\Delta_a}{\Omega}e^{\lambda_1 t}\sin(\Omega t)\langle S_y(0)\rangle \\ &+ \frac{\Delta_a\Omega_0}{\Omega^2}\left[e^{\lambda_2 t} - e^{\lambda_1 t}\cos(\Omega t)\right]\langle S_z(0)\rangle \\ &- \frac{\Delta_a\Omega_0}{\Omega^2}\frac{\gamma_a}{\lambda_2}\left(e^{\lambda_2 t} - 1\right), \qquad (5.4.25)\end{aligned}$$

$$\begin{aligned}\langle S_y(t)\rangle = &\frac{\Delta_a}{\Omega}e^{\lambda_1 t}\sin(\Omega t)\langle S_x(0)\rangle + e^{\lambda_1 t}\cos(\Omega t)\langle S_y(0)\rangle \\ &- \frac{\Omega_0}{\Omega}e^{\lambda_1 t}\sin(\Omega t)\langle S_z(0)\rangle, \qquad (5.4.26)\end{aligned}$$

$$\begin{aligned}\langle S_z(t)\rangle = &\frac{\Delta_a\Omega_0}{\Omega^2}\left[e^{\lambda_2 t} - e^{\lambda_1 t}\cos(\Omega t)\right]\langle S_x(0)\rangle + \frac{\Omega_0}{\Omega}e^{\lambda_1 t}\sin(\Omega t)\langle S_y(0)\rangle \\ &+ \left[\frac{\Delta_a^2}{\Omega^2}e^{\lambda_2 t} + \frac{\Omega_0^2}{\Omega^2}e^{\lambda_1 t}\cos(\Omega t)\right]\langle S_z(0)\rangle \\ &- \frac{\Delta_a^2}{\Omega^2}\frac{\gamma_a}{\lambda_2}\left(e^{\lambda_2 t} - 1\right), \qquad (5.4.27)\end{aligned}$$

where the (real) eigenvalues $\lambda_{1,2}$ for the three different cases are:

(a) Single-mode broad bandwidth squeezing:

$$\begin{aligned}\lambda_1 &= -\frac{\gamma_a}{2}\left\{\left(1 + \frac{\Omega_0^2}{2\Omega^2}\right) + N\left(2 + \frac{\Omega_0^2}{\Omega^2}\right) - M\cos(2\phi_0)\left(1 - \frac{\Delta_a^2}{\Omega^2}\right)\right\}, \\ \lambda_2 &= -\frac{\gamma_a}{2}\left\{\left(2 - \frac{\Omega_0^2}{\Omega^2}\right) + 2N\left(1 + \frac{\Delta_a^2}{\Omega^2}\right) + 2M\cos(2\phi_0)\left(1 - \frac{\Delta_a^2}{\Omega^2}\right)\right\}. \qquad (5.4.28)\end{aligned}$$

(b) Single-mode narrow bandwidth squeezing:

$$\begin{aligned}\lambda_1 &= -\frac{\gamma_a}{2}\left\{\left(1 + \frac{\Omega_0^2}{2\Omega^2}\right) + \frac{\Omega_0^2}{\Omega^2}[2N - 2M\cos(2\phi_0)]\right\}, \\ \lambda_2 &= -\frac{\gamma_a}{2}\left(2 - \frac{\Omega_0^2}{\Omega^2}\right). \qquad (5.4.29)\end{aligned}$$

(c) Two-mode narrow bandwidth squeezing:

$$\lambda_1 = -\frac{\gamma_a}{2}\left\{\left(1+\frac{\Omega_0^2}{2\Omega^2}\right)+N\left(1+\frac{\Delta_a^2}{\Omega^2}\right)+M\cos(2\phi_0)\left(1-\frac{\Delta_a^2}{\Omega^2}\right)\right\},$$
$$\lambda_2 = -\frac{\gamma_a}{2}\left\{\left(2-\frac{\Omega_0^2}{\Omega^2}\right)+2N\left(1+\frac{\Delta_a^2}{\Omega^2}\right)+2M\cos(2\phi_0)\left(1-\frac{\Delta_a^2}{\Omega^2}\right)\right\}. \quad (5.4.30)$$

For zero detuning, $\Delta_a = 0$, these results reproduce all of the basic predictions of earlier calculations. The eigenvalue $\lambda_1$ gives the decay rate of the $\langle S_y\rangle$ and $\langle S_z\rangle$ components, which may be inhibited, for an appropriate choice of phase, with narrow bandwidth squeezing (cases (b) and (c)), but not with the white noise squeezing of case (a). The component $\langle S_x\rangle$ decays at rate $\lambda_2$, which may be greatly reduced for cases (a) and (c), but for case (b) this rate is unchanged from its normal vacuum value.

With a nonzero detuning, the decay rates become mixed and the dynamics somewhat more complicated. However, following the approach of Courty and Reynaud (1989), we can uncover some interesting effects if we look at our results from the point of view of dressed states. In particular, the dressed-state inversion, $w_{dr}$, in the steady state, is related to $\langle S_x(\infty)\rangle$ and $\langle S_z(\infty)\rangle$ via

$$w_{dr} = \frac{\Delta_a}{\Omega}\langle S_z(\infty)\rangle + \frac{\Omega_0}{\Omega}\langle S_x(\infty)\rangle, \quad (5.4.31)$$

which, using (5.4.25-27), can be worked out explicitly as

$$w_{dr} = \frac{\Delta_a}{\Omega}\frac{\gamma_a}{\lambda_2}. \quad (5.4.32)$$

Clearly, for $\Delta_a = 0$, the population is evenly distributed between the dressed states. However, for $\Delta_a \neq 0$, and for $\lambda_2$ of the form found in cases (a) and (c), it is possible to have $|w_{dr}| = 1$, specifically, when

$$|\Delta_a/\Omega| = (2N + 2M + 1)^{-1}, \quad (5.4.33)$$

in which case the population is trapped in one of the dressed states. As a consequence, certain peaks will disappear from the fluorescence spectrum. The condition (5.4.33), which is in agreement with the findings of Courty and Reynaud (1989), is derived using $M^2 = N(N+1)$, and is unique to squeezing; in particular, it is not possible to have $|w_{dr}| = 1$ for a purely thermal field ($N \neq 0$, $M = 0$).

### 5.4.4 Fluorescence spectra

With the assumption that the dynamics are essentially Markovian, we can employ the familiar quantum regression theorem to compute correlation functions of the atomic variables. Omitting reflections, the spectrum is determined from the definition

$$S(\omega) = \int_{-\infty}^{\infty} d\tau\, e^{-i\omega\tau} \langle S^{+}(\tau) S^{-}(0) \rangle . \tag{5.4.34}$$

The form of the spectrum is identical for the three cases, and is given by

$$\begin{aligned} S(\omega) = {} & \frac{\pi}{2} \left( \frac{\Omega_0}{\Omega} w_{dr} \right)^2 \delta(\omega) \\ & - \frac{\gamma_a}{\lambda_2} \frac{\Omega_0^2}{2\Omega^2} \left[ 1 - (w_{dr})^2 \right] \frac{\lambda_2^2}{\lambda_2^2 + \omega^2} \\ & - \frac{\gamma_a}{\lambda_1} \frac{1}{4} \left( 1 + \frac{\Delta_a}{\Omega} \right)^2 (1 + w_{dr}) \frac{\lambda_1^2}{\lambda_1^2 + (\omega - \Omega)^2} \\ & - \frac{\gamma_a}{\lambda_1} \frac{1}{4} \left( 1 - \frac{\Delta_a}{\Omega} \right)^2 (1 - w_{dr}) \frac{\lambda_1^2}{\lambda_1^2 + (\omega + \Omega)^2} . \end{aligned} \tag{5.4.35}$$

It follows that, for $|w_{dr}| = 1$, two of the incoherent components of the spectrum vanish (of course, since we are observing the spectrum through a window of unsqueezed modes, the fluorescence lines will not completely disappear). As one might expect, this is accompanied by an increase in coherent scattering, as represented in (5.4.35) by the $\delta$-function term.

If we now return to the situation of Fig.5.13, for which $N = 0.03$ in the two-mode squeezing configuration, then, in fact, $|w_{dr}|$, as defined above, is identically one for $\phi_0 = \pi/2$. Hence, the features exhibited in Fig.5.13(b) are in general agreement with the analytical results of this section. In Fig.5.15, we plot the incoherent portion of the analytical spectrum (5.4.35) for the parameters of Fig.5.13. The agreement between analytical and simulation spectra is actually very good, if one takes into account the fact that the squeezing bandwidths involved in the simulation were quite small ($b_+ = 0.91\gamma_a$, $b_- = 1.09\gamma_a$).

In the series of figures that follow, we consider the variation in the fluorescence spectra, for the three varieties of squeezing, as we vary the ratio of the detuning $\Delta_a$ to the bare Rabi frequency $\Omega_0$ (keeping $\Omega = \sqrt{\Omega_0^2 + \Delta_a^2}$ fixed). The ordinary vacuum spectrum (which, for ease of comparison, is given in each figure) retains its symmetry as $\Delta_a$ is increased, and the sidebands decrease in size monotonically. With squeezing, the spectrum can become both phase dependent and asymmetric.

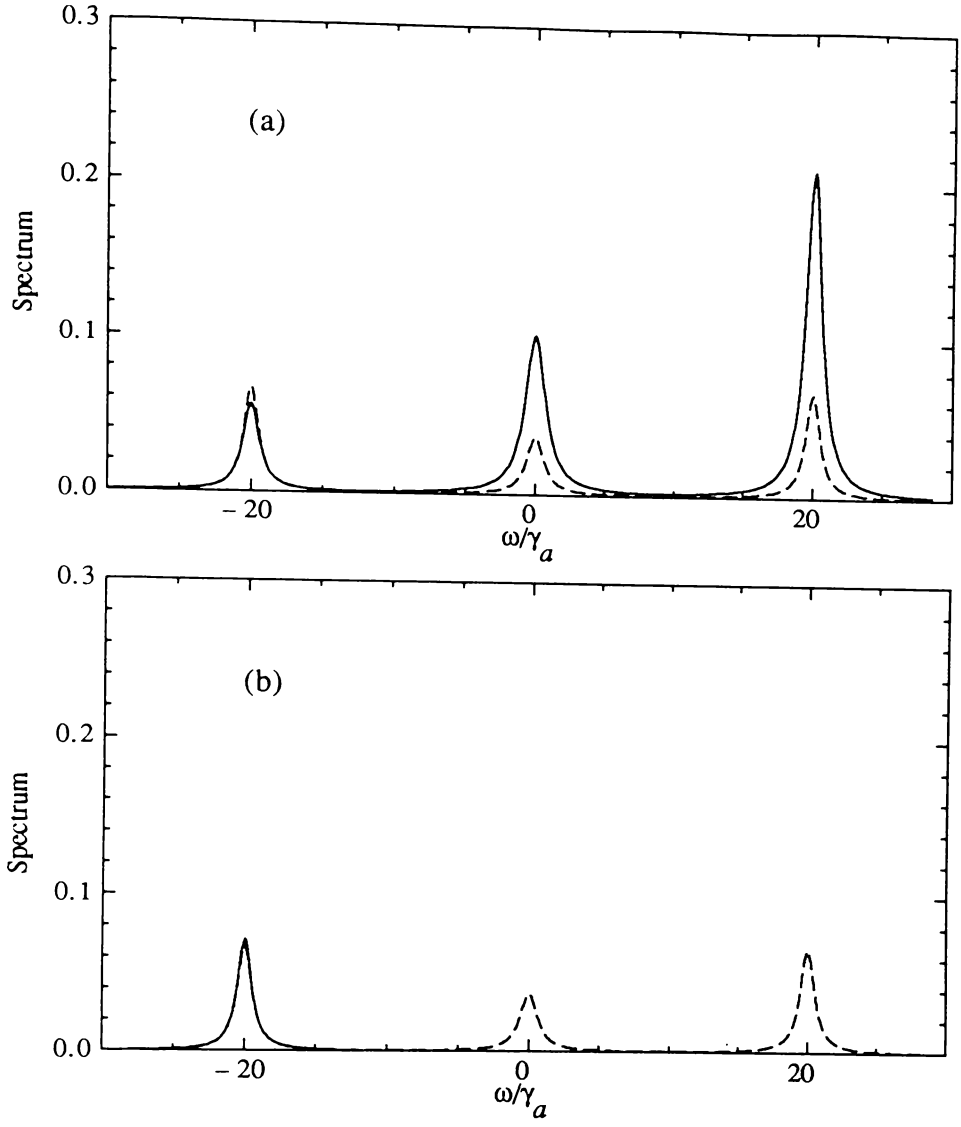


**Fig.5.15** Incoherent fluorescence spectrum computed from Eq.(5.4.35) for two-mode squeezing with $\Omega_0 = 14.14\gamma_a$, $\Delta_a = 14.14\gamma_a$, ($\delta_c = 20\gamma_a$), $N = 0.03$, and (a) $\phi_0 = 0$, (b) $\phi_0 = \pi/2$. The dashed curve in each figure is the ordinary vacuum spectrum.

In Fig.5.16, we plot the incoherent fluorescence spectrum for the case of white noise input squeezing, with $N = 0.125$ (50% squeezing). In addition to the striking phase dependence and asymmetry in the spectra, we see, of course, the disappearance of two spectral peaks for a particular value of the detuning (and of the phase $\phi_0$). This is a clear signature of squeezing, which is made particularly appealing, from an experimental point of view, by the fact that large squeezing is not required to produce it. We note that in Fig.5.16(c) the central peak for the case $\Delta_a = 0$ reaches the value 2.

The spectra one obtains with single-mode narrow bandwidth squeezed light are displayed in Fig.5.17. These spectra exhibit the same trends as the ordinary vacuum spec-

tra, differing only in the size and shape of the sidebands, where broadening or narrowing is now possible depending on the choice of phase. The results are certainly not as dramatic as those found with white noise squeezing.

Finally, in Fig.5.18, we consider two-mode squeezing, with $\delta_c = \Omega$. The spectra are very similar to the white noise spectra of Fig.5.16 (again, the central peak for $\Delta_a = 0$ in Fig.5.18(c) reaches a value of 2), but now some additional enhancement of the sidebands is possible for $\phi_0 = \pi/2$. This follows from the fact that $\lambda_1$ may be reduced below its normal vacuum value when the atom is placed in a two-mode squeezed vacuum.

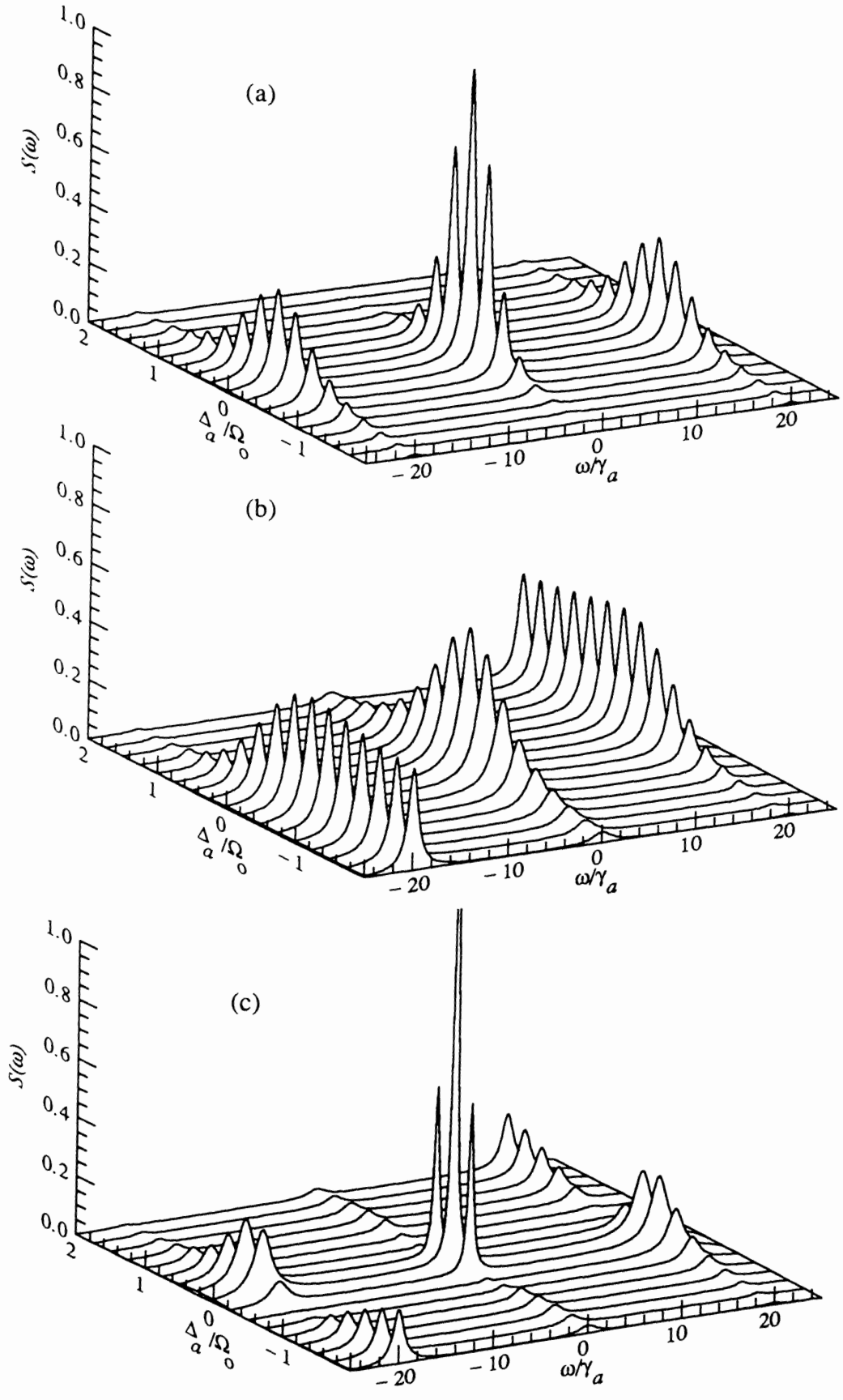


**Fig. 5.16** Incoherent fluorescence spectrum $S(\omega)$ as a function of the detuning $\Delta_a$ (in units of $\Omega_0$, keeping $\Omega = 20$), for (a) no squeezing, and for *single – mode broad bandwidth* squeezing with $N = 0.125$ (50% squeezing) and (b) $\phi_0 = 0$, (c) $\phi_0 = \pi/2$.

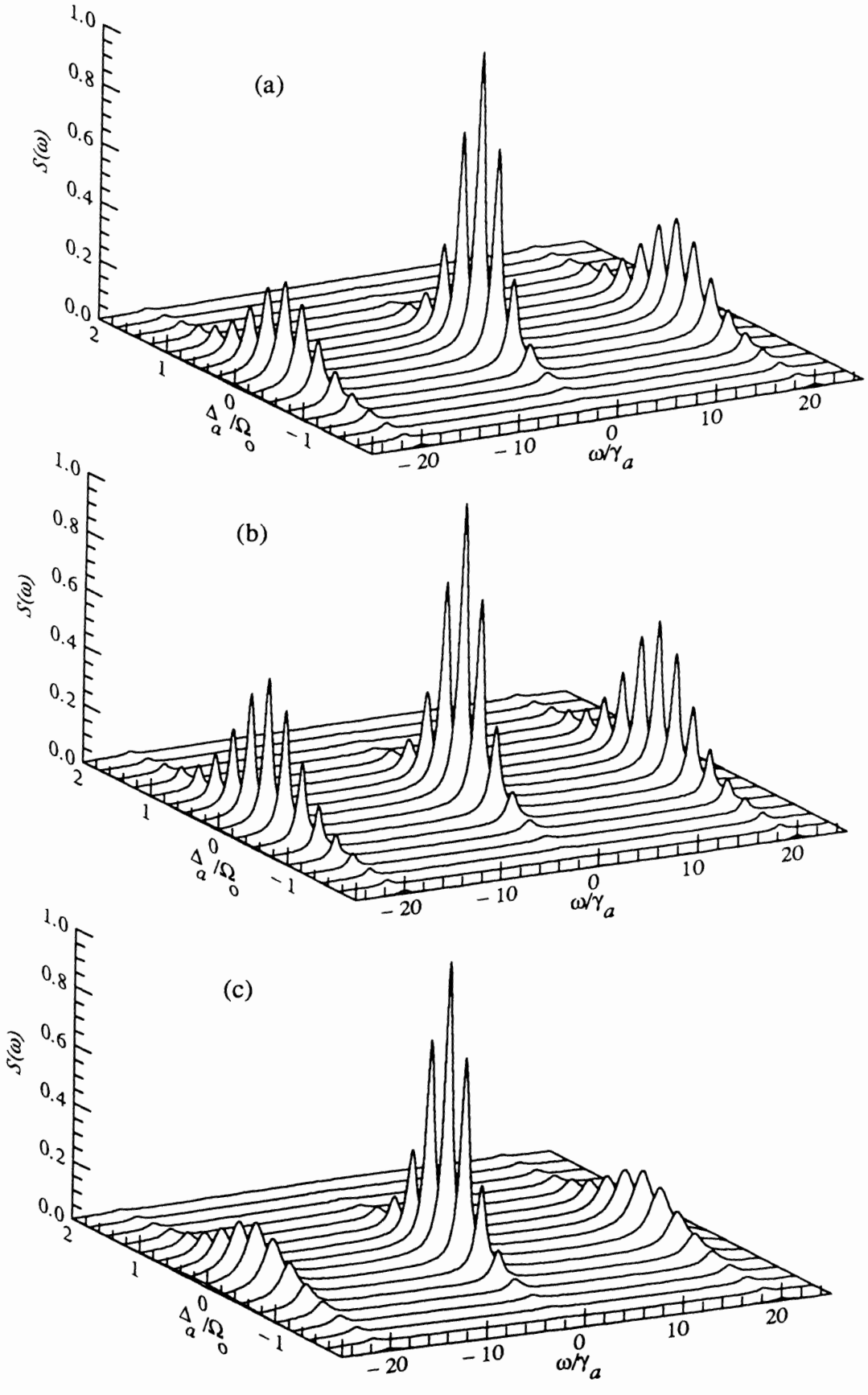


**Fig. 5.17** Incoherent fluorescence spectrum $S(\omega)$ as a function of the detuning $\Delta_a$ (in units of $\Omega_0$, keeping $\Omega = 20$), for (a) no squeezing, and for *single – mode narrow bandwidth* squeezing with $N = 0.125$ (50% squeezing) and (b) $\phi_0 = 0$, (c) $\phi_0 = \pi/2$.

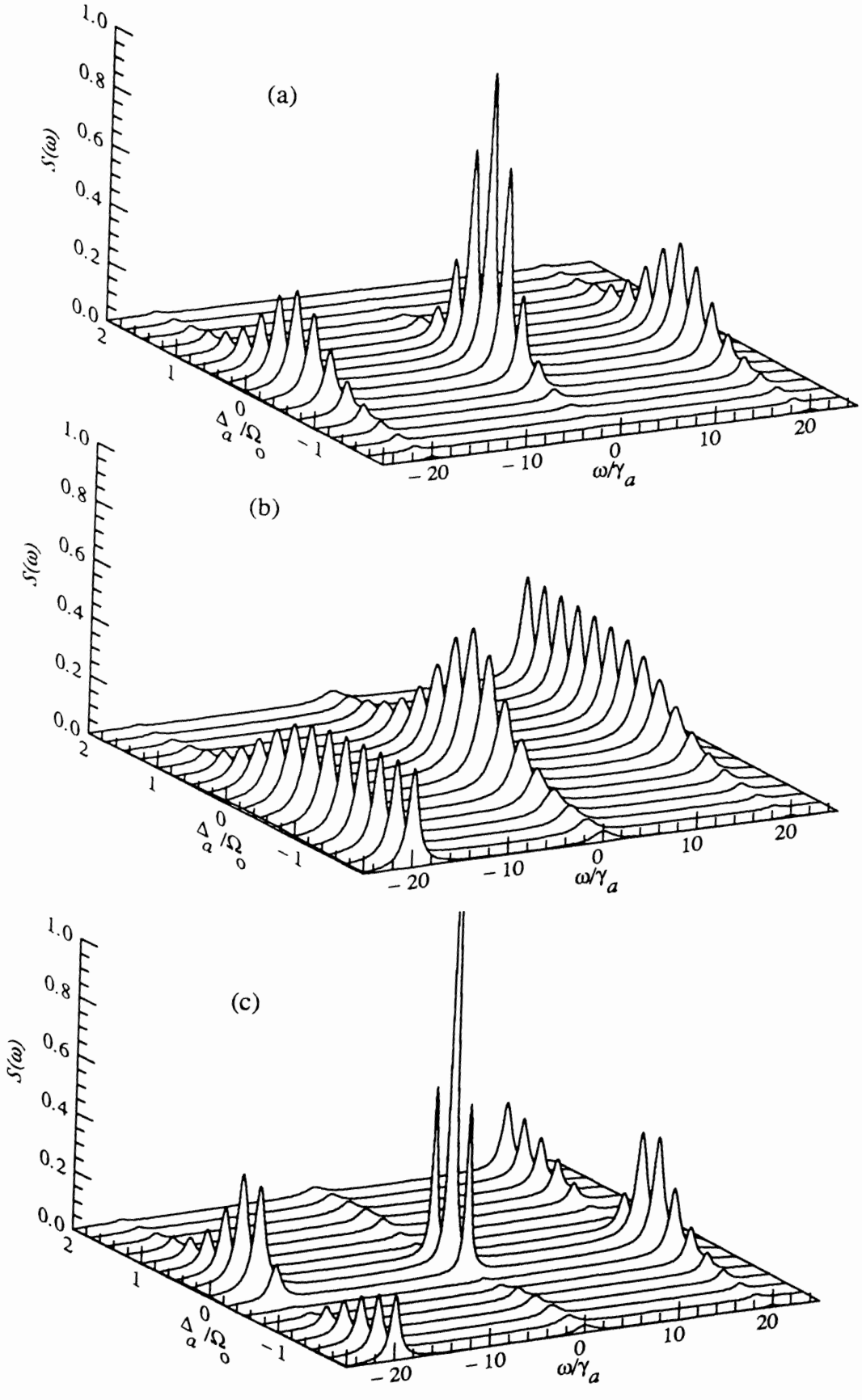


**Fig. 5.18** Incoherent fluorescence spectrum $S(\omega)$ as a function of the detuning $\Delta_a$ (in units of $\Omega_0$, keeping $\Omega = 20$), for (a) no squeezing, and for *two − mode narrow bandwidth* squeezing with $N = 0.125$ (50% squeezing) and (b) $\phi_0 = 0$, (c) $\phi_0 = \pi/2$.

## 5.5 Squeezed Cavity Dynamics

The frequency-dependent spectral density exhibited by an optical cavity offers interesting possibilities for the strongly driven resonance fluorescence of a single, cavity-confined, two-level atom. An analysis of the form given in Section 5.2.2 shows that the decay of the $S_x$ component of the Bloch vector is triggered by cavity vacuum fluctuations at the frequencies $\omega_0 \pm \Omega_0$ (we assume resonance between the atom, cavity, and driving field), while the decay of the $S_y$ and $S_z$ components is in response to fluctuations at the frequencies $\omega_0$ and $\omega_0 \pm \Omega_0$. As pointed out by Lewenstein *et al* (1987, 1988), if the Rabi frequency $\Omega_0$ is much larger than the cavity linewidth $\Gamma$, the cavity vacuum fluctuations that trigger the decay of the $S_x$ component will be negligible, and $S_x$ can be expected to remain virtually constant (as regards decay into the cavity modes). However, the decay of the $S_y$ and $S_z$ components can still be driven by cavity vacuum fluctuations at the frequency $\omega_0$, where the cavity spectral density reaches its peak. In terms of the spectrum of resonance fluorescence, these effects produce a dramatic narrowing of the central peak in the Mollow triplet, together with a limited narrowing of the Rabi sidebands.

Our interest in this particular problem stems from the fact that if we inject a broad bandwidth squeezed vacuum into the cavity, a cavity-confined atom can be made to experience squeezed vacuum fluctuations over a bandwidth $\Gamma$. If we consider the strong driving field limit $\Omega_0 \gg \Gamma$, then we have a close parallel with the work of Section 5.2, except that now the vacuum fluctuations that could not be eliminated for that system (and gave a limit to how narrow we could make the peaks) are removed through the action of the cavity (i.e. the cavity does not support vacuum fluctuations at the frequencies $\pm\Omega_0$). Our previous results therefore lead us to postulate that the decay of all three components of the Bloch vector may be strongly inhibited through the combined action of the injected squeezed vacuum and the cavity spectral density. To confirm this prediction we shall closely follow the working of Lewenstein *et al* (1987, 1988).

### 5.5.1 Cavity model

We consider a single two-level atom located in the centre of a cavity and driven by a laser field of frequency $\omega_0 = \omega_a$. The cavity spectral density is assumed to possess a peak

centered on the frequency $\omega_c = \omega_0$ and adjacent peaks in the spectral density are ignored. We must also allow for coupling to those modes unassociated with the cavity (i.e. modes out the side of the cavity), and hence the reservoir is divided into two parts corresponding to the cavity ($c_k$) and background ($b_k$) modes respectively. The Hamiltonian for this system is written (setting $\hbar = c = 1$), in the rotating wave approximation,

$$\begin{aligned} H =& \frac{\omega_a}{2} S_z + \int dk\ k c_k^\dagger c_k + \int dk\ k b_k^\dagger b_k \\ &+ \frac{\Omega_0}{2} \left( S^- e^{i\omega_0 t - i\phi_0} + S^+ e^{-i\omega_0 t + i\phi_0} \right) \\ &+ \int dk\ [g_c(k) S^+ c_k + h.c.] + \int dk\ [g_b(k) S^+ b_k + h.c.]. \end{aligned} \tag{5.5.1}$$

The coupling to each reservoir is described through the functions $g_c(k)$ and $g_b(k)$, which are proportional to the respective mode densities. The background modes correspond to a free space reservoir and hence contribute equally at all frequencies in the vicinity of $\omega_0$. Therefore, $g_b(k)$ can be regarded as constant, with

$$\int_{-\infty}^{\infty} dk\ |g_b(k)|^2 e^{-ik\tau} = \frac{\gamma_b}{2} \delta(\tau), \tag{5.5.2}$$

where the frequency $\omega_0$ corresponds to $k = 0$ in the rotating frame.

The function $|g_c(k)|^2$, representing the cavity mode density, is modelled as a simple Lorentzian with a maximum value at the cavity resonance frequency. The Lorentzian has a half width at half maximum of $\Gamma$, and satisfies

$$\int_{-\infty}^{\infty} dk\ |g_c(k)|^2 e^{-ik\tau} = \frac{\gamma_c}{2} \Gamma e^{-\Gamma\tau}. \tag{5.5.3}$$

More precisely, we choose

$$g_c(k) = \left( \frac{\gamma_c}{2\pi} \right)^{1/2} \left( \frac{\Gamma}{\Gamma - ik} \right). \tag{5.5.4}$$

The coefficients $\gamma_b$ and $\gamma_c$ give the contributions from the background and cavity modes to the overall (undriven) spontaneous emission rate of the atom. For significant effects to be observable, we will require $\gamma_c$ to be at least comparable to $\gamma_b$. This should be achievable in practice with, for instance, confocal optical resonators (Heinzen *et al*, 1987).

### 5.5.2 Modified Bloch equations

Following Lewenstein *et al*, we derive standard Heisenberg equations of motion from the Hamiltonian (5.5.1), and eliminate the cavity and background photon operators through a first-order expansion in $\gamma_c$ and $\gamma_b$ (Born approximation). In doing so, we require that $\Gamma$ and $\Omega_0$ be much larger than $\gamma_c$ and $\gamma_b$, but we do not perform a Markov approximation with respect to the cavity modes, as the cavity mode reservoir has a finite bandwidth, $\Gamma$, which may only be comparable with the frequency scale $\Omega_0$. The background mode reservoir effectively has an infinite bandwidth, and can therefore be treated as Markovian.

The difference between our work and that of Lewenstein *et al* (1987, 1988) arises when we perform the quantum mechanical average. We allow for cavity-mode correlation functions of the form

$$\langle c_k^\dagger(0)\, c_{k'}(0)\rangle = N\delta(k-k'), \tag{5.5.5}$$

$$\langle c_k^\dagger(0)\, c_{k'}^\dagger(0)\rangle = M\delta(k+k'), \tag{5.5.6}$$

where $M = [N(N+1)]^{1/2}$, and again we have made a choice of phase for the injected squeezed vacuum which corresponds to $M$ real. The relative phase between the coherent driving field and the squeezed vacuum can again be controlled through the phase of the coherent field $\phi_0$. The expressions (5.5.5,6) will be a valid description of the cavity-mode correlation functions provided the injected squeezed field is broadband compared to the cavity linewidth.

With these modifications to the statistics of the cavity-mode reservoir, we derive modified Bloch equations of the form

$$\begin{aligned}\langle \dot{S}_x\rangle = {} & \frac{\gamma_c}{2}\frac{\Gamma}{2}\int_0^t dt'\, e^{-\Gamma(t-t')}\{\langle S_z(t)S_x(t')\rangle - i\langle S_z(t)S_y(t')\rangle + c.c.\} \\ & - \gamma_c[N - M\cos(2\phi_0)]\Gamma\int_0^t dt'\, e^{-\Gamma(t-t')}\cos[\Omega_0(t-t')]\langle S_x(t')\rangle \\ & + \gamma_c M\sin(2\phi_0)\Gamma\int_0^t dt'\, e^{-\Gamma(t-t')}\cos[\Omega_0(t-t')]\langle S_y(t')\rangle \\ & - \gamma_c M\sin(2\phi_0)\Gamma\int_0^t dt'\, e^{-\Gamma(t-t')}\sin[\Omega_0(t-t')]\langle S_z(t')\rangle \\ & - \frac{\gamma_b}{2}\langle S_x\rangle,\end{aligned} \tag{5.5.7}$$

$$\langle \dot{S}_y\rangle = \frac{\gamma_c}{2}\frac{\Gamma}{2}\int_0^t dt'\, e^{-\Gamma(t-t')}\{i\langle S_z(t)S_x(t')\rangle + \langle S_z(t)S_y(t')\rangle + c.c.\}$$

$$
\begin{aligned}
&- \gamma_c[\,N + M\cos(2\phi_0)\,]\Gamma \int_0^t dt'\, e^{-\Gamma(t-t')} \cos[\,\Omega_0(t-t')\,]\langle S_y(t')\rangle \\
&+ \gamma_c M \sin(2\phi_0)\Gamma \int_0^t dt'\, e^{-\Gamma(t-t')} \cos[\,\Omega_0(t-t')\,]\langle S_x(t')\rangle \\
&+ \gamma_c[\,N + M\cos(2\phi_0)\,]\Gamma \int_0^t dt'\, e^{-\Gamma(t-t')} \sin[\,\Omega_0(t-t')\,]\langle S_z(t')\rangle \\
&- \Omega_0\langle S_z\rangle - \frac{\gamma_b}{2}\langle S_y\rangle, \qquad (5.5.8)
\end{aligned}
$$

$$
\begin{aligned}
\langle \dot{S}_z\rangle = &- \frac{\gamma_c}{2}\frac{\Gamma}{2}\int_0^t dt'\, e^{-\Gamma(t-t')}\{\langle S_x(t')S_x(t)\rangle - i\langle S_x(t')S_y(t)\rangle + c.c.\} \\
&- \frac{\gamma_c}{2}\frac{\Gamma}{2}\int_0^t dt'\, e^{-\Gamma(t-t')}\{\langle S_y(t')S_y(t)\rangle + i\langle S_y(t')S_x(t)\rangle + c.c.\} \\
&- \gamma_c[\,N + M\cos(2\phi_0)\,]\Gamma \int_0^t dt'\, e^{-\Gamma(t-t')} \sin[\,\Omega_0(t-t')\,]\langle S_y(t')\rangle \\
&- \gamma_c N\Gamma \int_0^t dt'\, e^{-\Gamma(t-t')}\{1 + \cos[\,\Omega_0(t-t')\,]\}\langle S_z(t')\rangle \\
&+ \gamma_c M\cos(2\phi_0)\Gamma \int_0^t dt'\, e^{-\Gamma(t-t')}\{1 - \cos[\,\Omega_0(t-t')\,]\}\langle S_z(t')\rangle \\
&+ \gamma_c M \sin(2\phi_0)\Gamma \int_0^t dt'\, e^{-\Gamma(t-t')} \sin[\,\Omega_0(t-t')\,]\langle S_x(t')\rangle \\
&+ \Omega_0\langle S_y\rangle - \gamma_b(1 + \langle S_z\rangle), \qquad (5.5.9)
\end{aligned}
$$

where $S_x$ and $S_y$ are as defined in (5.1.4,5).

To be consistent with our first order expansion in $\gamma_c$ and $\gamma_b$, it is sufficient to calculate the correlation functions occurring in (5.5.7-9) in zeroth order (i.e. neglecting all damping). The correlation functions are thus replaced with linear combinations of one-time averages of the spin operators (evaluated at the 'initial' time $t'$). We are again interested in the limit in which $\Omega_0 \gg \Gamma$, and so we in turn replace the $\langle S_i(t')\rangle$ appearing in the integrals with the expressions (5.2.17) (which relate $\langle S_i(t')\rangle$ to $\langle S_i(t)\rangle$ in zeroth order). We also require that $\Gamma$ be larger than any other decay rates featuring in the dynamics, which enables us to set the integrals equal to their stationary ($t \to \infty$) values. The Bloch equations can then be written in the approximate form

$$
\begin{aligned}
\langle \dot{S}_x\rangle \simeq &- \gamma_c\left[N - M\cos(2\phi_0) + \frac{1}{2}\right]\frac{\Gamma^2}{\Gamma^2 + \Omega_0^2}\langle S_x\rangle \\
&+ \gamma_c M \sin(2\phi_0)\langle S_y\rangle - \frac{\gamma_b}{2}\langle S_x\rangle, \qquad (5.5.10) \\
\langle \dot{S}_y\rangle \simeq &- \gamma_c\left[N + M\cos(2\phi_0) + \frac{1}{2}\right]\langle S_y\rangle \\
&+ \gamma_c M \sin(2\phi_0)\frac{\Gamma^2}{\Gamma^2 + \Omega_0^2}\langle S_x\rangle + \gamma_c\frac{\Omega_0\Gamma/2}{\Gamma^2 + \Omega_0^2}
\end{aligned}
$$

$$- \Omega_0 \langle S_z \rangle - \frac{\gamma_b}{2} \langle S_y \rangle, \tag{5.5.11}$$

$$\begin{aligned} \langle \dot{S}_z \rangle \simeq & - \frac{\gamma_c}{2} \left( 1 + \frac{\Gamma^2}{\Gamma^2 + \Omega_0^2} \right) - \gamma_c \left[ N + M \cos(2\phi_0) + \frac{1}{2} \right] \langle S_z \rangle \\ & - \gamma_c \left[ N - M \cos(2\phi_0) + \frac{1}{2} \right] \frac{\Gamma^2}{\Gamma^2 + \Omega_0^2} \langle S_z \rangle \\ & + \gamma_c \left[ N - M \cos(2\phi_0) + \frac{1}{2} \right] \frac{\Gamma \Omega_0}{\Gamma^2 + \Omega_0^2} \langle S_y \rangle \\ & + \gamma_c M \sin(2\phi_0) \frac{\Gamma \Omega_0}{\Gamma^2 + \Omega_0^2} \langle S_x \rangle \\ & + \Omega_0 \langle S_y \rangle - \gamma_b (1 + \langle S_z \rangle). \end{aligned} \tag{5.5.12}$$

With increasing $\Omega_0 / \Gamma$, many of the terms in (5.5.10-12) become very small. Neglecting these terms, we can further approximate the equations to finally produce

$$\begin{aligned} \langle \dot{S}_x \rangle &\simeq \gamma_c M \sin(2\phi_0) \langle S_y \rangle - \frac{\gamma_b}{2} \langle S_x \rangle, \\ \langle \dot{S}_y \rangle &\simeq - \gamma_c \left[ N + M \cos(2\phi_0) + \frac{1}{2} \right] \langle S_y \rangle - \Omega_0 \langle S_z \rangle - \frac{\gamma_b}{2} \langle S_y \rangle, \\ \langle \dot{S}_z \rangle &\simeq - \frac{\gamma_c}{2} - \gamma_c \left[ N + M \cos(2\phi_0) + \frac{1}{2} \right] \langle S_z \rangle + \Omega_0 \langle S_y \rangle - \gamma_b (1 + \langle S_z \rangle). \end{aligned} \tag{5.5.13}$$

The most interesting choice of the phase $\phi_0$ is that which gives $\cos(2\phi_0) = -1$, for in that case

$$\gamma_c \left[ N + M \cos(2\phi_0) + \frac{1}{2} \right] = \gamma_c \left( N - M + \frac{1}{2} \right) \simeq \frac{\gamma_c}{8N}, \tag{5.5.14}$$

for large $N$. Hence, with the addition of squeezing, the cavity-mode decay of *all three* components of the Bloch vector can, in principle, be strongly inhibited. The cavity spectral density provides the mechanism for the inhibition of the decay of $\langle S_x \rangle$, and for the partial (up to 33%) inhibition of the decay of $\langle S_y \rangle$ and $\langle S_z \rangle$, while the injected squeezed vacuum acts to remove the remaining decay channel for $\langle S_y \rangle$ and $\langle S_z \rangle$.

In contrast, the choice of phase $\cos(2\phi_0) = 1$ leads to a dramatic enhancement of the decay of $\langle S_y \rangle$ and $\langle S_z \rangle$.

If $\gamma_c$ is much larger than $\gamma_b$, then significant effects should be observable. The population decay is vitally dependent on the phase of the coherent field, varying between strongly inhibited and strongly enhanced regimes. If we assume that our observations of the behaviour of the Bloch vector components can be extended to the spectrum of resonance fluorescence out the side of the cavity (Lewenstein *et al*, 1988, have demonstrated

that such an extension is justified, and, indeed, our simulation work in the previous sections also supports this), then for the choice of phase $\cos(2\phi_0) = -1$, we predict dramatic narrowing of all three peaks in the Mollow triplet. The choice of phase $\cos(2\phi_0) = 1$ should result in strong broadening of the Rabi sidebands. We note that by observing the fluorescence out the side of the cavity, we obviate any complication associated with reflections of the squeezed vacuum input.

# 6. Atom-Squeezed-Vacuum Coupling in a Microcavity

The inhibition of atomic phase decays by squeezed light, and related effects such as those elucidated in previous chapters, have yet to be confirmed experimentally. The stumbling block to all of the work that has been done in the field of squeezed light spectroscopy is the requirement of an ideal squeezed-vacuum-atom coupling, so that the atom interacts only with squeezed modes of the radiation field. This is a significant practical problem which Gardiner (1986) pointed out in his original paper, stating the need for either an incoming squeezed electric dipole wave, or an appropriate one-dimensional situation.

The first suggestion presents somewhat formidable practical problems in holding atoms still at the focus, and consequently in minimising Doppler effects. We have therefore developed the second approach (Parkins and Gardiner, 1989b), using as experimental support, the recent work of De Martini and co-workers (1986, 1987) with microscopic plane mirror cavities. In their experiments, De Martini *et al* use two parallel plane mirrors, separated by a distance $L$ of the order of the spontaneous emission wavelength $\lambda$. With this microscopic Fabry-Perot cavity, a strong selection of radiation modes coupling to atoms within the cavity is possible. In particular, for $L = \lambda/2$, atoms whose dipole moments are parallel to the mirrors couple strongly and exclusively (for a cavity of sufficiently high finesse) to the modes whose propagation vectors lie within a small solid angle about a line perpendicular to the mirror surfaces. It is by squeezing these modes that we shall aim to achieve an effective squeezed-vacuum-atom coupling. Such a scheme would also seem to suit the likely source of squeezed light, a degenerate parametric oscillator, which in present experiments produces a near-plane-wave output.

## 6.1 Equations of Motion

In the electric dipole approximation, the atom-field interaction Hamiltonian has the form

$$H_{int} = -\mathbf{d} \cdot \mathbf{E}(\mathbf{h}, t), \tag{6.1.1}$$

where $\mathbf{d}$ is the atom's dipole moment operator, and $\mathbf{E}(\mathbf{h}, t)$ is the electric field operator evaluated at $\mathbf{h}$, the position of the atom. For a two-level atom, the dipole moment operator can be written in terms of the $2 \times 2$ matrix operators $S^{\pm}$ as (Allen and Eberly, 1975)

$$\mathbf{d} = (\mathbf{d}_r + i\mathbf{d}_i)S^+ + (\mathbf{d}_r - i\mathbf{d}_i)S^-, \tag{6.1.2}$$

where $\mathbf{d}_r$ and $\mathbf{d}_i$ are the real and imaginary parts of the dipole matrix element. The electric field operator is given by

$$\mathbf{E}(\mathbf{h}, t) = i\sum_{\mathbf{k},s}\left(\frac{\hbar\omega_k}{2}\right)^{1/2} a_{\mathbf{k}s}(t_0)e^{-i\omega_k(t-t_0)}\mathbf{f}_{\mathbf{k}s}(\mathbf{h}) + h.c.. \tag{6.1.3}$$

Here, $a_{\mathbf{k}s}$ is the annihilation operator for mode $\mathbf{k}$, with polarisation $s$, and $\mathbf{f}_{\mathbf{k}s}(\mathbf{h})$ is the mode function appropriate to the situation under investigation (e.g. a cavity).

Using the commutation relations for the spin matrices, and noting, as in Chapter 2, that the atom and field represent independent degrees of freedom, and hence that equal-time commutators of atomic operators with field operators are identically zero, the Heisenberg equations of motion for the "spin" operators $S^+$, $S_z$, can be derived in the form

$$\dot{S}^+ = i\omega_a S^+ + \frac{i}{2\hbar}(\mathbf{d}_r - i\mathbf{d}_i) \cdot [\mathbf{E}(\mathbf{h}, t), S_z]_+, \tag{6.1.4}$$

$$\dot{S}_z = \frac{i}{\hbar}(\mathbf{d}_r + i\mathbf{d}_i) \cdot [\mathbf{E}(\mathbf{h}, t), S^+]_+ - \frac{i}{\hbar}(\mathbf{d}_r - i\mathbf{d}_i) \cdot [\mathbf{E}(\mathbf{h}, t), S^-]_+, \tag{6.1.5}$$

where $\omega_a$ is the atomic transition frequency.

An equation of motion for the field operators $a_{\mathbf{k}s}(t)$ can also be derived, which, when formally solved, allows us to write the field $\mathbf{E}(\mathbf{h}, t)$ as a sum of two distinct contributions: a source-free or "input" term, and a radiated field due to the atom. That is, we write

$$\mathbf{E}(\mathbf{h}, t) = \mathbf{E}_{in}(\mathbf{h}, t) + \Gamma(\mathbf{h}, t), \tag{6.1.6}$$

where

$$\mathbf{E}_{in}(\mathbf{h}, t) = i\sum_{\mathbf{k},s}\left(\frac{\hbar\omega_k}{2}\right)^{1/2} a_{\mathbf{k}s}(t_0)e^{-i\omega_k(t-t_0)}\mathbf{f}_{\mathbf{k}s}(\mathbf{h}) + h.c., \tag{6.1.7}$$

and

$$\Gamma(\mathbf{h},t) = i\sum_{\mathbf{k},s}\frac{\omega_k}{2}[(\mathbf{d}_r - i\mathbf{d}_i)\cdot\mathbf{f}^*_{\mathbf{k}s}(\mathbf{h})]\mathbf{f}_{\mathbf{k}s}(\mathbf{h})S^-(t)\int_0^{t-t_0} d\tau e^{-i(\omega_k-\omega_a)\tau} + h.c.. \tag{6.1.8}$$

The result (6.1.8) is not exact, in that we have assumed the atom-field interaction to be weak, allowing us to make the approximation $S^-(t-\tau) \simeq S^-(t)e^{i\omega_a\tau}$ within the integral. This is generally referred to as the adiabatic approximation, and corresponds to a bad cavity limit, which, of course, is precisely the limit in which we are interested. Also, in deriving (6.1.8), we have neglected "off-resonant" terms involving exponentials of the form $e^{-i(\omega_k+\omega_a)\tau}$ (which corresponds to the rotating wave approximation).

Substituting the results (6.1.6-8) into (6.1.4,5), and using the properties of the spin matrices, we derive quantum Langevin equations in the form

$$\dot{S}^+ = i\omega_a S^+ + \frac{i}{2\hbar}(\mathbf{d}_r - i\mathbf{d}_i)\cdot[\mathbf{E}_{in}(\mathbf{h},t),S_z]_+, \tag{6.1.9}$$

$$\dot{S}_z = \frac{i}{\hbar}(\mathbf{d}_r + i\mathbf{d}_i)\cdot[\mathbf{E}_{in}(\mathbf{h},t),S^+]_+ - \frac{i}{\hbar}(\mathbf{d}_r - i\mathbf{d}_i)\cdot[\mathbf{E}_{in}(\mathbf{h},t),S^-]_+ - \gamma(\mathbf{h}), \tag{6.1.10}$$

where

$$\gamma(\mathbf{h}) = \frac{1}{2\hbar}\sum_{\mathbf{k},s}\omega_k|(\mathbf{d}_r + i\mathbf{d}_i)\cdot\mathbf{f}_{\mathbf{k}s}(\mathbf{h})|^2\int_{t_0-t}^{t-t_0} d\tau\, e^{i(\omega_k-\omega_a)\tau}. \tag{6.1.11}$$

With suitable approximation, the term $\gamma(\mathbf{h})$ gives the linewidth of the atomic transition. In free space, $\gamma(\mathbf{h})$, as we have defined it, takes the value $d_a^2\omega_a^3/3\pi\hbar c^3$, where $d_a = |\mathbf{d}_r + i\mathbf{d}_i|$.

Next, we move to a frame rotating at frequency $\omega_0$, which we shall assume represents the carrier frequency of the input squeezed field. For simplicity, we shall assume resonance between this frequency and the atomic transition frequency, $\omega_0 = \omega_a$. We define polarisation quadratures in the standard way by

$$S_x = S^+e^{-i\omega_0 t} + S^-e^{i\omega_0 t}, \tag{6.1.12}$$

$$S_y = -i\left(S^+e^{-i\omega_0 t} - S^-e^{i\omega_0 t}\right). \tag{6.1.13}$$

The rotating wave approximation is invoked, and the equations of motion that result can be written as follows

$$\dot{S}_x = \frac{1}{2\hbar}[X_{in}(\mathbf{h},t),S_z]_+, \tag{6.1.14}$$

$$\dot{S}_y = \frac{1}{2\hbar}[Y_{in}(\mathbf{h},t), S_z]_+, \tag{6.1.15}$$

$$\dot{S}_z = -\gamma(\mathbf{h}) - \frac{1}{2\hbar}[X_{in}(\mathbf{h},t), S_x]_+ - \frac{1}{2\hbar}[Y_{in}(\mathbf{h},t), S_y]_+, \tag{6.1.16}$$

where

$$X_{in}(\mathbf{h},t) = \sum_{\mathbf{k},s}\left(\frac{\hbar\omega_k}{2}\right)^{1/2} a_{\mathbf{k}s}(t_0)e^{-i(\omega_k-\omega_0)t}(\mathbf{d}_r + i\mathbf{d}_i)\cdot\mathbf{f}_{\mathbf{k}s}(\mathbf{h}) + h.c., \tag{6.1.17}$$

$$Y_{in}(\mathbf{h},t) = i\sum_{\mathbf{k},s}\left(\frac{\hbar\omega_k}{2}\right)^{1/2} a_{\mathbf{k}s}(t_0)e^{-i(\omega_k-\omega_0)t}(\mathbf{d}_r + i\mathbf{d}_i)\cdot\mathbf{f}_{\mathbf{k}s}(\mathbf{h}) + h.c.. \tag{6.1.18}$$

These equations are of the form derived in earlier chapters, and, once again, the adjoint equation formulation, together with the operator definitions

$$\beta_X(\mathbf{h},t)\rho \equiv \frac{1}{2\hbar}[X_{in}(\mathbf{h},t), \rho]_+, \tag{6.1.19}$$

$$\beta_Y(\mathbf{h},t)\rho \equiv \frac{1}{2\hbar}[Y_{in}(\mathbf{h},t), \rho]_+, \tag{6.1.20}$$

enables us to treat the equations as classical stochastic differential equations. The statistics of $\beta_X(\mathbf{h},t)$ and $\beta_Y(\mathbf{h},t)$, as defined by the correlation functions $\langle\beta_X(\mathbf{h},t)\beta_X(\mathbf{h},t')\rangle$ and $\langle\beta_Y(\mathbf{h},t)\beta_Y(\mathbf{h},t')\rangle$, determine the behaviour of $\langle S_{x,y,z}(t)\rangle$ and, of course, whether or not the decay of one of $\langle S_x(t)\rangle$ or $\langle S_y(t)\rangle$ can be inhibited. Specification of the correlation functions will of course require specifications of, for instance, $\langle a_{\mathbf{k}s}(t_0)a_{\mathbf{k}'s'}(t_0)\rangle$ for a squeezed input field, incident over some finite solid angle, and we will consider this in Section 6.3. Most importantly, the dependence of the atomic dipole decay on the surrounding mode structure is now explicitly included through the definition of $\beta_X(\mathbf{h},t)$ and $\beta_Y(\mathbf{h},t)$.

## 6.2 Mode Functions of the Cavity

The action of the cavity in restricting the number of modes that couple to the atom is central to our investigation, and is described through the cavity mode functions. The particular configuration that we have in mind is a plane-mirror Fabry-Perot cavity, as shown

in Fig.6.1. The mode functions give the spatial dependence of the field, and can be computed using classical electromagnetic theory. In our configuration, two plane mirrors are assumed to lie parallel to the $xy$ plane, the first a perfectly reflecting mirror at $z = 0$, and the second a partially transmitting lossless mirror at $z = L$, with real reflectivity $R$, and transmittivity $i\sqrt{1 - R^2}$ (the same for both directions). We assume that the mirrors are very large, so that end effects can be ignored.

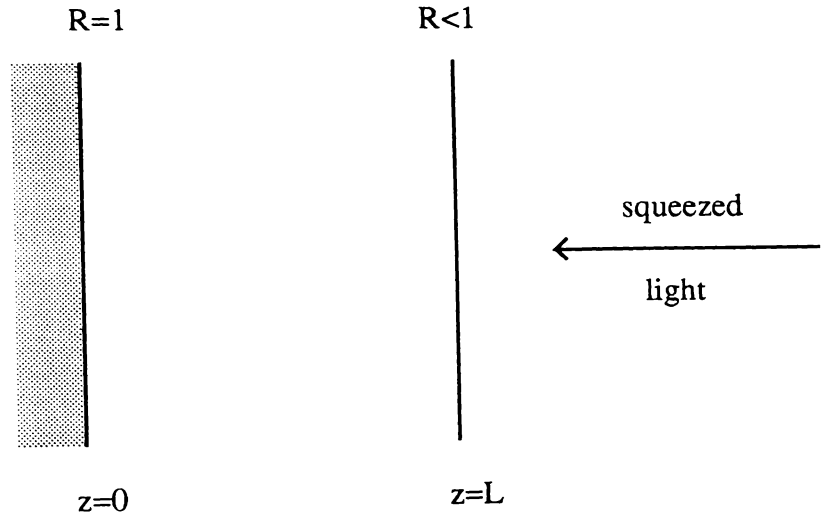


**Fig.6.1** Cavity configuration.

By a consideration of boundary conditions at the mirrors, we can derive the following expression for the mode functions inside the cavity

$$\mathbf{f}_{\mathbf{k}s}(\mathbf{r}) = V^{-1/2} g(k_z) \left( \boldsymbol{\epsilon}_{\mathbf{k}s} e^{i\mathbf{k}\cdot\mathbf{r}} + \boldsymbol{\epsilon}'_{\mathbf{k}s} e^{i\mathbf{k}'\cdot\mathbf{r}} \right), \tag{6.2.1}$$

where $V$ is the quantisation volume, and $g(k_z)$ is taken to have the form

$$g(k_z) = \frac{i(1 - R^2)^{1/2}}{1 - Re^{-i2k_zL}}. \tag{6.2.2}$$

We have assumed that the reflectivity $R$ is the same for both polarisations. The polarisation vector $\boldsymbol{\epsilon}_{\mathbf{k}s}$, and the wave vector $\mathbf{k}$, can be written as a sum of components parallel and perpendicular to the $xy$ plane respectively,

$$\boldsymbol{\epsilon}_{\mathbf{k}s} = \boldsymbol{\epsilon}^{\perp}_{\mathbf{k}s} + \boldsymbol{\epsilon}^{\parallel}_{\mathbf{k}s}, \quad \mathbf{k} = \mathbf{k}^{\perp} + \mathbf{k}^{\parallel}. \tag{6.2.3}$$

The primed quantities in (6.2.1) are then defined by

$$\boldsymbol{\epsilon}'_{\mathbf{k}s} = \boldsymbol{\epsilon}^{\perp}_{\mathbf{k}s} - \boldsymbol{\epsilon}^{\parallel}_{\mathbf{k}s}, \quad \mathbf{k}' = -\mathbf{k}^{\perp} + \mathbf{k}^{\parallel}. \tag{6.2.4}$$

We note that the following identities hold:

$$\mathbf{k} \cdot \boldsymbol{\epsilon}_{\mathbf{k}s} = \mathbf{k}' \cdot \boldsymbol{\epsilon}'_{\mathbf{k}s} = 0 \quad , \quad \boldsymbol{\epsilon}_{\mathbf{k}s} \cdot \boldsymbol{\epsilon}^*_{\mathbf{k}s} = \boldsymbol{\epsilon}'_{\mathbf{k}s} \cdot \boldsymbol{\epsilon}'^*_{\mathbf{k}s} = 1 . \tag{6.2.5}$$

For our purposes, we need only know the mode functions inside the cavity. For a precise check on the orthogonality of the mode functions, one must of course take account of the partially-transmitting mirror. In the case of an infinitely thin mirror, this necessitates an additional surface term in the orthogonality integral (see, for example, Ley and Loudon, 1987). If the mirror is given a finite thickness and finite dielectric constant, an approach such as is used by Carniglia and Mandel (1971) for the quantisation of fields about an interface is then required.

The effect of the cavity is most clearly exhibited in the form of $|g(k_z)|^2$, which we identify as the Airy function of the cavity

$$|g(k_z)|^2 = \frac{1 - R^2}{(1 - R)^2 + 4R\sin^2(k_z L)} . \tag{6.2.6}$$

If $R$ is close to one, then this function displays a series of sharp peaks for angles of incidence such that $\sin(k_z L) = \sin(kL\cos\theta_k) = 0$. If, therefore, $L = \lambda/2$, the function given in (6.2.6) will exhibit a peak centered at $\cos\theta_k = 1$ (the peak at $\cos\theta_k = 0$ can be ignored, as other factors that enter our calculations later are zero at this angle), that is, a strong coupling is effected only with those modes in a small solid angle about the $z$ axis (i.e. perpendicular to the mirrors). In the next section we shall examine the requirements for producing an effective squeezing of these modes.

## 6.3 Squeezed Vacuum Input

The formulation of squeezing in a full three dimensional electromagnetic field has not been considered before, so it is appropriate that this be set out with some care. In a one dimensional situation, a multimode squeezed state can be specified by operators $A(\omega)$, $A^\dagger(\omega)$, such that

$$\begin{aligned} [A(\omega), A^\dagger(\omega')] &= \delta(\omega - \omega'), \\ \langle A^\dagger(\omega) A(\omega') \rangle &= \delta(\omega - \omega') N(\omega), \\ \langle A(\omega) A(\omega') \rangle &= \delta(2\omega_0 - \omega - \omega') M(\omega), \end{aligned} \tag{6.3.1}$$

where $\omega_0$ is the central frequency about which squeezing takes place. To generalise this to three dimensions, let us define an operator analogous to $A(\omega)$,

$$A(k) = \sum_{\hat{\mathbf{k}},s} \alpha_s^*(\mathbf{k}) a_{\mathbf{k}s}, \tag{6.3.2}$$

where $\alpha_s(\mathbf{k})$ is a square normalised mode function satisfying

$$\sum_{\hat{\mathbf{k}},s} |\alpha_s(\mathbf{k})|^2 = 1. \tag{6.3.3}$$

Here, $\hat{\mathbf{k}}$ is a unit vector in the direction of $\mathbf{k}$. We want the same kind of relations as for $A(\omega)$ to be true. But further, let us specify that the field is not squeezed in any other modes. This can be achieved by defining the state by

$$[a_{\mathbf{k}s}, a^\dagger_{\mathbf{k}'s'}] = \delta^3_{\mathbf{k},\mathbf{k}'}\delta_{s,s'}, \tag{6.3.4}$$

$$\langle a^\dagger_{\mathbf{k}s} a_{\mathbf{k}'s'} \rangle = N(k)\alpha_s^*(\mathbf{k})\alpha_{s'}(\mathbf{k}')\delta_{k,k'}, \tag{6.3.5}$$

$$\langle a_{\mathbf{k}s} a_{\mathbf{k}'s'} \rangle = M(k)\alpha_s(\mathbf{k})\alpha_{s'}(\mathbf{k}')\delta_{k,2K-k'}. \tag{6.3.6}$$

In this case, we can see that

$$\langle A^\dagger(k)A(k') \rangle = N(k)\delta_{k,k'}, \tag{6.3.7}$$

$$\langle A(k)A(k') \rangle = M(k)\delta_{k,2K-k'}. \tag{6.3.8}$$

However, if

$$B(k) = \sum_{\hat{\mathbf{k}},s} \beta_s^*(\mathbf{k}) a_{\mathbf{k}s}, \tag{6.3.9}$$

and

$$\sum_{\hat{\mathbf{k}},s} \alpha_s(\mathbf{k})\beta_s^*(\mathbf{k}) = 0, \tag{6.3.10}$$

then the operator $B(k)$ is not squeezed, and indeed has no excitation in it at all. Thus the definitions (6.3.4-6) represent a situation in which there is squeezing only between modes with wavefunction $\alpha_s(\mathbf{k})$.

## 6.4 Correlation Functions for the Cavity Field

Computation of the correlation function $\langle \beta_Y(\mathbf{h},t)\beta_Y(\mathbf{h},t')\rangle$, from which we may determine the decay rate of $\langle S_y\rangle$, proceeds as follows. If $\rho_b$ is the bath density operator, then, using the properties of the trace, one can write

$$\begin{aligned}\langle \beta_Y(\mathbf{h},t)\beta_Y(\mathbf{h},t')\rangle &\equiv Tr_b\{\beta_Y(\mathbf{h},t)\beta_Y(\mathbf{h},t')\rho_b\}\\ &= \frac{1}{4\hbar^2}Tr_b\{[Y_{in}(\mathbf{h},t),[Y_{in}(\mathbf{h},t'),\rho_b]_+]_+\}\\ &= \frac{1}{2\hbar^2}Tr_b\{[Y_{in}(\mathbf{h},t),Y_{in}(\mathbf{h},t')]_+\rho_b\}\\ &\equiv \frac{1}{2\hbar^2}\langle [Y_{in}(\mathbf{h},t),Y_{in}(\mathbf{h},t')]_+\rangle. \end{aligned} \tag{6.4.1}$$

Using (6.1.18) and (6.3.4-6), and moving to an integral representation (for the necessary modifications to our discrete expressions, see, for example, Kibble, 1969), we derive

$$\begin{aligned}&\langle \beta_Y(\mathbf{h},t)\beta_Y(\mathbf{h},t')\rangle =\\ &-\frac{Vc}{2\hbar(2\pi)^3}\sum_{s,s'}\int_0^{2K} dk\, k^2[k(2K-k)]^{1/2}e^{-ic(k-K)(t-t')}M(k)\\ &\times\int_{\Omega_{sq}}d\Omega_k\int_{\Omega_{sq}}d\Omega_{k'}\,\alpha_s(\mathbf{k})\mathrm{F}_{\mathbf{k}s}(\mathbf{h})\alpha_{s'}((2K-k)\hat{\mathbf{k}}'))\mathrm{F}_{(2K-k)\hat{\mathbf{k}}'s'}(\mathbf{h}) \;+\; c.c.\\ &+\frac{Vc}{2\hbar(2\pi)^3}\sum_{s,s'}\int_0^{\infty} dk\, k^3 e^{-ic(k-K)(t-t')}N(k)\\ &\times\int_{\Omega_{sq}}d\Omega_k\int_{\Omega_{sq}}d\Omega_{k'}\,\alpha_s(\mathbf{k})\mathrm{F}_{\mathbf{k}s}(\mathbf{h})\alpha^*_{s'}(k\hat{\mathbf{k}}')\mathrm{F}^*_{k\hat{\mathbf{k}}'s'}(\mathbf{h}) \;+\; c.c.\\ &+\frac{Vc}{2\hbar(2\pi)^3}\int_0^{\infty} dk\, k^3 e^{-ic(k-K)(t-t')}\int_{halfsphere}d\Omega_k\sum_s|\,\mathrm{F}_{\mathbf{k}s}(\mathbf{h})\,|^2, \end{aligned} \tag{6.4.2}$$

where $K=\omega_0/c=\omega_a/c$ is the central squeezing wavenumber, and, for brevity, we have introduced the quantity $\mathrm{F}_{\mathbf{k}s}(\mathbf{h})$, defined by

$$\mathrm{F}_{\mathbf{k}s}(\mathbf{h}) = (\mathbf{d}_r + i\mathbf{d}_i)\cdot\mathbf{f}_{\mathbf{k}s}(\mathbf{h}). \tag{6.4.3}$$

### 6.4.1 Ideal mode matching of the input to the cavity

In his original work, Gardiner (1986) considered the case of an atom in free space, noting that $\alpha_s(\mathbf{k})$ should, in that case, correspond as closely as possible to an electric dipole

wave, with $\Omega_{sq}$, the solid angle over which the input is squeezed, approximately $4\pi$, giving the maximum overlap of $\alpha_s(\mathbf{k})$ with $F_{\mathbf{k}s}(\mathbf{h})$. Similarly, we may attempt to maximise this overlap for our particular situation by choosing

$$\alpha_s(\mathbf{k}) = \mathcal{N}^{-1/2}\, F^*_{\mathbf{k}s}(\mathbf{h}_0), \tag{6.4.4}$$

where

$$\mathcal{N} = \int_{\Omega_{sq}} d\Omega_k \sum_s |\, F_{\mathbf{k}s}(\mathbf{h}_0)\,|^2, \tag{6.4.5}$$

and $\mathbf{h}_0 = (0, 0, h_z)$. As we shall see, a choice such as (6.4.4) is important, otherwise the phase of the squeezing can be altered to an extent that a significant reduction in fluctuations is no longer possible. In simple terms, the mode structure of the squeezing incident upon the cavity should match as closely as possible the mode structure of the cavity in which we aim to carry out the experiment. In practice, some approximation will be necessary, but for the moment we consider the "ideal" case (6.4.4). Later we shall examine other possible choices of $\alpha_s(\mathbf{k})$, at which stage the importance of matching will be emphasized more definitively.

Having made the choice (6.4.4), we then assume that, over the bandwidth of interest, the functions inside the integrals are slowly varying functions of $k$ (apart from the complex exponential), and can be set equal to their values at $k = K$. We then approximate the integrals by

$$\int_0^{2k} dk\; e^{-ic(k-K)(t-t')} \simeq \int_0^{\infty} dk\; e^{-ic(k-K)(t-t')} \simeq \frac{2\pi}{c}\delta(t-t'), \tag{6.4.6}$$

to give

$$\begin{aligned}
\langle \beta_Y(\mathbf{h},t)\beta_Y(\mathbf{h},t')\rangle \simeq\ & \\
& -\frac{V}{(2\pi)^2}\frac{K^3}{2\hbar} M(K)\;\delta(t-t')\int_{\Omega_{sq}} d\Omega_k \int_{\Omega_{sq}} d\Omega_{k'}\, \mathcal{N}(K)^{-1} \\
& \quad \times \sum_{s,s'} F^*_{K\hat{\mathbf{k}}s}(\mathbf{h}_0) F_{K\hat{\mathbf{k}}s}(\mathbf{h}) F^*_{K\hat{\mathbf{k}}'s'}(\mathbf{h}_0) F_{K\hat{\mathbf{k}}'s'}(\mathbf{h}) \;+\; c.c. \\
& + \frac{V}{(2\pi)^2}\frac{K^3}{2\hbar} N(K)\;\delta(t-t')\int_{\Omega_{sq}} d\Omega_k \int_{\Omega_{sq}} d\Omega_{k'}\, \mathcal{N}(K)^{-1} \\
& \quad \times \sum_{s,s'} F^*_{K\hat{\mathbf{k}}s}(\mathbf{h}_0) F_{K\hat{\mathbf{k}}s}(\mathbf{h}) F_{K\hat{\mathbf{k}}'s'}(\mathbf{h}_0) F^*_{K\hat{\mathbf{k}}'s'}(\mathbf{h}) \;+\; c.c. \\
& + \frac{V}{(2\pi)^2}\frac{K^3}{2\hbar}\,\delta(t-t') \int_{halfsphere} d\Omega_k \sum_s |\, F_{K\hat{\mathbf{k}}s}(\mathbf{h})\,|^2 .
\end{aligned} \tag{6.4.7}$$

To carry out the polarisation sums, we adopt the circular polarisation vectors

$$\epsilon_{\mathbf{k}+} = -\frac{e^{i\phi_k}}{\sqrt{2}} \times (-\cos\theta_k \cos\phi_k + i\sin\phi_k, -\cos\theta_k \sin\phi_k - i\cos\phi_k, \sin\theta_k), \quad (6.4.8)$$

$$\epsilon_{\mathbf{k}-} = \frac{e^{-i\phi_k}}{\sqrt{2}} \times (-\cos\theta_k \cos\phi_k - i\sin\phi_k, -\cos\theta_k \sin\phi_k + i\cos\phi_k, \sin\theta_k). \quad (6.4.9)$$

With this particular choice, the polarisations are unique when $\theta_k = 0$ (i.e. the same for any $\phi_k$).

We shall assume that with suitable optical pumping the atoms can be prepared in a state from which only a $\Delta M = \pm 1$ transition is possible (Jhe *et al*, 1987). For our cavity configuration, this shall correspond to transitions in which the emitted photons are polarised in a plane parallel to the mirror surfaces (i.e. the atom quantisation axis is chosen as the normal to the mirrors), and for which the dipole moment can be written (Allen and Eberly, 1975)

$$\mathbf{d}_r + i\mathbf{d}_i = \frac{d_a}{\sqrt{2}}(1, i, 0). \quad (6.4.10)$$

We then find

$$\mathrm{F}_{K\hat{\mathbf{k}}+}(\mathbf{h}) = -iV^{-1/2}\, d_a\, g(K\cos\theta_k)(1-\cos\theta_k)\, e^{i2\phi_k} \sin(Kh_z\cos\theta_k) \times \exp[iK(h_x \sin\theta_k \cos\phi_k + h_y \sin\theta_k \sin\phi_k)], \quad (6.4.11)$$

and

$$\mathrm{F}_{K\hat{\mathbf{k}}-}(\mathbf{h}) = -iV^{-1/2}\, d_a\, g(K\cos\theta_k)(1+\cos\theta_k) \sin(Kh_z\cos\theta_k) \times \exp[iK(h_x \sin\theta_k \cos\phi_k + h_y \sin\theta_k \sin\phi_k)]. \quad (6.4.12)$$

We note at this point that with $|g(K\cos\theta_k)|^2$ sharply-peaked about $\cos\theta_k = 1$, the dominant contribution to the quantities we compute will come from terms involving $\mathrm{F}_{K\hat{\mathbf{k}}-}(\mathbf{h})$ (rather than $\mathrm{F}_{K\hat{\mathbf{k}}+}(\mathbf{h})$, which is small), that is, from only a single polarization.

To simplify matters we set $h_y = 0$, so that we shall be considering variations in the atom's position along the $x$ axis (from the "central squeezing position" $\mathbf{h}_0 = (0, 0, h_z)$). By varying $h_x$, we will be able to gauge the area inside the cavity over which reduced fluctuations can be achieved.

The solid angle over which the squeezing shall be incident is defined by

$$\int_{\Omega_{sq}} d\Omega_k \equiv \int_0^{\theta_{sq}} d\theta_k \sin\theta_k \int_0^{2\pi} d\phi_k, \quad (6.4.13)$$

that is, we consider a cone centered on the $z$ axis. After some calculation, and a change of integration variable ($u = \cos\theta_k$), we can write (with $N \equiv N(K)$, $M \equiv M(K)$)

$$\langle \beta_Y(\mathbf{h},t)\beta_Y(\mathbf{h},t')\rangle = \gamma_a \mathcal{B}(\mathbf{h})\delta(t-t'), \tag{6.4.14}$$

where $\gamma_a = d_a^2\omega_a^3/3\pi\hbar c^3$, and

$$\begin{aligned}\mathcal{B}(\mathbf{h}) &= 3(N-M)\frac{1+R}{1-R}\frac{1}{\mathcal{N}'} \\ &\quad\times\left\{\int_{\cos\theta_{sq}}^{1} du\,(1+u^2)\frac{\sin^2(Kh_z u)}{1+F\sin^2(KLu)}J_0(Kh_x\sqrt{1-u^2})\right\}^2 \\ &\quad+\frac{3}{2}\frac{1+R}{1-R}\int_0^1 du\,(1+u^2)\frac{\sin^2(Kh_z u)}{1+F\sin^2(KLu)},\end{aligned} \tag{6.4.15}$$

with

$$\mathcal{N}' = \int_{\cos\theta_{sq}}^{1} du(1+u^2)\frac{\sin^2(Kh_z u)}{1+F\sin^2(KLu)}. \tag{6.4.16}$$

Here $F = 4R/(1-R)^2$, and $J_0$ is the zeroth-order Bessel function. A similar correlation function can be derived for $\beta_X(\mathbf{h},t)$, and on averaging the equations of motion we find

$$\langle \dot{S}_y\rangle = -\frac{\gamma_a}{2}\mathcal{B}(\mathbf{h})\langle S_y\rangle. \tag{6.4.17}$$

Under free-space (and no squeezing) conditions, which can be modelled here by the limits $N = M = 0$, $R = 0$, and $h_z \to \infty$, we find that $\mathcal{B}(\mathbf{h})$ is equal to 1.

The integrals appearing above will be evaluated numerically. However, to obtain some estimate by analytical means, we can consider $h_x = 0$, and approximate the sharply peaked Airy function by a Lorentzian (after a suitable change of integration variable). We further assume that the other factors in the integrands do not vary significantly over the width of this Lorentzian, and hence that they can be removed from the integral and set equal to their values at $u = 1$. Considering the case where $KL = \pi$ ($L = \lambda/2$), and $Kh_z = \pi/2$ (i.e. the atom is at the centre of the cavity), we find

$$\begin{aligned}&\mathcal{B}(h_x = 0, h_z = L/2) \\ &\quad\simeq \frac{3}{\pi}\frac{1+R}{2\sqrt{R}}\left\{\tan^{-1}(\pi\sqrt{F}) + 2(N-M)\tan^{-1}[\pi\sqrt{F}(1-\cos\theta_{sq})]\right\}.\end{aligned} \tag{6.4.18}$$

For an ideal broadband squeezed light input, one has $M = [N(N+1)]^{1/2}$, so that for large squeezing $N - M$ approaches $-1/2$. Hence, choosing $\cos\theta_{sq} = 0$ the term in brackets may become very small. However, if $F$ is large, this requirement may

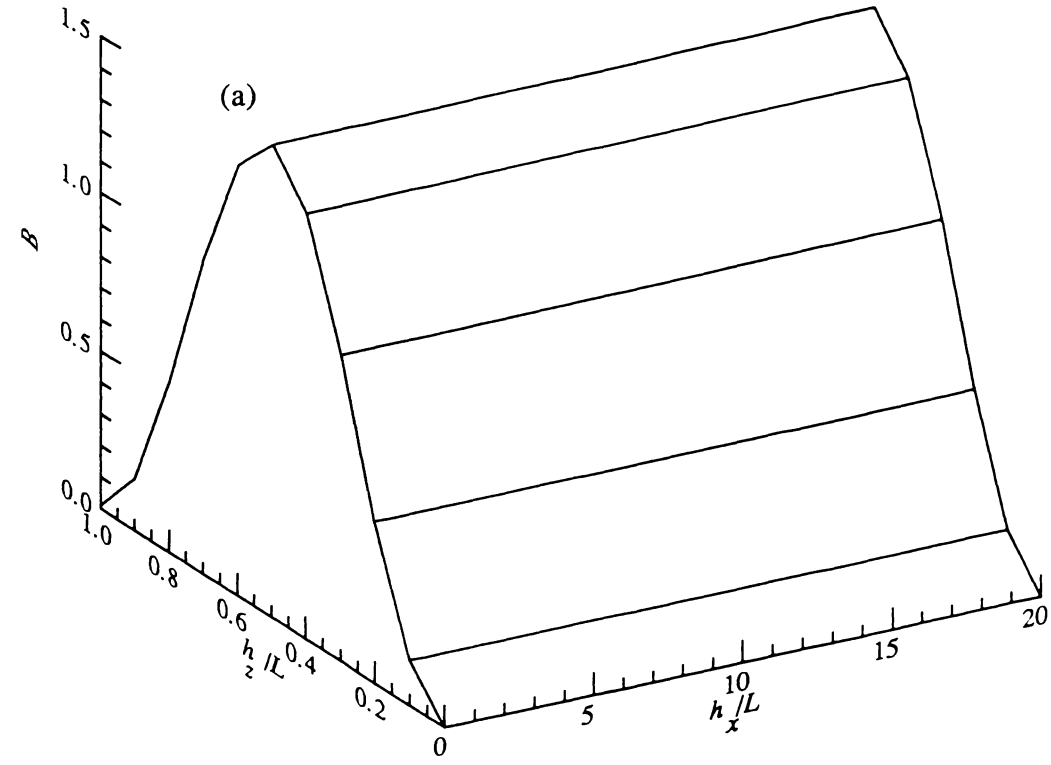
(a)
1.5
1.0
0.5
0.0
B
1.0
0.8
0.6
$h_z/L$
0.4
0.2
0
5
10
15
20
$h_x/L$

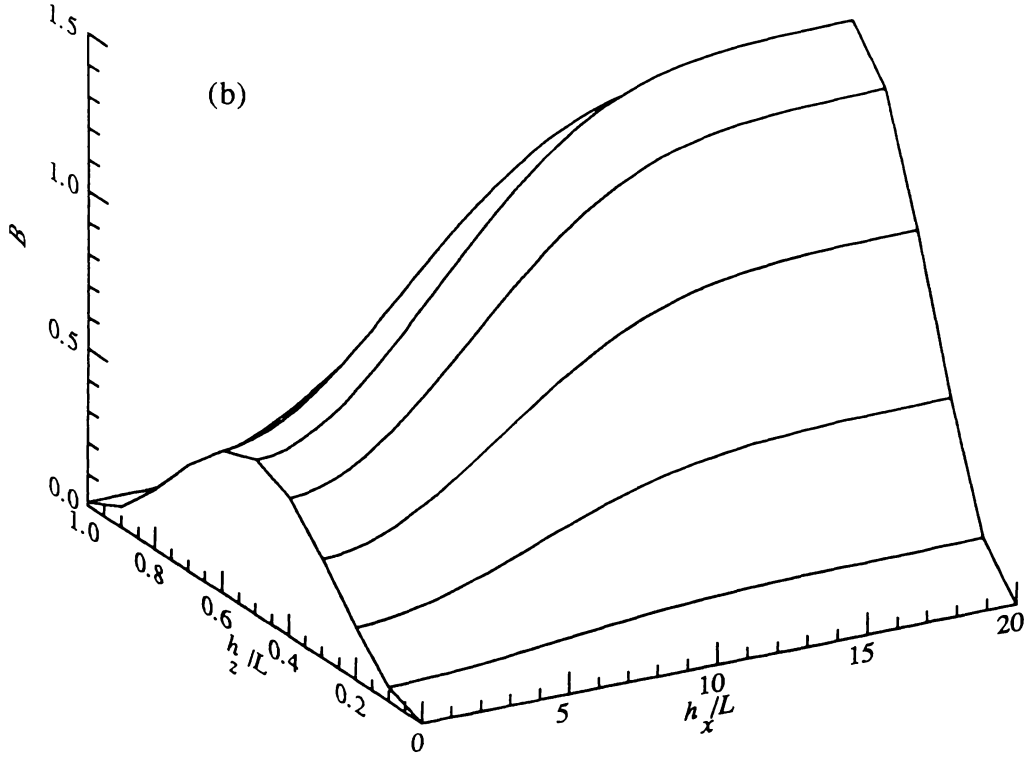
(b)
1.5
1.0
0.5
0.0
B
1.0
0.8
0.6
$h_z/L$
0.4
0.2
0
5
10
15
20
$h_x/L$

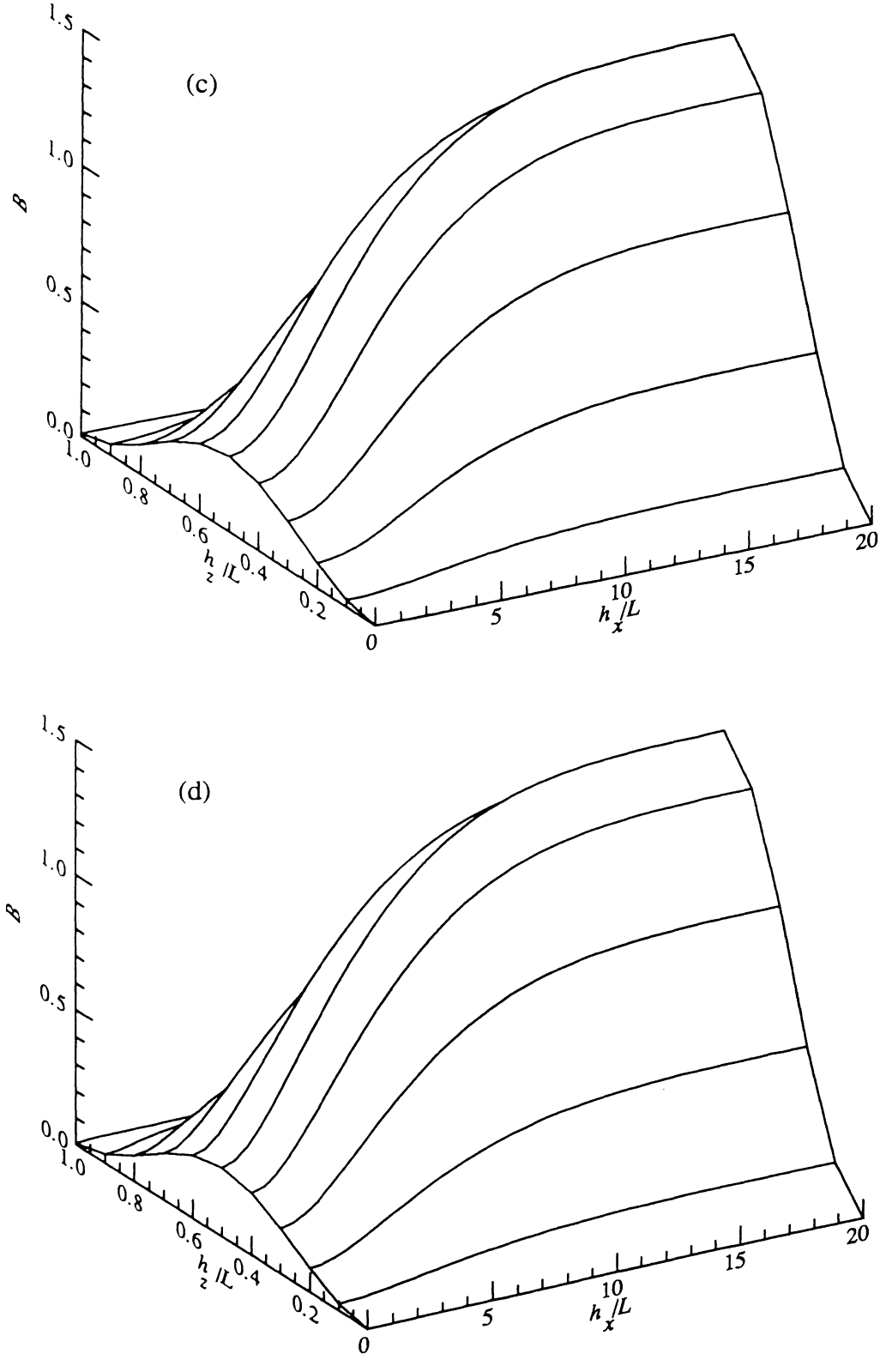


**Fig.6.2** $\mathcal{B}$ as a function of $h_x$ and $h_z$, for $L = \lambda/2$, $R = 0.99$, and $N = 1$ (83% squeezing), with (a) $\theta_{sq} = 0$, (b) $\theta_{sq} = 0.1$, (c) $\theta_{sq} = 0.3$, (d) $\theta_{sq} = 1.0$.

be relaxed; for instance, if $R = 0.98$, and $\theta_{sq} = 0.3$ radians, then $\tan^{-1}(\pi\sqrt{F}) = 1.57$, while $\tan^{-1}[\pi\sqrt{F}(1 - \cos\theta_{sq})] = 1.50$. Hence, a substantial reduction in fluctuations is still possible at the point we have chosen midway between the mirrors with a squeezed light input of modest angular dimensions.

### Numerical results

The results of computer evaluation of $\mathcal{B}(\mathbf{h})$ are shown in Figs.6.2-3. In Fig.6.2 we display four plots for $L = \lambda/2$, $R = 0.99$, and $N = 1$ (83% squeezing), with $\theta_{sq} = 0$, 0.1, 0.3, and 1.0 radians respectively. As one can see there is relatively little variation in going from $\theta_{sq} = 0.1$ to $\theta_{sq} = 1.0$, emphasising the function of the cavity in isolating those modes nearly perpendicular to the mirrors. The maximum reduction in fluctuations relative to the vacuum occurs in each case at $h_z/L = 0.5$, $h_x/L = 0$. These reductions are 67%, 81%, and 82% for $\theta_{sq} = 0.1$, 0.3, and 1.0 respectively. Hence, for $\theta_{sq} > 0.3$, with $R = 0.99$, the reductions possible are limited essentially by the available squeezing.

A good amount of squeezing is available in the $x$ direction for several times the width $L$ of the cavity. This "width" of squeezing depends on the reflectivity $R$, as shown in Fig.6.3 where we consider $\theta_{sq} = 0.3$ with $R = 0.95$ and $R = 0.995$. With increasing $R$, the area over which significant squeezing occurs increases substantially. We note, however, that significant reductions are possible with fairly modest values of the reflectivity $R$, as demonstrated in Fig.6.3(a). In terms of the maximum achievable inhibition, a decrease in $R$ may be compensated for by an increase in the angular limit $\theta_{sq}$ of the squeezed input. For instance, with $R = 0.95$, and with the same input squeezing as above, a maximum reduction of 82% is possible with $\theta_{sq} = 1.0$, as opposed to 74% with $\theta_{sq} = 0.3$.

### Effect of mirror spacing

It is important to consider also the sensitivity of the effects to small changes in the mirror spacing $L$. This will be very pertinent to any practical experimental arrangement as the distances involved are extremely small. For $L < \lambda/2$, the mode density inside the cavity is greatly diminished, and we enter the regime of inhibited spontaneous emission (Hulet *et al*, 1985, Jhe *et al*, 1987), remembering that the dipole moment is assumed to be parallel to the mirrors.

In Fig.6.4 we display the result, with squeezing, for $L = 0.495\lambda$. In all regions, the decay rate is significantly reduced from the free-space rate. The effect of squeezing

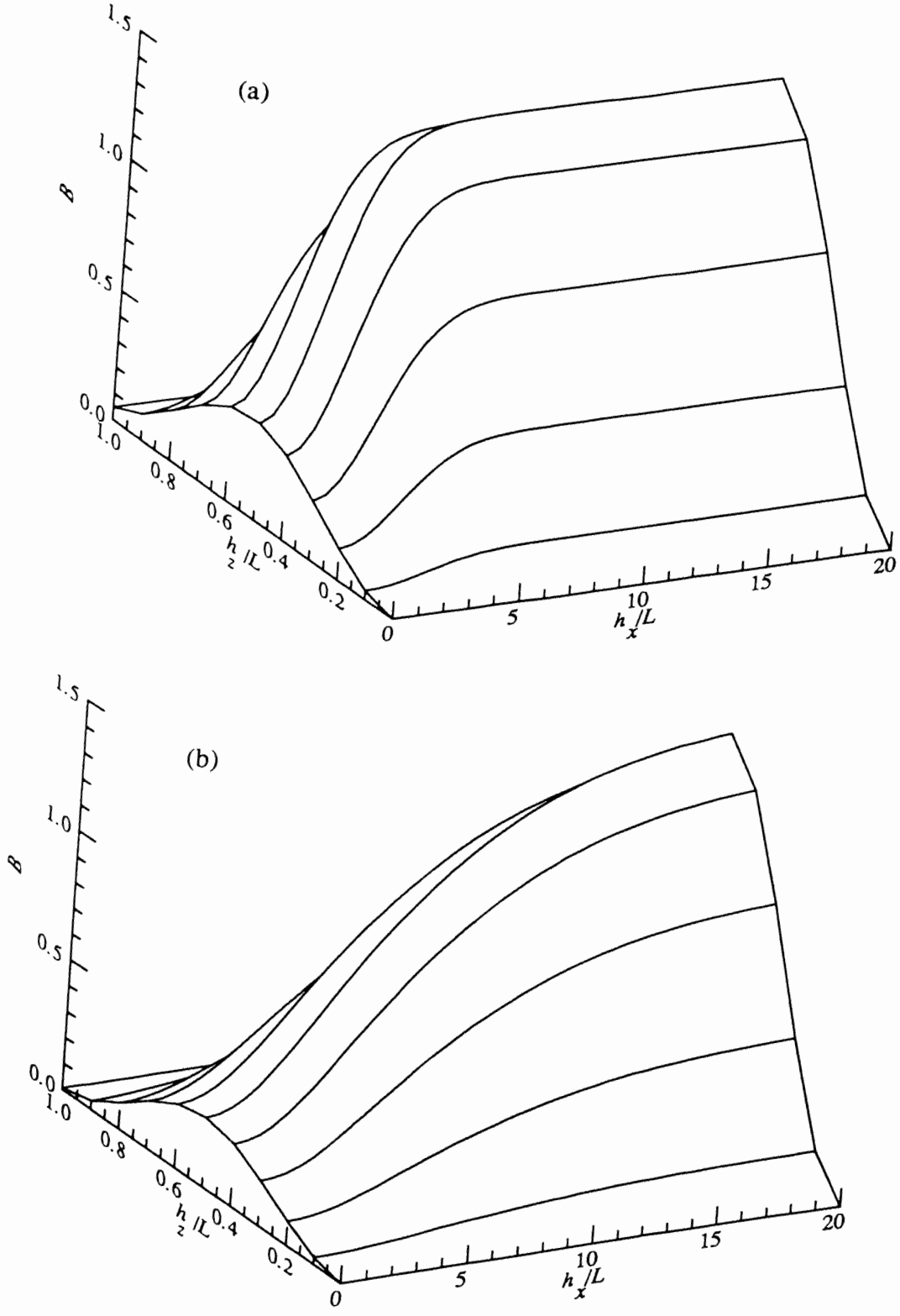


**Fig.6.3** $\mathcal{B}$ as a function of $h_x$ and $h_z$, for $L = \lambda/2$, $\theta_{sq} = 0.3$, $N = 1$, with (a) $R = 0.95$, (b) $R = 0.995$.

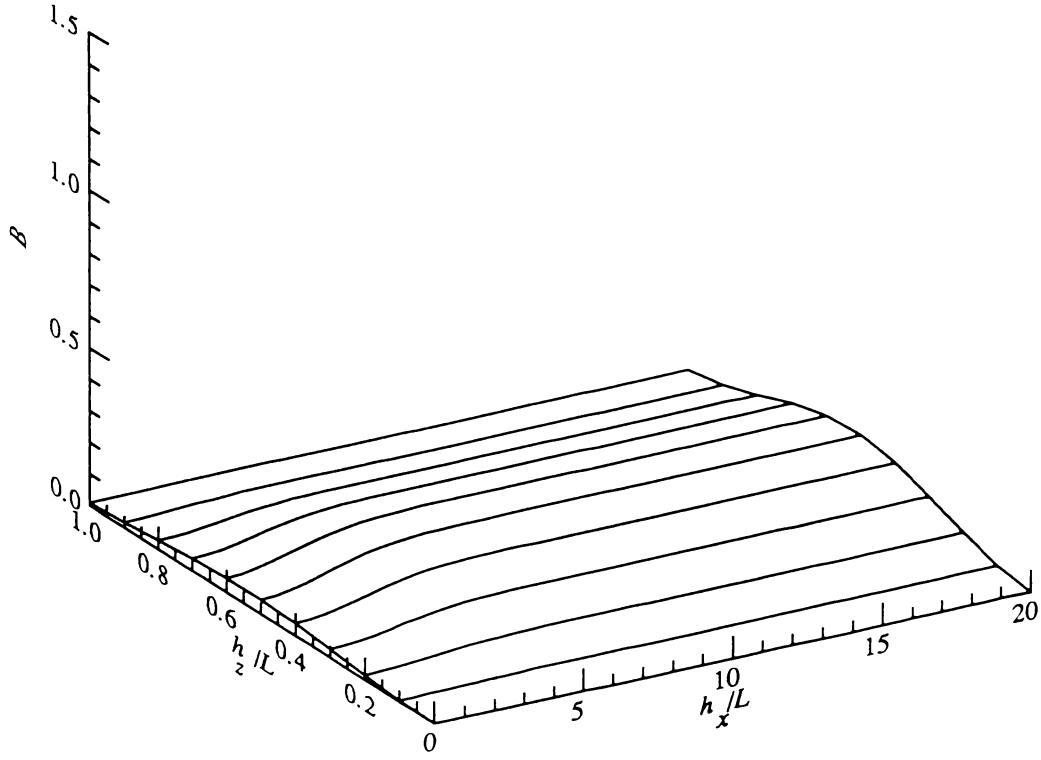


**Fig.6.4** $\mathcal{B}$ as a function of $h_x$ and $h_z$, for $L = 0.495\lambda$, $R = 0.99$, $N = 1$, and $\theta_{sq} = 0.3$.

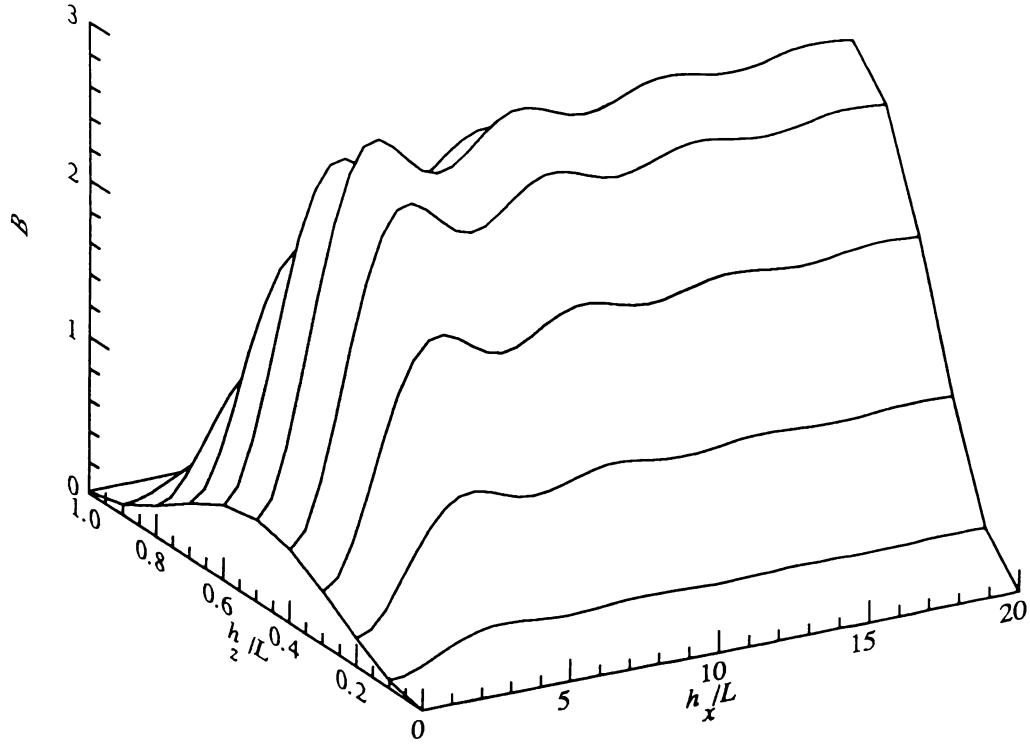


**Fig.6.5** $\mathcal{B}$ as a function of $h_x$ and $h_z$, for $L = 0.51\lambda$, $R = 0.99$, $N = 1$, and $\theta_{sq} = 0.3$.

can still be seen for sufficiently small $h_x/L$, however, the maximum relative reduction in $\mathcal{B}$ (69%) is less than that obtained with the same parameters for $L = \lambda/2$ (81%). Clearly, also, the absolute difference between the results obtained with and without squeezing is much smaller than for $L = \lambda/2$.

For smaller values of $R$, the cutoff in mode density is less sharp, and the drop-off in decay rate due to inhibited spontaneous emission is somewhat less dramatic. However, the effects of reducing $L$ below $\lambda/2$ are clearly undesirable if one hopes to see a large absolute reduction in the decay rate as a consequence of squeezing.

If $L$ is slightly greater than $\lambda/2$, we find that significant further enhancement of the decay rate, both with and without squeezing, is possible. This occurs as the remainder of the first-order Fabry-Perot maximum (i.e. the peak of the Airy function) is incorporated in the integrals of (6.4.15-16). Where squeezing is not significant, $\mathcal{B}(h_z = L/2)$ now approaches 3, as shown in Fig.6.5, where we consider the case $R = 0.99$, $L/\lambda = 0.51$. As $L$ is increased beyond this value, this enhancement is reduced, with the next maximum occurring around $L/\lambda = 1$. The maximum reduction due to squeezing ($N = 1, \theta_{sq} = 0.3$) is 81%, the same as was found with $L = \lambda/2$. The inhibition does not persist over as large an area as before, but the advantage now is that the absolute magnitude of the reduction is increased.

For lower values of $R$, a graph similar to that in Fig.6.5 is found, but with the maximum inhibition at $h_x = 0$ reduced (with increased $\theta_{sq}$, this may be improved).

If $L$ is too much greater than $\lambda/2$ (greater than $\sim 0.52$ for $R = 0.99$), an increase in $\theta_{sq}$ (from 0.3 radians) is needed to maintain a significant inhibition. We demonstrate this in Fig.6.6, where we display the results for $L/\lambda = 0.525$, and $R = 0.99$, with $\theta_{sq} = 0.3$ and $\theta_{sq} = 1.0$. These results emphasise the importance of matching the input to the cavity over a sufficiently large solid angle.

In conclusion, there appears to be a reasonable range over which $L$ may be varied and yet allow a significant reduction in the decay rate B relative to the normal vacuum level. This range is biased towards values of $L$ equal to or slightly larger than $\lambda/2$, as opposed to values of $L$ less than $\lambda/2$, where inhibited spontaneous emission becomes the dominant effect.

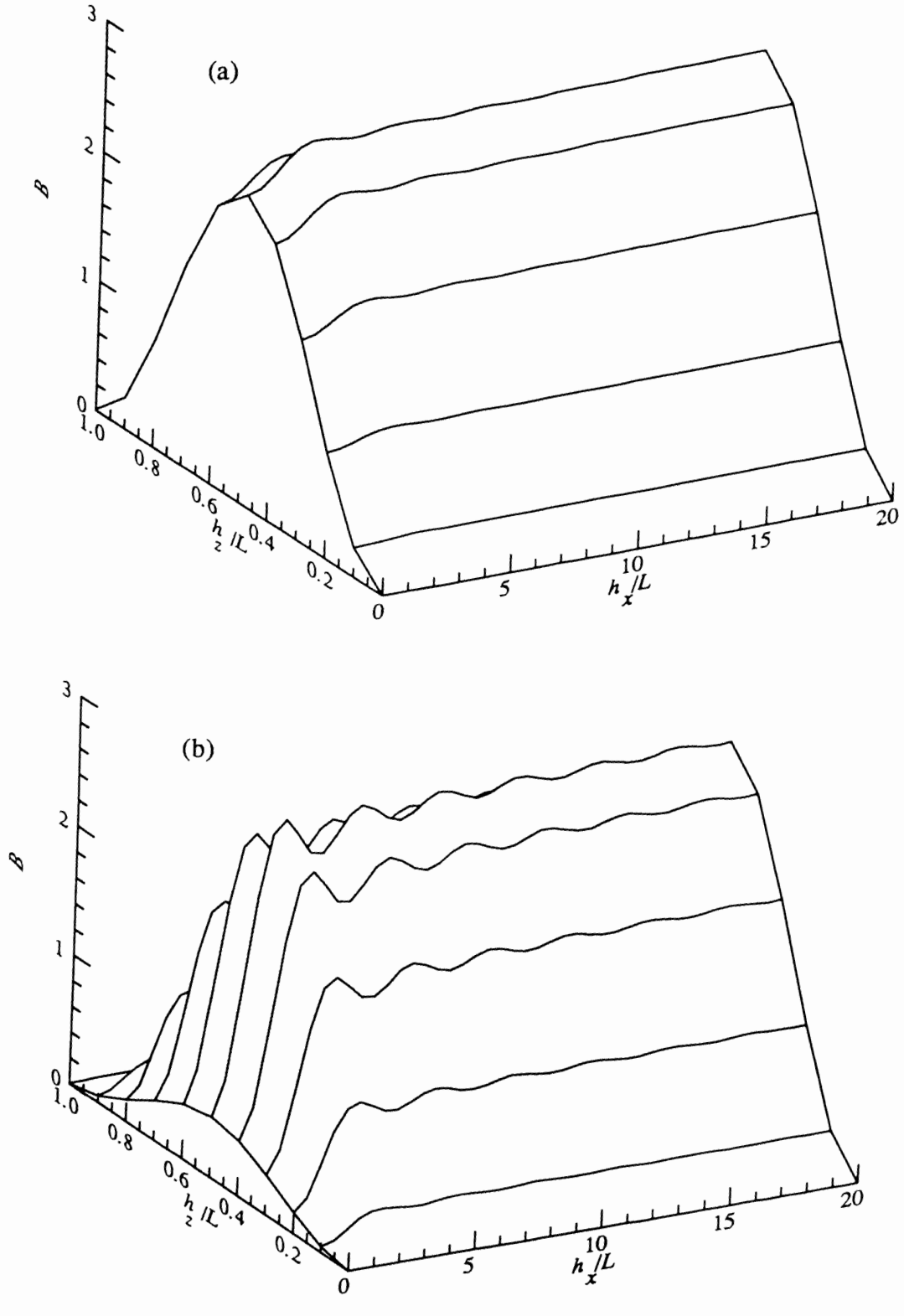


**Fig.6.6** $\mathcal{B}$ as a function of $h_x$ and $h_z$, for $L = 0.525\lambda$, $R = 0.99$, $N = 1$, with (a) $\theta_{sq} = 0.3$, (b) $\theta_{sq} = 1.0$.

### 6.4.2 Nonideal mode matching of the input to the cavity

In practice, a perfectly mode-matched input is unlikely to be possible, so it is important to repeat our calculations with $\alpha_s(\mathbf{k})$ given not by (6.4.4), but rather by some approximation to that function. It is instructive to consider the form of the exact mode function; if $R$ is close to one then, to a good approximation

$$F_{K\hat{\mathbf{k}}+}(\mathbf{h}_0) \simeq 0, \tag{6.4.19}$$

$$F_{K\hat{\mathbf{k}}+}(\mathbf{h}_0) \simeq -2iV^{-1/2} d_a \sin(Kh_z \cos\theta_k) g(K\cos\theta_k), \tag{6.4.20}$$

from which it is clear that we must try to match the function $g(K_z)$, as given by (6.2.2), for a particular polarisation. We choose a Gaussian distribution over angle as an example of an approximate match, which will enable us to check how critical the requirement of matching is. In particular, we choose

$$\alpha_-(\mathbf{k}) = 0, \tag{6.4.21}$$

$$\alpha_+(\mathbf{k}) = \mathcal{N}_g^{-1/2} \exp[-\delta \sin^2\theta_k - i(\eta + \xi \sin^2\theta_k)] \times i \sin(Kh_z \cos\theta_k), \tag{6.4.22}$$

where $\delta$, $\eta$, and $\xi$ are real constants, and the normalisation factor $\mathcal{N}_g$ is given by

$$\mathcal{N}_g = \int_{\Omega_{sq}} d\Omega_k \exp(-2\delta \sin^2\theta_k) \sin^2(Kh_z \cos\theta_k), \tag{6.4.23}$$

with $\int_{\Omega_{sq}} d\Omega_k$ as defined in (6.4.13). This form may be considered to model a focussed Gaussian beam in the paraxial approximation (Yariv, 1985).

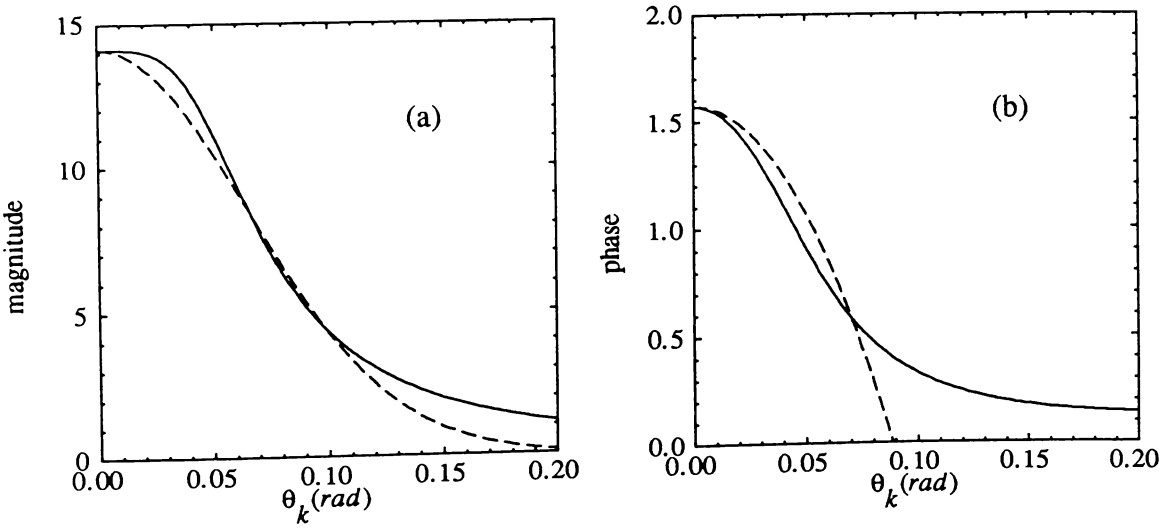


**Fig.6.7** (a) Magnitude and (b) phase of $g(K_z)$ (solid lines) for $L = \lambda/2$, $R = 0.99$, compared with $14\exp(-120\sin^2\theta_k)$ and $\pi/2 - 200\sin^2\theta_k$ (dashed lines) respectively.

A comparison of the magnitude and phase of $g(K_z)$ with $\exp(-\delta \sin^2\theta_k)$ (appropriately scaled) and $(\eta + \xi \sin^2\theta_k)$ respectively is shown in Fig.6.7, for $R = 0.99$, and $L = \lambda/2$, with $\delta = 120$, $\eta = \pi/2$, and $\xi = -200$ (a particular choice of parameters we shall consider later). The Lorentzian-type long-time tails of $g(K_z)$ are not well matched, but in the more important small angle region, where $g(K_z)$ is sharply peaked, the approximation is much better.

Using the expressions (6.4.21,22) for $\alpha_\pm(\mathbf{k})$ in (6.4.2), we obtain,

$$\langle \beta_Y(\mathbf{h},t)\beta_Y(\mathbf{h},t')\rangle = \gamma_a \mathcal{B}_g(\mathbf{h})\,\delta(t-t'), \tag{6.4.24}$$

where

$$\begin{aligned}\mathcal{B}_g(\mathbf{h}) =& 3\pi\mathcal{N}_g^{-1}\frac{1+R}{(1-R)^3}\left\{N\,|\mathcal{I}(\mathbf{h})|^2 - M\,\mathrm{Re}[\mathcal{I}(\mathbf{h})^2]\right\} \\ &+ \frac{3}{2}\frac{1+R}{1-R}\int_0^1 du\,(1+u^2)\frac{\sin^2(Kh_zu)}{1+F\sin^2(KLu)},\end{aligned} \tag{6.4.25}$$

with

$$\begin{aligned}\mathcal{I}(\mathbf{h}) = ie^{-i\eta}\int_{\cos\theta_{sq}}^1 du(1+u)\sin^2(Kh_zu)J_0(Kh_x\sqrt{1-u^2}) \\ \times\frac{1-R\cos(2KLu)-iR\sin(2KLu)}{1+F\sin^2(KLu)} \\ \times\exp\left[-(\delta+i\xi)(1-u^2)\right].\end{aligned} \tag{6.4.26}$$

Evidently, for maximum effect we require (i) that $\mathrm{Re}[\mathcal{I}(\mathbf{h})^2]$ be as close as possible to $|\mathcal{I}(\mathbf{h})|^2$, and (ii) that the factors multiplying $N$ and $M$ be maximised relative to the corresponding factor in the second term of (6.4.25) (i.e. the "normal" vacuum term).

**Numerical results**

In our first set of diagrams we display the results obtained with $L = \lambda/2$ and $R = 0.99$, with $\theta_{sq} = 0.1$ radians. In Fig.6.8 we give the profile of $\mathrm{B}_g(\mathbf{h})$ at $h_x = 0$ (where maximum reductions are to be expected), for a series of values of $\xi = 50, 150, 200, 300$, with $\delta = 120$ and $\eta = -\pi/2$ fixed. Once again, we assume an input squeezed by 83% ($N = 1$). The magnitude of fluctuations relative to the vacuum depends strongly on the choice of $\xi$, emphasising the need for good matching of the mode functions (in particular, the phase). For $N = 1$, reduced fluctuations at $h_x = 0$ are found for values of $\xi$ in the range 80 to 340. At the position $h_z/L = 0.5$, the optimum choice of parameters ($\delta \simeq 120$, $\xi \simeq 200$, $\eta = -\pi/2$) gives a maximum reduction below the vacuum level of approximately 64%, which compares very favourably with that obtained with ideal matching when $\theta_{sq} = 0.1$.

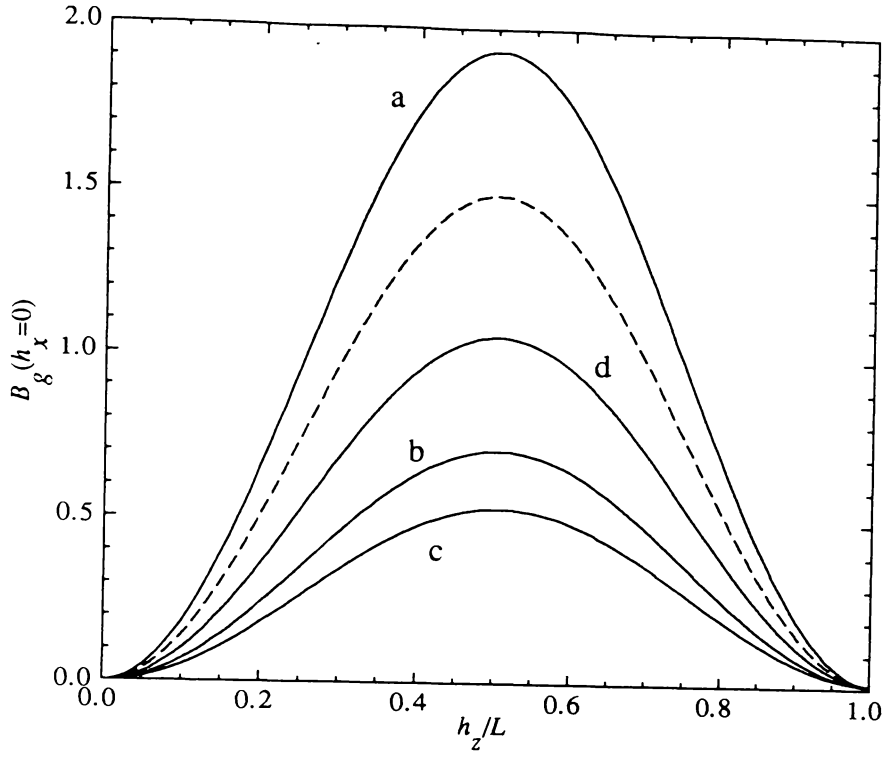


**Fig.6.8** $\mathcal{B}_g(h_x = 0)$ for $L = \lambda/2$, $R = 0.99$, with $\theta_{sq} = 0.1$, $\delta = 120$, $\eta = -\pi/2$, $N = 1$, and (a) $\xi = 50$, (b) $\xi = 150$, (c) $\xi = 200$, and (d) $\xi = 300$. The dashed line is the result obtained with no squeezed input.

While our results are very dependent on $\xi$, they are much less sensitive to variations in $\delta$, as we demonstrate in Fig.6.9, where we fix $\xi = 200$ and compare results for $\delta = 0$ and $\delta = 500$. The curves are very similar, and give maximum reductions below the vacuum level of 55% and 45% for $\delta = 0$ and $\delta = 500$ respectively (the optimum choice of $\delta = 120$ gives a 64% reduction).

In Fig.6.10, we display the behaviour in the $x$ direction for the optimum choice of $\xi$ and $\delta$ given above. This figure is to be compared with Fig.6.2(b). Reduced values of $B_g$ are found over a similar area to that when the input is ideally-matched.

Unlike the ideally-matched case, increasing the angular limit $\theta_{sq}$ does not lead to an appreciable improvement in the amount of noise reduction possible. This is not surprising as the phase approximation used ceases to be effective for $\theta_k > 0.1$, as shown in Fig.6.7(b). If $R$ is decreased slightly, then values of $\theta_{sq}$ larger than 0.1 give the best results (provided $\delta$ and $\xi$ are fitted appropriately). However, a limit (above which no further improvement occurs) is again reached, with a maximum reduction in fluctuations similar to those found above. Our approximation to the phase is obviously limited, and some more accurate approximation would be needed to yield better reductions.

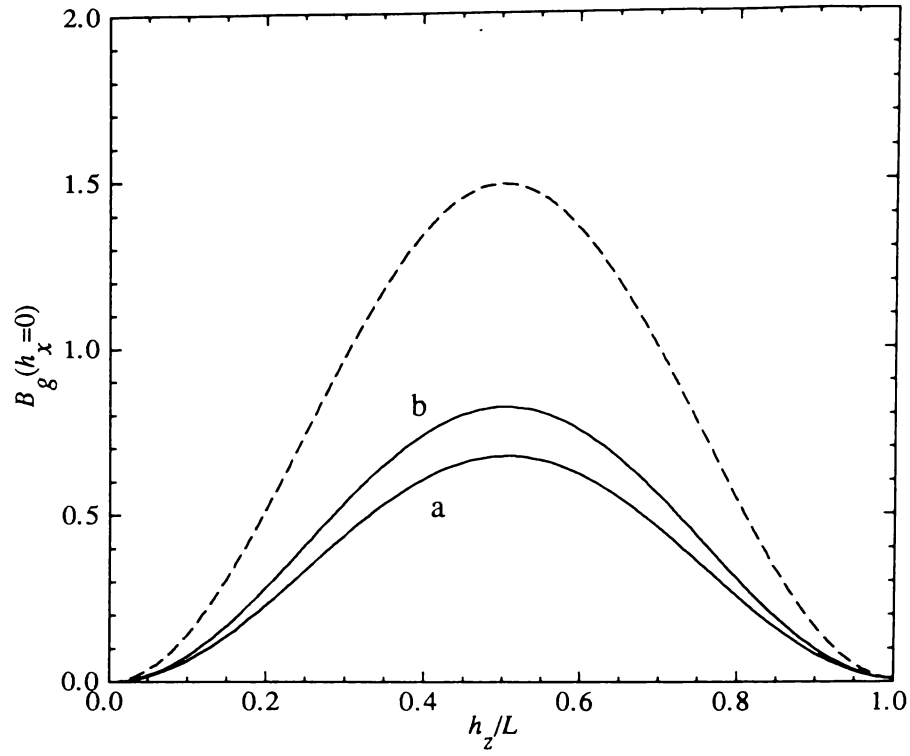


**Fig.6.9** $\mathcal{B}_g(h_x = 0)$ for $L = \lambda/2$, $R = 0.99$, with $\theta_{sq} = 0.1$, $\xi = 200$, $\eta = -\pi/2$, $N = 1$, and (a) $\delta = 0$, (b) $\delta = 500$. The dashed line is the result obtained with no squeezed input.

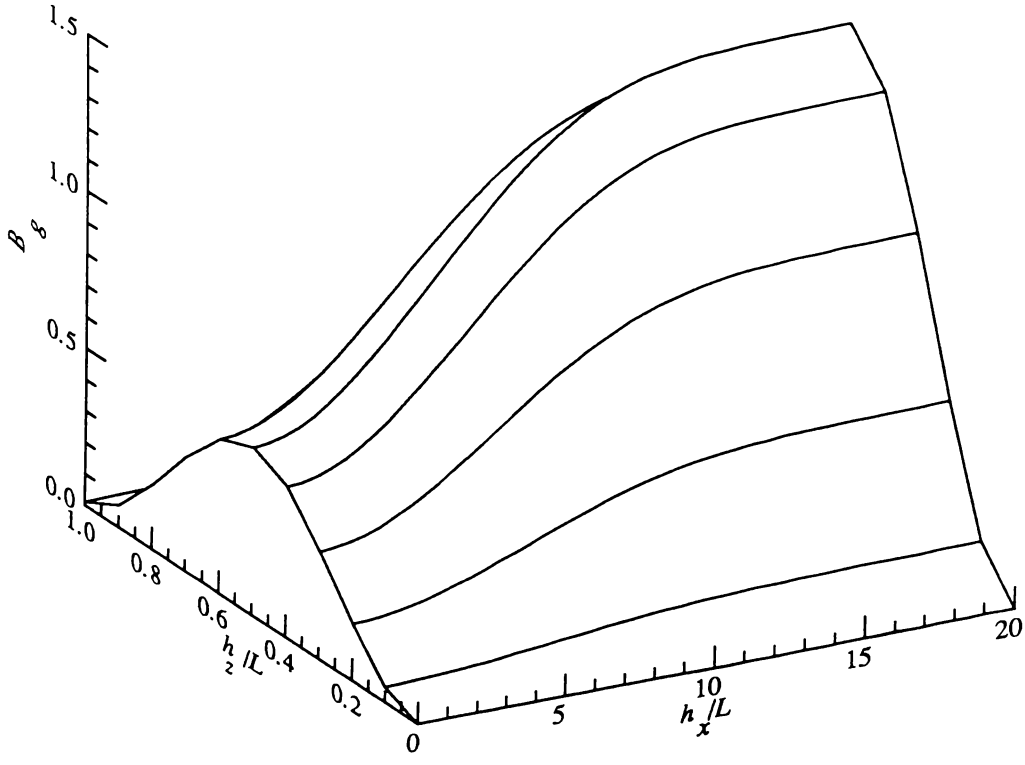


**Fig.6.10** $\mathcal{B}_g$ as a function of $h_x$ and $h_y$, for $L = \lambda/2$, $R = 0.99$, with $\theta_{sq} = 0.1$, $\delta = 120$, $\xi = 200$, $\eta = -\pi/2$, and $N = 1$.

We shall not consider in detail any further approximations, but, as one might expect, Lorentzian approximations to the phase are found to give significant improvements over the above results, particularly as the angular limit $\theta_{sq}$ is increased. That is, if we replace $\eta + \xi \sin^2 \theta_k$ by a function of the form

$$-\frac{\pi}{2}\frac{w^2}{w^2 + \theta_k^2} \tag{6.4.27}$$

in (6.4.22), then, for a suitable choice of the parameter $w$, one can almost reproduce the results obtained under conditions of ideal matching.

### 6.4.3 Experimental Considerations

As we have found, suitably-prepared atoms inside the cavity will be sensitive to only a single (circular) polarisation of the field. Hence, a single source of circularly-polarised squeezed light should suffice. This squeezed light would have to be passed through a system of lenses and phase plates in order to produce a focused beam of squeezed light with characteristics of the sort discussed earlier, that is, with appropriately matched phase and amplitude.

The cavity itself should be a bad cavity (i.e. low $Q$), which, in the case of a microscopic optical cavity, does not seem too difficult to achieve. In particular, we have, for the lifetime $t_c$ of a photon within the cavity

$$t_c = \frac{L}{(1 - R)c} \sim 10^{-13} s, \tag{6.4.28}$$

for $L \sim 10^{-6} m$ and $R = 0.99$ (i.e. $Q \sim 100$). This time is clearly much shorter than a typical spontaneous emission lifetime, so it should be safe to regard the process as irreversible. If this is not the case new effects may arise, such as the collective stimulated emission process observed by De Martini and Jacobovitz (1988), in which long-range atom-atom correlations occur when more than one atom undergoes a radiative decay within a period $t_c$. A low density atomic or molecular sample would therefore also seem appropriate in avoiding such cooperative effects.

# Appendix A: Higher order terms in the cumulant expansion

In this appendix, the cumulant expansion introduced in Chapters 2 and 3 is expanded to fourth order in the expansion parameter, which we denote by $\epsilon$ (later, we set $\epsilon$ equal to one). To this order in $\epsilon$, and with the assumption that the odd moments of the noise $\beta_{hf}(t)$ are zero (i.e. $\langle\beta_{hf}(t_1)\rangle = \langle\beta_{hf}(t_1)\beta_{hf}(t_2)\beta_{hf}(t_3)\rangle = 0$), the cumulant expansion yields (Collett, 1987)

$$\begin{aligned}
\dot{\mu}_{hf} =& A_0\mu_{hf} + \beta_{lf}(t)A_1\mu_{hf} \\
&+ \epsilon^2\int_{t_0}^{t} d\tau\,\langle\beta_{hf}(t)\beta_{hf}(\tau)\rangle A_1 e^{A_0(t-\tau)}A_1 e^{-A_0(t-\tau)}\mu_{hf} \\
&- \epsilon^4\int_{t_0}^{t} d\tau\,\langle\beta_{hf}(t)\beta_{hf}(\tau)\rangle A_1 e^{A_0(t-\tau)}A_1 e^{A_0\tau} \\
&\quad\times\int_{t_0}^{t} d\tau_1\int_{t_0}^{\tau_1} d\tau_2\,\langle\beta_{hf}(\tau_1)\beta_{hf}(\tau_2)\rangle e^{-A_0\tau_1}A_1 e^{A_0(\tau_1-\tau_2)}A_1 e^{A_0(\tau_2-t)}\mu_{hf} \\
&+ \epsilon^4\int_{t_0}^{t} d\tau_1\int_{t_0}^{\tau_1} d\tau_2\int_{t_0}^{\tau_2} d\tau_3\,\langle\beta_{hf}(t)\beta_{hf}(\tau_1)\beta_{hf}(\tau_2)\beta_{hf}(\tau_3)\rangle \\
&\quad\times A_1 e^{A_0(t-\tau_1)}A_1 e^{A_0(\tau_1-\tau_2)}A_1 e^{A_0(\tau_2-\tau_3)}A_1 e^{A_0(\tau_3-t)}\mu_{hf}. \qquad (A1)
\end{aligned}$$

For consistency with a fourth order expansion, we must note that $A_0$ in fact contains a damping term and should be written in the form

$$A_0 = A_{sys} + \epsilon^2 A_2\ , \qquad (A2)$$

where

$$A_2\mu_{hf} \equiv \frac{i}{2\hbar}[\,[\Gamma,\mu_{hf}]_+, X]. \qquad (A3)$$

In the third term in (A1) we therefore write

$$e^{A_0\tau} \simeq e^{A_{sys}\tau}\left\{1 + \epsilon^2\int_0^{\tau} d\tau'\,e^{-A_{sys}\tau'}A_2 e^{A_{sys}\tau'}\right\}\ , \qquad (A4)$$

while in the final two terms we simply make the replacement $e^{A_0\tau} \rightarrow e^{A_{sys}\tau}$. Since the correlation time of $\beta_{hf}(t)$ is short, we can set $t_0 = -\infty$, and noting that $\beta_{hf}(t)$ is Gaussian, the fourth order moments can be factorised into products of the two-time correlation

functions. After some manipulation, we find (setting $\epsilon = 1$)

$$
\begin{aligned}
\dot{\mu}_{hf} &= A_{sys}\mu_{hf} + A_2\mu_{hf} + \beta_{lf}(t)A_1\mu_{hf} \\
&- \frac{1}{\hbar^2}\int_0^\infty d\tau\, \langle \beta_{hf}(t)\beta_{hf}(t-\tau)\rangle\, [X,[X(-\tau),\mu_{hf}]] \\
&+ \frac{i}{2\hbar^3}\int_0^\infty d\tau_1 \int_0^{\tau_1} d\tau_2\, \langle \beta_{hf}(t)\beta_{hf}(t-\tau_1)\rangle \\
&\quad \times [X,[X(-\tau_2),[\Gamma(-\tau_2),[X(-\tau_1),\mu_{hf}]]_+]] \\
&- \frac{i}{2\hbar^3}\int_0^\infty d\tau_1 \int_0^{\tau_1} d\tau_2\, \langle \beta_{hf}(t)\beta_{hf}(t-\tau_1)\rangle \\
&\quad \times [X,[X(-\tau_1),[X(-\tau_2),[\Gamma(-\tau_2),\mu_{hf}]_+]]] \\
&+ \frac{1}{\hbar^4}\int_0^\infty d\tau_1 \int_0^{\tau_1} d\tau_2 \int_0^{\tau_2} d\tau_3 \\
&\quad \times \{\langle \beta_{hf}(t)\beta_{hf}(t-\tau_3)\rangle \langle \beta_{hf}(t-\tau_2)\beta_{hf}(t-\tau_1)\rangle \\
&\quad + \langle \beta_{hf}(t)\beta_{hf}(t-\tau_2)\rangle \langle \beta_{hf}(t-\tau_3)\beta_{hf}(t-\tau_1)\rangle \\
&\quad + \langle \beta_{hf}(t)\beta_{hf}(t-\tau_1)\rangle \langle \beta_{hf}(t-\tau_3)\beta_{hf}(t-\tau_2)\rangle\} \\
&\quad \times [X,[X(-\tau_3),[X(-\tau_2),[X(-\tau_1),\mu_{hf}]]]] \\
&- \frac{1}{\hbar^4}\int_0^\infty d\tau_1 \int_0^{\tau_1} d\tau_2 \int_0^{\infty} d\tau_3 \\
&\quad \times \langle \beta_{hf}(t)\beta_{hf}(t-\tau_3)\rangle \langle \beta_{hf}(t-\tau_2)\beta_{hf}(t-\tau_1)\rangle \\
&\quad \times [X,[X(-\tau_3),[X(-\tau_2),[X(-\tau_1),\mu_{hf}]]]]. \qquad (A5)
\end{aligned}
$$

In deriving Eqs.(3.1.31), we neglected terms that are proportional to $q_{k1}$ and $q_{k2}$ with $k \geq 3$. In keeping with this approximation, we consider $X$ to have the reduced form

$$X = q_{21}(A_{12} + A_{21}) \qquad (A6)$$

for the purpose of evaluating (A5). Having made this assumption, if one then evaluates the equations of motion for the matrix elements of $\mu_{hf}(t)$, one finds that the final two terms in (A5) merely yield higher order corrections to damping terms that we have already neglected on the basis that $\kappa_{hf}(\omega_{21})^2 = 0$, that is, the high frequency portion of the bath gives rise to a frequency renormalisation, but plays no part in the dynamics of the two lowest levels in the system. Hence, the last two terms in (A5) are neglected. The fifth and sixth terms in (A5) do however yield a significant correction, but then only to the inhomogeneous term occurring in the equation for $\dot{S}_z$. It is straightforward to show that

this correction has the form

$$
\begin{aligned}
&-\frac{\pi\omega_{21}q_{21}^4\kappa(\omega_{21})^2}{2\hbar^3}\int_0^\infty d\tau\,\tau\langle\beta_{hf}(\tau)\beta_{hf}(0)\rangle e^{i\omega_{21}\tau} \\
&=\frac{\pi\omega_{21}q_{21}^4\kappa(\omega_{21})^2}{\hbar^2}P\int_0^\infty d\omega\,\kappa_{hf}(\omega)^2\omega\left\{\frac{1}{(\omega-\omega_{21})^2}+\frac{1}{(\omega+\omega_{21})^2}\right\},
\end{aligned}
\tag{A7}
$$

where again we have assumed that $\kappa_{hf}(\omega_{21})^2 \simeq 0$.

# Appendix B: Simulation of Thermal Quantum Noise

Thermal quantum noise is numerically simulated using a Fast Fourier Transform technique. To show how this may be formulated, we begin with the correlation function in the form

$$\langle \beta_{lf}(t)\beta_{lf}(t')\rangle = \int_{-\infty}^{\infty} df\ S(f)e^{i2\pi f(t-t')}, \qquad (B1)$$

where $f = \omega/2\pi$. The function $S(f)$ is assumed to be negligible outside the region $(-F, F)$. Dividing this region into $2N$ equal intervals, we can approximate the integral with the discrete form

$$\begin{aligned}\int_{-\infty}^{\infty} df\ S(f)e^{i2\pi f(t-t')} &\simeq \int_{-F}^{F} df\ S(f)e^{i2\pi f(t-t')} \\ &\simeq \frac{F}{N}\sum_{j=-(N-1)}^{N-1} S_j\ e^{i2\pi jF(t-t')/N}, \qquad (B2)\end{aligned}$$

where $S_j = S(jF/N) = S(-jF/N)$. We discretise time by identifying the timestep as

$$\Delta t = \frac{1}{2F}, \qquad (B3)$$

and by setting $t = k\Delta t$, and $t' = k'\Delta t$, after which the correlation function follows in the form

$$\langle \beta_{lf}^{k}\beta_{lf}^{k'}\rangle = \frac{F}{N}\sum_{j=-(N-1)}^{N-1} S_j\ e^{i2\pi j(k-k')/(2N)}. \qquad (B4)$$

A noise source satisfying this correlation function can be constructed from

$$\beta_{lf}^{k} = \sqrt{\frac{F}{N}}\sum_{j=-(N-1)}^{N-1} g_j\sqrt{S_j}\ e^{i2\pi jk/(2N)}, \qquad (B5)$$

where $g_j$ $(=g_{-j})$ is a Gaussian random number with zero mean and unit variance ($\langle g_i g_j\rangle = \delta_{ij}$). Hence, to generate a sequence of random numbers $\{\beta_{lf}^{k},\ k = 1, N\}$ for a single trajectory of the variables $S_x$, $S_y$, and $S_z$, we multiply each element $\sqrt{S_j}$ by a random number $g_j$, and calculate the discrete Fourier transform of the resulting sequence. This calculation is carried out by the NAG routine C06FBF, which uses the Fast Fourier Transform algorithm (Brigham, 1974).

The maximum time to which one can compute a single trajectory is determined from

$$t_{max} = N\left(\frac{1}{2F}\right), \qquad (B6)$$

which is constrained by the requirement that $S(F) \simeq 0$. Noting that $S(f)$ is a maximum at $f = f_c = \omega_c/2\pi$, this corresponds to the condition $F \gg f_c$ (from which it follows that $\Delta t \ll 2\pi/\omega_c$).

In practice, there is a limit to the number of points $N$ that one can handle, which therefore limits the maximum value of $f_c$ that one can consider while still maintaining a reasonable value of $t_{max}$. In our simulations, we use $N = 98304$ $(=2^{15} \times 3)$, with $F$ typically $15 - 30$ times greater than the cutoff frequency $f_c$. On average, the computation of 1000 trajectories of the variables $S_x$, $S_y$, and $S_z$ requires approximately 4.25 hours of CPU time using a VAX 6000-430 mainframe computer.

# Appendix C: Modelling of Exponentially-Correlated Noise

The noise sources that we aim to simulate are Gaussian and obey the statistics

$$\langle \beta_1^c(t) \rangle = \langle \beta_2^c(t) \rangle = \langle \beta_1^c(t) \beta_2^c(t') \rangle = 0 , \tag{C1}$$

$$\langle \beta_1^c(t) \beta_1^c(t') \rangle = \gamma_a (N - M) b_- e^{-b_- |t-t'|} , \tag{C2}$$

$$\langle \beta_2^c(t) \beta_2^c(t') \rangle = \gamma_a (N + M) b_+ e^{-b_+ |t-t'|} , \tag{C3}$$

These sources are modelled using summations of suitably weighted Gaussian distributed random numbers. Two sequences of Gaussian random numbers $\{g_n\}$ and $\{h_n\}$ are generated with the properties

$$\begin{aligned} &\langle g_n \rangle = \langle h_n \rangle = 0 , \\ &\langle g_n g_m \rangle = \langle h_n h_m \rangle = \delta_{nm} \quad , \quad \langle g_n h_m \rangle = 0 , \end{aligned} \tag{C4}$$

from which $\beta_1^c(t_n)$ and $\beta_2^c(t_n)$ are constructed as

$$\beta_1^c(t_n) = \left[ \gamma_a (N - M) b_- (1 - e^{-2 b_- \Delta t}) \right]^{1/2} \sum_{r=0}^{n} e^{-r b_- \Delta t} g_{n-r} , \tag{C5}$$

$$\beta_2^c(t_n) = \left[ \gamma_a (N + M) b_+ (1 - e^{-2 b_+ \Delta t}) \right]^{1/2} \sum_{r=0}^{n} e^{-r b_+ \Delta t} h_{n-r} , \tag{C6}$$

where $\Delta t$ is the timestep, and $n$ is assumed to be large. Simple recursion relations follow from $(C5)$ and $(C6)$ in the form

$$\beta_1^c(t_n) = g_n \left[ \gamma_a (N - M) b_- (1 - e^{-2 b_- \Delta t}) \right]^{1/2} + e^{-b_- \Delta t} \beta_1^c(t_{n-1}) , \tag{C7}$$

$$\beta_2^c(t_n) = h_n \left[ \gamma_a (N + M) b_+ (1 - e^{-2 b_+ \Delta t}) \right]^{1/2} + e^{-b_+ \Delta t} \beta_2^c(t_{n-1}) . \tag{C8}$$

The random numbers $g_n$ and $h_n$ are generated by successive calls to the NAG (Numerical Algorithms Group) routine G05DDF. The independence of the noise sources constructed by this means is maintained, since the routine G05DDF updates the seed of the underlying multiplicative congruential generator with each call. The overall random number sequence is initialised by the NAG routine G05CCF, which sets the basic generator routine to a non-repeatable initial state, thereby ensuring that a different sequence of random numbers is

used for each different run of the program. Inbetween individual trajectories, the recursion relations are iterated for a certain number of timesteps to ensure that the noise in each trajectory is uncorrelated with the noise in other trajectories.

In the case of two-mode squeezing, in which $\beta_1^c(t)$ and $\beta_2^c(t)$ satisfy

$$\langle \beta_1^c(t) \rangle = \langle \beta_2^c(t) \rangle = \langle \beta_1^c(t) \beta_2^c(t') \rangle = 0, \tag{C9}$$

$$\langle \beta_1^c(t) \beta_1^c(t') \rangle = 2\gamma_a(N - M) b_- e^{-b_-|t-t'|} \cos[\delta_c(t - t')], \tag{C10}$$

$$\langle \beta_2^c(t) \beta_2^c(t') \rangle = 2\gamma_a(N + M) b_+ e^{-b_+|t-t'|} \cos[\delta_c(t - t')], \tag{C11}$$

we require four independent sequences of random numbers. That is, we write $\beta_1^c(t)$ and $\beta_2^c(t)$ as

$$\beta_1^c(t) = \beta_{1a}^c(t) \cos(\delta_c t) + \beta_{1b}^c(t) \sin(\delta_c t), \tag{C12}$$

$$\beta_2^c(t) = \beta_{2a}^c(t) \cos(\delta_c t) + \beta_{2b}^c(t) \sin(\delta_c t), \tag{C13}$$

where $\beta_{1a}^c(t)$, $\beta_{1b}^c(t)$, $\beta_{2a}^c(t)$, and $\beta_{2b}^c(t)$ are independent noise sources satisfying

$$\langle \beta_{1a}^c(t) \beta_{1a}^c(t') \rangle = \langle \beta_{1b}^c(t) \beta_{1b}^c(t') \rangle = 2\gamma_a(N - M) b_- e^{-b_-|t-t'|}, \tag{C14}$$

$$\langle \beta_{2a}^c(t) \beta_{2a}^c(t') \rangle = \langle \beta_{2b}^c(t) \beta_{2b}^c(t') \rangle = 2\gamma_a(N + M) b_+ e^{-b_+|t-t'|}. \tag{C15}$$

We model these four sources using the method outlined above.

# References


Allen, L., and J.H. Eberly, 1975, *Optical Resonance and Two-Level Atoms* (Wiley, New York), Ch.2.

An, S., M. Sargent, and D.F. Walls, 1988, Optics Comm. **67**, 373.

Aslangul, C., N. Pottier, and D. Saint-James, 1985, Phys. Lett. 110A, 249.

Aslangul, C., N. Pottier, and D. Saint-James, 1986, J. Phys. (Paris) **47**, 1657.

Brigham, E.O., 1974, *The Fast Fourier Transform* (Prentice-Hall, Englewood Cliffs).

Carmichael, H.J., and D.F. Walls, 1976, J. Phys. B**9**, 1199.

Carmichael, H.J., A.S. Lane, and D.F. Walls, 1987a, Phys. Rev. Lett. **58**, 2539.

Carmichael, H.J., A.S. Lane, and D.F. Walls, 1987b, J. Mod. Opt. **34**, 821.

Carniglia, C.K., and L. Mandel, 1971, Phys. Rev. D **3**, 280.

Chakravarty, S., and A.J. Leggett, 1984, Phys. Rev. Lett. **52**, 5.

Collett, M.J., 1983, *Input, Output, and Dissipation in the Theory of Quantum and Classical Amplifiers*, M.Sc. Thesis (unpublished), University of Waikato.

Collett, M.J., 1987, *Environmental Correlations in the Theory of Open Quantum Systems*, Ph.D. Thesis (unpublished), University of Essex.

Collett, M.J., and C.W. Gardiner, 1984, Phys. Rev. A **30**, 1386.

Collett, M.J., R. Loudon, and C.W. Gardiner, 1987, J. Mod. Opt. **34**, 821.

Courty, J.-M., and S. Reynaud, 1989, Europhys. Lett. **10**, 237.

Cresser, J.D., J. Häger, G. Leuchs, M. Rateike, and H. Walther, 1982, in *Dissipative Systems in Quantum Optics*, edited by R. Bonifacio (Springer-Verlag, Berlin).

Dekker, H., 1987, Phys. Rev. A **35**, 1436.

De Martini, F., and G. Innocenti, 1986, in *Quantum Optics IV*, edited by J.D. Harvey and D.F. Walls (Springer-Verlag, Berlin).

De Martini, F., G. Innocenti, G.R. Jacobovitz, and P. Mataloni, 1987, Phys. Rev. Lett. **59**, 2955.

De Martini, F., and G.R. Jacobovitz, 1988, Phys. Rev. Lett. **60**, 1711.

Dorsey, A.T., M.P.A. Fisher, and M.S. Wartak, 1986, Phys. Rev. A **33**, 1117.

Drummond, P.D., and C.W. Gardiner, 1980, J. Phys. A **13**, 2353.

Ford, G.W., and R.F. O'Connell, J. Opt. Soc. Am. B**4**, 1710.

Gardiner, C.W., 1983, *Handbook of Stochastic Methods* (Springer-Verlag, Berlin).

Gardiner, C.W., and M.J. Collett, 1985, Phys. Rev. A **31**, 3761.

Gardiner, C.W., 1986, Phys. Rev. Lett. **56**, 1917.

Gardiner, C.W., A.S. Parkins, and M.J. Collett, 1987, J. Opt. Soc. Am. B**4**, 1683.

Gardiner, C.W., 1988, IBM J. Res. Dev. **32**, 127.

Gradshteyn, I.S., and I.M. Ryzhik, 1965, *Table of Integrals, Series, and Products* (Academic Press, New York).

Heinzen, D.J., J.J. Childs, J.E. Thomas, and M.S. Feld, 1987, Phys. Rev. Lett. **58**, 1320.

Hulet, R.G., E.S. Hilfer, and D. Kleppner, 1985, Phys. Rev. Lett. **55**, 2137.

Jhe, W., A. Anderson, E.A. Hinds, D. Meschede, L. Moi, and S. Haroche, 1987, Phys. Rev. Lett. **58**, 666.

Kennedy, T.A.B., and D.F. Walls, 1990, Phys. Rev. A **42**, 3051.

Kibble, T.W.B., 1969, in *Quantum Optics*, edited by S.M. Kay and A. Maitland (Academic Press, London).

Lane, A.S., 1988, *Generation and Applications of Squeezed Coloured Noise*, Ph.D. Thesis (unpublished), University of Waikato.

Leggett, A.J., S. Chakravarty, A.T. Dorsey, M.P.A. Fisher, A. Garg, and W. Zwerger, 1987, Rev. Mod. Phys. **59**, 1.

Lewenstein, M., T.W. Mossberg, and R.J. Glauber, 1987, Phys. Rev. Lett. **59**, 775.

Lewenstein, M., and T.W. Mossberg, 1988, Phys. Rev. A **37**, 2048.

Ley, M., and R. Loudon, 1987, J. Mod. Opt. **34**, 227.

Marte, M.A.M., and D.F. Walls, 1988, Phys. Rev. A **37**, 1235.

Marte, M.A.M., H. Ritsch, and D.F. Walls, 1988a, Phys. Rev. Lett. **61**, 1093.

Marte, M.A.M., H. Ritsch, and D.F. Walls, 1988b, Phys. Rev. A **38**, 3577.

McNeil, K.J., and I.J.D. Craig, 1990, Phys. Rev. A **41**, 4009.

Milburn, G.J., 1986, Phys. Rev. A **34**, 4882.

Mollow, B.R., 1969, Phys. Rev. **188**, 1969.

Orozco, L.A., M.G. Raizen, M. Xiao, R.J. Brecha, and H.J. Kimble, 1987, J. Opt. Soc. Am. B **4**, 1490.

Parkins, A.S., and C.W. Gardiner, 1988, Phys. Rev. A **37**, 3867.

Parkins, A.S., and C.W. Gardiner, 1989a, Phys. Rev. A **40**, 2534.

Parkins, A.S., and C.W. Gardiner, 1989b, Phys. Rev. A **40**, 3796.

Parkins, A.S., 1990a, Phys. Rev. A **42**, 4352.

Parkins, A.S., 1990b, to appear in Phys. Rev. A.

Raizen, M.G., L.A. Orozco, M. Xiao, T.L. Boyd, and H.J. Kimble, 1987, Phys. Rev. Lett. **59**, 198.

Ritsch, H., 1989, private communication.

Reid, M.D., and P.D. Drummond, 1990, Phys. Rev. A **41**, 3930.

Ritsch, H., and P. Zoller, 1987, Optics Comm. **64**, 523.

Ritsch, H., and P. Zoller, 1988a, Phys. Rev. Lett. **61**, 1097.

Ritsch, H., and P. Zoller, 1988b, Phys. Rev. A **38**, 4657.

Slusher, R.E., P. Grangier, A. LaPorta, B. Yurke, and M.J. Potasek, 1987, Phys. Rev. Lett. **59**, 2566.

Smith, A.M., and C.W. Gardiner, 1989, Phys. Rev. A **39**, 3511.

van Kampen, N.G., 1974, Physica **74**, 215.

van Kampen, N.G., 1981, *Stochastic Processes in Physics and Chemistry* (North-Holland, Amsterdam).

Weiss, U., H. Grabert, and S. Linkwitz, 1987a, J. Low Temp. Phys. **68**, 213.

Weiss, U., H. Grabert, P. Hänggi, and P. Riseborough, 1987b, Phys. Rev. B **35**, 9535.

Wu, L.-A., H.J. Kimble, J.L. Hall, and H. Wu, 1986, Phys. Rev. Lett. **57**, 2520.

Wu, L.-A., M. Xiao, and H.J. Kimble, 1987, J. Opt. Soc. Am. B **4**, 1465.

Yariv, A., 1985, *Optical Electronics*, 3rd Ed. (Holt, Rinehart and Winston, New York).